
**PROCEEDINGS OF THE 2001 ANTENNA APPLICATIONS
SYMPOSIUM –VOLUME I**

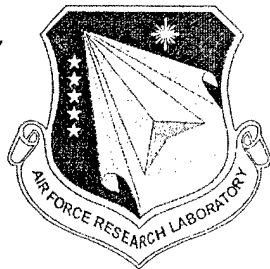
**Daniel H. Schaubert, et al
Electrical and Computer Engineering Department
University of Massachusetts
Amherst MA 01002**

**Electromagnetics Laboratory
University of Illinois
Urbana-Champaign**

FINAL REPORT : September 19 – 21 2001

APPROVED FOR PUBLIC RELEASE: DISTRIBUTION UNLIMITED

20020717 123

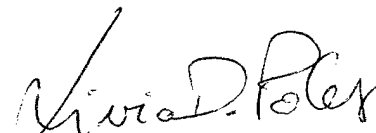


**AIR FORCE RESEARCH LABORATORY
Sensors Directorate
Electromagnetics Technology Division
80 Scott Dr
Hanscom AFB MA 01731-2909**

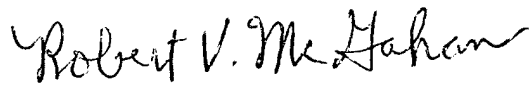
TITLE OF REPORT:
2001 Antenna Applications Symposium
VOLUME I
PUBLICATION REVIEW

This report has been reviewed and is approved for publication.

APPROVED:


Livio D. Poles
Antenna Technology Branch
Electromagnetics Technology Division

FOR THE DIRECTOR


Robert V. McGahan,
Division Technical Advisor
Electromagnetics Technology Division

REPORT DOCUMENTATION PAGE					Form Approved OMB No. 0704-0188	
The public reporting burden for this collection of information is estimated to average 1 hour per response, including the time for reviewing instructions, searching existing data sources, gathering and maintaining the data needed, and completing and reviewing the collection of information. Send comments regarding this burden estimate or any other aspect of this collection of information, including suggestions for reducing the burden, to Department of Defense, Washington Headquarters Services, Directorate for Information Operations and Reports (0704-0188), 1215 Jefferson Davis Highway, Suite 1204, Arlington, VA 22202-4302. Respondents should be aware that notwithstanding any other provision of law, no person shall be subject to any penalty for failing to comply with a collection of information if it does not display a currently valid OMB control number.						
1. REPORT DATE (DD-MM-YYYY) 11 February 2002		2. REPORT TYPE Final		3. DATES COVERED (From - To) 19-21 September 2001		
4. TITLE AND SUBTITLE PROCEEDINGS OF THE 2001 ANTENNA APPLICATION SYMPOSIUM				5a. CONTRACT NUMBER GS01K99BKM0012		
				5b. GRANT NUMBER TASK ORDER NUMBER R15701321		
				5c. PROGRAM ELEMENT NUMBER		
				5d. PROJECT NUMBER		
6. AUTHOR(S) Daniel H. Schaubert et, al				5e. TASK NUMBER		
				5f. WORK UNIT NUMBER		
7. PERFORMING ORGANIZATION NAME(S) AND ADDRESS(ES) Air Force Research Laboratory 80 Scott Rd Electromagnetics Technology Division Sensors Directorate Hanscom AFB, MA 01731				8. PERFORMING ORGANIZATION REPORT NUMBER Volume II		
9. SPONSORING/MONITORING AGENCY NAME(S) AND ADDRESS(ES) Air Force Research Laboratory 80 Scott Rd Electromagnetics Technology Division Sensors Directorate Hanscom AFB, MA 01731				10. SPONSOR/MONITOR'S ACRONYM(S)		
				11. SPONSOR/MONITOR'S REPORT NUMBER(S)		
12. DISTRIBUTION/AVAILABILITY STATEMENT Approved for Public Release; Distribution Unlimited.						
13. SUPPLEMENTARY NOTES SNHA Project Engineer Volume I consists of Pages 1-249, Volume II consists of Pages 250-587						
14. ABSTRACT The proceedings of the 2001 Antenna Applications Symposium is a collection of state-of-the-art papers relating to phased array antennas, Reconfigurable Antennas, Microstrip Antennas, Fractal Antennas.						
15. SUBJECT TERMS Antennas, Phased Array, Reconfigurable, Fractal Antennas, Digital Beamforming, Microstrip Antennas						
16. SECURITY CLASSIFICATION OF:			17. LIMITATION OF ABSTRACT SAR	18. NUMBER OF PAGES 337	19a. NAME OF RESPONSIBLE PERSON Livio D. Poles	
a. REPORT U	b. ABSTRACT U	c. THIS PAGE U			19b. TELEPHONE NUMBER (Include area code) 781-377-4087	

2001 ANTENNA APPLICATIONS SYMPOSIUM

WEDNESDAY, SEPTEMBER 19, 2001
MORNING

Fifty Years of Antennas Midst Corn and Soybeans	1
P. E. Mayes	

RECONFIGURABLE ANTENNAS

Architecture and Performance of Reconfigurable Aperture	36
L. Pringle, P. Friederich, L. Fountain, P. Harms, D. Denison, E. Kuster, S. Blalock, R. Prado, G. Kiesel, G. Smith, M. Allen, K. Kim, J. Maloney, M. Kesler	
Stacked Reconfigurable Antennas For Space-Based Radar Applications	59
J. Hazen, R. Clark, P. Mayes and J. Bernhard	
Broadband Antennas Over Electronically Reconfigurable Artificial Magnetic Conductor Surfaces	70
V. C. Sanchez, W. E. McKinzie III and R. E. Diaz	
Patch Antennas with Switchable Slots (PASS): Concept, Theory and Applications	84
F. Yang and Y. Rahmat-Samii	
Piezo-Electric Modulation of Microstrip Elements	104
M. Banerjee and P. K. Bondyopadhyay	

WEDNESDAY, SEPTEMBER 19, 2001
AFTERNOON

ANTENNAS

Antenna Efficiency and Gain of Two New Compact Microstrip Antennas	108
S. Zhang, G. Huff, and J. T. Bernhard	
Experimental Investigation of Antenna-Handset-Feed Interaction During Wireless Product Testing	117
J. Haley, T. Moore and J. T. Bernhard	
Accurate Analysis of Electrically Small Conical Antennas by Using the Low-Frequency Method	135
J-S. Zhao, W. C. Chew and P. E. Mayes	
Inductively Loaded, Stacked Sector Antennas	152
P. E. Mayes	
Performance Enhancements with Applications of the Coaxial Cavity Antenna	171
T. Holzheimer and S. Schneider	
The Koch Fractal Monopole Antenna: The Significance of Fractal Geometry in Determining Antenna Performance	194
S. R. Best	
On The Performance Trade-Offs Associated with Fractal Antenna Designs	206
S. R. Best	
Printed Circuit Board Implementation of Log-Periodic Parasitic Monopole Arrays	214
P. G. Ingerson, S. C. Kuo, P. E. Mayes and C. C. Liu	

THURSDAY, SEPTEMBER 20, 2001
MORNING

ARRAYS I

Some Notable Firsts in Array Antenna History	231
H. E. Schrank	
Predicted Performance of Small Arrays of Dielectric-Free Tapered Slot Antennas	250
A. Boryssenko and D. H. Schaubert	
Decade Bandwidth Tapered Notch Antenna Array Element	280
N. Schuneman, J. Irion and R. Hodges	
Radio Direction-Finding for Wildlife Research	295
W. W. Cochran, G. W. Swenson, Jr. and L. L. Pater	
Computer Model For The Design of a VHF Antenna Test Range	308
S. Santarelli and H. Steyskal	
Conformal Array Control Using Digital Beamforming	336
D. Curtis, M. Champion, B. Tomasic, H. Tobin, R. Thomas, S. Santarelli, H. Steyskal, J. Kenney, E. Martin and J. Tenbarga	
Use of Scan Impedance and Scan Element Pattern	364
R. C. Hansen	

THURSDAY, SEPTEMBER 20, 2001
AFTERNOON

ARRAYS II

Phased Array Technology and Allerton	372
R. J. Mailloux	
A Study of Phased Array Antennas for NASA's Deep Space Network	391
V. Jamnejad, J. Huang and R. Cesarone	
RF Isolation of Separate Transmit and Receive Phased Array Antennas in a Multifunction Environment	413
M. G. Parent, D. Taylor, G. Tavik, M. Kluskens and J. A. Valenzi	
Analysis of a Thick Dichroic Plate with Arbitrarily Shaped Holes	443
W. A. Imbriale	
Ranking and Selection Applied to Eigen-Analysis of Array	464
M. C. Wicks and P. Chen	
Vertical Diversity in Array of Collocated HF Loop Antennas	477
G. Le Bouter, L. Bertel, D. Lemur and Y. Erhel	
Antenna Diversity as a Means of Improving HF Transmissions	501
A Bisiaux and L. Bertel	

FRIDAY, SEPTEMBER 21, 2001
MORNING

APERTURES

Geodesic Sphere Phased Arrays for LEO Satellite Communications- Array Symmetry Issues P. K. Bondyopadhyay	525
About Possibility The Vector's Parabolic Antenna DP To Improve Radar Resolution V. Ginzburg	533
Accurate Analysis of Reflector Antennas Using FAFFA-MLFMA Algorithm T. J. Cui, W. C. Chew and J. Song	544
A New Class of Broadband Planar Apertures P. Friederich, L. Pringle, L. Fountain, P. Harms, D. Denison, E. Kuster, S. Blalock, G. Smith, J. Maloney and M. Kesler	561

Identifiers for Proceedings of Symposia
The USAF Antenna Research and Development Program

Year	Symp. No.	Identifier
1951	First	
1952	Second	C054 520
1953	Third	AD63794
1954	Fourth	AD63139
1955	Fifth	AD90397
1956	Sixth	AD114702
1957	Seventh	AD138500
1958	Eighth	AD301151
1959	Ninth	AD314721
1960	Tenth	AD244388 (Vol. 1) AD319613 (Vol. 2)
1961	Eleventh	AD669109 (Vol. 1) AD326549 (Vol. 2)
1962	Twelfth	AD287185 (Vol. 1) AD334484 (Vol. 2)
1963	Thirteenth	AD421483
1964	Fourteenth	AD609104
1965	Fifteenth	AD474238L
1966	Sixteenth	AD800524L
1967	Seventeenth	AD822894L
1968	Eighteenth	AD846427L
1969	Nineteenth	AD860812L
1970	Twentieth	AD875973L
1971	Twenty-First	AD888641L
1972	Twenty-Second	AD904360L
1973	Twenty-Third	AD914238L

Antenna Applications Symposium

		TR#	ADA#
1977	First	None	955413
1978	Second	None	955416
1979	Third	_____	077167
1980	Fourth	_____	205907
1981	Fifth	_____	205816
1982	Sixth	_____	129356
1983	Seventh	_____	142003; 142754
1984	Eighth	85-14	153257; 153258
1985	Ninth	85-242	166754; 165535
1986	Tenth	87-10	181537; 181536
1987	Eleventh	88-160	206705; 206704
1988	Twelfth	89-121	213815; 211396
1989	Thirteenth	90-42	226022; 226021
1990	Fourteenth	91-156	237056; 237057
1991	Fifteenth	92-42	253681; 253682
1992	Sixteenth	93-119	268167; 266916
1993	Seventeenth	94-20	277202; 277203
1994	Eighteenth	95-47	293258; 293259
1995	Nineteenth	96-100	309715; 309723
1996	Twentieth	97-189	341737
1997	Twenty First	1998-143	
1998	Twenty Second	1999-86	
1999	Twenty Third	2000-008 (I), (II)	

Silver and Gold at Allerton

In the fall of 2001, antenna engineers gathered near Monticello, Illinois, for a very special meeting. It was the 50th anniversary of the first antenna symposium at Allerton House and the 25th meeting in the current series known as the Antenna Applications Symposium. The Allerton House and Conference Center is located on a 1500-acre wildlife preserve of woodlands, gardens and prairie. In 1946 Robert Allerton donated this part of his homestead to the University of Illinois, which manages it as a conference center and nature preserve. In 1951, the first US Air Force Antenna Research and Development Symposium was convened at the Allerton Conference Center. (The IEEE Antennas and Propagation Society was formed in 1949 and held its first international symposium in 1963.) No proceedings exist for the 1951 meeting, but proceedings were produced for the 1952 and subsequent symposia, and they are archived at DTIC.



Allerton House Conference Center near Monticello, Illinois, site of antenna symposia since 1951.

Twenty-three USAF Antenna R&D Symposium were held at Allerton House. These symposia were cosponsored by the US Air Force through Wright-Patterson Air Force Base, Ohio and by the University of Illinois. They were organized by the Antennas and Radomes Group until 1973, when, after a reorganization, Wright-Patterson terminated its support. In 1977, after numerous requests from the antenna community, Paul Mayes and the staff of the University of Illinois Electromagnetics Laboratory restarted the popular meeting under the moniker of Antenna Applications Symposium. The University of Illinois sponsored the 1977 and 1978 symposia. In 1979, the Air Force rejoined the symposium as cosponsor through Rome Laboratory (now the Air Force Research Laboratory, Sensors Directorate) at Hanscom Air Force Base, Massachusetts.

From the earliest meetings in the 1950s, the Allerton Symposium has emphasized antenna hardware and applications. The majority of papers presented at Allerton are authored by antenna engineers working in industry. The symposium is organized with a single session, affording flexibility for extended discussion of papers.



A much smaller than usual group conquered post-September 11 travel problems to attend the opening session of the 2001 symposium.

Throughout the years, attendees of the Allerton Symposium have enjoyed walking and jogging the pathways of the estate's formal gardens and woodland trails, and often have learned of significant developments in antennas long before they were disclosed in archival journals. George Deschamps reported the radiation properties of some microstrip-fed arrays at the 1953 symposium. Since that time a number of authors have chronicled the history of microstrip patch and other printed circuit antennas at Allerton. These papers include the first published array work by Bob Munson, the theoretical development of the cavity model by Y. T. Lo and his students, and a progression toward increasingly practical elements with wider bandwidth.

Experimental results for the equiangular spiral antenna were presented by John Dyson at the Fifth AF Symposium, October 1955. Dwight Isbell's disclosure of the first unidirectional log-periodic antennas was made at the Seventh Symposium. Bob Carrel's "An Analysis of the Log-Periodic Dipole Antenna" was presented at the Tenth Symposium, a year before his Ph. D. thesis on the subject was issued as the much-requested Tech. Rep. 52, AF33(616)-6079, October 1961.

Early descriptions of important military and commercial systems have included the limited-field-of-view AGILTRAC array fed reflector, the Joint Stars EHF airborne SATCOM arrays and most recently the IRIDIUM multiple beam array.

In 1994, following the retirement of Mayes from the University of Illinois, the University of Massachusetts joined as a cosponsor of the symposium and Dan Schaubert assumed the duties of symposium organizer. Currently the organizational team includes Jennifer Bernhard and Weng Chew of the University of Illinois, Bob Mailloux and Livio Poles of AFRL, and Dan Schaubert of the University of Massachusetts. They are assisted by several others at the cosponsoring organizations and elsewhere.

The 2001 Antenna Applications Symposium was held in late October, postponed from its original dates in the third week of September due to travel restrictions following the September 11 terrorist attacks. Most authors were able to attend and present their papers, and the discussions during sessions and breaks were characteristically lively. Papers at the 2001 symposium included historical surveys to commemorate the occasion and new work on reconfigurable arrays, wide bandwidth antennas, wireless communication, phased arrays, microstrip antennas, and computational analysis of complex electromagnetic radiating structures.



Formal gardens of Allerton Park afford a pleasant surrounding for informal discussions during breaks.

The Proceedings of the symposium contain full-length papers. Proceedings of recent symposia are available from the organizers (contact Dan Schaubert) and archival copies of all available Allerton Symposium Proceedings may be obtained by qualified users through DTIC. A few of the recent proceedings are also available at the symposium web site, <http://www.ecs.umass.edu/ece/allerton>.

The 2002 Antenna Applications Symposium will be September 18-20. Authors wishing to contribute papers describing antenna developments, applications or characterization may contact Dan Schaubert, schaubert@ecs.umass.edu, or see the web site for information, <http://www.ecs.umass.edu/ece/allerton>.

Paul Mayes
Electromagnetics Laboratory
Univ. of Illinois
Urbana, IL 61801
pemayes@ix.netcom.com

Dan Schaubert
Antenna Laboratory
Univ. of Massachusetts
Amherst, MA 01003
schaubert@ecs.umass.edu

Robert Mailloux
Sensors Directorate
Air Force Research Lab
Hanscom AFB, MA 01731
robert.mailloux@hanscom.af.mil

FIFTY YEARS OF ANTENNAS MIDST CORN AND SOYBEANS

Paul E. Mayes
Electrical and Computer Engineering Department
University of Illinois at Urbana-Champaign
1406 West Green Street
Urbana, IL 61801

Abstract: The year 2001 marks the fiftieth anniversary of the first antenna symposium held at Allerton Park. From 1951 until 1975, the Symposium of the U. S. Air Force Antenna Research and Development Program met annually. This meeting was a cooperative effort involving the Antenna and Radomes Group at Wright-Patterson Air Force Base (WPAFB) and the Antenna Laboratory at the University of Illinois at Urbana-Champaign (UIUC). In 1977, after a two-year hiatus, the Antenna Applications Symposium began under the sponsorship of the Antenna (renamed Electromagnetics) Laboratory of UIUC. Two years later, the Air Force joined once again through the Cambridge Air Force Research Center and has continued to the present, currently through the Sensors Directorate of the Air Force Research Laboratory at Hanscom Air Force Base. In 1994 major responsibility for organization of the symposium was assumed by the Antenna Laboratory of the University of Massachusetts. This paper presents a summary of the history of the antenna meetings at Allerton Park. Consideration is given to the evolution of the discipline during this era and to the people who have contributed to making these meetings special.

1. Post-war Antenna Research Started

After World War II several engineering researchers relocated from Ohio to Illinois. They were recruited by Professor W. L. Everitt, Head of the Department of Electrical Engineering, UIUC, from 1945 to 1949 and Dean of the College of Engineering (UIUC) from 1949 to 1968 [1](See Figure 1). Some of these recruits came from antenna jobs at WPAFB in Dayton. They realized the importance of continuing during a period of peace some of the defense research that had started during the war. Professor E. C. Jordan came from Ohio State University where he had been associated with Everitt in antenna research [2]. The Antenna Laboratory was established in the Electrical Engineering Department of UIUC. Principal support for the new laboratory came from WPAFB. Walt Portune was the contract monitor for the Air Force and Cleve Nash directed the research at the University (Figure 2). After Nash left in 1952, Jordan served as Director of the Antenna Laboratory until he became Head of EE in 1954. During this time the tradition of Antenna Symposia at Allerton Park began.

2. The First Symposia

The need to exchange information among various AF contractors led to the initiation of the Symposium on the USAF Antenna R & D Program. This meeting was sponsored by WPAFB. Local arrangements were made by the staff of the EE Department, UIUC. The first meeting was held in 1951 with unclassified sessions at Allerton House and classified sessions at Chanute AFB in Rantoul, Illinois. From 1960 onward the meetings have been unclassified. If Proceedings were published for the first symposium, they unfortunately seem to have been lost. However, records are available for many years and they have been scanned in gathering material for this paper. Looking through these volumes gives a perspective of the history of progress in antenna design and an acquaintance with the engineers who made it possible.

In 1952 there were 33 papers presented. The favorite topics were: (a) flush-mounted antennas, and (b) direction-finding antennas. Some of the authors are familiar names: E. C. Jordan, author of the widely used text, *Electromagnetic Waves and Radiating Systems*, (Figure 3), R. C. Hansen, well known author, editor and consultant, former president and life member of the IEEE Antennas and Propagation Society (Figure 4), Arthur Dorne, a principal of the antenna company, Dorne and Margolin, Vic Rumsey, (Figure 5), author of seminal papers on electromagnetics, especially frequency-independent antennas, Director of the Antenna Laboratory at UIUC from 1954 to 1957, Walter Rotman, antenna inventor, author and long-time employee of Air Force research agencies, C. H. Walter, professor in the Antenna Laboratory of Ohio State University and author of the book, *Traveling Wave Antennas*, to name just a few.

3. Papers of the Air Force Antenna R & D Symposia

Over the years, a wide variety of subjects related to antennas have been presented in the library of Allerton House and discussed at length on the grounds of Allerton Park. In attempting an analysis of the subjects of the papers presented between 1952 and 1973, twenty-five categories were used initially. Since such a fine subdivision of subjects proved to be overwhelming, they were later combined as listed in Table 1. The distribution of papers in these categories for the USAF Antenna R & D Symposia (1952-1973) is illustrated in Figure 6.

The program of the 1952 Symposium was dominated by papers about flush-mounted antennas. Interest in conformal antennas has remained high, particularly with the development of patch antenna technology. Interest in antenna arrays increased rapidly between 1954 and 1955, and peaked in 1972 when fifteen papers on arrays were included in the program. Various solutions to increased antenna bandwidth have been offered, beginning with the advent of spiral antennas in 1955 and log-periodic antennas in 1957. Although never dominating the program, there has never failed to be at least one paper, as many as five, on the subject of broadband or frequency-independent antennas. Since 1961 papers

Table 1. Subject categories used in the classification of papers presented at the Symposia on the USAF Antenna Research and Development Program

Cat. No.	Category Name	Subcategories
1	Antenna Properties	Impedance, Pattern, Efficiency, Gain, Polarization, Specifications
2	Evaluation of Antennas	Testing, Measurement, Modeling, Near Field
3	Conformal Antennas	Microstrip, Flush, Slot, Hidden, EW, DF, Homing, Special Purpose, Satellite and Space Antennas
4	Transmission and Radiating Lines	Waveguides, Radiation, Miscellaneous
5	Aperture Antennas	Radomes, Reflectors, Feeds, Propagation and Environmental Effects,
6	Arrays and Array Elements	Phased Arrays, Slot Arrays, Elements for Arrays
7	Broadband and Frequency Independent Antennas	Spiral, Helical and Log-Periodic Antennas, Broadband Elements and Systems
8	Electrically Small Antennas	

on electrically small antennas have also appeared steadily in numbers only slightly less than those for broadband antennas.

Numerous notable papers appeared in the program between 1951 and 1973. A complete list would total several hundred, but a sampling gives a picture of how the antenna field was developing. Rumsey (Figure 5) initiated a major advance in antenna technology, frequency-independent antennas, during this time. Figure 3 shows E. C. Jordan with a display that features several frequency-independent antennas that have been described at Allerton Symposia. Several papers about logarithmic spiral antennas, e.g. [3, 4, 5], were presented by John Dyson (Figure 7). In Figure 3 Jordan is pointing to a model of the conical log-spiral, described at the symposium in 1958, and he is holding a prototype of the conical log-spiral that was used on the UIUC radio telescope.

Ray DuHamel (Figure 8), inventor of several log-periodic antennas, was an active participant in the early symposia. Dwight Isbell, (Figure 9) who later invented the

log-periodic dipole array, described the first unidirectional log-periodic in 1957[6]. R. L. Carrel, (Figure 8) while a graduate student at UIUC, presented his method for the analysis of the LP dipole array in 1960[7].

Very early work on microstrip antennas was reported by Georges Deschamps (Figure 8) in 1953 while he was an engineer at Federal Telecommunications Laboratory [9]. In 1958 he became Director of the Antenna Laboratory of UIUC, renamed the Electromagnetics Laboratory in 1973, and remained until his retirement. His theory of partially polarized antennas was presented to the Symposium in 1966 [10]. Microstrip patch antennas have been described from the practical standpoint by Robert Munson (Figure 10) [11] and theoretically by Y. T. Lo (Figure 8) [12].

In 1953 A. A. Oliner outlined the slot radiation research underway at that time at the Microwave Research Institute of the Polytechnic Institute of Brooklyn [13]. In the same year, L. G. Fubini of Airborne Instruments Lab reviewed strip transmission lines [14], Ray DuHamel and R. L. Warnock discussed the measurement of antenna gain and efficiency [15], S. B. Cohn talked about flush airborne radar antennas [16], and R. C. Hansen and E. C. Jordan presented ferrite loop antenna systems for aircraft [17].

Consideration of antenna arrays began to surface in 1954 with the idea of using ferrite phase shifters for scanning by A. J. Simmons of Naval Research Lab [18]. Feeding of a traveling wave array of thin wire radiators by using a surface wave on a dielectric rod waveguide was the subject of a paper by H. E. King and Ray DuHamel in 1955 [19]. Interest in spiral antennas was generated in 1955 by papers on Archimedian spirals by B. H. Burdine of MIT [20] and the equiangular spiral antenna by J. D. Dyson [3]. Dyson gave another paper about the equiangular spiral the following year [21].

Additional fundamental material on arrays was contained in papers on mutual coupling by R. S. Elliott and L. A. Kurtz of Rantec Corporation [22] and antennas for wide angle scanning by A. S. Dunbar of Dalmo-Victor Company [23].

Spiral antennas were also an important part of the program in 1958. Dyson introduced the unidirectional log-spiral [4] and A. E. Marston of NRL described the application of the spiral antenna to scanning array systems [24]. In 1961 Dyson talked about using conical log-spiral antennas in simple arrays [25]. Roy Spencer of NRL treated the operation and analysis of point sources in antenna arrays in 1960 [26].

The first of several studies related to electrically small antennas, by J. A. M. Lyon and his colleagues at the University of Michigan appeared in 1961 [27]. Also that year, Ed Altshuler discussed the concept of using a large spherical reflector for aerospace research [28].

Fabrication and testing of step-index realizations of a Luneberg lens was the subject of a paper by Eino J. Luoma of Emerson-Cuming in 1962 [29]. Now also began to appear papers about the use of digital computers in the analysis and design of antennas and antenna systems. C. A. Bolt of Westinghouse discussed the design of antennas using digital computers [30] and P. A. Michelson and James Schomer of Boeing considered the application of non-linear programming to the pattern synthesis problem [31].

Many attempts to rely on log-periodic geometry alone to produce an antenna with frequency-independent properties had met with failure. Now came work that sought to explain why some log-periodic structures were good antennas while others were not. P. Ingerson (Figure 11) and P. Mayes (Figure 11) showed the results of some measurements on backfire periodic dipole arrays [32] and W. T. Patton of UIUC (Figure 12) presented his analysis of the backfire bifilar helix [33].

Antenna engineers continued to push the boundaries to produce high-performance antennas. These include not only electrically small antennas, but also superdirective ones. In 1965 H. A. Ecker and D. E. Svoboda of WPAFB treated superdirective antennas [34].

The availability of antenna with very wide impedance and pattern bandwidths called for extensions to the bandwidth of related components in the radiating system. Such a component was described by R. H. DuHamel and M. E. Armstrong of Hughes Aircraft in their paper on a wide-band monopulse antenna using the tapered-line magic-T [35].

Conformal antennas have long been of interest to the Air Force, becoming more and more important with the increase in speed of aircraft. A series of papers about the TEM-line antenna developed at Ohio State University began in 1965 with one by J. R. Copeland [36].

A flurry of activity in the millimeter wave band resulted in development of millimeter wave biconical horn and slot array antennas as described by F. R. Ore of UIUC in 1965 [37].

Robert Mailloux started his participation as a presenter at the Symposia in 1965 with his paper on the long Yagi-Uda array [38]. At this time he was with NASA Electronics Research Center in Cambridge, MA.

Broadband antennas continued to be of interest in 1966 when C. T. Tai of the University of Michigan described the concept of a multi-wire dipole which he called the Saguaro antenna [39]. P. Ingerson and P. Mayes explained how to design log-periodic structures to increase the likelihood of achieving frequency independent performance through the use of dispersion data for the corresponding periodic structure [40].

The continuing advance in applications of digital computers to antenna analysis was illustrated in the paper by V. R. Arens, C. T. Elfving, U. R. Embry, and D. L. Johnstone of Sylvania and K. K. Mie of the University of California at Berkeley [41].

Dealing with the large number of elements required in a high gain array was considered by W. H. Nester of General Electric in his paper about element thinning [42].

A unique real-time field-measuring technique using liquid crystals was proposed by Carl F. Augustine and Wilfred G. Jaeckle of Bendix Research Labs in 1968 [43]. The problem of producing circularly polarized radiation at large polar angles was considered in a paper by J. Rosa and E. W. Case of Radiation, Inc. [44]. Airborne long-wire antennas of astonishing length were described by R. L. Carrel and R. C. Fenwick of Collins Radio Company [45].

The problem of achieving broadband performance without dispersion was tackled by D. L. Sengupta and J. E. Ferris of the University of Michigan in a paper presented in 1969 [46]. This problem was addressed again in 1970 by Robert J. Wohlers of Cornell Aeronautical Lab [51]. Also in 1969 Georges Deschamps, J. J. Sweeney and F. R. Ore of UIUC proposed a new method for evaluating the noise performance of two-port networks [47].

Some new broadband antennas were introduced in 1970. P. E. Mayes and F. M. Wiesenmeyer of UIUC described an electrically small antenna comprising a monopole and cavity-backed slot fed from the same microstrip line [48]. P. G. Ingerson, now at TRW, found a way to change the radiation characteristics of equiangular spiral antennas by periodically changing the width of the spiral arms [49].

Reduction of mutual coupling in antenna arrays was the objective of the paper by Robert Mailloux, now at AFCRL [50]. Computer software had by now advanced to the point that antennas no longer were required to be in free space, as shown by the paper by G. J. Burke, S. Gee, E. K. Miller, A. J. Poggio, and E. S. Selden [52].

The fact that "blind angles" were a serious problem with large phased arrays and, more importantly, what to do about it, were addressed in a 1972 paper by Robert Mailloux [53]. The very useful quadrifilar helix antenna was discussed by A. T. Adams and colleagues of Syracuse University [54].

The sponsorship by WPAFB ended with the Twenty-Third Symposium, October 10-12, 1973. Harold Weber of WPAFB was the conference chairman. The keynote address, "Small Antennas," was given by Harold Wheeler of WPAFB [9]. Near-field measurements were being studied as a viable alternative for the testing of large phased arrays, as pointed out by Allen Newell of NBS [55]. For

some problems of antenna design, just *any* solution would no longer do. R. C. Hansen produced the optimum inductive loading for a short monopole [56] and W. A. Imbriale and P. G. Ingerson of TRW optimized the design of a broadband parabolic reflector antenna fed with a log-periodic dipole array [57].

4. The Antenna Applications Symposium

In 1975, the University of Illinois at Urbana was host to the International Symposium of APS/ URSI. Several attendees inquired about the future of the "Allerton" Symposium. This expression of interest prompted the mailing of a questionnaire asking for opinions about restarting an antenna meeting at Allerton Park. The response was overwhelmingly favorable. In April 1977 the First Antenna Applications Symposium was sponsored by the Electromagnetics Laboratory of UIUC.

Once again, 33 papers were presented. Among the presenters were William Kreutel, of NASA who delivered the keynote address [58], Georges Deschamps, Professor of ECE, UIUC, and Director of the Antenna/Electromagnetics Laboratory, 1959-1989 [59], Robert Munson of Ball Aerospace, a leading proponent of microstrip antenna technology, [60], R. S. Elliott, professor at UCLA [61], C. H. Walter, Professor at OSU, later with TRW [62], and John Kerr, long-time employee at Army research agencies, developer of numerous conformal antennas [63].

Ed Turner (Figure 13), who had been the organizer and sponsor of the Air Force Symposium, was an enthusiastic supporter of the successor meeting. He attended and presented papers in 1977 and 1978, his last. The proceedings of the 1979 symposium is prefaced by a memorial to Ed. His irrepressible enthusiasm and unabashed humor were hallmarks of the meeting for sixteen years.

The results of an analysis using the subdivisions of Table 1 are shown in Figure 14. The dominant theme from 1977 to 2000 has been antenna arrays. Only in 1981, 1995, 1996 and 1998 has there been a more popular topic. On the other hand, electrically small antennas received little attention.

It is impossible to adequately review the hundreds of papers that have been presented during the years since 1977, but, once again, it is useful to trace the movement of antenna research and development by presenting a sampling.

The advent of log-periodic antennas had been closely followed by attempts to increase the gain by using them in arrays. One mystery related to disappointing results in this effort was solved by J. M. Tranquilla and K. Balmain of the University of Toronto in their 1977 paper revealing resonances excited by currents on parallel feeders to be at fault [64].

A widened scope of the field was one goal of the new meeting. Much desired papers from the world of commercial applications were typified by the presentation about mobile antenna gain near 900 MHz by A. L. Davidson and W. J. Turney of Motorola [65].

During the 1978 Symposium there was a special session on numerical techniques, now entering a certain stage of maturity. Papers were presented by A. J. Poggio and E. K. Miller of Lawrence Livermore [66], L. N. Medgyesi-Mitschang of McDonnell Douglas [67], and W. Gee (Figure 15), T. H. Lee and E. K. Okubo of Lockheed Missiles and Space Company [68].

This was an active time for practitioners of the conformal antenna art, as illustrated by a paper on the spiral slot by A. R. Sindoris of North Carolina State, D. H. Schaubert and F. G. Farrar of the Harry Diamond Labs of the U. S. Army [69] and another on microstrip polarization techniques by J. L. Kerr, mentioned above [70]. In fact, theoretical analysis was becoming useful to designers. Such was demonstrated by the description and application of the cavity model by Y. T. Lo, D. Solomon, and W. F. Richards of UIUC [71].

That radar scattering was also of interest to antenna engineers was shown by UIUC researchers W. L. Ko and R. Mittra (Figure 15) [72].

Allan Schell of RADC/EEA presented the Air Force requirements for antenna technology as the keynote address in 1979 [73]. Richards, Lo and P. Simon extended the cavity model to the design of circularly polarized microstrip antennas [74].

A special session on near-field techniques was held in 1979 with papers by David Staiman of RCA [75], Carl Stubenrauch (Figure 11) of NBS [76], Jerome Hanfling of Raytheon [77], and C. E. Kirchhoff of Martin Marietta [78].

The burgeoning use of satellites in communications systems was acknowledged in the 1980 keynote address by Leon Ricardi of MIT Lincoln Labs [79] while in 1981 the emphasis shifted to millimeter wave technology. The keynote address in the latter year was given by J. Wiltse of Georgia Tech [80] and the area was further addressed in papers by N. Deo of Epsilon Lambda Electronics and R. Mittra of UIUC [81] and S. Ray, R. Mittra, T. Trinh and L. Paleta, all of UIUC [82].

The maturity of near-field measurement technology was demonstrated by W. T. Patton of RCA [83].

The 1981 session on microstrip antennas contained papers by R. Munson, [84], J. D. Ou, W. F. Richards and Y. T. Lo [85] and M. Campi of Harry Diamond Labs [86].

The keynote of 1982 again featured Allan Schell with an overview of the Air Force antenna needs [87]. The beginnings of what later developed into the principal software for target identification was described by M. Hurst, R. Mittra and S. W. Lee of UIUC [88].

Millimeter waves were still stirring interest as shown by papers by R. B. Dybdal of the Aerospace Corporation [89], O. B. Kesler (Figure 17) of Texas Instruments [90], and F. Lalezari and R. Munson of Ball [91].

The search was on for economical ways to build large phased arrays in 1983. F. I. Diamond of RADC gave the keynote address [92] and the monolithic approach was expanded by Harold Weber of WPAFB [93], R. Stockton of Ball [94], and B. J. Edward of General Electric [95]. Expanding the match bandwidth of microstrip antennas was addressed by D. A. Paschen of Ball [96].

The extension of monolithic phased arrays to higher frequencies was addressed in 1984. The keynote speaker was W. T. Patton [97] and D. H. Schaubert, D. M. Pozar, K. S. Yngvesson, and R. W. Jackson of UMass spoke to the issues of millimeter wave arrays [98]. Y. T. Lo and colleagues revisited the design of circularly polarized microstrip antennas [99]. The theme was little changed in 1985 with R. C. Johnson of Georgia Tech giving the keynote [100], D. H. Schaubert, R. W. Jackson, and D. M. Pozar [101] and D. B. Rutledge and colleagues from CalTech and UCLA [102] expanding upon the theme. Y. Rahmat-Samii of JPL added an overview of reflector antenna technology [103].

A historical note was added to the program in 1986 when H. Schrank of Westinghouse traced the practice of electromagnetics through the preceding century [104]. D. M. Pozar and D. H. Schaubert added consideration of aperture coupling to the discussion of patch antennas in arrays [105]. Enhancing the impedance bandwidths of microstrip antennas was addressed by D. Tanner and P. Mayes [106] and by D. A. Paschen [107]. Near-field measurement techniques were extended to spherical geometry by D. W. Hess of Scientific-Atlanta [108].

J. Schindler of RADC returned to the topic of economical phased arrays in his keynote talk of 1987 [109]. The theme was expanded in talks by A. J. Zaghloul of COMSAT and R. Mailloux of RADC [110], and C. D. Pepe, M. J. Povinelli, and J. J. Kennick of General Electric [111].

John Kraus of Ohio State declined to travel to Allerton for the 1988 Symposium, but he produced a video tape that dramatized some of the memorable moments in the history of electromagnetics [112]. Further discussion of the work at General Electric on flared slot antennas in very wide band phased arrays was presented by M. J. Povinelli [113].

The topic of solid-state millimeter-wave arrays resurfaced in the keynote by J. Kinzel of General Electric in 1989 [114]. Microstrip antennas in composite layers

were analyzed by D. R. Jackson, University of Houston, N. G. Alexopoulos, UCLA, and A. A. Oliner, Polytechnic University of Brooklyn [115]. P. Franchi and H. Tobin of RADC told how to measure large arrays with random errors [116].

Over-the-horizon (OTH) radar was a special topic of the 1990 Symposium. The keynote was delivered by J. L. Poirier of RADC [117]. A. J. Gould of RADC discussed using a thinned HF array to study the ionosphere [118] and Y. T. Lo gave an update on CP patch antennas [119].

Electronic surveillance became the theme in 1991 when Gary Grann of ESD, Hanscom AFB entitled his keynote, "Beyond AWACS" [120]. R. Hansen discussed transient effects in reflector antennas [121].

Opto-electronics was the theme in 1992, the keynote was by P. R. Herzfeld of Drexel University [122] and consideration of true-time-delay beamsteering with fiber optics was done by I. L. Newberg of Hughes [123]. Commercial applications were represented in a paper by R. L. Niekamp of Harris Broadcast Division about an HDTV antenna [124]. In the session on computational electromagnetics, E. K. Miller, now at Los Alamos National Lab, talked about conditions that EM software should satisfy [125].

A new emphasis in government funding, dual-use, provided a session topic for 1993. How the antenna community might respond was discussed in the keynote by J. K. Schindler [126], use of waveguide arrays for both commercial and military applications was suggested by I. Karlsson of Ericsson Radar [127] and millimeter-wave phased arrays for communications were discussed by G. E. Miller [128].

A special session of the 1994 Symposium honored the author upon his retirement. P. W. Klock of UIUC (Figure 17), who has provided great assistance in symposium operations over many years, summarized the author's career [129].

Array technology enjoyed a rebound in 1995. The keynote paper was delivered by C. Raquet of NASA [130]. The international nature of the recent symposia was reflected in the discussion of low-cost millimeter-wave phased arrays by P. Pons and C. Renard of Dassault Electronique, France [131]. The merging of optics and microwaves began to emerge with papers by M. G. Parent of NRL [132] and T. L. Larry, C. J. Swann, and M. L. VanBlaricum of Toyon Research [133]. Commercial antennas were also represented in the paper by A. Adrian of Ford [134].

Although many excellent papers were presented in recent years, perhaps the essence of the symposia can be captured to some degree by considering only the keynote and/or tutorial papers. In 1996 there was a special session on photonics. The keynote was delivered by Brian Hendrickson of ARPA [135]. The main

mission antenna for the ill-fated Iridium system was combined with other advanced phased array concepts by Jack Schuss of Raytheon in 1997 [136]. Warren Stutzman of Virginia Tech gave an overview of the antenna needs of industry and government in the new century [137].

The 1998 and 1999 Proceedings can be found on the web at www.ecs.umass.edu/ece/allerton/greetings.html. Great interest in MEMS prompted a tutorial session in 1999. Among the papers presented was an assessment of using MEMS in large antennas for radar by J. Smith of DARPA [138].

5. The Site and Extra-Curricular Activities

One of the attractive features of holding meetings at Allerton Park is the surroundings. The surprising appearance of conference facilities in a wide expanse of agricultural area provides an isolation that is conducive to intermingling of the attendees. Thus it is that the information exchange is not limited to the technical sessions, but occurs in the halls, the dining room, the formal gardens, and along hiking trails. Nor is all of the exchange of purely technical nature. In the early days Dean Everitt regaled the diners with stories and jokes and his rendition of "the bald-headed end of the broom" to his own piano accompaniment. It was not unusual to hear music emanate from the piano at the coaxing of one of the attendees. Sometimes informal sing-a-longs occurred. Bob Carrel, among others, was known to pound the ivories for such events.

Allerton House is the centerpiece of the park, a seeming oasis buried in fields of corn and soybeans. Figure 18 is a picture of the house as it looked in the early days of the Symposia, the picture from the UIUC archives is dated 1958. A striking feature of the photograph is the reflection of the building in the pond. Just a few weeks ago a photographer was asked to take another picture with a similar view. He refrained from using the pond, there was too much algae. So the building in Figure 19 looks very much like it did almost fifty years ago. Not so for its environment.

6. The People of the Symposia

Many names have already appeared, but there are many more who have made significant contributions to the success of the antenna symposia. It is risky to attempt to identify them; some deserving of mention will undoubtedly be left out. Nevertheless, it seems imperative to give recognition to those that come to mind. It has already been mentioned that Walt Portune, Antennas and Radomes Group, WPAFB, initiated the meeting and for several years served as contract monitor for the Air Force. He was followed, for a few years, by Fred Burnham. Then came Ed Turner with his free flowing ideas and irrepressible humor. Many attendees will remember Ed Turner and his pistol as he very effectively called the symposium back into session with bursts of (blanks, we hope) gunfire. In the

final years of sponsorship by WPAFB, the meeting was shepherded by Harold Weber.

On the side of the University of Illinois, local arrangements were initially handled by John Hoffman, Research Laboratory Manager. Later this position was filled by Carl Mensendick. In 1956 Harold Lawler assumed these duties which he continued until his retirement in 1989. Harold recalls the days when UIUC owned Hott House in Monticello. Rooms at this converted mansion included the servants quarters tucked away behind the kitchen. It was quite challenging to guide sleepy travelers through the house to locate these rooms at one or two o'clock in the morning.

Able assistance with registration and housing has been given by Rosa Townsend, Melinda Suits and Shirley Dipert. Richard Ripper, Don Pritchard and Lee McWhorter have spent many hours behind the wheel of UIUC wagons providing transportation between airport and Allerton House, Hott House and other UIUC lodging. When arriving at Allerton House one morning, Harold Lawler was surprised to see corn stalks protruding from underneath the UIUC station wagon. He later learned that Ed Turner had volunteered to relieve the UIUC drivers for a late trip from the airport. On the way to Allerton House, Ed forgot that the road takes an abrupt jog, missed the turn entirely and wound up deep in the corn field.

Of course, there have been a host of people from Cambridge Air Force Research Center (and the follow-on agencies with ever-changing names), some of whom continue to attend after their employment by the Air Force has ceased. Ed Altshuler was a contributing author in the very early years and continues even to the present. Peter Franchi and Hugh Southall have presented frequently. The names of Allan Schell, Ron Fante, R. Steyskal, N. Kernweiss, D. McGrath, D. Jacavanco and others from RADC appear in the program. Recently, we find the names of L. Poles and S. Santarelli as authors.

Bob Mailloux has not only presented many papers over the years, he has provided impetus behind the participation by the Air Force. He has served as contact person at Hanscom since the Air Force sponsorship was renewed in 1977.

As sponsoring institutions, the University of Massachusetts and University of Illinois have provided numerous authors. Dan Schaubert was an author of symposia papers before he joined UMass and continues, not only to supply manuscripts, but also to handle the many tasks of organizing the meetings. Schaubert, a three-time UIUC graduate, was an engineer at Harry Diamond Laboratories 1974-1980. Later he was Professor and then Head of the Electrical and Computer Engineering Department, University of Massachusetts, Amherst, (1994-1998). Now he is once again a professor, but he continues to promote and organize the Antenna Applications Symposium, as he has since 1994.

We end by observing that there are many unique features of antenna symposia at Allerton Park, but it is the people that make these meetings great.

8. References

Note: To shorten the references in the following list, the title of the Proceedings of the Antenna Symposia is reduced to the symposium number and the year. Those that were held between 1951 and 1973 are for the Proceedings of the Annual Symposium on the United States Air Force Antenna Research and Development Program, Allerton Park, Illinois. Those after 1974 are for the Antenna Applications Symposium, Allerton Park, Illinois. Printed versions of some of the Symposium papers listed below may not appear in the Proceedings.

- [1] E. C. Jordan, Wendell Miller, and Mac E. Van Valkenburg, "Centennial History of the Department of Electrical and Computer Engineering: 1891-1991," College of Engineering, University of Illinois at Urbana-Champaign, Nov. 1991.
- [2] E. C. Jordan and W. L. Everitt, "Acoustic Models of Radio Antennas," Proc. IRE, vol. 29, no.4, p.186, 1941.
- [3] J. D. Dyson, "The Equiangular Spiral Antenna," Fifth Symp., 1955.
- [4] J. D. Dyson, "The Non-Planar Equiangular Spiral Antenna," Eighth Symp., 1958.
- [5] J. D. Dyson and P. E. Mayes, "Multi-Arm Log-Spiral Antennas," Tenth Symp., 1960.
- [6] D. Isbell, "Unidirectional Log-Periodic Antenna," Seventh Symp., 1957.
- [7] R. L. Carrel, "Analysis of the Log-Periodic Dipole Antenna," Tenth Symp., 1960.
- [8] R. L. Carrel, "Analysis and Design of the Log-Periodic Dipole Antenna," Tech. Rep. No. 52, Contract AF33(616)-6079, Aeronautical Systems Division, WPAFB, Ohio, 1961.
- [9] Georges Deschamps, "Microstrip Microwave Antennas," Third Symp., 1953.
- [10] Georges Deschamps, "Partially Polarized Antennas," Sixteenth Symp., 1966.
- [11] Robert Munson, "Microstrip Phased Array Antennas," Twenty-Second Symp., 1972.
- [12] Y. T. Lo, D. Solomon, and W. F. Richards, "Theory and Experiment on Microstrip Antennas," Twenty-Eighth Symp., 1978.

- [13] A. A. Oliner, "Slot Radiation Research Program," Third Symp., 1953.
- [14] L. G. Fubini, "Strip Transmission Lines," Third Symp., 1953.
- [15] R. H. DuHamel and R. L. Warnock, "Antenna Gain and Efficiency Measurement," Third Symp., 1953.
- [16] S. B. Cohn, "Flush Airborne Radar Antennas," Third Symp., 1953
- [17] R. C. Hansen and E. C. Jordan, "Ferrite Loop Antenna Systems for Aircraft," Third Symp., 1953.
- [18] A. J. Simmons, "Scanning Antenna Arrays Using Ferrite Phase Shifters," Fourth Symp., 1954.
- [19] H. E. King and R. H. DuHamel, "Coupling of Antenna Elements to a Circular Surface Waveguide," Fifth Symp., 1955.
- [20] B. H. Burdine, "Radiation from the Double Spiral Antenna," Fifth Symp., 1955.
- [21] J. D. Dyson, "An Experimental Investigation of the Equiangular Spiral Antenna," Fifth Symp., 1955.
- [22] R. S. Elliott and L. A. Kurtz, "Mutual Coupling in Large UHF Scanning Arrays," Fifth Symp., 1955.
- [23] A. S. Dunbar, "Some Antennas for Wide Angle Scanning," Seventh Symp., 1957.
- [24] A. E. Marston, "Appliction of the Spiral Antenna to Scanning Array Systems," Eighth Symp., 1958.
- [25] J. D. Dyson, " The Conical Log-Spiral in Simple Arrays," Eleventh Symp., 1961.
- [26] Roy C. Spencer, "Operation and Analysis of Point Source Antenna Arrays," Tenth Symp., 1960.
- [27] R. M. Kalafus and J. A. M. Lyon, "Feasibility of Electrically Small Antennas on an Energy Basis," Eleventh Symp., 1961.
- [28] E. Altshuler, "Large Spherical Antennas for Aerospace Research," Eleventh Symp., 1961.

- [29] Eino J. Luoma, "Fabrication and Testing of Step-Index Luneberg Lenses with High Directional Accuracy," Twelfth Symp., 1962.
- [30] C. A. Bolt, Jr., "Antenna Design with Digital Computers," Twelfth Symp., 1962.
- [31] R. A. Michelson and J. W. Schomer, "The Application of Nonlinear Programming to Pattern Synthesis Problems," Twelfth Symp., 1962.
- [32] P. E. Mayes and P. G. Ingerson, "Near-Field Measurements on a Backfire Periodic Dipole Array," Twelfth Symp., 1962.
- [33] W. T. Patton, "The Backfire Bifilar Helix," Twelfth Symp., 1962.
- [34] H. A. Ecker and D. E. Svoboda, "Superdirective Antennas," Twelfth Symp., 1962.
- [35] R. H. DuHamel and M. E. Armstrong, "A Wide-Band Monopulse Antenna Using the Tapered-Line Magic-T," Twelfth Symp., 1962.
- [36] J. R. Copeland, "A Surface-Mounted Slotted TEM-Line Antenna," Twelfth Symp., 1962.
- [37] F. R. Ore, "Millimeter Wave Biconical Horn and Slot Array Antennas," Twelfth Symp., 1962.
- [38] Robert J. Mailloux, "The Long Yagi-Uda Array," Twelfth Symp., 1962.
- [39] C. T. Tai, "The Saguaro Antenna," Sixteenth Symp., 1966.
- [40] P. G. Ingerson and P. E. Mayes, "Design of Log-Periodic Structures Using Dispersion Data for Periodic Lines," Sixteenth Symp., 1966.
- [41] V. R. Arens, C. T. Elfving, U. R. Embry, D. L. Johnstone, and K. K. Mie, "Integral Equation Formulation of a Log-Periodic Antenna," Seventeenth Symp., 1967.
- [42] W. H. Nestor, "Element Thinning in Large Arrays," Seventeenth Symp., 1967.
- [43] Carl F. Augustine and Wilfred G. Jaekle, "Real-Time Area Detection of Electromagnetic Fields Using Cholesteric Liquid Crystals," Eighteenth Symp., 1968.
- [44] J. Rosa and E. W. Case, "A Wide Angle Circularly Polarized Omnidirectional Array Antenna," Eighteenth Symp., 1968.

- [45] R. L. Carrel and R. C. Fenwick, "Airborne VLF Transmitting Antennas," Eighteenth Symp., 1968.
- [46] D. L. Sengupta and J. E. Ferris, "Investigation of the Rudimentary Horn," Nineteenth Symp., 1969.
- [47] Georges Deschamps, J. J. Sweeney, and F. R. Ore, "A New Method of Evaluating the Noise Performance of Two-Port Networks," Nineteenth Symp., 1969.
- [48] P. E. Mayes and F. M. Wiesenmeyer, "The Monopole-Slot – An Electrically Small DF and Communications Antenna," Twentieth Symp., 1970.
- [49] P. G. Ingerson, "Modulated Arm Width (MAW) Log-Spiral Antenna," Twentieth Symp., 1970.
- [50] R. J. Mailloux, "A Study of the Use of Conducting Fences for Reducing Mutual Coupling," Twentieth Symp., 1970.
- [51] Robert J. Wohlers, "The GWIA – An Extremely Wide Bandwidth Low-Dispersion Antenna," Twentieth Symp., 1970.
- [52] G. J. Burke, S. Gee, E. K. Miller, A. J. Poggio, and E. S. Selden, "Analysis of Antennas Over Lossy Half-Space," Twentieth Symp., 1970.
- [53] R. J. Mailloux, "Blind Spot Occurrence in Phased Arrays – When to Expect It and How to Cure It," Twenty-Second Symp., 1972.
- [54] A. T. Adams, R. Greenough, R. Wallenberg, A. Mendelovieg, and C. Lumjick, "The Quadrifilar Helix Antenna," Twenty-Second Symp., 1972.
- [55] Allen Newell, "Planar Near Field Measurements," Twenty-Third Symp., 1973.
- [56] R. C. Hansen, "Optimum Inductive Loading of Short Monopoles," Twenty-Third Symp., 1973.
- [57] W. A. Imbriale and P. G. Ingerson, "Optimum Design of Broadband Parabolic Reflector Antennas Fed with Log-Periodic Dipole Arrays," Twenty-Third Symp., 1973.
- [58] W. Kreutel, "Satellite Communications: New Challenges for Antenna Engineers," First Symp., 1977.
- [59] A. R. Jamieson and G. A. Deschamps, "Off-Set Fed Reflector Antennas with Multiple Beam Capability," First Symp., 1977.

- [60] R. Munson and G. G. Sanford, "Conformal Microstrip Antenna Arrays," First Symp., 1977.
- [61] R. S. Elliott and L. A. Kurtz, "The Design of Small Slot Arrays," First Symp., 1977.
- [62] E. H. Newman and C. H. Walter, "A Comparison of the Efficiency of Electrically Small Dipole and Loop Antennas," First Symp., 1977.
- [63] J. L. Kerr, "Other Microstrip Antenna Applications," First Symp., 1977.
- [64] J. M. Tranquilla and K. G. Balmain, "A Study of TEM Resonances on a Class of Parallel Dipole Arrays," First Symp., 1977.
- [65] A. L. Davidson and W. J. Turney, "Mobile Antenna Gain in the 900 MHz Band," First Symp., 1977.
- [66] A. J. Poggio and E. K. Miller, "A Perspective on Numerical Methods for Antennas," Second Symp., 1978.
- [67] L. N. Medgyesic-Mitschang, "Method of Moments Modeling of Aperture and Wire Radiators on Surfaces," Second Symp., 1978.
- [68] W. Gee, T. H. Lee, and E. K. Okubo, "Computer-Aided Radome Effect Analysis," Second Symp., 1978.
- [69] A. R. Sindoris, D. H. Schaubert, and F. G. Farrar, "The Spiral Slot – A Unique Microstrip Antenna," Second Symp., 1978.
- [70] J. L. Kerr, "Microstrip Polarization Techniques," Second Symp., 1978.
- [71] W. L. Ko and R. Mittra, "Modeling the X-Band Radar Augmentation System of a High Altitude Supersonic Target," Second Symp., 1978.
- [72] A. C. Schell, "Air Force Requirements for Antenna Technology," Third Symp., 1979.
- [73] W. F. Richards, Y. T. Lo, and P. Simon, "Design and Theory of Circularly Polarized Microstrip Antennas," Third Symp., 1979.
- [74] D. Staiman, "Automated Near Field Antenna Test Set for Phased Array Antennas," Third Symp., 1979.
- [75] Carl Stubenrauch, "Some Recent Near Field Measurements at NBS," Third Symp., 1979.

- [76] J. D. Hanfling, "Planar Near Field Measurement for Aircraft Antenna Applications," Third Symp., 1979.
- [77] C. E. Kirchhoff, "Near Field Pattern Measurement Facility," Third Symp., 1979.
- [78] L. Ricardi, "Antenna Technology for Satellite Communications Systems," Fourth Symp., 1980.
- [79] J. Wiltse, "Millimeter-Wave Technology," Fifth Symp., 1981.
- [80] N. Deo and R. Mittra, "Millimeter-Wave Integrated Circuits," Fifth Symp., 1981.
- [81] S. Ray, R. Mittra, T. Trinh, and L. Paleta, "Recent Development in Millimeter-Wave Antennas," Fifth Symp., 1981.
- [82] W. T. Patton, "Phased Array Alignment with Planar Near-Field Scanning," Fifth Symp., 1981.
- [83] R. Munson, "Advances in Microstrip Antenna Technology," Fifth Symp., 1981.
- [84] J. D. Ou, W. F. Richards, and Y. T. Lo, "An Analysis of Annular, Annular Sector, and Circular Sector Microstrip Antennas," Fifth Symp., 1981.
- [85] M. Campi, "Design of Microstrip Linear Array Antennas," Fifth Symp., 1981.
- [86] A. Schell, "Overview of Air Force Antenna Needs," Sixth Symp., 1982.
- [87] M. Hurst, R. Mittra, and S. W. Lee, "An Approach to Radar Target Identification," Sixth Symp., 1982.
- [88] R. B. Dybdal, "Millimeter-Wave Antenna Development," Sixth Symp., 1982.
- [89] O. B. Kesler, "94 GHz Antenna Techniques," Sixth Symp., 1982.
- [90] F. Lalezari and R. Munson, "Millimeter-Wave Microstrip Antennas," Sixth Symp., 1982.
- [91] F. I. Diamond, "Antenna Applications and System Engineering," Seventh Symp., 1983.
- [92] H. Weber, "Solid State Phased Array Technology," Seventh Symp., 1983.

- [93] R. Stockton, "Fundamental Design Issues for Monolithic Phased Arrays," Seventh Symp., 1983.
- [94] B. J. Edwal, "Integration of Monolithic Microwave Integrated Circuits into Phased Array Antenna Systems," Seventh Symp., 1983.
- [95] D. A. Paschen, "Broadband Microstrip Matching Techniques," Seventh Symp., 1983.
- [96] W. T. Patton, "New Antenna Technology," Eighth Symp., 1984.
- [97] D. H. Schaubart, D. M. Pozar, K. S. Yngvesson, and R. W. Jackson, "Considerations for Millimeter-Wave, Monolithic Phased Arrays," Eighth Symp., 1984.
- [98] Y. T. Lo, B. Engst, and R. Q. H. Lee, "Circularly Polarized Microstrip Antennas," Eighth Symp., 1984.
- [99] R. C. Johnson, "Antenna Technology," Ninth Symp., 1985.
- [100] D. H. Schaubart, R. W. Jackson, and D. M. Pozar, "Antenna Elements for Integrated Phased Arrays," Ninth Symp., 1985.
- [101] W. W. Lam, C. F. Jou, N. C. Luhmann, Jr., and D. B. Rutledge, "Diode Grid for Electronic Beam-Steering and Frequency Multiplication," Ninth Symp., 1985.
- [102] Y. Rahmat-Samii, "Overview of Reflector Antenna Technology," Ninth Symp., 1985.
- [103] H. Schrank, "A Centennial of Electromagnetics," Tenth Symp., 1986.
- [104] D. M. Pozar and D. H. Schaubart, "Aperture Coupled Patch Antennas and Arrays," Tenth Symp., 1986.
- [105] D. Tanner and P. Mayes, "Wideband, Double-Tuned Microstrip Elements," Tenth Symp., 1986.
- [106] D. A. Paschen, "Practical Examples of Integrated Broadband Matching of Microstrip Antennas," Tenth Symp., 1986.
- [107] D. W. Hess, "Review of Spherical Near-Field Measurements," Tenth Symp., 1986.

- [108] J. Schindler, "MMIC's – The Key to Affordable Arrays," Eleventh Symp., 1987.
- [109] A. J. Zaghloul and R. Mailloux, "MMIC Phased Arrays," Eleventh Symp., 1987.
- [110] C. D. Pepe, M. J. Povinelli, and J. J. Kennick, "Wideband Active Phased Array," Eleventh Symp., 1987.
- [111] J. Kraus, "Antennas: Our Eyes and Ears on the World," (video), Twelfth Symp., 1988.
- [112] M. J. Povinelli, "Experimental Design and Performance of Endfire and Conformal Flared Slot (Notch) Antennas and Application to Phased Arrays: An Overview of Development," Twelfth Symp., 1988.
- [113] J. Kinzel, "Future Directions in Solid State Millimeter-Wave Arrays," Thirteenth Symp., 1989.
- [114] D. R. Jackson, N. G. Alexopoulos, and A. A. Oliner, "Microstrip Antennas in Composite Layers," Thirteenth Symp., 1989.
- [115] P. Franchi and H. Tobin, "Techniques to Measure Large Antenna Arrays with Random Errors," Thirteenth Symp., 1989.
- [116] J. L. Poirier, "HF Antennas: Application to OTH Radars," Fourteenth Symp., 1990.
- [117] A. J. Gould, "A Thinned High Frequency Linear Antenna Array to Study Ionospheric Structure," Fourteenth Symp., 1990.
- [118] Y. T. Lo, "Design of Circularly Polarized Patch Antennas," Fourteenth Symp., 1990.
- [119] G. Grann, "Beyond AWACS," Fifteenth Symp., 1991.
- [120] R. C. Hansen, "Transient Effects in Reflector Antennas," Fifteenth Symp., 1991.
- [121] P. R. Herzfeld, "Optically Fed and Controlled Phased Array Antennas – A Dream or a Real Possibility?" Sixteenth Symp., 1992.
- [122] I. L. Newberg, "Antenna True-Time-Delay Beamsteering Utilizing Fiber Optics," Sixteenth Symp., 1992.

- [123] R. L. Niekamp, "A Broadband Panel Antenna for HDTV Applications," Sixteenth Symp., 1992.
- [124] E. K. Miller, "Necessary and Sufficient Conditions for Portable, Reliable and Useful CEM," Sixteenth Symp., 1992.
- [125] J. K. Schindler, "Dual-Use Technology – Past and Future," Seventeenth Symp., 1993.
- [126] G. E. Miller, "Integrated Circuit Active Phased Array Antenna for Millimeter-Wave Communication Applications," Seventeenth Symp., 1993.
- [127] I. Karlsson, "Applications of Waveguide Arrays in Commercial and Military Radars," Seventeenth Symp., 1993.
- [128] P. W. Klock, "Antennas, Antenna Laboratory, Allerton Antenna Symposium and Paul E. Mayes," Eighteenth Symp., 1994.
- [129] C. Raquet, "MMIC Array Demonstration with the NASA Advanced Communications Technology Satellite (ACTS): Technology, Teamwork and Transition," Nineteenth Symp., 1995.
- [130] P. Pons and C. Renard, "Low-Cost Millimeter-Wave Phased Array Antennas," Nineteenth Symp., 1995.
- [131] M. G. Parent, "A Survey of Optical Beamforming Techniques," Nineteenth Symp., 1995.
- [132] Photonic-Based Tuning and Control of Antenna Elements," Nineteenth Symp., 1995.
- [133] A. Adrian, "Performance Analysis for a Concealed Automobile Entertainment Radio Antenna Subsystem," Nineteenth Symp., 1995.
- [134] B. Hendrikson, "Military Application of Lightwaves – Present and Future," Twentieth Symp., 1996.
- [135] J. Schuss, "The Iridium Main Mission Antenna and Other Advanced Phased Array Concepts," Twenty First Symp., 1997.
- [136] W. Stutzman, "Antennas for Industry and Government in the Next Century," Twenty Second Symp., 1998.
- [137] J. Smith, "MEMS and Advanced Radar," Twenty Third Symp., 1999.



Fig. 1. Dr. W. L. Everitt, Dean of College of Engineering , University of Illinois at Champaign-Urbana, 1949-1968. Dean Everitt was after-dinner speaker/entertainer at some of the early symposia. In 19?? He gave the keynote address as Dean Emeritus.

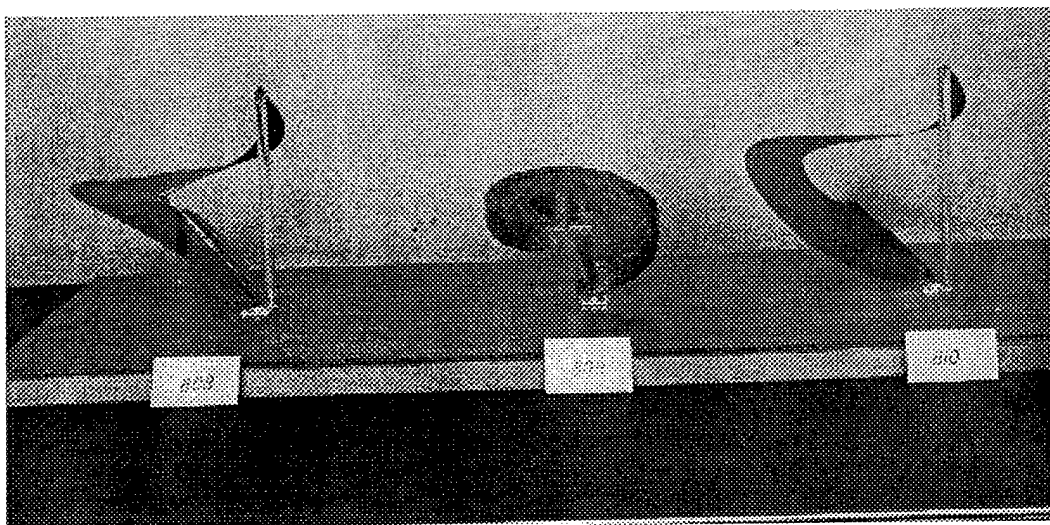


Figure 2. Some typical antenna models subject to research in the early days of the Antenna Laboratory at UIUC. As far as has been determined, none of these antennas were ever described at the Symposium, but notice the similarity to log-spirals that were later presented in great detail.

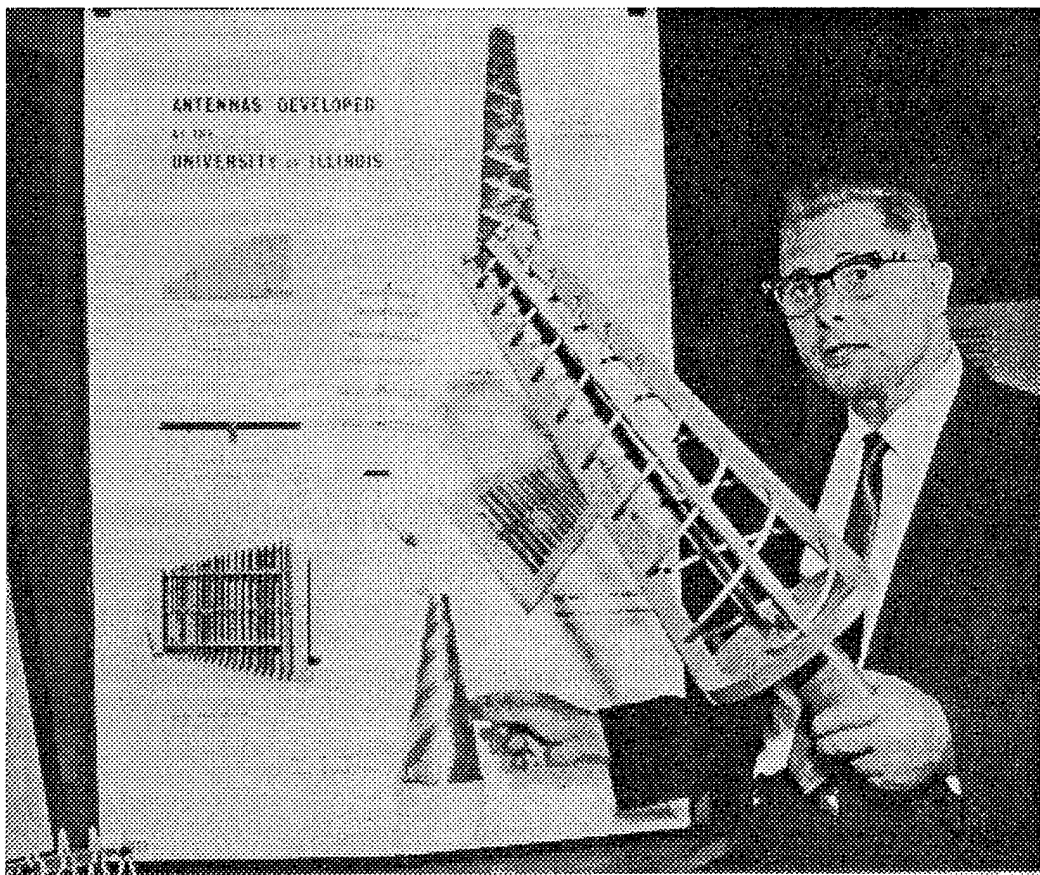
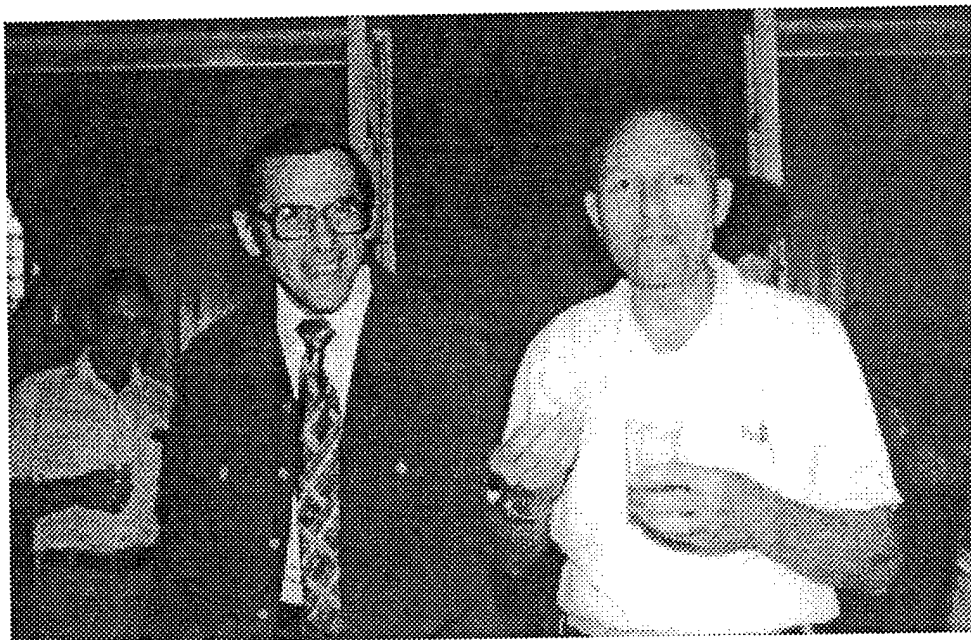


Figure 3. Dr. E. C. Jordan, Director of the Antenna Lab, UIUC, 1952-1954, Head of Electrical and Computer Engineering Department, UIUC, 1954-1979. Ed is pointing to a conical log-spiral antenna that was described by John Dyson in a paper presented at the 1958 Symposium. Ed is holding a conical spiral of the type used in the UIUC radio telescope. In the background can be seen: (a) the log-periodic vertical zigzag, (b) the balanced log-periodic zigzag, (c) a log-periodic array of helical dipoles, (d) the “letter-rack” antenna, and (e) a log-periodic folded dipole array. The development of log-periodic antennas has also been described by papers presented at several Symposia.



Harold Lawler

R. C. Hansen

1978 Antenna Applications Symposium

Figure 4. Lawler was Laboratory/Business Manager for the UIUC ECE Department from 1956 to 1989 and handled many organizational details for the antenna symposia during that time. Hansen was a graduate student at UIUC ECE Department when the first antenna symposium was held in 1951. After graduation, he worked in industry for several years before becoming an independent consulting engineer. He has attended and presented papers at numerous symposia at Allerton Park.

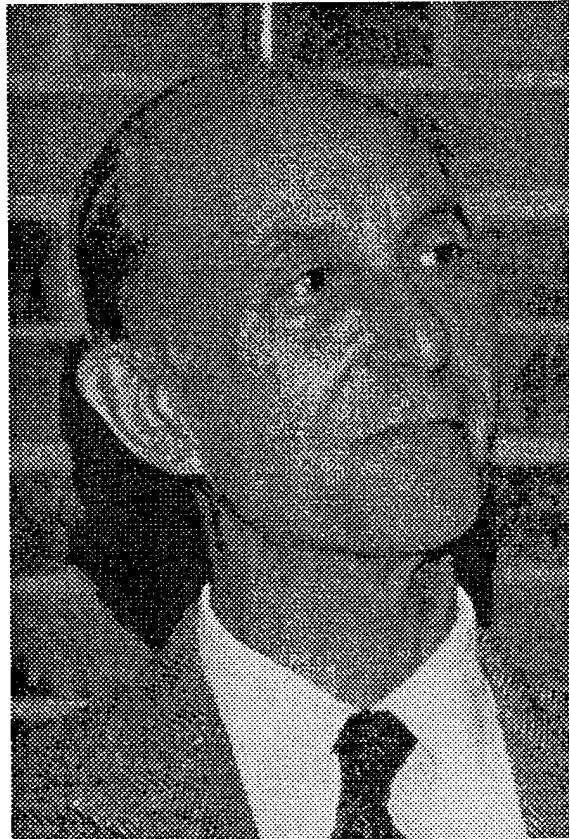


Figure 5. Victor H. Rumsey was employed by the Antenna Laboratory of Ohio State University in the early years of the Symposium. He was widely known as the author of papers and reports on the “reaction theory” in electromagnetics. He attended and presented papers at the Symposium before he moved to UIUC in 1954 to assume duties as the Director of the Antenna Laboratory. At Illinois, he developed several principles for the realization of “frequency-independent” antennas. In 1957 he moved to the University of California at Berkeley and later to UC, San Diego.

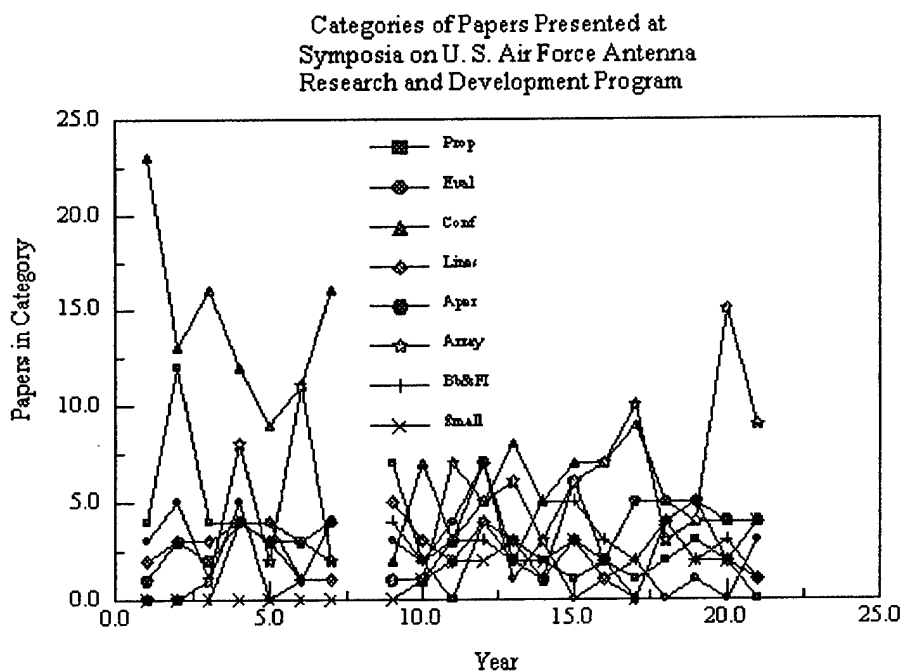


Figure 6. The distribution of papers, 1952-1972, classified into the categories shown in Table 1. (The 1959 Proceedings was not available at the time these data were compiled.) Note the early interest in flush-mounted (conformal) antennas which was revived in the early 70's by the introduction of patch antenna technology. Other popular topics have been the properties of antenna elements and antenna arrays.



Figure 7. John Dyson demonstrated the frequency independent performance of log-spiral antennas in 1957 and described his early work at the Symposium in 1958 while a graduate student at UIUC. He continued to investigate the properties of log-spiral antennas for many years as ECE Professor in the Antenna Lab, UIUC, and presented several more papers on spirals at the Allerton Symposia.



Figure 8. From left to right, Robert L. Carrel, Georges Deschamps, Ray DuHamel and Y. T. Lo. Carrel was a graduate student in the Antenna Laboratory, UIUC, during the development of log-periodic antennas and wrote a widely distributed thesis on the analysis of log-periodic dipole arrays. He first described his work at the 1957 Antenna Symposium. Georges Deschamps was an engineer with Federal Telecommunications Laboratory when he presented a paper on microstrip antennas in 1953. He later became Director of the Antenna Laboratory, UIUC. Ray DuHamel, inventor and developer of several log-periodic antennas, was a faculty member and research supervisor at the Antenna Laboratory, UIUC, from 1952 to 1958 when he left to join Collins Radio. Later, he worked for Hughes Aircraft and became an independent consultant. Y. T. Lo joined the Antenna Laboratory, UIUC, in 1955. Much of his work on microstrip patch antennas appears in the Proceedings of the Symposia.

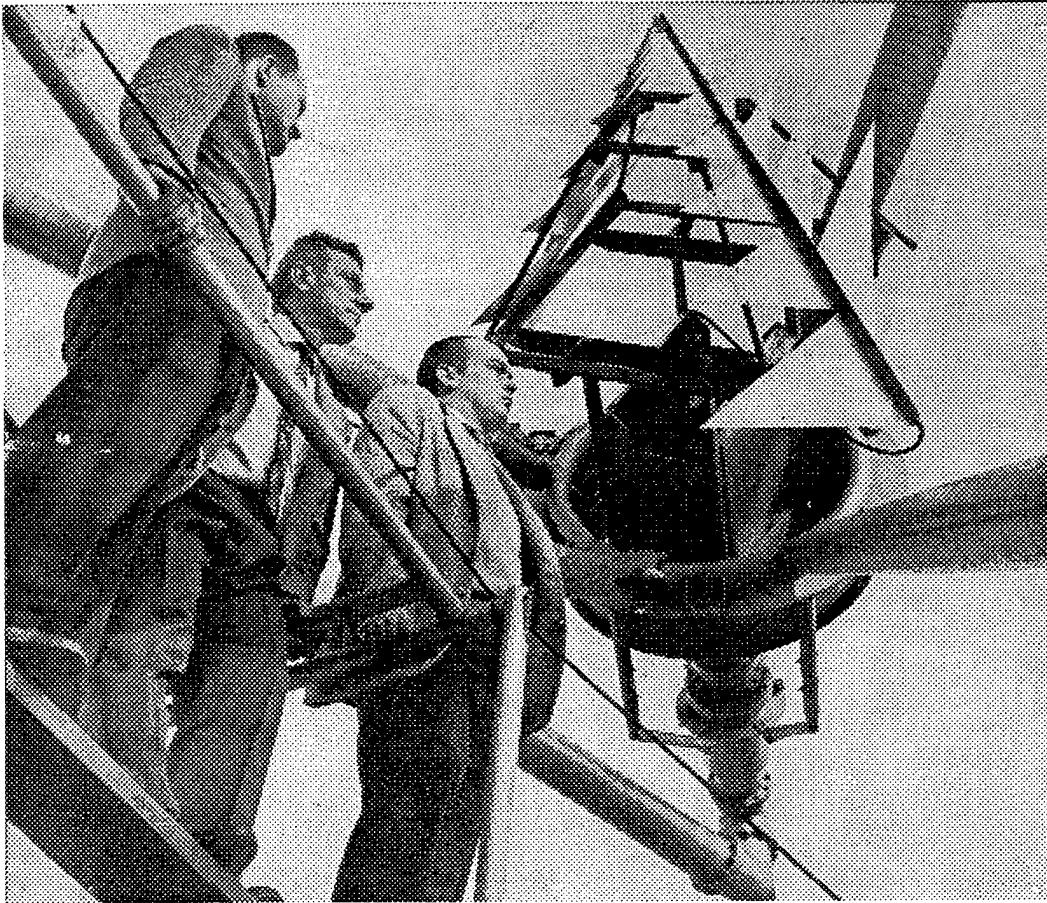


Figure 9. From left to right, Paul Mayes, Harold Webb, and Dwight Isbell. Mayes joined the faculty of the Antenna Laboratory, UIUC, in 1954 and remained until his retirement at the end of 1993. Harold Webb was Professor, ECE Department, and director of the Moon Bounce Program that operated the reflector antenna shown here. Dwight Isbell was an Antenna Technician in the Antenna Laboratory and developed the first unidirectional log-periodic antenna. He described the antenna in an Antenna Symposium paper presented in 1957. A later model of his antenna is shown here as it was installed on the Moon Bounce reflector, the first use of a log-periodic antenna as a reflector feed.

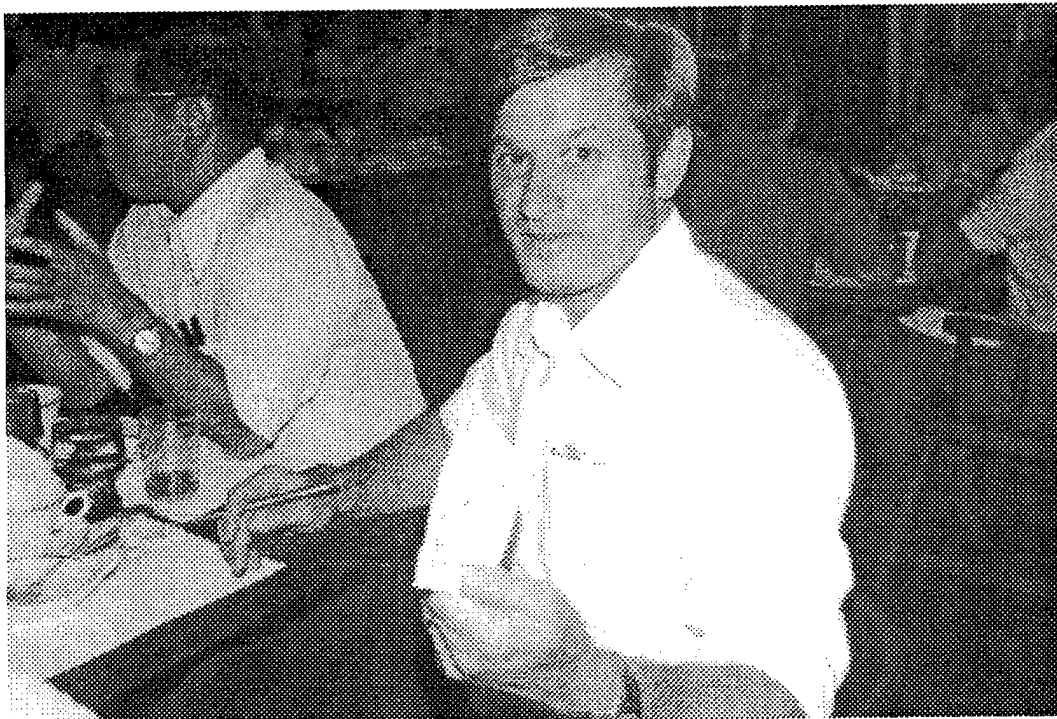
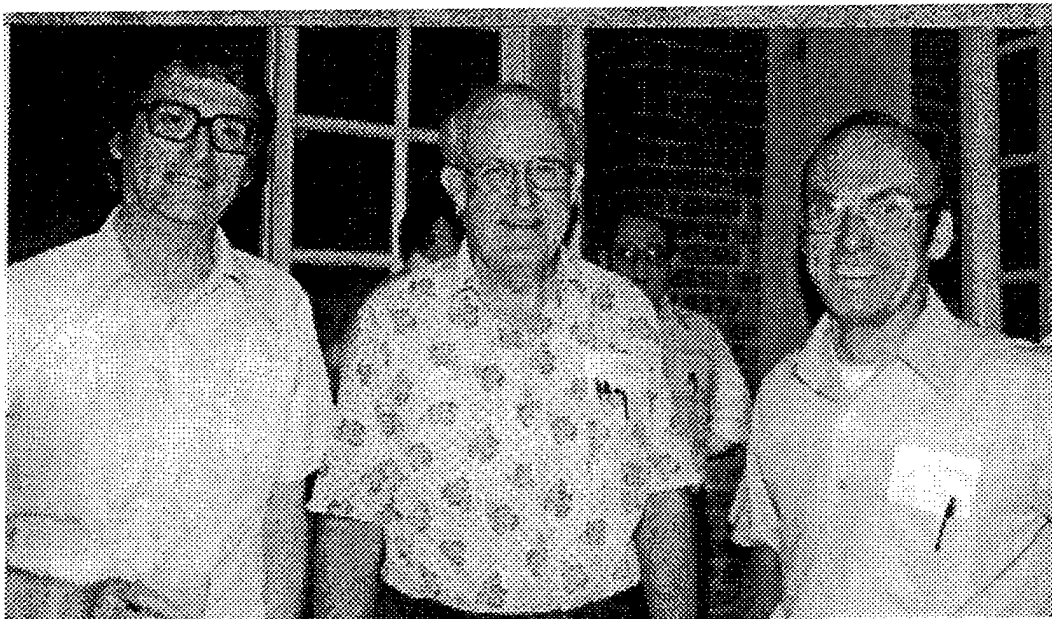


Figure 10. Robert Munson and C. H. Tang (in background) in the dining hall at Allerton House. Munson has presented several papers on microstrip patch technology at the Symposium.



Paul Ingerson

Paul Mayes

Carl Stubenrauch

1978 Antenna Applications Symposium

Figure 11.



Figure 12. W. T. Patton, RCA, keynote speaker at the 1984 Antenna Applications Symposium.

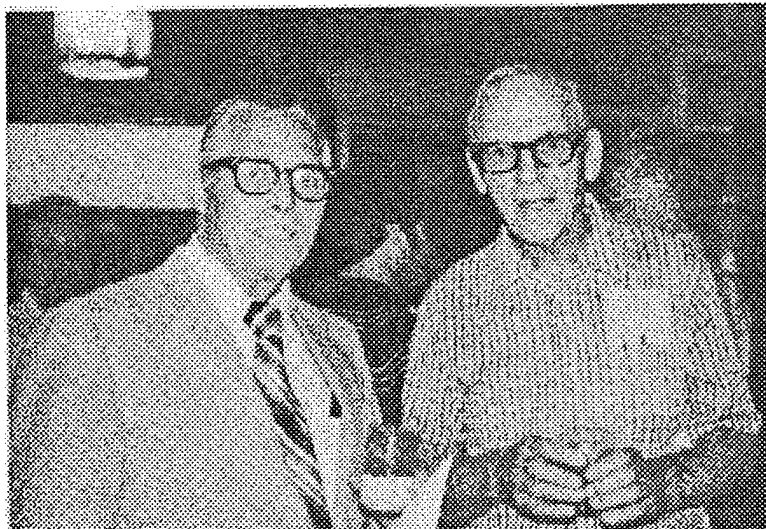


Figure 13. Ed Turner (right) with Ed Jordan at the 1978 Antenna Applications Symposium.

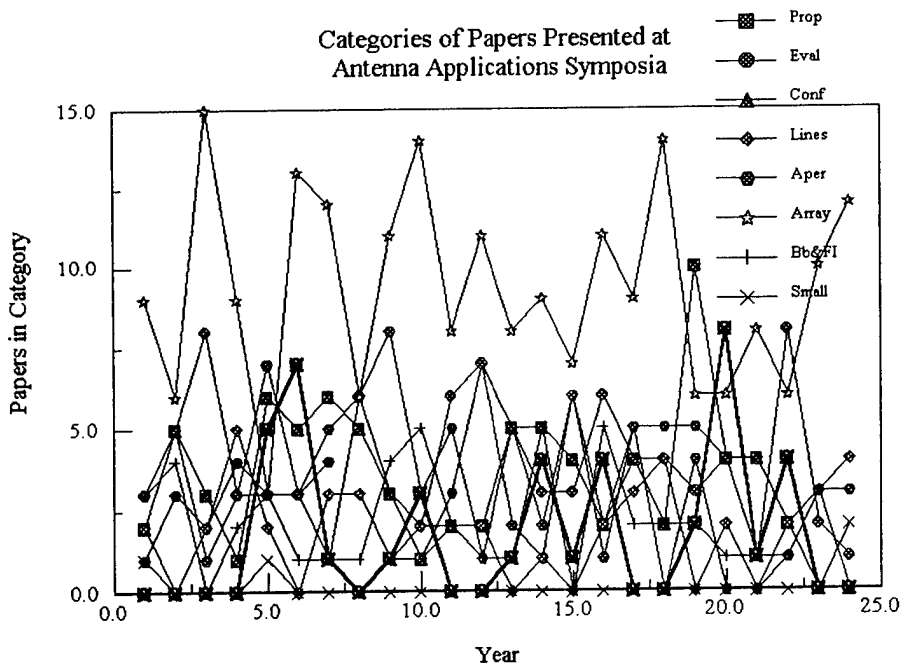


Figure 14. The distribution of papers, 1977-2001, classified into the categories shown in Table 1. The most popular category during these years was antenna arrays. No other topic has provoked the extended period of interest of arrays.



Figure 15. Walter Gee (center) with unidentified other attendees at the 1982 Antenna Applications Symposium.



Figure 16. Raj Mittra, Director of the Electromagnetic Communications Lab, UIUC. Mittra and his colleagues have contributed numerous papers to the Antenna Symposium.



Figure 17. P. W. Klock (left) and O. B. Kesler at the 1968 Symposium.



Figure 18. Allerton House, circa 1958.

(Photo courtesy of University of Illinois Archives)

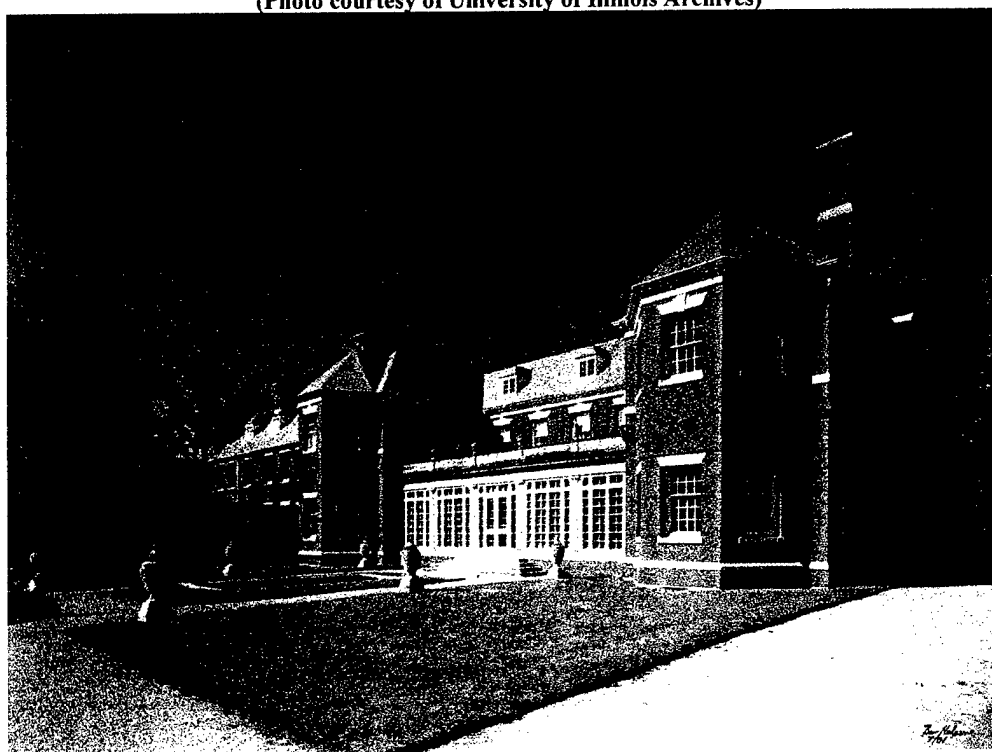


Figure 19. Allerton House, July 2001.

(Photo copyright, Benjamin Halpern, Photographer.)



J. Ned Hines

1982 Antenna Applications Symposium

Figure 20. If loyalty awards were offered, this man would surely be a candidate. Hines has been attending the Antenna Symposia at Allerton Park since he was a graduate student at OSU shortly after the meetings began. He has attended, authored papers and served as session chairman throughout his career at Bell Laboratories and successor companies.

Architecture and Performance of a Reconfigurable Aperture

L. Pringle, P. Friederich, L. Fountain, P. Harms,
D. Denison, E. Kuster, S. Blalock, R. Prado, G. Kiesel
Georgia Tech Research Institute
400 10th Street NW
Atlanta, GA 30332-0866

G. Smith, M. Allen, K. Kim
School of Electrical And Computer Engineering
Georgia Institute of Technology
Atlanta, GA 30332-

J. Maloney, M. Kesler
Photonex Corporation

This paper introduces a reconfigurable aperture architecture consisting of a matrix of conducting pads with switches between some or all of the patches. Each switch has two states: open and closed (conducting). This reconfigurable aperture can change functionality-for example, instantaneous bandwidth and steering angle-by switching the connections between the patches. A genetic search is utilized to find the optimum configuration (set of switch openings and closings) for a particular functionality, and the finite-difference time-domain method is utilized to calculate the performance of each candidate configuration during the search process. The anticipated performance of this architecture as a single feed aperture and as an element in an array is quantified through the measurement of a series of experimental test beds, each test bed embodying a different level of sophistication or a different method for control of the switches. Two switches are considered in support of this architecture: a FET switch and a MEMS switch. The FET switch limits the aperture performance to frequencies below 1.75GHz and to feed currents less than 0.1 Amps, while the MEMS switch performs well up to 10GHz and can maintain an RF current of 1 Amp. However, the FET switch is readily available while the MEMS switch is under development. There are three candidate architectures for controlling the switches: inductive coupling, resistive grid lines on the aperture, and conducting grid lines interrupted by surface-mount resistors. The expected performance of each of these candidates is quantified.

1. Introduction

Here we briefly review the architecture, switches, and switch control strategy for this aperture.

Aperture Architecture: The concept of a reconfigurable aperture reviewed here is derived from fragmented aperture design. (The reader should note that a separate paper on fragmented aperture design is to be presented in this forum.) In general, a "fragmented aperture" consists of sets of connected conducting structures such that each conducting structure is fabricated as a connected set of small "pads" on a low-loss, insulating substrate. One can think of the size and shape of these structures as being specified to optimally resonate over the desired frequency band of operation. The conducting structures are disconnected from each other, but interact with each other through radiative coupling. The key to designing a broadband fragmented aperture is the derivation of the optimal placement of conductor for the coupling of far-field energy at a particular steering angle and over a bandwidth of interest into the feed. This optimal placement is accomplished with a computer search algorithm.

This novel aperture design, which was developed at GTRI, enables nearly diffraction-limited performance with a single feed point for aperture sizes of several wavelengths on a side. Figure 1 shows a picture of a fragmented aperture and its realized gain (including mismatch) vs frequency over the designed band of operation (0.24-2.04 GHz) as compared to what can ideally be achieved from this aperture size (10 inch square) with a uniform current excitation. Note that typical broadband antennas, such as a spiral or bow tie typically approach this ideal only at a single low frequency, above which the gain tends to "flatten out" with frequency.

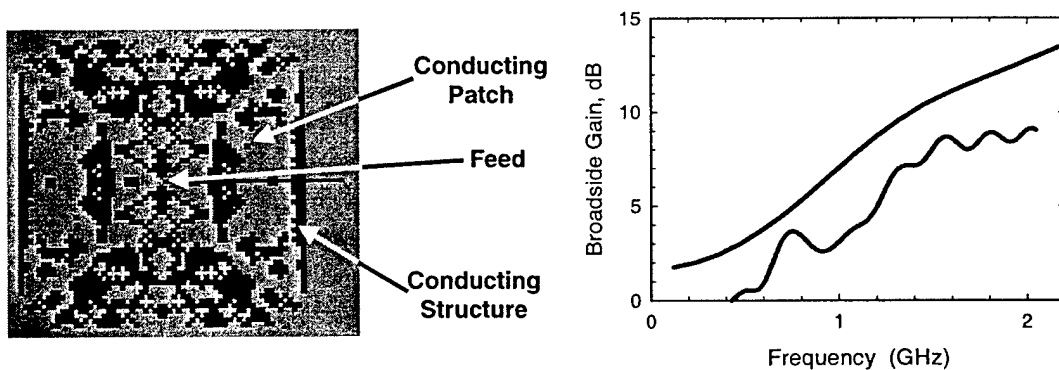


Figure 1. Left, fragmented aperture. Right, measured gain with mismatch (lower curve) as compared to the gain of an aperture with a continuous current sheet (upper curve).

The reconfigurable antenna element proposed by GTRI is essentially an *adaptable* fragmented aperture, in that switches control the size and shape of the resonant structures in order to optimize performance for the particular function at hand. For example, the antenna might be configured to maximize gain in a particular direction over a particular band, or to minimize side lobes (to reduce jamming vulnerability), or to place nulls in certain angular sectors. A notional drawing of a reconfigurable antenna is presented in Figure 2. The aperture is filled with conducting pads that provide the building blocks from which the conducting regions are assembled. (Note that the individual pads are not patch antennas, and do not have associated feeds.) Each pad site controls two switches with a single logic chip associated with that site. In actual antenna test coupons built so far, the logic chip and associated circuitry are actually located behind each conducting pad.

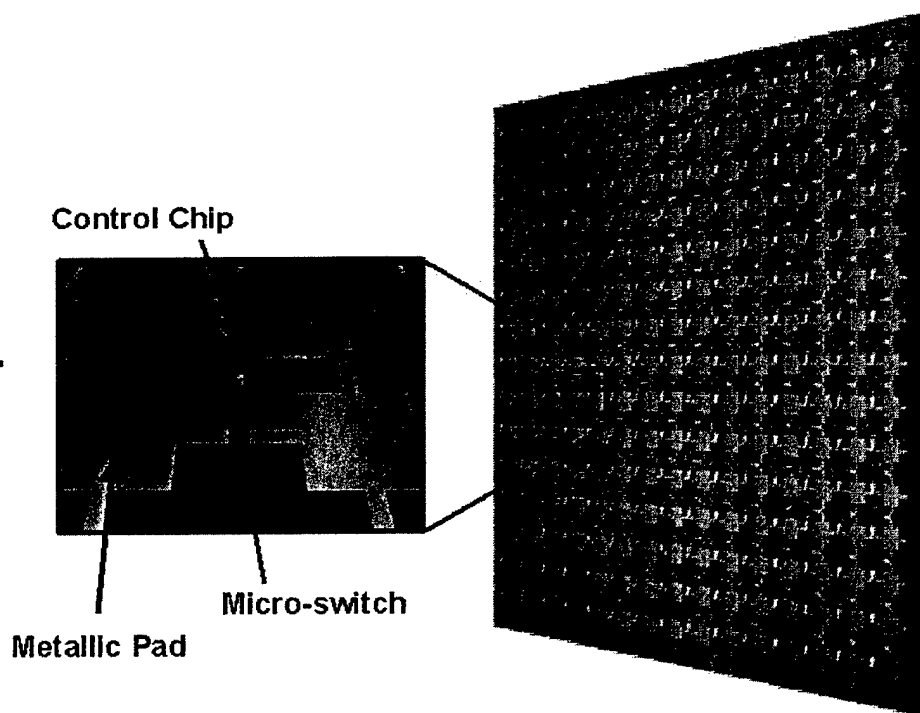


Figure 2. Notional drawing of the reconfigurable aperture concept. Each pad may be connected to any or all of its four neighbor pads. The total number of switches is slightly less than twice the number of pads. The logic chip at each location controls two of the switches.

The major differences between a fragmented aperture and the proposed reconfigurable aperture are as follows. 1) The reconfigurable aperture has the ability to change its configuration, and thus its functionality, on demand; 2) there

is a constant presence of disconnected conducting patches (those patches that do not get “switched into” the structure for a particular configuration) and of switches on the aperture surface of the reconfigurable aperture, which represents scattering sources; and 3) the density of the pads is lower for a reconfigurable aperture than a fragmented aperture. Note that fragmented apertures are typically designed with a pad size of $\lambda/20$ or less. For a reconfigurable aperture this would require a great number of switches, thus the number of pads per wavelength is typically reduced to 10 per wavelength. Simulations show that the lower pad density does sacrifice performance, as will be quantified below. We have not quantified any degradation in performance due to the presence of the parasitic scatterers on the surface. Still, the presence of the disconnected pads cannot be ignored and must be accounted for when designing a configuration.

Switches: The switch characteristic with the greatest impact on aperture performance is the open state capacitance. The capacitance limits the upper frequency of operation, since this capacitance renders all switches to appear closed at some sufficiently high frequency. The second important characteristic is the closed-state resistance. The presence of this resistance results in resistive losses, although the amount of loss depends on the particular configuration. A third consideration is the current required by the switches. Note that these switches must be controlled in some manner that is non-intrusive to the aperture. Switches that require a large control current (such as PIN diodes) require some well-conducting structure to carry this current, which represents additional scatterers on the aperture. Finally, the RF current carrying ability of the switch limits the power of the antenna.

With these criteria in mind, GTRI is testing two switches for use in the reconfigurable aperture. The first is a standard GaAs FET switch (ATF10136), which has an open state capacitance of 0.45 pF (measured) and a closed state resistance of about 4 Ohms (measured). This FET represents a state-of-the-art RF-FET that can pass high current and be easily purchased on the open market. Simulations and measurements show that the capacitance limits the reconfigurable aperture to frequencies below 1.75 GHz. The effect of the resistance is small, costing about 0.5dB in efficiency for configurations with large instantaneous bandwidths (40%) and negligible loss in efficiency for small bandwidth configurations (5%).

The second switch under consideration is a Georgia Tech developed direct-contact MEMS. This particular micro-switch is unique in that it is a magnetically closed, electrostatically held latch that makes true electrical contact between the terminals for broadband RF operation. Figure 3 presents a diagram of the switch construction. This choice of switch is driven by the need for good isolation when operating at high frequencies (up to 10 GHz). In order to achieve this isolation the

separation distance between contacts in the open position must be large, requiring a large force to close the switch. Supplying large voltages to operate switches distributed over the aperture is impractical. Thus, GTRI intends to change the antenna configuration by first closing all switches magnetically using a momentary external magnetic field. Then a latching voltage will be applied only to those switches that are to remain closed. When the external magnetic field is turned off, switches that are latched will remain closed and all others will return to an open state. Note that the voltage required to latch a closed switch is much smaller than the electrostatic voltage that would be required to close the switch initially.

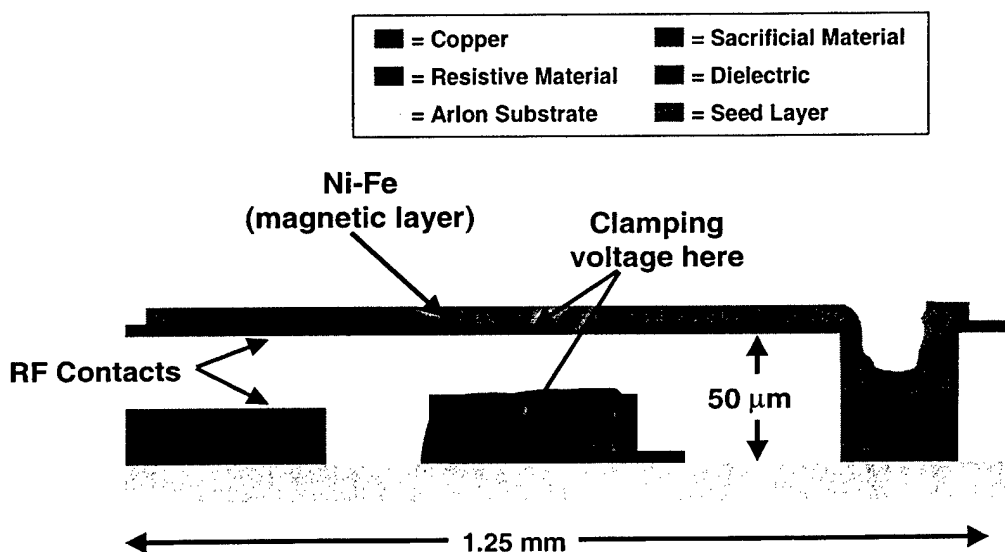


Figure 3. Micro-switch concept, with magnetic activation/electrostatic hold.

Switch Activation Technology. The greatest engineering challenge presented by this aperture is a method for communicating with and controlling the switches that does not interfere with RF performance. GTRI is investigating three architectures to support this function. All architectures utilize a logic chip to control the two switches that accompany each pad. An aperture controller (computer) communicates with each chip via a digital control signal for the purpose of setting the required states of the two switches under the chip's control. The chip also rectifies and smoothes the control signal for use in powering the chip.

The three architectures under consideration represent three methods for sending the control signals to the chip. The first of these is the use of highly resistive grid lines. Since the chips require little current (10 μ Amps) the resistance of the lines can be high enough to have negligible effect on the aperture. Calculations show that lines on the order of 100-200 K Ω per wavelength should be sufficient.

Because of the difficulty in fabricating highly resistive grid lines, a back-up architecture is also under consideration. This architecture utilizes conducting grid lines that are periodically interrupted by surface mount resistors. Note that the conducting wires represent additional scatterers on the aperture surface, which seems to degrade performance somewhat, as will be described below.

The final switch control concept under consideration utilizes a modulated RF signal (magnetic field) that is inductively coupled to a small coil located within each pad. The received energy is used to communicate and power the microchip at each pad location. The technology to accomplish this activation strategy is already present in consumer electronics (RF “tags” to identify ID badges, for example). The technical challenge is to fabricate the necessary magnetic field transmitter and receivers/control chips (at each latch position) within the antenna structure in a way that each chip has enough power to accomplish its task, while still maintaining antenna performance at microwave frequencies. For this reason, the success of this control system depends greatly on the number of switches required and the necessary size and separation of the conducting patches.

The following text reviews the expected performance of the reconfigurable aperture based on simulations and measurements. This review includes discussions of the effects on performance due to the architecture, switch choice, and switch control. Finally, this paper concludes with the expected utility of this aperture for phased array antennas.

2. Architecture

For the purpose of this paper, the baseline architecture is an aperture comprised of an 11 X 11 array of pads (216 switches) as shown in Figure 4. Each pad is one square centimeter, and the separation between pads is 2 cm (center-to-center). The size of the entire aperture is thus 22 cm on a side, which was chosen for operation down to about 800 MHz (at which frequency the aperture is a bit over $\lambda/2$ on a side). This baseline aperture is chosen for historical reasons that are not of importance here, but quantification of improvements in performance due to changes in architecture, switch control, and switch choice will be made with reference to this architecture.

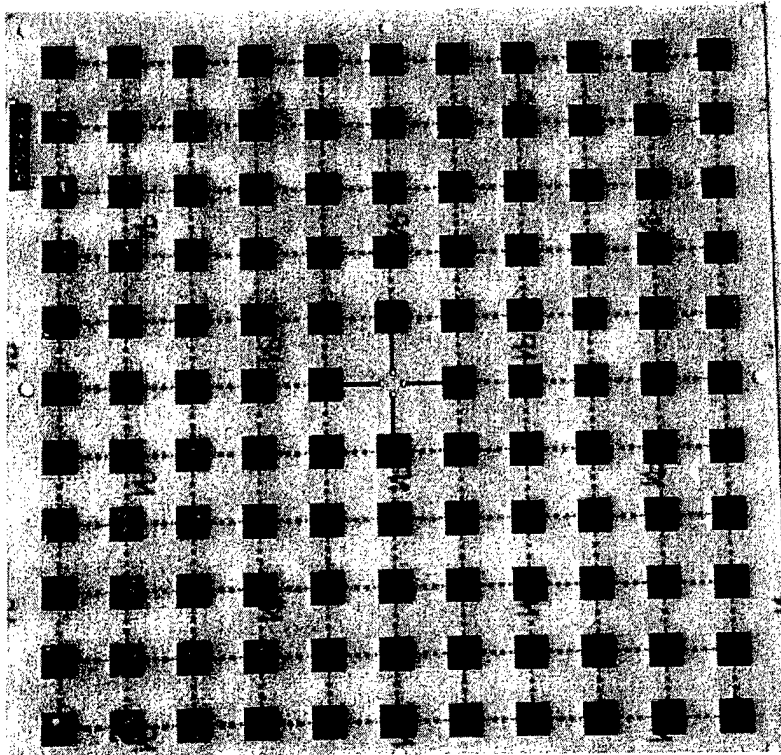


Figure 4. Picture of the front surface of the baseline reconfigurable aperture design showing the matrix of conducting pads.

In order to quantify performance we first compare the performance of the reconfigurable architecture, as described above, with fragmented apertures. Figure 5 shows the realized gain vs. frequency (broadside) for two configurations designed for the reconfigurable architecture. These designs were accomplished assuming “perfect” switches. That is, the open switches were assumed to be perfect open connections, and the closed switches were assumed to be perfect wires. The upper curve on the plot is the directivity of a uniform sheet of current on the same size aperture. This upper curve, a common-sense limit to the achievable gain for practical designs, acts as the “goal” in the search process. In this case all of the curves (including the goal) assume that there is no ground plane. Thus, these apertures radiate energy in both directions, decreasing the gain by 3dB from what might be achieved from this architecture with a ground plane.

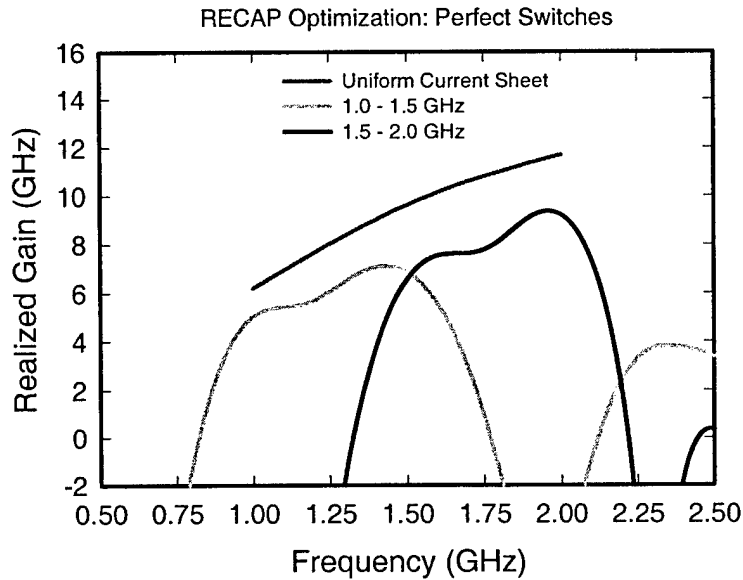


Figure 5. Results of two designs with perfect switches and no ground plane.

Figure 6 shows similar configurations for fragmented apertures of 10 inches on a side, which is only 10% larger on a side than the reconfigurable aperture architecture. Thus, we use the performance of these apertures as an indicator of the capability of the reconfigurable architecture as compared to a good broadband aperture.

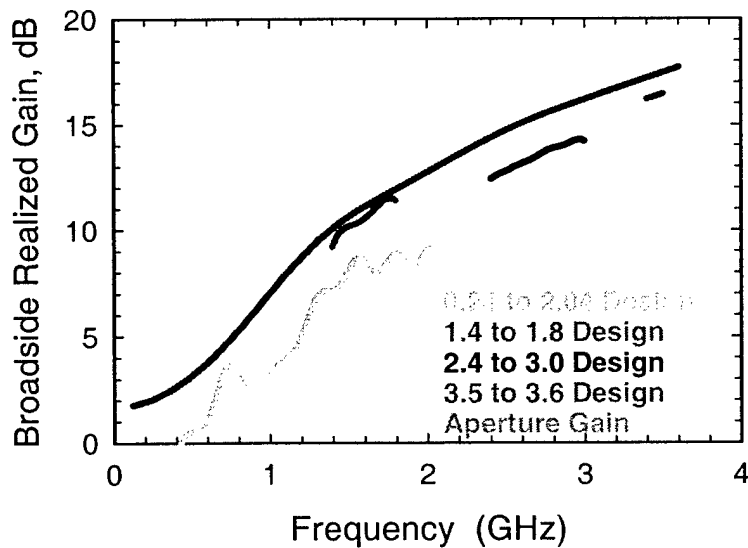


Figure 6. Four designs optimized for a 10-inch fragmented aperture

In general, for a particular aperture size, fragmented aperture performance and reconfigurable aperture performance (as compared to the directivity of a uniform sheet of current) decreases with increasing bandwidth, and for a given bandwidth it decreases with increasing frequency. With these trends in mind Figures 5 and 6 clearly show that the fragmented aperture designs out-perform the reconfigurable designs. For example, the 2.4 – 3.0 GHz fragmented configuration performs better (as compared to a uniform sheet of current) than the reconfigurable 1.5 - 2.0 GHz configuration, even though the reconfigurable configuration is lower in frequency.

1.5 - 2.0 GHz There are two possibilities for this loss in performance. First, the pad density of the reconfigurable designs is much less than the fragmented designs. Second, the reconfigurable designs contain parasitic scatterers that are always present (those pads that are not “connected into” the pattern). In an attempt to sort out these effects GTRI re-designed the reconfigurable configurations using 15 X 15 pads with the same size aperture. This doubles the number of switches. Figure 7 shows the results of this redesign. Note that the performance in both bands improves significantly.

Thus, the performance of a reconfigurable aperture can improve with increased pad density. However, increasing the pad density increases the number of switches, and thus increases the complexity of the structure. The authors are unable to say whether the fragmented aperture performance level can be reached with the reconfigurable architecture, as the configuration search for a fragmented-like pad density is prohibitive.

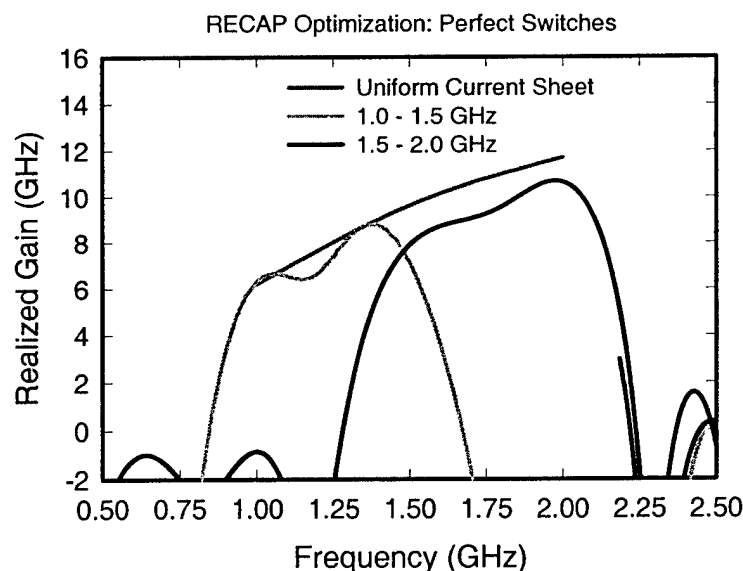


Figure 7. Results of redesign from Figure 5 at higher resolution.

Experimental verification of the model used to calculate antenna performance is very important, since the designs of the configurations are accomplished through simulation. Until a robust reconfigurable board is completed experimental verification is accomplished by “hard-wiring” the connections corresponding to closed switches. Figure 8 shows a prediction of a 1.0-1.4 GHz configuration (black curve) calculated at the resolution used in the search process (0.25 cm grid). The light gray curve represents a measurement of the same configuration. Note that the trends are predicted, but there is a frequency shift of 12% between the measurement and the model.

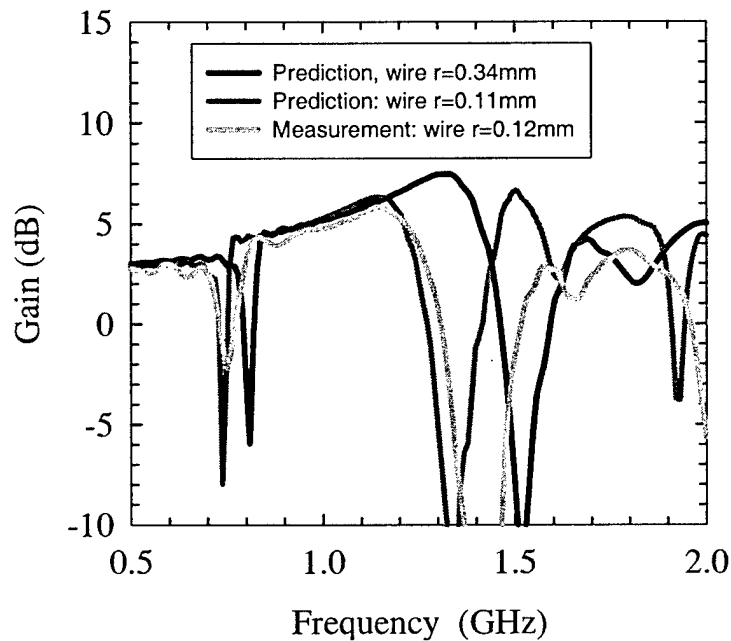


Figure 8. Actual test coupon measurement compared to two simulations with different resolution grids.

This discrepancy can be corrected by accomplishing the finite difference time domain calculation using a higher resolution grid. The medium gray curve represents the model result using a 1/12 cm grid, and this curve shows good agreement with the measurement. The cause of the frequency shift in the model is two-fold. First, the higher resolution allows for a more accurate prediction. Second, the wire connections are modeled as a perfectly conducting grid edge, and increasing the grid size increases the effective radius of the wire connecting the pads. Note that the effective radius of the modeled wires and the radius for the wire used in the measurement are displayed on the figure.

These two effects were studied independently by “gridding up” two different sized wires in the FDTD model (for this exercise flat conducting strips were used instead of round wires, to aid the modeling) with a very high-resolution grid. This calculation showed that the frequency shift due to the resolution of the model is about 8%, and the remainder of the 12% frequency shift is caused by discrepancies in wire diameters.

Unfortunately, a grid size fine enough for high modeling accuracy requires run times in excess of what is tolerable for design purposes. For that reason, efficient searches for antenna configurations are accomplished using an under-resolved grid size, and a frequency shift of about 8% is expected. Other verified measurements show this to be a good rule of thumb.

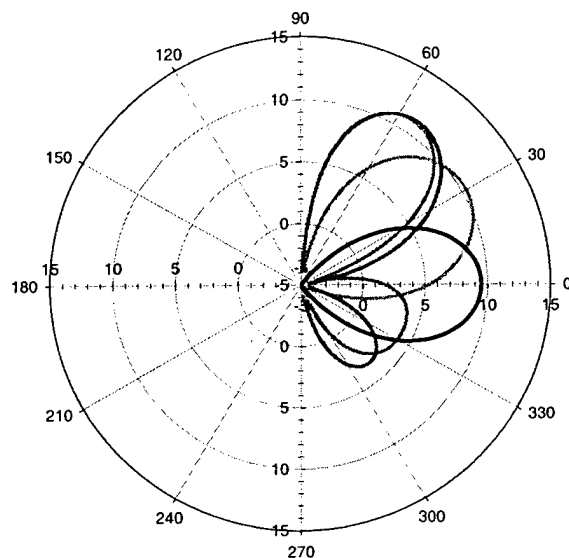


Figure 9. Demonstration of steering from a single feed antenna. The plot shows predicted directive gain for four configurations (0, 30, 45, and 60 degree scan angles) at 1.5 GHz.

The ability of the aperture to steer has also been demonstrated through simulation and verified through measurement. Note that the steering is accomplished from a single feed point and without phase shifters. Figure 9 shows four steered patterns generated at 1.5 GHz through simulation (these plots show directive gain). The desired steer angles are 0 degrees (broadside), 30 degrees, 45 degrees, and 60 degrees. These patterns were generated in the presence of an infinite ground plane 6 cm behind the aperture (this ground plane spacing is used for all subsequent results pertaining to a single feed aperture). The gain for all configurations is between 10 and 11 dB, except for the broadside case. The directivity for the

broadside case is slightly lower, as the broadside case represents a wideband configuration (1.0-1.5 GHz, 40% bandwidth) while the others are narrow band configurations (5% bandwidth).

Experimental verification of a 45 degree steered pattern is shown in Figure 10. The plot shows the predicted (as modeled for the purpose of the configuration search) and the measured directive gain for a “hard-wired” configuration. The comparison is made at two different frequencies because of the phase shift alluded to earlier. Note that both patterns are steered to 45 degrees. The discrepancy in the directive gain (and thus the width of the main lobe) is due to the decrease in frequency of operation (and thus a decrease in gain for the same size aperture) for the measured pattern as compare to the modeled pattern.

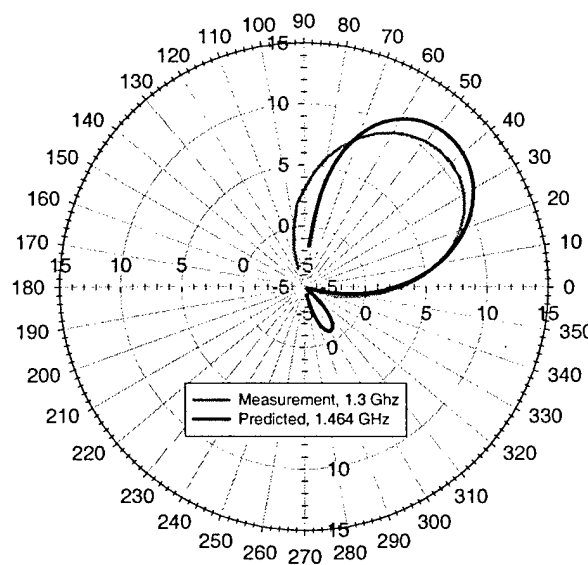


Figure 10. Design prediction and measurement for a 45 degree scan angle at 1.3 GHz.

3. Switches

The choice of switch has a great impact on aperture performance. As previously mentioned, switch capacitance and resistance are the two main contributors to a loss of performance as compared to “perfect” switches. The effect of the capacitance is displayed in Figure 11, which plots the realized gain for two 1.75-2.0 GHz configurations - a “perfect switch” configuration and a FET switch configuration. Note that the FET switch clearly does not support operation at these frequencies. A similar FET switch configuration has been shown to be successful in the 1.5-1.75 GHz, indicating that the FET capacitance of 0.45 pF supports operation of the aperture only at frequencies less than 1.75 GHz. GTRI

measured the capacitance of several off-the-shelf RF FETs, but the capacitance of all FETs measured to be in the neighborhood of 0.45pF. Researchers speculate that the packaging of the FET is the limiting factor in achieving a low capacitance.

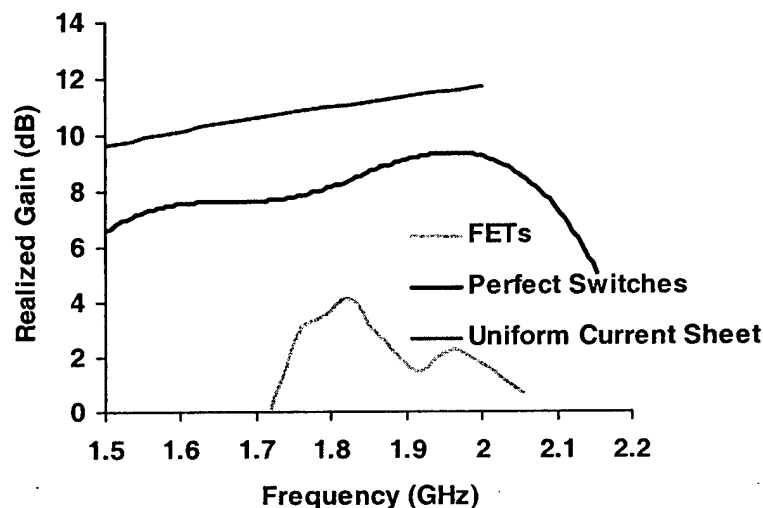


Figure 11. Comparison of designs using a perfect switch and a realistic FET switch model. The plot demonstrates the upper frequency limit of 1.75 GHz for use of FETs.

FET switch resistances were measured to be 4 Ohms and greater, depending on the FET. The degradation in performance due to a 4 Ohm closed state resistance has been quantified and found to be greatest for wideband configurations. For example, Figure 12 shows the predicted gain of two 1.0-1.5 GHz configurations. The plot on the right corresponds to a configuration for perfect switches, the plot on the left corresponds to the FET switches. Note that the gain decreases by an average of about 0.5dB across the band with the insertion of the FET, although the loss is as high as 1dB at 1.5 GHz. Other simulations show that this loss is smaller for narrow band configurations. Configurations with bandwidths of 5% show negligible loss due to the switch resistance.

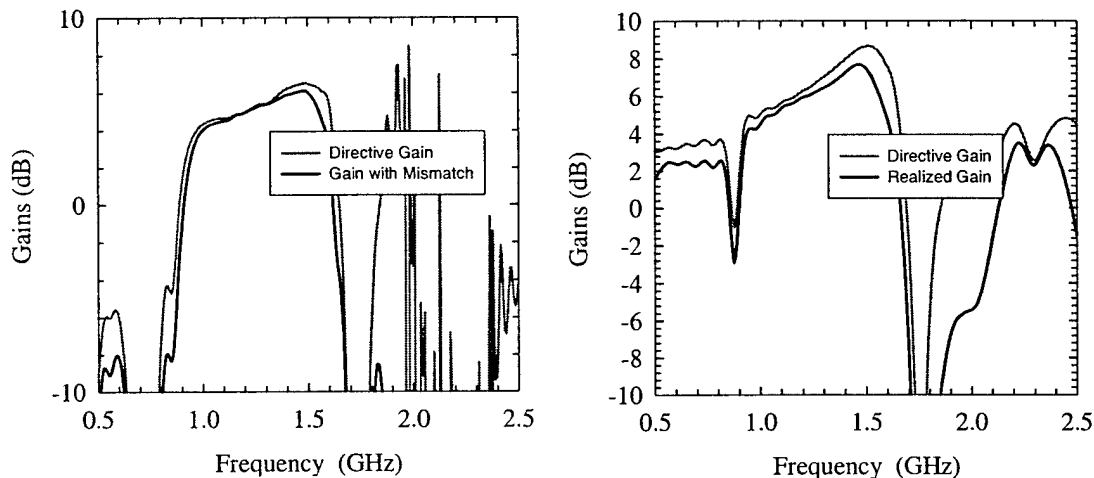


Figure 12. Effect of switch resistance on antenna performance. The simulation plotted on the left modeled the switches with 4 ohms of resistance, while the plot on the right assumed perfect (0-ohm) switch resistance.

In order to improve the characteristics of the switch, the Georgia Tech Electrical and Computer Engineering Department is developing a MEMS switch. As explained in the introduction, this switch is magnetically activated and electrostatically latched. The latch operation is to be accomplished using the same logic chip as is used for the FET switches.

GTRI has not reached a point in the development of the MEMS switch to insert it into the aperture, so tests of the MEMS switch have been accomplished using the loop test bed shown in Figure 13. The gray strips are conductor, the light gray features are the switches, and the dark traces are the resistive traces that activate the switches. Note that the loop test bed is designed to be sitting on top of a reflection plane in the lab (the reflection plane is shown as a dark strip at the bottom), thus this test fixture represents a full loop of circumference 60 mm. An actual photo of one of the MEMS switches is shown to the right of the figure. The switch is 1.2 mm long.

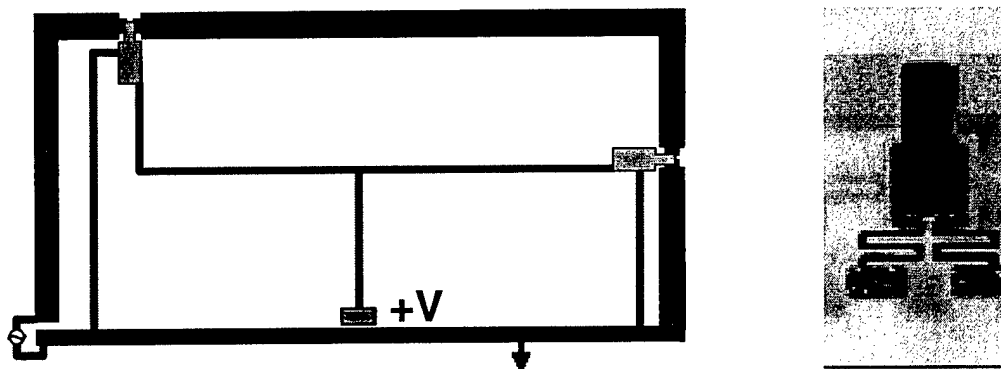


Figure 13. Photograph of a single MEMS (right) and a picture of the test figure used to characterize the MEMS on the GTRI image plane.

Opening the switches will make the test bed act as a monopole, while closing the switches will make the test bed act as a loop. Figure 14 shows a comparison of the input impedance of this fixture compared to the same fixture with no MEMS present ("perfect" opens at the switch points). Note that the open impedance of the MEMS matches the perfect open impedance for all frequencies less than about 9.5 GHz, suggesting that the switch isolation is good enough for antenna operation up to that frequency. In addition, the MEMS closed state resistance has been measured to be less than 1 Ohm, and operating MEMS have been manufactured that pass over 1 Amp of current.

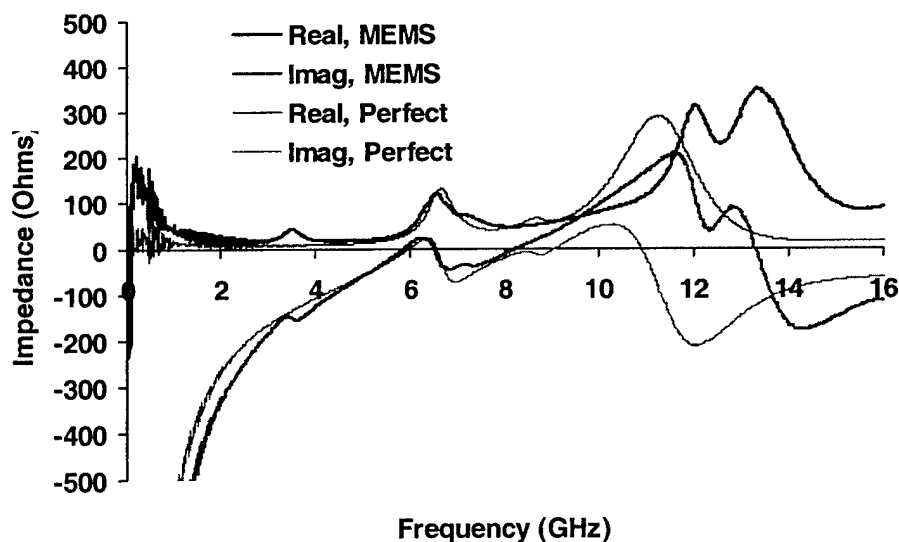


Figure 14. Comparison of antenna input impedance with MEMS in the open state and with no switch present (perfect open).

4. Switch Control

By far the greatest engineering challenge in bringing the reconfigurable aperture to reality is the development of a switch control system that does not significantly interfere with antenna performance. Figure 15 illustrates the three methods currently under development. The three methods are illustrated using a single “stick” of pads, but each strategy is designed to operate for the entire aperture.

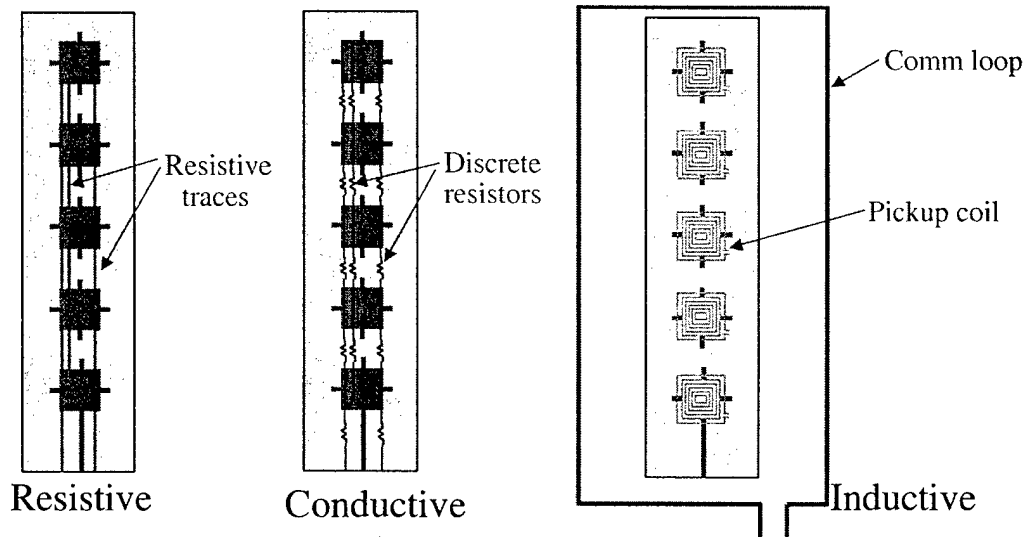


Figure 15. Three methods for controlling and powering the switches in the aperture are currently under investigation.

The first method considered for switch control uses resistive traces to provide the control signal (and power) to the logic chips driving each switch site. Since the current demand of the chips is so small ($\sim 10 \mu\text{A}$) they can be controlled through lines with resistances in the tens of Kohms. At those values, simulations indicate that the control lines would have negligible impact on the antenna's radiation characteristics. A second method was conceived in response to the difficulty of fabricating boards with the requisite high-resistance control lines. In this method, the resistive lines are replaced with conducting lines that are interrupted with discrete resistors. The discrete resistors offer virtually any value of resistance that circuit operation will permit. However, the conductive grid lines induce a frequency shift to the antenna operation as well as narrowing the achievable bandwidth with a given configuration. A third means of controlling the switches was devised to provide a method that did not introduce more conducting structures on the surface of the aperture. With this method, the solid conducting pads are replaced with small pickup coils that inductively couple power and control signals from a communications loop that surrounds the entire aperture.

The current test coupons being investigated are all designed to work with FET switches that effectively limit operation to frequencies below 2 GHz. Concurrent efforts are directed toward development of integrated circuitry that will extend FET performance to 5 GHz, and MEMS switches for operation up to 10 GHz. Both approaches will still require control signals and power, so it is germane to consider the problems of scaling the control strategies to higher frequencies.

4.1 Resistive control lines

Figure 16 shows the results of simulations to determine the impact of various values of resistive grid lines for control of the switches. These simulations indicate that traces with a resistance on the order of $10 \text{ K}\Omega / \text{cm}$ should have negligible impact on the antenna performance up to 2 GHz. As operation is extended to higher frequencies, higher resistance values per unit length will be required (i.e., constant values per wavelength). Thus, any difficulty achieving functional control lines at higher resistance values will only be magnified. However, measurements of actual traces with resistance near $1 \text{ K}\Omega / \text{cm}$ showed an additional loss in the aperture about 1.5 dB beyond what was predicted. Efforts are currently under way to measure a test coupon with $8 \text{ K}\Omega / \text{cm}$ resistive traces to determine if the offset from prediction continues to be an issue at the higher resistance values.

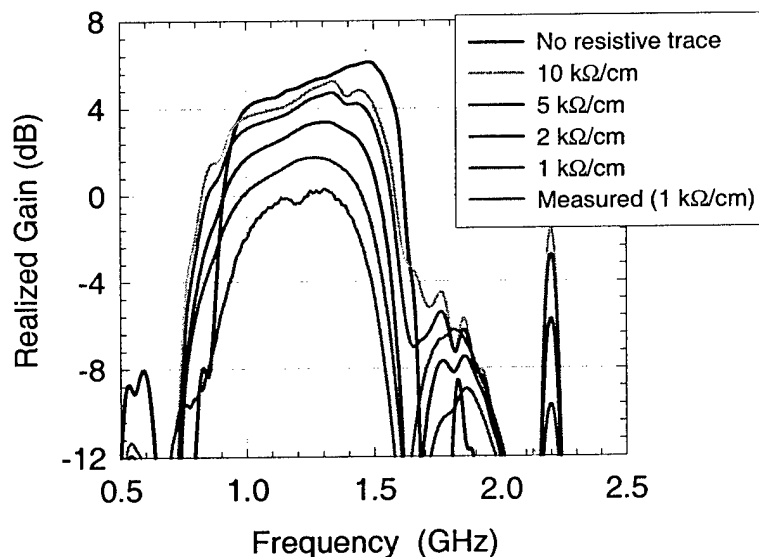


Figure 16. Predicted loss of antenna efficiency due to various values of resistive control line traces, along with measured values at $1 \text{ K}\Omega / \text{cm}$.

4.2 Conductive control lines with discrete resistors

Fabrication of test coupons with resistive traces involves etching resistive foils that are laminated to Cu-clad substrates. Linear resistance values are controlled by choice of the surface impedance of the foil layer and the line widths to which the traces are etched. As noted earlier, the higher resistance values tend to stress the capability of standard printed circuit fabrication processes. Use of discrete resistors permits resistance values as high as desired. However, the presence of the associated conducting lines introduces additional capacitance that results in a significant downward frequency shift in the performance of a configuration compared to the predicted performance with no conducting grid lines present. In addition, the conducting lines restrict the achievable bandwidth with a given configuration. This is illustrated in Figure 17, where a configuration with conducting grid lines is measured for comparison to the design with no grid lines. The design goal was an operating band from 1.2 – 1.5 GHz. The actual frequencies of operation are shifted down by about 20%, reducing the operating bandwidth from 300 MHz to about 250 MHz.

For operation over smaller instantaneous bandwidths, however, this strategy may be the most easily scaled to higher frequencies.

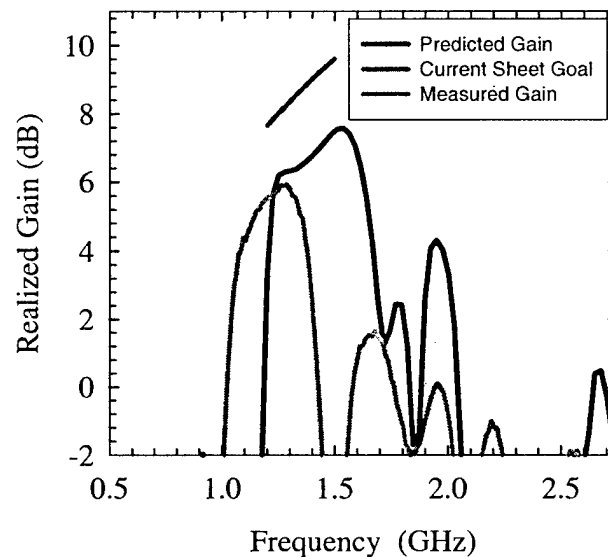


Figure 17. Effect on the performance of a design configuration when conducting grid lines and discrete resistors are present on the board.

4.3 Inductively coupled control signals

The third strategy for coupling of power and control signals to the logic chips uses an external communications loop around the entire aperture. A major advantage

of this approach is that it keeps perturbing structures such as the conductive grid lines off of the board and out of the aperture. Of course, the presence of the communication loop will impact configurations steered far from broadside. The control signal / power is coupled to the pads at 13.6 MHz, far from intended operating bands of 800 MHz and above. In order to achieve the coupling, a pickup coil surrounded by a solid conducting perimeter ring replaces each solid conducting pad. Without the ring, the pad doesn't radiate efficiently. Unfortunately, with the ring, control signals don't couple efficiently. The solution was to introduce a cut in the perimeter ring and bridge it with a capacitor. Measurements to date show effective coupling of signals with moderate currents in the communication loop (100 mA input currents and up to 1 A actually present in the loop). The inductive coupling strategy has been successfully employed in the reconfigurable test beds at frequencies up to 1.75 GHz (again limited by the FET switches). However, scaling to higher frequencies will present difficulties, because the requisite smaller pickup pads will not have enough area to accommodate as many loops, and so will not as effectively couple the power necessary to drive the control circuits.

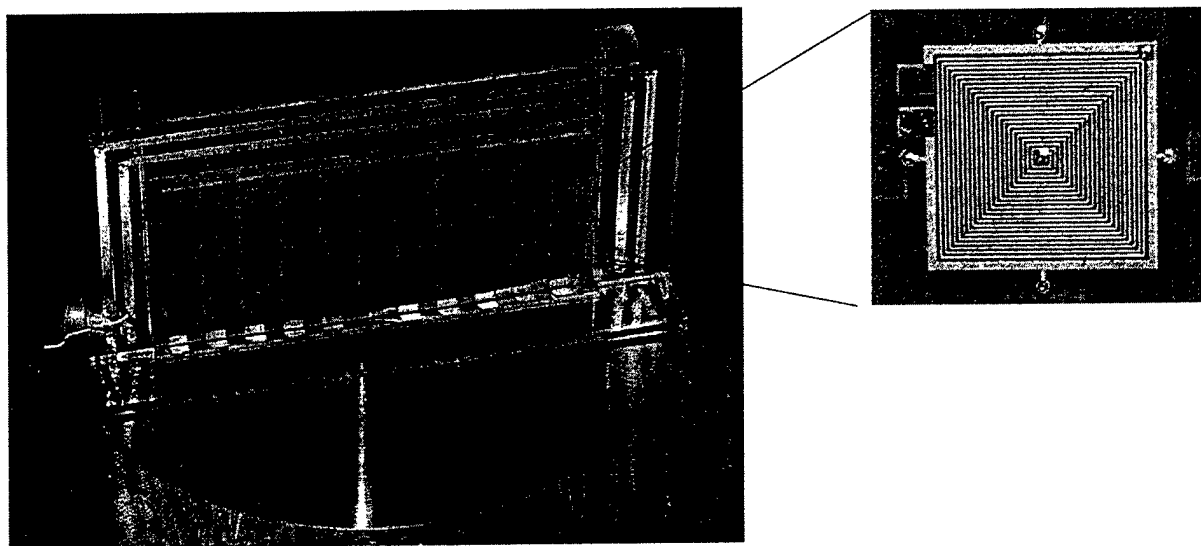


Figure 18. Photo of the inductive test coupon showing the external comm. loop and a close-up of the individual element / pickup coil. The inset shows the break in the perimeter ring around each pad where a capacitor is mounted to maintain simultaneous inductive coupling and efficient radiation at RF frequencies.

4.4 Control strategies: projected performance

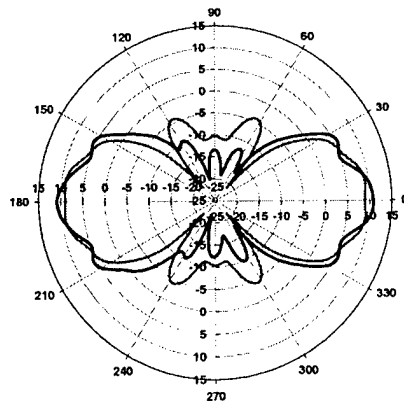
GTRI expects that three test beds, one for each of the switch control strategies discussed above, will be completed for testing by late September, 2001. From simulation the expectation is that the resistive test bed will suffer some small resistive losses and that the conductive grid line test bed will not be able to achieve as wide an instantaneous bandwidth as the other two strategies. The performance of the inductive test board will depend on the ability of the inductive pad to perform as well as a solid pad.

5. Arraying Reconfigurable Elements

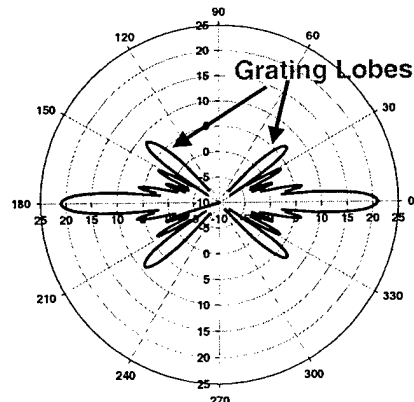
The previous discussion has focused on the use of the reconfigurable aperture as a single feed antenna. There are also applications for this aperture as an element in an array. The advantage of using a reconfigurable element are two-fold: 1) the embedded element pattern of each element can be steered concurrently with the typical phase steering of the array for the purpose of minimizing scan loss and decreasing loss to grating lobes (for sparsely fed arrays); 2) neighboring reconfigurable elements can be connected through switch points so that, if desired, the array can be configured to be a connected array, allowing operation at frequencies much lower than is typical for traditional arrays at the same feed density. For operation at low frequencies, the element architecture can be configured for minimal mismatch in the presence of a closely spaced ground plane (the ground plane spacing most likely being determined by higher frequencies).

In order to illustrate the first of these advantages, the left plot of Figure 19 shows the measured and predicted embedded element pattern for a single element in an array. The element configuration was designed for 7-8 GHz broadside operation (plots are for 7.5 GHz), and the configuration was "hard-wired" for measurement. Note that there was no ground plane for this design, thus the pattern shoots energy to the front and back. The design of the configuration was accomplished using the same genetic search as is used for the single feed configurations, but the performance calculation that is accomplished for each candidate in the search is accomplished using a periodic code, thus assuming an infinite array. The array spacing in this case is 6 cm, which is $3\lambda/2$ in this band. Thus, this is a sparse array.

The plot to the right of Figure 19 displays an artificially constructed array pattern generated by combining the measured embedded element pattern with the calculated array factor for a 5 X 5 array. Note the presence of the grating lobes. Because the search process is seeking a configuration with maximum broadside gain, the embedded element pattern tends to have a "tucked-in" shape that tries to minimize the loss of power into the grating lobes.



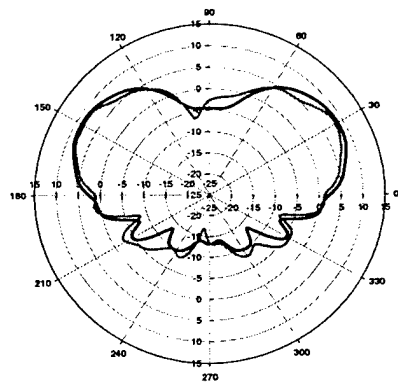
**Embedded Element Gain-with-Mismatch
Measured, Predicted**



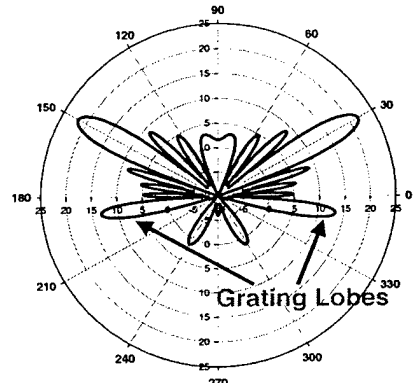
**Measured Element Pattern
Combined with Array Factor**

Figure 19. Left, measured and predicted patterns for an embedded element at 7.5 GHz. Right, projected array performance using the element in a sparse array to squelch grating lobes.

The ability to minimize loss into the grating lobes is most effective for steered configurations. Figure 20 illustrates the embedded element pattern for a 30 degree steered case for the same 7-8 GHz band. Note that the reconfigurable element steers the pattern, which minimizes the energy directed into the grating lobes. For this case the grating lobes are about 9dB below the main peak. Note that if a similarly spaced array used a typical un-switched broadside element, the grating lobe would actually peak higher than the main lobe. Thus, the reconfigurable element allows for sparse arrays that effectively manage loss due to grating lobes.



**Embedded Element Gain-with-Mismatch
Measured, Predicted**



**Predicted Array
Gain-with-Mismatch**

Figure 20. Left, measured and predicted patterns for an embedded element at 7.5 GHz, steered to 30 degrees. Right, projected array performance using the element in a sparse array.

In order to illustrate the ability of the reconfigurable element to perform over extremely wide bandwidths in an array environment, eight broadside configurations were designed for operation from 800 MHz to 10 GHz. Figure 21 shows the predicted realized gain of these configurations as compared to the directivity of a uniform current sheet of the same size. For each of these configurations the element spacing is 6 cm. These designs were accomplished in the presence of a ground plane spaced 1.2 cm behind the aperture. The performance for the 0.8 – 1.4 GHz, 1.4 – 2.5 GHz, and 7 – 8 GHz configurations were verified by measurement.

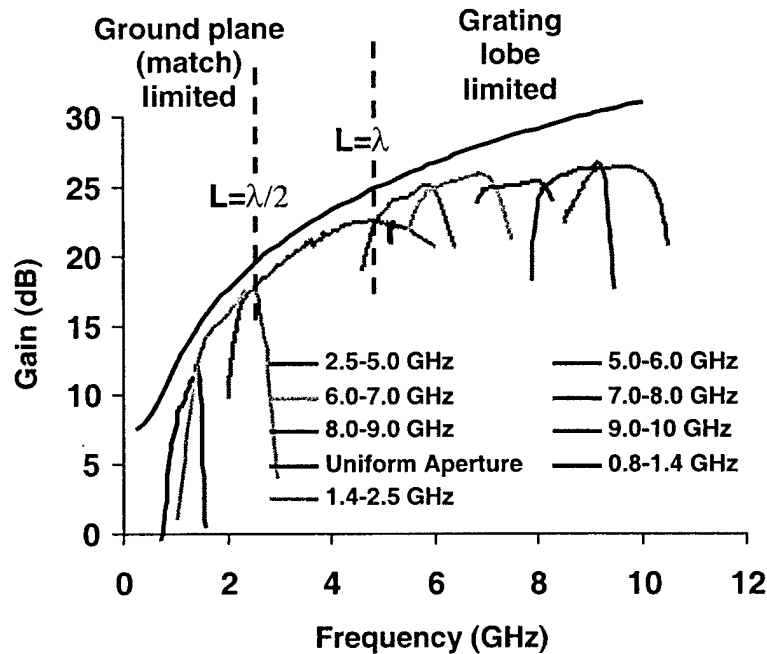


Figure 21. Predicted realized gain for eight configurations of a 5 x 5 array of reconfigurable elements with a 6 cm square lattice spacing (L).

The bands of operation naturally divide themselves into three regions. The region below 2.5 GHz corresponds to frequencies for which the dominant role played by reconfiguration is to reduce reflections at the feed in the presence of the closely spaced ground plane. Thus, the bandwidth is limited in order to achieve low reflection losses. The frequency region between 2.5 and 5 GHz represents the typical broadband aperture region, where the ground plane is placed at a sufficient distance that mismatch is not a problem, and where the element spacing is sufficient so that no grating lobes propagate. Above 5 GHz grating lobes appear, and at frequencies above 5 GHz the reconfiguration is used to minimize the energy that goes into the grating lobes. Over a wide bandwidth this cannot be achieved, since the grating lobes change their position with frequency. Thus, the

bandwidth at these high frequencies is limited by the ability to effectively squelch energy in the grating lobes. The reader will notice that this operation becomes less effective at frequencies above 8 GHz, at which point the aperture gain begins to level off. GTRI researchers speculate that improvement at these very high frequencies can be accomplished for even narrower bandwidths.

6. Conclusion

This paper has reviewed the expected performance of a reconfigurable element, both as a single-feed antenna and as an element in an array. In general, this element has the ability to steer its pattern from a single feed point and optimize its architecture for different bands of operation. The performance of the aperture is determined by the switches used to open and close the connections between the conducting pads that make up the aperture. We have considered two switch types: FETS, which have limited performance but which are easily available, and a MEMS switch, which is presently under development. The greatest engineering challenge of making this architecture a reality is the development of an effective way to control the switches without interfering with the performance of the antenna. Three suggested methods for accomplishing this were outlined in the paper. GTRI expects to have a test bed for each of these architectures fabricated by late September.

7. Acknowledgement

Much of the work described in this paper was funded by DARPA through the US Army CECOM. The authors would like to thank Barry Perlman and Ernie Potenziani at CECOM, Larry Corey from DARPA, and J.K. Smith, formerly of DARPA for continued support, encouragement, and useful suggestions.

STACKED RECONFIGURABLE ANTENNAS FOR SPACE-BASED RADAR APPLICATIONS

J. Hazen, R. Clark, P. Mayes, and J. T. Bernhard
Electromagnetics Laboratory
Department of Electrical and Computer Engineering
University of Illinois at Urbana-Champaign
Urbana, IL 61801

Abstract: This paper demonstrates a new stacked antenna that will serve as the radiating element in a reconfigurable array. In its final form, this array will use RF MEMS switching to provide operation over two bands, a wide range of polarizations, and multiple or scanned beams. The basic antenna structure consists of a microstrip bowtie with a mixed dielectric substrate. Polarization variability at each feed point is supported by orthogonal placement of two balanced bowtie elements that can be driven to produce linear, elliptical, or circular polarization. Array operation in the lower band requires that the upper-band elements be disconnected via switches below the ground plane. In this stacked configuration, the upper-band elements act as floating parasitic elements for the lower-band elements, slightly broadening the impedance bandwidth. Operation of the upper-band elements requires that the lower-band elements be grounded via switches. In this configuration, the lower-band elements act as the ground plane for the upper-band elements. Measured impedance and radiation characteristics of the stacked configuration over both operating bands are presented and discussed.

1. Introduction

A number of groups have recently shown interest in reconfigurable antennas for providing multi-band radar and/or communications over the same radiating aperture. These antennas include switched arrays composed of quasi-Yagi and traditional microstrip patches that alternately provide either broadband endfire operation or narrowband broadside operation [1]. Other approaches use Micro-ElectroMechanical Systems (MEMS) switches to change the resonant length of narrowband radiators such as dipoles [2] slot-ring antennas [3], and resonant slots [4]. In contrast, two groups propose use of switches[5] or frequency selective volumes [6] to change the location of ground planes to tune antennas across

frequency bands. One group is developing fragmented apertures with each pixel controlled by MEMS switches to create both narrowband and broadband antenna operation [7]. Another group implemented a fixed antenna configuration with dual-polarization using a stacked dual-band slot and patch antenna to supply moderate bandwidth for each band [8]. Each of these techniques provides a reconfigurable antenna aperture, but none demonstrate the simultaneous needs for large instantaneous bandwidth, dual-polarization and array reliability using minimum RF MEMS switch density in a prototype antenna.

A proof-of concept antenna with a dual-band reconfigurable aperture for use with isolated MEMS switches is presented in this paper. The S and X bands were chosen for demonstration, though antennas radiating at other microwave bands can be designed using a similar technique. This antenna can provide up to 25% impedance bandwidth at both bands, more than double that of previously reported microstrip bowtie antennas [9-10].

Section 2 presents the conceptual analysis and design of the antenna. Fabrication issues are presented in Section 3, and simulation and measured results are found in Section 4. The final section discusses the results and directions for future work.

2. Conceptual Analysis and Design

Microstrip patch and slot antennas have been the antenna of choice for most of the antennas mentioned previously, with their low profile and low cost of fabrication being the main advantages. Bowties and stacked antennas with multiple dielectric substrates [9-12] have been repeatedly demonstrated to produce high bandwidth. In light of these advantages, a stacked balanced bowtie with a mixed dielectric substrate was designed as shown in Figures 1 and 2. The antenna dimensions were refined numerically using IE3D [13], a method of moments simulator. Coaxial feeds drive each element, and MEMS switches located behind the ground plane will switch between antenna arrays. When driving the lower array of S-band elements, the X-band elements are disconnected via MEMS switches so that they behave as parasitic radiators. When driving the top array of X-band elements, the S-band elements are switched to ground and act as the ground plane for the X-band array [14].

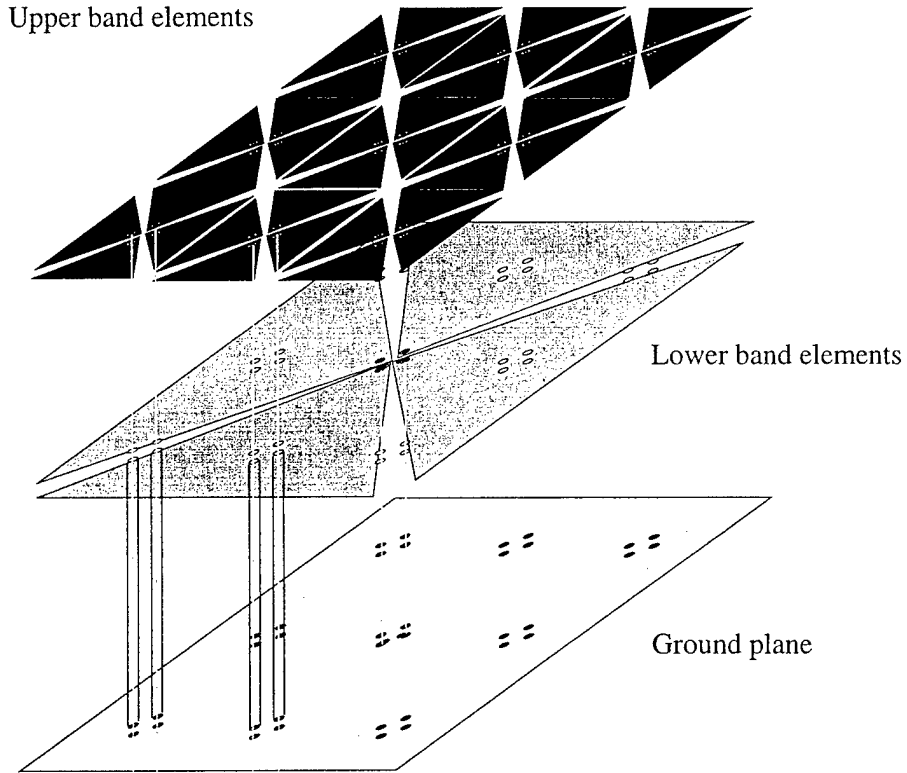


Figure 1: Stacked reconfigurable array concept. Lower and upper band elements are alternatively activated using RF MEMS switches below the ground plane.

2.1 Single Linearly-Polarized Element Design

The basic antenna structure, shown in Figure 2, consists of a balanced bowtie antenna with a mixed dielectric substrate composed of a polymer material ($\epsilon_r = 3.0$) and air ($\epsilon_r = 1.0$). The specific dimensions for the two sizes of antenna elements necessary to provide switched band operation from 3 GHz and 8 GHz are provided in Table 1.

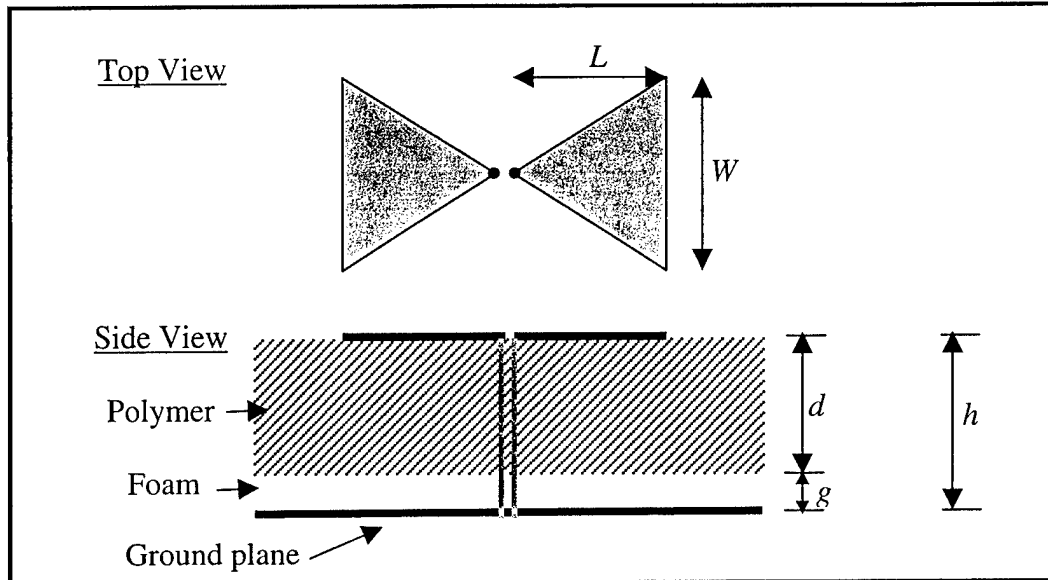


Figure 3: Basic structure of reconfigurable array antenna element consisting of balanced bowtie element with mixed dielectric substrate materials.

Dimension Variable	S Band Element	X Band Element
L	34 mm	11.5 mm
W	72.8 mm	19.2 mm
s	6.8 mm	1.8 mm
p_i	0.9 mm	0.3 mm
p_o	3.6 mm	1.2 mm
d	8.25 mm	3.75 mm
g	2.75 mm	0.75 mm
h	11.0 mm	4 mm

Table 1: p_i is the coaxial feed inner diameter, and p_o is the outer diameter of the coaxial cable. S is the spacing between the feed centers, also the vertex of the triangular patch.

The probe diameter (p_i) greatly affected the bandwidth and center frequency of the antenna in the simulations performed. Feeds also needed sufficient separation to reduce coupling between the bowtie elements and to preserve bandwidth. However, the separation between the balanced feeds (S) did not affect the bowtie operation as much as the probe diameter -- for small changes-- so it was adjusted as necessary for fabrication requirements.

Since the S-band feeds must not interfere spatially or electrically with the X-band feeds, and since the coaxial shields to the X-band feeds must be soldered to the S-band patches, the S-band antenna geometry depends on the geometry of the X-band array. The balanced feed for the S-band elements was spaced so that the center X-band coax could fit in between. Also, the width of the S-band bowtie was adjusted so that X-band feed shields on the diagonals would solder to the patch. Therefore, the X-band elements should be designed first.

2.2 Stacked S-band Element with Uniformly-Spaced X-band Array

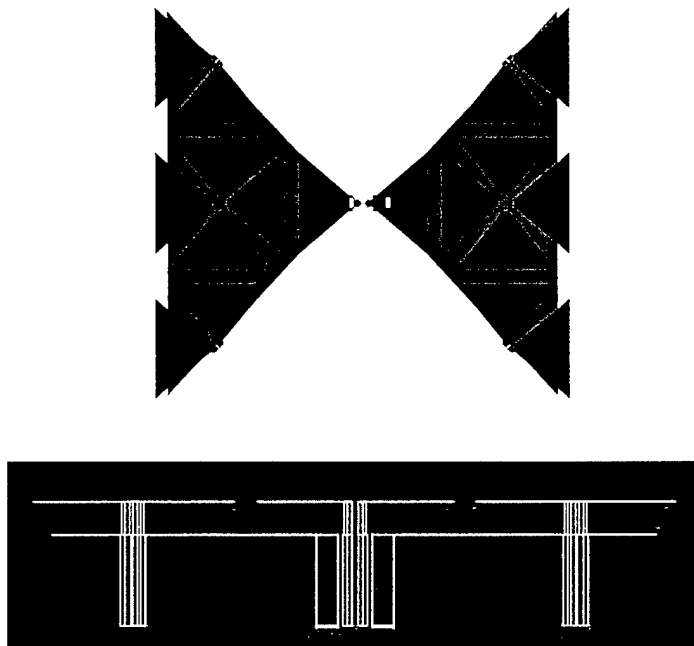


Figure 4: Top and side view of a stacked configuration with one S-band bowtie element.

Since an array of X-band elements covering an S-band bowtie would be too computationally intensive for the IE3D program to solve, the X-band elements were simulated over an infinite ground plane. The following antenna was simulated in IE3D for its S_{11} parameters.

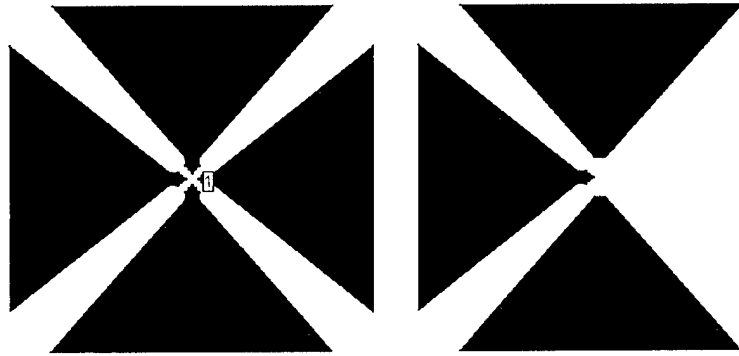


Figure 5: Top view of X-band array simulation.

The elements that would play the largest role in determining the S_{11} were identified as the elements pictured above. Coupling between feeds and patches affected the S -parameters significantly. From several of these simulations, the element spacing was chosen at 27.8mm.

3. Fabrication

For fabrication, three sheets of 128 mil Liquid Crystal Polymer (LCP) laminate and one sheet of 69mil LCP laminate were used to assemble the substrate for the lower band element. The 128 mil boards were fabricated using an uncontrolled process, so thickness varied by at least 20 mil over the antenna aperture. Two 128 mil boards were attached around the 69mil board, with one of them being milled for the patch antenna for the S-band antenna. One 128 mil board was milled for the X-band bowtie array. Unwanted copper was chemically removed using HCL and HNO_3 .

Nylon screws were used to fix the stacked antenna together and fix the antenna to its stand in the antenna testing range. The screws were placed at the diagonals of the S-band bowtie. Nylon spacers were used to create an air gap rather than use foam dielectric to simplify prototype fabrication.

Feeds were created using 3.6 mm and 1.2 mm diameter 50 ohm coaxial cables. SMA connectors were soldered to the 3.6 mm coax by hand, whereas the 1.2mm coax had SMA connector soldered on industrially. The outer shield was stripped on both coaxial cables to the patch height mentioned above.

4. Measurement Results

Several versions of each design have been tested. Here we present some of the measurements and others will be presented at the conference. Both lower and upper band elements were tested for impedance bandwidth and radiation characteristics in a number of configurations. 180° phase shifts between the two inputs of the antennas were accomplished using 180° hybrid couplers. The results of the impedance bandwidth measurements of each half-bowtie antenna are provided in Figures 6 and 7 for configurations with only one bowtie present (as depicted in Figure 3). Figure 6 also includes simulation results using IE3D [13]. Each antenna is intended to have a 25% impedance bandwidth as defined by a 2:1 VSWR. The measured bandwidths for the lower and upper frequency bands are 23% and 25% respectively with small frequency shifts away from the intended bands. The differences between the intended operation and the measurements were caused by fabrication inaccuracies in the heights of the foam layers of the substrates.

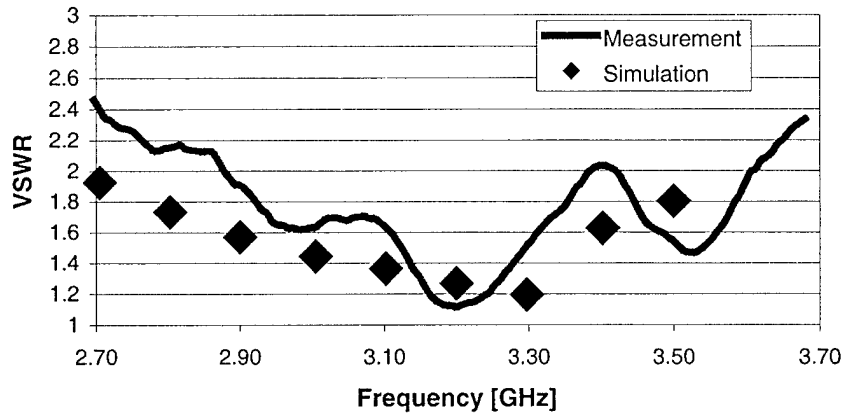


Figure 6: Measured and simulated VSWR for the lower band (2.7-3.5 GHz) antenna.

Figures 8 and 9 provide representative E-plane and H-plane radiation pattern measurements of the two antennas near their midbands. Across their entire frequency bandwidths, all of the patterns exhibit good broadside characteristics that support scanning to 45 degrees and reasonable cross-polarization levels.

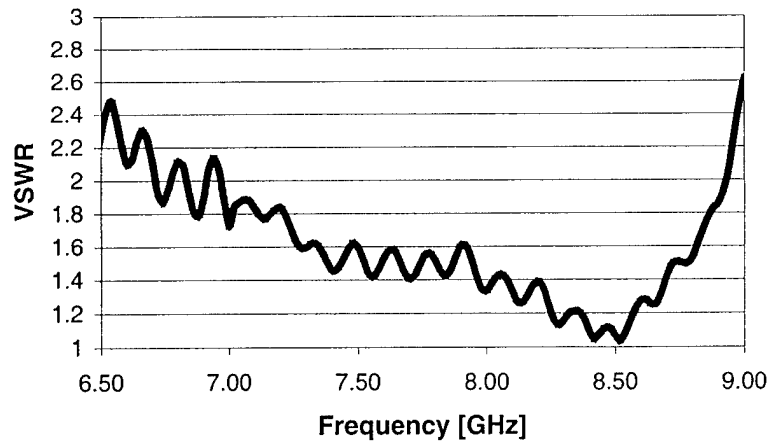


Figure 7: Measured VSWR for upper band (7-9 GHz) antenna.

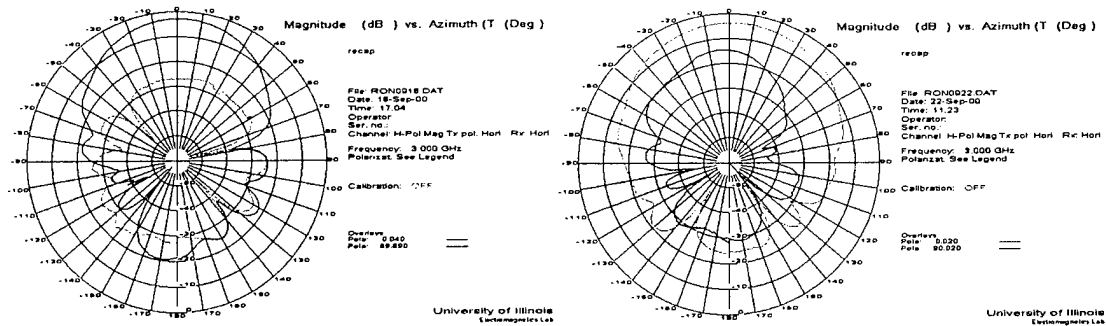


Figure 8: E-plane (left) and H-plane (right) radiation pattern measurements for the lower band antenna at 3.0 GHz.

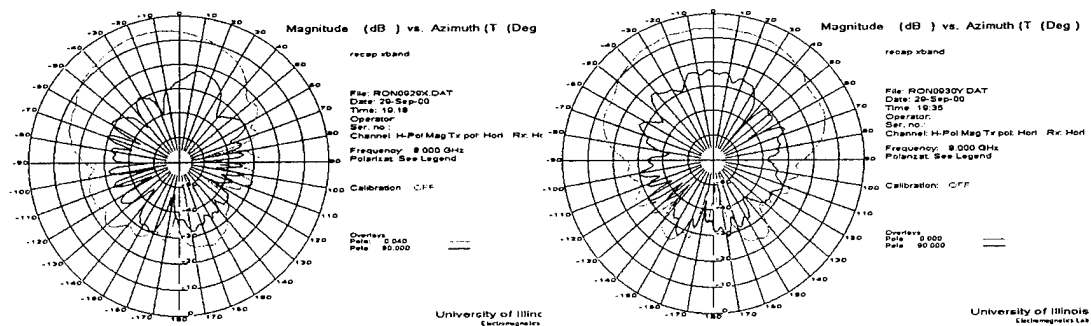


Figure 9: E-plane (left) and H-plane (right) radiation pattern measurements for the upper band antenna at 8.0 GHz.

Fabrication and measurement of the dual-bowtie configuration in the lower band proved more difficult, since the feed structure is difficult to solder by hand. Preliminary return loss data from one port of a full dual bowtie element is presented in Figure 10. Differences between measured and simulated data on this prototype may be due to inconsistent substrate properties (both thickness and permittivity) as well as the fabrication sensitivity of the vertical feed probes.

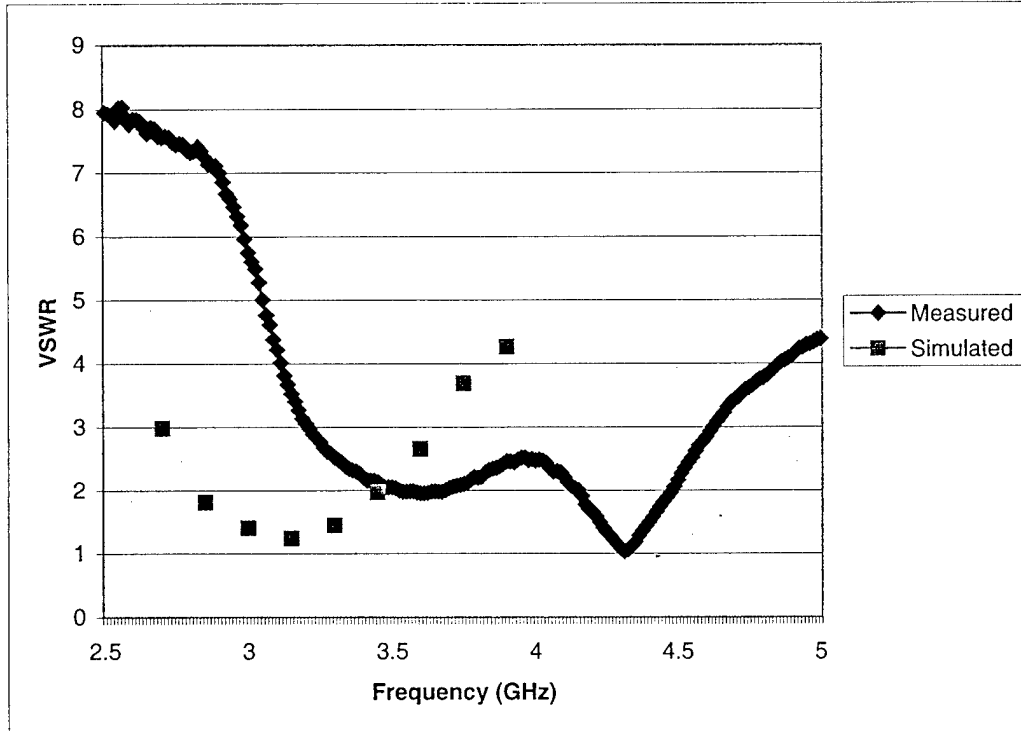


Figure 10: Measured and simulated VSWR for a one-half bowtie element in a quad configuration.

5. Discussion and Directions for Future Work

A stacked reconfigurable antenna with multiple polarizations with reasonable bandwidth is presented in this work. This paper has included the design process, fabrication issues and preliminary test results. Measurements of the laboratory prototype in the stacked configuration prove the viability of the concept. Additional measurement results for both frequency bands will be presented at the conference.

In the future, this concept will be applied to higher frequency bands where the required substrate thicknesses are more practical than used in this demonstration.

Strategies for minimization of coupling between contiguous array elements and mitigation of blind angles in large arrays are currently being investigated. Additionally, a study of feed point location sensitivity of upper element characteristics relative to the lower element geometries is underway.

6. Acknowledgments

This work was sponsored in part by the DARPA RECAP Program under grant # F33615-99-C-1519.

7. References

- [1] J. Sor, Y. Qian, M.F. Chang and T. Itoh, "Multi-mode microstrip antennas for reconfigurable apertures," *Proc. IEEE/URSI Symp. on Antennas and Propagation*, **AP-1**, pp. 318-320, 2000.
- [2] J. H. Schaffner, R. Y. Loo, D. F. Sievenpiper, F. A. Dolezal, G. L. Tangonan, J. S. Colburn, J. J. Lynch, J. J. Lee, S. W. Livingston, R. J. Broas, and M. Wu, "Reconfigurable aperture antennas using RF MEMS switches for multi-octave tenability and beamsteering," *Proc. IEEE/URSI Symp. on Antennas and Propagation*, **AP-1**, pp. 321-324, 2000.
- [3] K. C. Gupta, J. Li, R. Ramadoss, C. Wang, Y.C. Lee and V.M. Bright, "Design of frequency-reconfigurable rectangular slot ring antennas," *Proc. IEEE/URSI Symp. on Antennas and Propagation*, **AP-1**, p. 326, 2000.
- [4] R. Gilbert, D. Kopf, and J. Volakis, "A reconfigurable slot aperture," *Proc. IEEE/URSI Symp. on Antennas and Propagation*, **URSI**, p. 97, 2000.
- [5] J. C. Veihl, R. E. Hodges, D. McGrath, and C. Monzon, "Reconfigurable aperture decade bandwidth array," *Proc. IEEE/URSI Symp. on Antennas and Propagation*, **AP-1**, pp. 314-317, 2000.
- [6] R.E. Diaz, J. T. Aberle, and W. E. McKinzie, "TM Mode Analysis of a Sievenpiper high-impedance reactive surface," *Proc. IEEE/URSI Symp. on Antennas and Propagation*, **AP-1**, pp. 327-330, 2000.
- [7] J.C. Maloney, M. P. Kelser, L.M. Lust, L.N. Pringle, T. L. Fountain, P. H. Harms, and G.S. Smith, "Switched fragmented aperture antennas," *Proc. IEEE/URSI Symp. on Antennas and Propagation*, **AP-1**, pp. 310-313, 2000.
- [8] R. Pokuls, J Uher, and D. M. Pozar, "Dual-Frequency and Dual-Polarization Microstrip Antennas for SAR Applications," *IEEE Trans. Antennas Propagat.*, vol. 46, pp. 1289-1296, Sept. 1998.
- [9] S. Uysal, M. S. Leong, and C. H. Ng, "Bowtie patch antennas and simple arrays for wireless indoor communications," *IEEE Trans. on Microwave Theory & Techniques*, **47**, no. 6, pt. 1, pp. 738-745, June 1999.

- [10] K. W. Loi, S. Uysal, and M. S. Leong, "Design of a wideband microstrip bowtie patch antenna," *IEE Proc.-Microwaves Antennas & Propagation*, **145**, no. 2, pp. 137-140, April 1998.
- [11] R. Q. Lee, K. F. Lee, and J. Bobinchak, "Characteristics of a two-layer electromagnetically-coupled rectangular patch antenna," *Electron Lett.*, vol. 23, pp. 1070-1072, Sept. 1987.
- [12] S. D. Targonski, R. B. Waterhouse, and D. M. Pozar, "Design of wide-band aperture-stacked patch microstrip antennas," *IEEE Trans. Antennas Propagat.*, vol. 46, pp. 1245-1251, Sept. 1998.
- [13] IE3D, version 8.0. Zeland Software Inc.
- [14] R. Bancroft, "Accurate design of dual-band patch antennas," *Microwaves RF*, Sept. 1988.

Broadband Antennas Over Electronically Reconfigurable Artificial Magnetic Conductor Surfaces

Victor C. Sanchez

Titan Systems Corporation - Aerospace Electronics Division, Greenbelt, MD
vsanchez@titan.com

William E. McKinzie III
e-tenna Corporation, Laurel, MD
wmckinzie@titan.com

Rodolfo E. Diaz
Arizona State University, Tempe, AZ
rudydiaz@asu.edu

Abstract: Artificial magnetic conductor (AMC) surfaces allow flush-mounted wire or strip antennas to radiate efficiently by exhibiting both a high surface impedance and a surface wave bandgap over some limited frequency range. In this paper, an electronically reconfigurable AMC is presented which dramatically increases the range of operating frequencies for an AMC device of specified thickness. Broadband planar antennas placed in close proximity to the reconfigurable AMC surface have been shown to radiate efficiently only in the surface wave bandgap of the AMC, and therefore are themselves tuned by the AMC structure. A planar spiral antenna has been demonstrated to tune over more than 3:1 bandwidth in a thickness of one-twentieth of a wavelength ($\lambda/20$) at band-center with instantaneous bandwidths ranging from 5 to 20%.

1. Introduction

An artificial magnetic conductor (AMC) - sometimes referred to as a high impedance surface - is a lossless reactive surface, usually realized as a printed circuit board that inhibits the flow of tangential electric surface current. This approximates a zero tangential magnetic field and results in a high equivalent surface impedance over some finite frequency range. This property allows wire

antennas (electric currents) to be placed flush in close proximity to the surface ($< \lambda/100$ away) without adversely affecting the antenna's input impedance.

AMCs have the second property that both transverse magnetic (TM) and transverse electric (TE) surface waves are cutoff over some frequency range. This property is critical for maintaining good radiation efficiency. When properly designed, the AMC surface wave bandgap will correspond to same frequency band where the AMC exhibits a high surface impedance - thus enabling realization of an efficient, electrically thin antenna structure.

Figure 1-1 shows one AMC embodiment, invented at UCLA in the late 1990's by Dan Sievenpiper et. al. [1-4]. It consists of an electrically thin, planar, periodic structure with vertical and horizontal conductors, which can be fabricated using low cost printed circuit technologies.

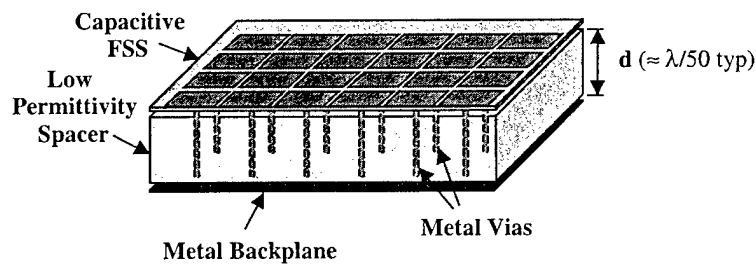


Figure 1-1 - Sievenpiper high-impedance surface.

The impedance properties of an AMC surface can be derived using the simple circuit model shown below in Figure 1-2.

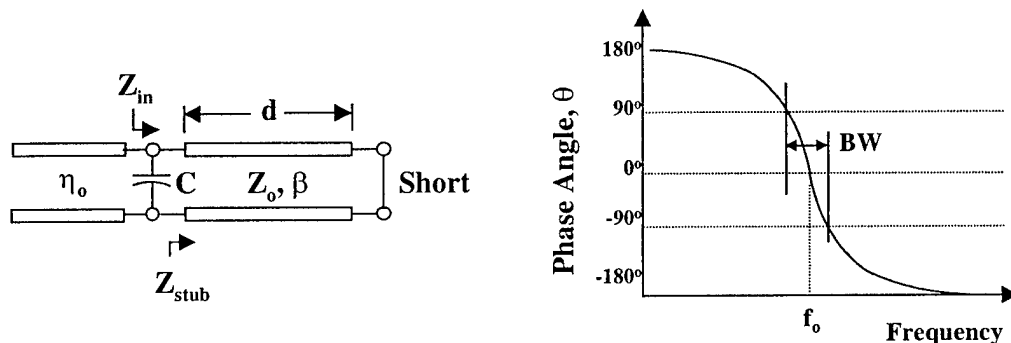


Figure 1-2 - AMC Equivalent Circuit Model and Phase Response.

The fractional bandwidth of a non-magnetically loaded Sievenpiper type AMC structure, defined by the $\pm 90^\circ$ reflection phase points, is described by equation 1

$$\frac{\omega_2 - \omega_1}{\omega_0} = 2\pi \frac{d}{\lambda_0} \quad (1)$$

where d is the thickness of the spacer layer, and λ_0 is the free space wavelength at resonance where a zero degree reflection phase is observed. Thus, to support a wide instantaneous bandwidth, the AMC must be relatively thick. For example, to accommodate an octave frequency range (*fractional BW* = 0.667), the AMC thickness must be over a tenth of a free space wavelength thick ($d = 0.106 \lambda_0$). This thickness is too large for many practical applications. The limiting case of a passive Sievenpiper AMC is one whose thickness is a full $\lambda_0/4$, and whose FSS capacitance has gone to zero. The phase bandwidth for this case (maximum instantaneous bandwidth for an AMC) is 3:1 or 100% fractional bandwidth.

Because antenna applications often do not require a broad instantaneous bandwidth but rather a narrow instantaneous bandwidth that is tunable over a broad frequency range, a viable alternative is to realize an electrically thin AMC structure that is electronically reconfigured. This reconfiguration can be achieved by adjusting the electrical properties of either the spacer layer (using ferrites or ferro-electrics) or by adjusting the capacitance of the FSS region. The FSS capacitance can be adjusted using PIN diodes, MEMs switches or MEMS actuators to adjust overlap area in two-layer FSSs, or via varactor diodes in a single layer FSS configuration [5]. The latter approach is the subject of this paper.

2. Varactor-Tuned AMC Implementation

A reconfigurable AMC (RAMC) realized by integrating varactor diodes into a single layer FSS is illustrated conceptually in Figure 2-1. This figure shows the general layout and the biasing scheme. The basic idea is that the varactor diodes add a voltage-variable capacitance in parallel to the intrinsic capacitance of the FSS layer. In this embodiment, the bias voltage is applied through the RF backplane. The vias, indigenous to the high-impedance surface, are used to route DC bias currents and voltages from stripline control lines buried inside the RF

backplane. RF bypass capacitors are used to decouple RF current at the base of the biasing vias. A ballast resistor of large value is placed in parallel with each diode to ensure an equal voltage drop across each series diode in the strings that are found between the biasing vias and the grounded vias. In practice, varactor diodes can be installed in a “thinned” pattern as shown in Figure 2-1 so as to reduce the number of varactors per unit area, and hence the cost, weight, and complexity. In the example shown, every other row and column is “thinned” for the integration of diodes. However, we could also skip two, three, or N rows of patches between diode strings (so long as the spacing of diodes remains smaller

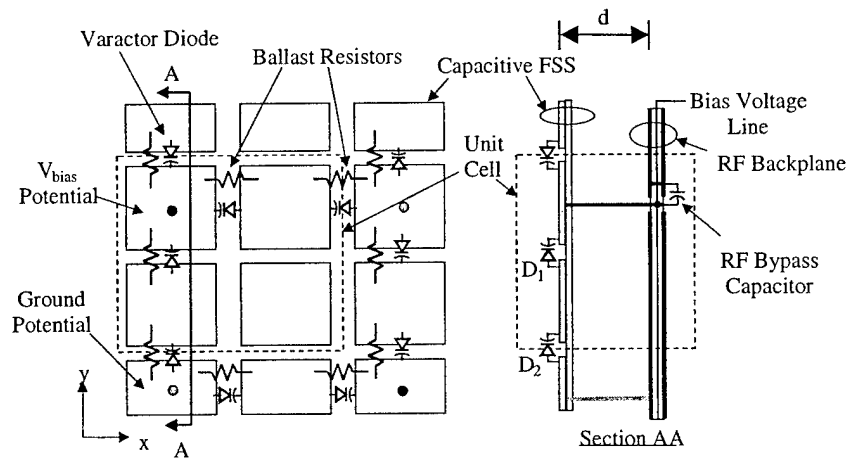


Figure 2-1. Conceptual schematic of varactor-tuned single layer AMC

than approximately one quarter of a free space wavelength).

A physical realization of this approach, where every third unit cell contains a varactor is shown in Figure 2-2. This model was fabricated by sandwiching a 250 mil thick foam core ($\epsilon_r=1.07$) between two printed circuit boards. The upper board is single-sided 60 mil Rogers R04003 board and forms the FSS. Plated through holes are located in the center of one out of every nine square patches, 300 mils on a side with a period of 360 mils. Tuning diodes are M/A-COM GaAs MA46H202 diodes, and the ballast resistors are each 2.2 M Ω chips. The RAMC is assembled by installing 22 AWG wire vias between the FSS board and the RF backplane on 1080 mil centers. The RF backplane is a 3 layer FR4 board, 62 mils thick, which contains an internal stripline bias network. Ceramic decoupling capacitors are used on the bottom side of the RF backplane, one at every biasing via (providing an RF short while maintaining DC isolation from ground). The size of the RAMC substrate is 10"x16"

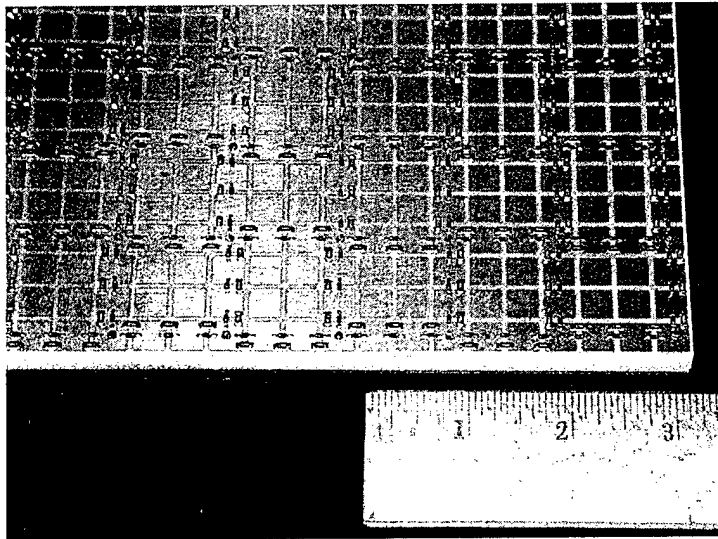


Figure 2-2. Physical realization of varactor-tuned RAMC. Total thickness is 375 mils, excluding surface mount components.

The design was accomplished initially using a simple equivalent circuit model analysis followed by rigorous analysis using a commercial TLM tool (Flomerics' Microstripes) and rigorous surface wave analysis after Diaz, et. al. [6-7]. The equivalent circuit model for the FSS shown in figure 2-3 below included the extended unit cell (with diodes on every third patch) as well as practical implementation effects including diode packaging capacitance and necking inductance at the leads of each diode).

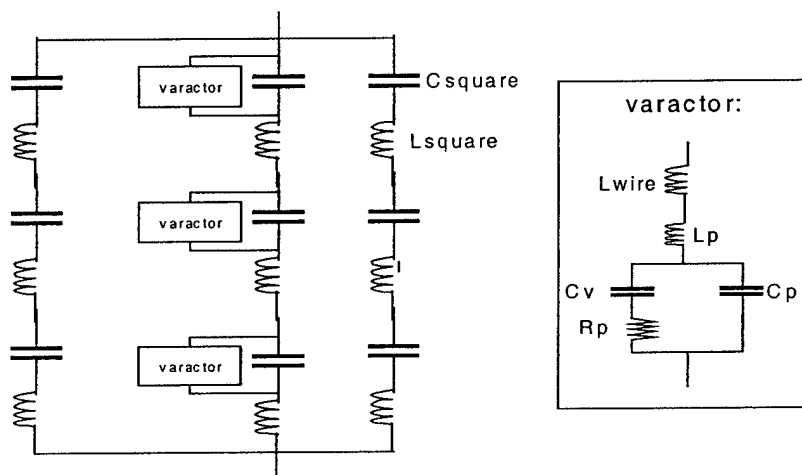


Figure 2-3. Equivalent circuit model for FSS portion of RAMC.

The measured reflection coefficient phase angle versus frequency is shown in Figure 2-4 with the varactor bias voltage as a parameter. At each bias level, the instantaneous ± 90 -degree bandwidth of the device is relatively

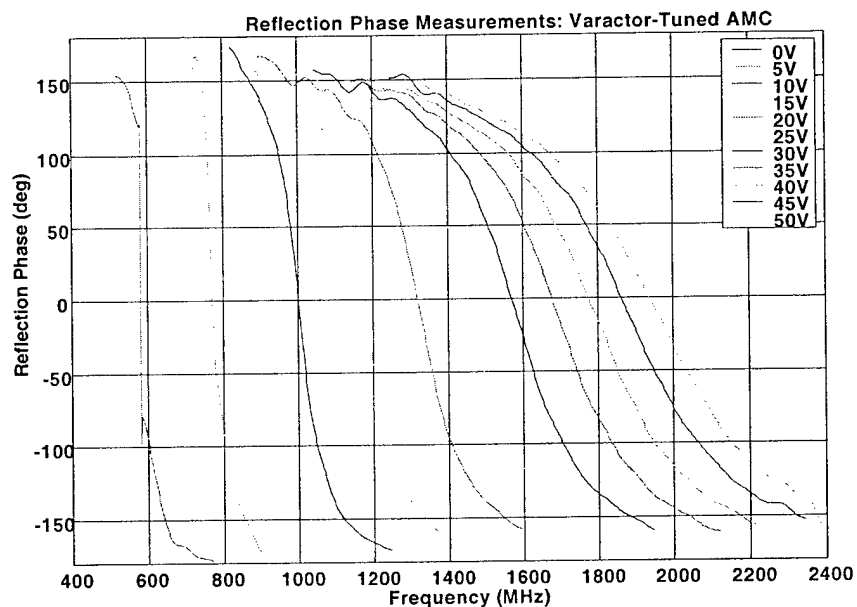


Figure 2-4. Measured reflection phase of the varactor-tuned RAMC with varactor bias voltage as a parameter. Note that d/λ_0 is $1/52$ at 600 MHz & $1/16$ at 1920 MHz.

narrow. However, as the bias level changes, the instantaneous ± 90 -degree bandwidth continuously moves across a much wider frequency band from 590 to 2110 MHz (0° reflection phase tunes from approximately 590 to 1920 MHz)

Figure 2-5 shows the test set-up that is used to experimentally verify the existence of a TE surface wave bandgap. In this case, the transmission response (S_{21}) is measured between two Vivaldi-notch radiators that are mounted so as to excite the dominant electric field polarization for TE modes on the AMC surface. For the TE set-up, both antennas are oriented horizontally. For the TM set-up (not shown), the antennas are oriented vertically. Absorber is placed around the surface-under-test to minimize the space wave coupling between the antennas. The optimal configuration – defined empirically as “that which gives us the smoothest, least-noisy response and cleanest surface wave cutoff” – is obtained by trial and error. This optimal configuration is obtained by varying the location of the antennas, the placement of the absorber, the height of absorber above the surface-under-test, the thickness of absorber, and by placing a conducting foil “wall” between layers of absorber.

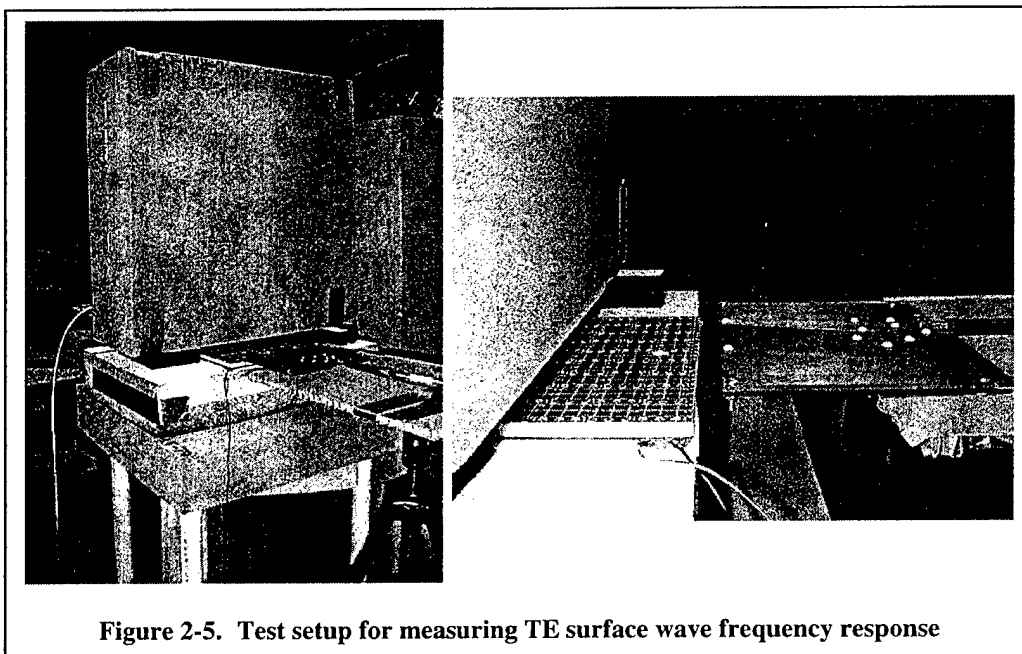


Figure 2-5. Test setup for measuring TE surface wave frequency response

Figures 2-6 through 2-8 show the measured S_{21} for the TE and TM surface wave measurements as described above for 50, 20 and 0 volt bias levels, respectively. The surface wave bandgaps observed are correlated closely to the ± 90 -degree reflection phase bandwidths at each bias level.

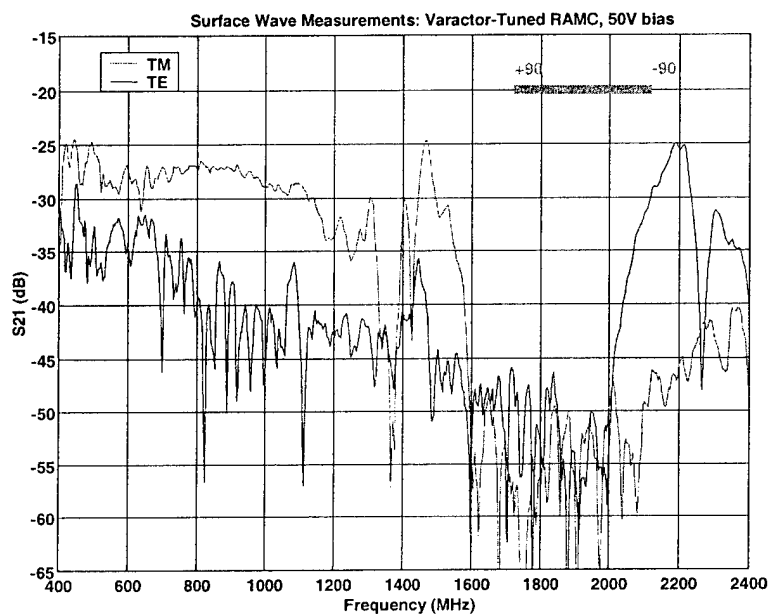


Figure 2-6. Surface wave measurements for RAMC w/bias voltage of 50V. The ± 90 degree reflection phase bandwidth is indicated by the green bar.

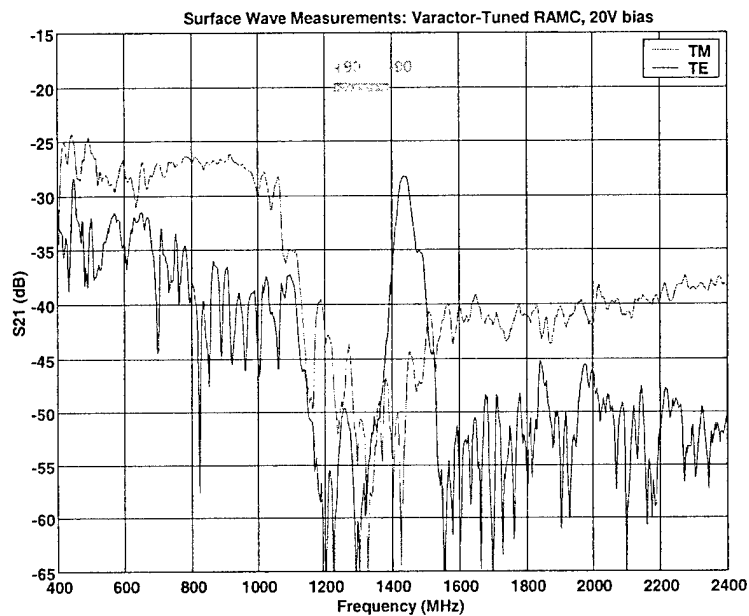


Figure 2-7. Surface wave measurements for RAMC w/bias voltage of 20V. The +/- 90 degree reflection phase bandwidth is indicated by the green bar.

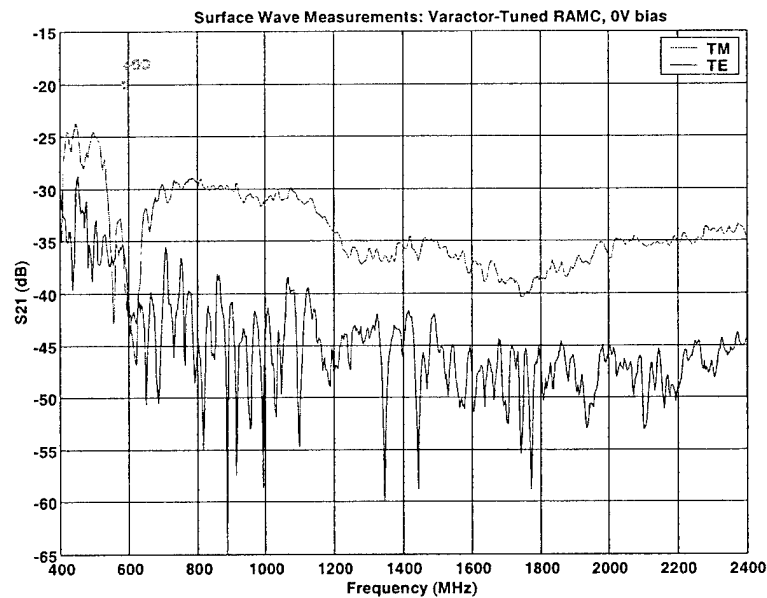


Figure 2-8. Surface wave measurements for RAMC w/bias voltage of 0V. The +/- 90 degree reflection phase bandwidth is indicated by the green bar.

For expediency, the results above show only a few discrete bias conditions. However, it should be noted, that as bias voltage was changed in analog fashion, both the high-impedance band and the surface wave bandgap tuned continuously over more than 3:1 bandwidth. We next consider antennas in proximity to the tunable AMC surface.

3. Broadband Spiral Antenna Over Varactor-Tuned AMC

Demonstration of the properties in the previous section is necessary in order to characterize the AMC surface. However, in order for the AMC to be of practical use, we now consider integrated wire antenna/AMC radiating structures consisting of flush-mounted wire elements in close proximity to the AMC. Similar to the choice for the AMC itself, we can choose an antenna element with broad instantaneous bandwidth or a narrowband element which is tuned. In this case, the tradeoff in complexity associated with tuning is not favorable because broadband elements can be realized without severe penalties in size/weight.

Figure 3-1 below shows an 8 inch diameter, non-complementary, equiangular spiral flush mounted above the reconfigurable AMC. Note that the spiral arms contain less metal than a complementary spiral structure. This was done to minimize the capacitive perturbation to the AMC FSS layer. The spiral

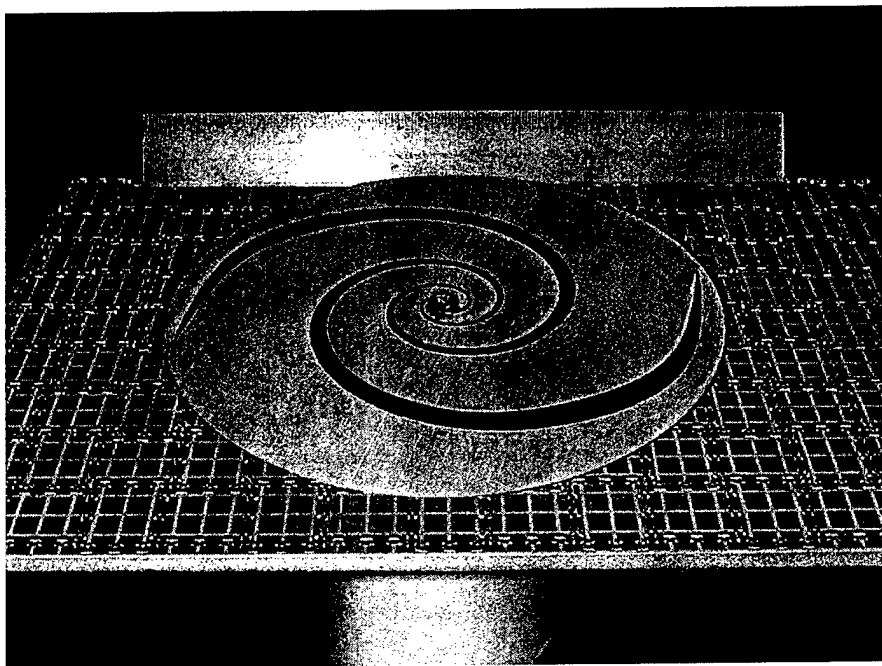


Figure 3-1. Printed spiral antenna located above the varactor-tuned RAMC.

was etched on a 60 mil substrate of Rogers R04003. On the lower side of the substrate was attached a 100 mil thick foam spacer layer. This foam rested against the surface mounted diodes and chip resistors installed on the RAMC, such that the printed spiral was about 0.150" above the printed FSS surface. This spiral was fed with a Chebyshev-Duncan coaxial balun, which exhibited approximately a 3:1 impedance transformation ration ($50:150\Omega$). When the spiral is in a free space environment, the return loss looking into the balun-fed spiral with a 50 ohm system is less than -8 dB over 400 MHz to 1000 MHz, less than -10 dB over 1000 MHz to 1200 MHz, and less than -15 dB over 1200 MHz to 2 GHz.

Figures 3-2 and 3-3 illustrate the fact that the broadband printed spiral antenna has a high gain bandwidth and a good impedance match over a range of frequencies defined explicitly by the surface wave bandgap of the RAMC upon which it rests. For the case of a 20 volt bias, the return loss has a plateau at approximately -15 dB over the frequency range of 1100 to 1400 MHz, which is effectively the surface wave bandgap as illustrated in Figure 2-7. Also, the swept gain plot of Figure 3-3 reveals that the broadside gain of the RAMC backed spiral is at least 3 dB higher than the case of the same spiral located above an absorber (i.e. in free space), for a frequency range from about 1150 to 1350 MHz, which is within the frequency range of the surface wave bandgap.

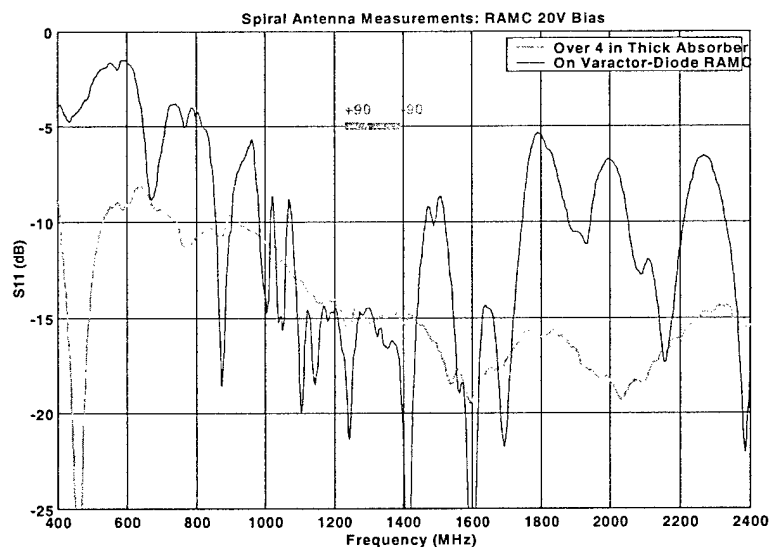


Figure 3-2 Return loss measurement for the RAMC backed spiral antenna with bias set to 20 volts.

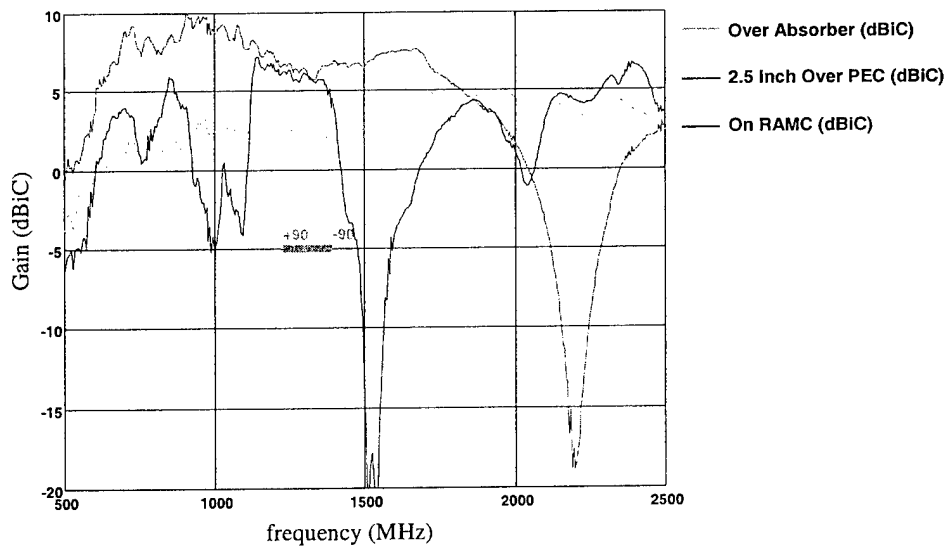


Figure 3-3. Swept boresight gain for the RAMC backed spiral with 20 volt bias.

When the RAMC is biased to 50 volts, the surface wave bandgap, observed in Figure 2-6, extends from approximately 1600 to 2100 MHz. Figure 3-4 reveals that the return loss of the spiral element on this RAMC drops below -15 dB over this same frequency range. The swept gain shown in Figure 3-5 reveals that the boresight gain is at least 3 dB higher than the case of the same spiral located above an absorber, for the same frequency range of 1600 MHz to 2100 MHz.

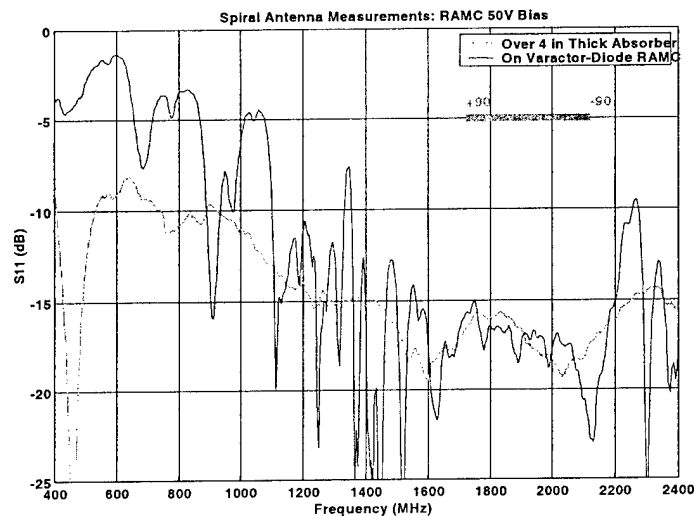


Figure 3-4 Return loss measurement for the RAMC backed spiral antenna with the RAMC bias set to 50 volts.

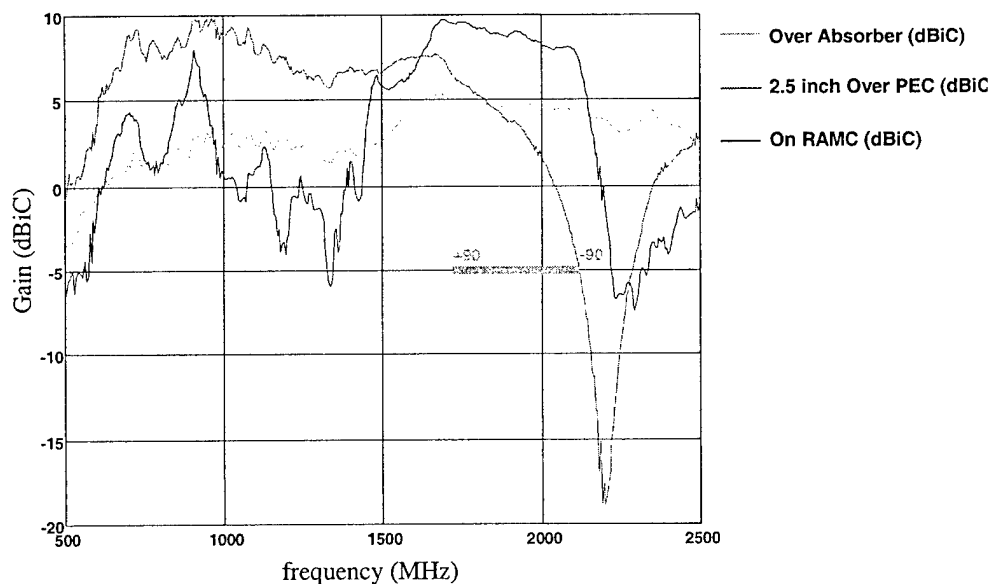


Figure 3-5. Swept boresight gain for the RAMC backed spiral antenna with 50 V bias.

Thus, by electronically adjusting the surface wave bandgap of the RAMC, we can obtain the desirable properties of an integrated planar broadband element over a wide tuning range. Just as the AMC reflection phase and surface wave bandgap are tuned smoothly by analog changes to the bias voltage, the antenna match and gain characteristics tuned smoothly across more than 3:1 bandwidth. We suspect that this behavior is possible in other classic broadband elements such as a bowtie antenna, a log-periodic bowtie, other planar log-periodic structures, etc.

For comparison, consider the commercially available Spiral Antenna Model 2090 from Microwave Engineering Corporation. This antenna is a spiral over an absorber-filled cavity with 9" diameter and 3.5" depth. The published gain characteristic (available on their web site) is very similar to the spiral presented here when placed over an absorber (cyan curve in Figure 3-5). In essence the RAMC approach allows us to achieve at least 3 dB more gain in a much thinner structure at a cost of decreased instantaneous bandwidth and added complexity.

4. Conclusions

We have demonstrated that a broadband spiral antenna can be mounted over a reconfigurable artificial magnetic conductor (AMC) and exhibit good impedance and gain performance over the range of frequencies defined by the high impedance band and surface wave bandgap of the AMC. As the RAMC is tuned over a wide range of frequencies, the spiral antenna can operate efficiently in the surface wave bandgap, even though the entire structure is only $\lambda_0/30$ thick at the lowest frequency.

This experiment demonstrates several key concepts. (1) A very physically and electrically thin antenna can be fabricated by installing a broadband printed element very close to a RAMC surface. In this case, the RAMC plus spiral has a total height of $\lambda/20$ at 1 GHz. (2) Over the frequency range defined by the tunable surface wave bandgap, the gain of this spiral at boresight, or broadside, is at least 3 dB greater than for the case of the same spiral element backed by an absorber. (3) The impedance match for the antenna is good (-15 dB or better) only over the high-impedance band for the AMC.

Acknowledgement

This work was sponsored by DARPA contract no. F19628-99-C-0080 and maintained by AFRL/SNHA, Hanscom AFB, MA .

References

- [1] D. Sievenpiper, "High-impedance electromagnetic surfaces," Ph.D. dissertation, UCLA electrical engineering department, filed January 1999
- [2] D. Sievenpiper, L. Zhang, and E. Yablonovitch, "High-impedance electromagnetic ground planes," *IEEE Intl. MTT Symp.*, June 13-19, 1999, Anaheim, CA
- [3] D. Sievenpiper, R. Broas, and E. Yablonovitch, "Antennas on high-impedance ground planes," *IEEE Intl. MTT Symp.*, June 13-19, 1999, Anaheim, CA
- [4] D. Sievenpiper, L. Zhang, R. Jimenez Broas, N. Alexopoulos, and E. Yablonovitch, "High-impedance electromagnetic surfaces with a forbidden frequency band," *IEEE Trans. Microwave Theory and Techniques*, Vol 47, No. 11, November 1999, pp. 2059-2074.
- [5] Sievenpiper, D., J. Schaffner, B. Loo, G. Tangonan, R. Harold, J. Pikulski and R. Garcia, "Electronic Beam Steering Using a Varactor-Tuned Impedance Surface," *IEEE Ant. and Prop. Intl. Symp.*, July13-18, 2001, Boston, MA
- [6] Diaz, R. E., J. T. Aberle, W. E. McKinzie, "TM Mode Analysis of a Sievenpiper High-Impedance Reactive Surface," *IEEE Ant. and Prop. Intl. Symp.*, 2000. IEEE, Volume: 1 , 2000, Page(s): 327 -330
- [7] Diaz, R. E., J. T. Aberle, W. E. McKinzie, "Analysis of the Surface Wave Suppression Band of the Sievenpiper High-Impedance Ground Plane in Terms of its Effective Medium Properties," *National Radio Science Meeting*, January 8-11, 2001, University of Colorado at Boulder, Colorado.

PATCH ANTENNAS WITH SWITCHABLE SLOTS (PASS): CONCEPT, THEORY AND APPLICATIONS

Fan Yang and Yahya Rahmat-Samii

Department of Electrical Engineering, University of California at Los Angeles
Los Angeles, CA 90095-1594

Email: rahmat@ee.ucla.edu

Tel: (310) 206-2275, Fax: (310) 206-8495

Abstract

This paper presents a novel kind of microstrip antenna, a patch antenna with switchable slots (PASS). Slots are incorporated into the patch and switches are positioned in the center of the slots to control their status. By turning the switches on or off, different radiation features can be achieved. PASS can be widely used in wireless communications and three examples are discussed in the paper. The first example is for dual-band operation. A patch antenna with a switchable slot resonates at two different frequencies with the switch at on and off modes. This design has the attracting features of small and flexible frequency ratio and similar patterns at two bands. The second example is a dual-band CP patch antenna. The antenna can generate circularly polarized pattern at two frequencies with only one patch and a single feed. The third example is a polarization diversity PASS. A diagonal fed square patch antenna with switchable slots shows the ability to change polarization sense between different switches modes. By properly incorporating the switchable slots, the antenna can switch between right hand circular polarization and left hand circular polarization. PASS appears to be promising for wireless communications applications such as PCS, GPS, WLAN, satellite links and planetary robots.

Keywords: patch antenna, slot, switch, dual frequency, CP, polarization diversity

1. Introduction

Microstrip antennas are widely used in wireless communications due to their advantages of low profile, light weight, low production cost and conformability with RF circuitry. The development of wireless communications has led to many new requirements for microstrip antennas, such as dual bands, CP operation and

polarization diversity. To this end, a novel design concept, a patch antenna with switchable slots (PASS) as shown in Fig. 1, is proposed and investigated herein.

Slots have been integrated with patch antennas to realize different functionalities. For examples, it can be utilized to tune the resonant frequency [1], to reduce the patch size [2]-[4], to expand the antenna bandwidth [5][6] and to obtain CP performance[7]. In this paper, a novel slot implementation is explored. Switches are inserted in the center of slots to control their status. The slots will have different effects on a patch antenna when switches are on or off. Therefore, it can be used to realize various functionalities.

Based on this idea, three designs are presented for different applications. The first design is a PASS for dual-band operation. A patch antenna with a switchable slot has been designed and fabricated. When the switch is on, the antenna resonates at 4.82 GHz and it resonates at 4.38 GHz when the switch is off. A small frequency ratio of 1.10 is achieved in this design and it can be tuned by adjusting the slot length and position. It also shows similar patterns at two bands.

The second design is a dual-band circularly polarized PASS. A diagonally fed square patch with a pair of tuning stubs and switchable slots is investigated and it is simpler than previous designs because it has only one patch and a single feed. The structure has features of low profile, small frequency ratio and similar CP patterns at two bands and it will be used for future planetary robots.

The third design is a PASS, which can switch between RHCP and LHCP at the same feeding port. This design also uses a diagonally fed square patch with switchable slots, but there is no tuning stub here. The CP performance is realized by slots and the right hand or left hand polarized sense is determined by the switches status. This idea is verified by both FDTD simulation and experimental results.

In summary, the PASS demonstrates useful features for wireless communications applications such as PCS, GPS, WLAN, satellite links and planetary robots.

2. The operating mechanism of the PASS

A basic PASS structure is shown in Fig. 2. The patch size is $L \times W$ and it is built on dielectric substrate with permittivity ϵ_r and thickness h . A probe is located at (X_f, Y_f) to activate the TM_{10} mode of the patch. A slot with length L_s , width W_s and position P_s is incorporated into the patch and a switch is inserted in the center

of the slot to control its status. The switch can be either a pin diode [8][9] or a MEMS based switch [11].

When the switch is in the OFF mode, the currents on the patch have to flow around the slot, as shown in Fig. 3a, resulting in a relatively long length of electrical current path. Therefore, the antenna resonates at a low frequency [1]. In contrast, when the switch is in the ON mode, some of the electrical currents can go directly through the switch, as shown in Fig. 3b. In this case, the length of current path is shorter than previous case so that the antenna has a higher resonant frequency. As a result, the PASS has different resonant features with different status of the switch. It should be pointed out that even when the switch is on, it still has a longer current path length than the patch antenna without a slot. Thus, its resonant frequency should be lower than the case without a slot.

To demonstrate this idea, the finite difference time domain (FDTD) method is utilized to analyze the antenna properties. When the switch is in the OFF mode, it is removed from simulation and when the switch is in the ON mode, it is modeled as a metal tab. The antenna is mounted on a finite substrate of 50 mm \times 50 mm size, 3 mm thickness and $\epsilon_r=2.20$. The patch parameters are listed below (Unit: mm):

$$L=W=18, (X_f, Y_f)=(5,9) \quad (1)$$

$$L_s=16, W_s=1, P_s=13 \quad (2)$$

The initial patch without slot works at 4.85 GHz as shown in Fig.4. When the slot is incorporated into the patch and the switch is turned on, the antenna resonates at 4.75 GHz. Once the switch is turned off, the antenna frequency shifts to 4.40 GHz. These results agree with the expectation: when the switch is on, the slot has less effect so that the resonant frequency decreases a little; when the switch is off, the slot effect is significant so that the resonant frequency decreases a lot.

The effects of slot length and slot position are studied and depicted in Fig. 5. It is noticed from Fig. 5a that the resonant frequency will decrease when the slot length increases. In all these cases, the antennas have better matches than -10 dB. Another important feature in this figure is that the slot length effect on the switch OFF mode is more significant than its effect on the switch ON mode. According to this feature, one can choose appropriate slot length to get suitable frequency ratio, which means that the frequency ratio is flexible in this design, varying from 1.0 to 1.10 according to the figure. As revealed in Fig. 5b, slot position also has some effect on the antenna frequencies. The resonant frequency is the lowest when the slot position is at 9 mm. The reason is that in this case, the slot is located

in the center of the patch where the currents are maximum so that the slot effect is the most significant.

3. Applications of the PASS: Dual frequency operation

Dual-frequency operation is an important topic in the applications of microstrip antennas. Typically, there are two main approaches to solve this problem: one is to use stacked patches [11][12] and the other is to activate different modes of the patch [13]. The first approach stacks two or more patches that resonate at different frequencies. A disadvantage of this method is the increased height of the antenna. The second approach achieves dual frequency operation by activating two different modes under the patch such as the TM₁₀ and TM₃₀ modes or the TM₁₀ and TM₀₁ modes. However, this approach has some limitations. For example, when the TM₁₀ and the TM₃₀ modes are activated, the frequency ratio is very large, approximately around 3. When the TM₁₀ and TM₀₁ modes are activated, the two modes will have different polarizations. In this paper, the PASS concept is applied to realize dual frequency operation. This design is very simple considering that it has only one patch and a single feed. It is also worthwhile to point out that the frequency ratio of this structure is small and very flexible. Another attracting feature is that the antenna has same polarizations and similar patterns at two frequencies.

Experiments have been carried out to demonstrate this PASS concept. Four antennas have been built for comparison and their parameters are the same as described in equation (1) and (2) except that the thickness of the substrate RT/duroid 5880 ($\epsilon_r=2.20$) is 3.18 mm. Fig. 6 shows the photos of these four antennas: Fig. 6a is an initial patch antenna without a slot, Fig. 6b is a patch antenna with a switchable slot (PASS), Fig. 6c is a reference patch antenna for the switch OFF mode and Fig. 6d is a reference patch antenna for the switch ON mode. The last two are the same as the FDTD models. In Fig. 6b, a pin diode (HPND-4005) is inserted in the center of the slot. To isolate the DC, the slot is cut the full width of the patch and two capacitors are soldered on the edges of the slot for RF continuity. A shorted quarter-wavelength strip is connected to the right edge of the patch for grounded DC while not affecting the RF. A 2 Volt voltage is supplied from the coax probe.

As predicted by the FDTD simulation, the dual frequency performance can be observed in Fig. 7. The PASS resonates at 4.38 GHz when the pin diode is in the OFF mode and resonates at 4.82 GHz when the pin diode is turned ON. The input match is better than -10 dB at the two resonant frequencies and the frequency ratio is only 1.10. The reference antennas c and d show the similar resonant

frequencies as the PASS results, which proves the validity of metal tab representation. There are some differences between the PASS and the reference antennas, which may be a result from the resistance and capacitance of the pin diode and two capacitors. The radiation patterns are measured and displayed in Fig. 8. As revealed by the figures, the PASS has very similar patterns at two frequencies and they are very close to the patterns of the patch antenna without the slot. It is also noticed that when the diode is turned ON, the antenna gain is about 1.5 dB lower than the other two cases, which may attribute to the diode loss. Ongoing research plans to use MEMS based switches to reduce the loss.

4. Applications of the PASS: Dual band CP performance

Dual-band circularly polarized patch antennas have attracted much attention recently due to the applications of differential GPS, planetary robots and other wireless communications. Some related designs have been reported including stacked microstrip antennas [14][15] and a slot loaded circular microstrip antenna [16]. However, the stacked antennas greatly increase the antenna height and the circular microstrip antenna has a large frequency ratio and different patterns at two bands due to the different modes activated.

In this paper, the PASS concept is also used to achieve dual-band CP performance. The proposed antenna structure is shown in Fig. 9a. A square patch with length L is mounted on a substrate of thickness h and permittivity ϵ_r . The feeding probe is located on the diagonal line of the patch at (X_f, Y_f) and a pair of rectangular stubs with size $L_r \times W_r$ are attached to opposite patch edges. Thus, both the TM_{01} and TM_{10} modes will be excited with the same amplitude and they are tuned 90 degrees out of phase by properly selecting the size of the small rectangular stubs. Therefore, the antenna can generate a circularly polarized pattern. To realize frequency agility, two orthogonal switchable slots are incorporated into the patch with parameters L_s , W_s and P_s . After loading the slots, the currents on the patch for both modes are affected by the slots so that the electrical length of the currents path changes, resulting in different resonant frequencies. Due to the symmetry of the slots and the feeding port, the slots have the same effect on both modes and hence the antenna retains the CP performance. By turning the switches on or off, the circularly polarized pattern can be obtained at dual bands. To design a desired antenna, a combination of FDTD simulation and empirical tuning is used and a photo of the final design is shown in Fig. 9b. The antenna parameters are listed below (Unit: mm):

$$L=19, h=3.18, \epsilon_r=2.20, (X_f, Y_f)=(6,6) \quad (3)$$

$$L_s=16, W_s=1, P_s=13, L_r=4, W_r=2 \quad (4)$$

The antenna was mounted on a finite ground plane of $40 \text{ mm} \times 40 \text{ mm}$. In the experiments, removable metal tabs are used to represent the on and off states of the diodes and the previous experiments have demonstrated the applicability of this representation. Fig. 10a presents the return loss of the antenna and Fig. 10b shows the axial ratio of the antenna at the boresight. It can be seen from the figures that by turning the diodes on and off, dual-band CP operation can be achieved. The axial ratio is 2.9 dB at 4.0 GHz and 1.6 dB at 4.37 GHz and a frequency ratio of only 1.09 is obtained. Although the return loss at 4.37 GHz is -9 dB, it can be further improved by properly adjusting probe position and slot position. Spinning linear radiation patterns in xz plane are shown in Fig. 11 at two frequencies 4.0 GHz (switch ON mode) and 4.37 GHz (switch OFF mode). As revealed by the figure, the pattern shape and beam angle are very similar to each other. Similar radiation patterns can be observed in yz plane. Fig. 12 plots the axial ratios of the PASS at the switches ON and OFF modes.

5. Applications of the PASS: CP polarization diversity

Polarization diversity antennas are of growing interest due to the development of wireless communications in recent years. In broadband wireless communication systems, such as PCS system [17] and wireless local area networks (WLAN) [18][19], they are used to mitigate the detrimental fading caused by multipath phenomenon. In active read/write microwave tagging systems, they provide a powerful modulation scheme [20]. In satellite communication systems, they are utilized to realize frequency reuse for doubling the system capability [21]. In a recent project to build a Mars rover, a patch antenna with dual-frequency and dual-polarization capabilities is required [22]. In light of these applications, we use the PASS concept to design a patch antenna that can achieve RHCP and LHCP diversity with a single feeding port.

Fig. 13 shows the schematic of the proposed antenna. A square patch with length L is mounted on a square substrate with thickness h , permittivity ϵ_r and a feeding probe is located on the diagonal line of the patch at (X_f, Y_f) . Two orthogonal slots are incorporated symmetrically into the patch with parameters L_s , W_s and P_s and two switches are inserted in the center of the slots. The switches directions are important in this case: the diode number 1 orients toward the feeding point and diode number 2 orients away from the feeding point. Thus, when a positive voltage is provided, the diode 1 is off and the diode 2 is on; when a negative voltage is provided, the diode 1 is on and the diode 2 is off. This leads to different functionality. The radiation principle of the antenna is briefed next. Since the feeding point is on the diagonal line of the square patch, both the TM_{10} and TM_{01} modes are activated at the same frequency. After incorporating the slots, the

resonant features of both modes are affected. If diode 1 is on and diode 2 is off, the electrical current of the TM₁₀ mode can go through diode 1, whereas the current of the TM₀₁ mode cannot go through diode 2 and is forced to flow around the slot. Therefore, the resonant frequency of the TM₁₀ mode changes little while the resonant frequency of the TM₀₁ mode decreases a lot. If the frequencies of these two modes are tuned properly, in the middle of these two frequencies, the radiation fields of the TM₁₀ mode and the TM₀₁ mode have the same magnitude and are 90 degrees out of phase. As a result, a RHCP pattern can be obtained. On the other hand, if the diode 1 is off and diode 2 is on, the opposite situation happens and a LHCP pattern can be obtained.

Several experiments have been carried out to demonstrate the functionality of this polarization diversity PASS. Two square patch antennas are fabricated to represent two modes of the patch with following parameters (Unit: mm):

$$L=18, h=3.18, \epsilon_r=2.20, (X_f, Y_f)=(5, 5) \quad (5)$$

$$L_s=12, W_s=1, P_s=13 \quad (6)$$

The antenna was mounted on a finite ground plane of 40 mm × 40 mm. Fig. 14 shows the photos of these two antennas: Fig. 14a has a metal tab in the center of the vertical slot and Fig. 14b has a metal tab in the horizontal slot. The metal tab is used to represent the on status of the switches. Fig. 14a represents the situation when diode 1 is off and diode 2 is on, which results in a LHCP pattern. In contrast, Fig. 14b represents a RHCP antenna. Due to the symmetry, the LHCP and RHCP antenna show very similar S₁₁ and they are better than -10 dB from 4.5 GHz to 5.1 GHz, as shown in Fig. 15. This frequency range was chosen for the ease of the measurement setup at the UCLA antenna lab and it can be readily scaled to other frequencies. As revealed in Fig. 16, the best axial ratio at the boresight is achieved at 4.64 GHz and 3% CP bandwidths (according to 3 dB axial ratio criterion) are obtained for both cases. Fig. 17 presents the measured spinning linear patterns and axial ratios of the RHCP antenna in xz and yz plane. An acceptable axial ratio (AR<3dB) is obtained in a broad angular range from -70 to 70 degrees in xz plane and from -90 to 90 degrees in yz plane. Fig. 18 shows the radiation properties of the LHCP antenna and similar radiation features can be observed.

6. Conclusion

A novel design scheme for microstrip antennas, a patch antenna with switchable slots (PASS) is presented in this paper. By incorporating slots into the patch and using switches to control their status, the antenna is capable for different

functionalities. The validity of this concept is demonstrated by both FDTD simulation and experimental results. It has been used to achieve dual frequency operation, dual band CP performance and polarization diversity. The PASS demonstrates useful features for wireless communications applications such as PCS, GPS, WLAN, satellite links and planetary robots.

7. Acknowledgement

This work was supported in part by JPL under Contract 442520-79278.

Reference:

1. X. X. Zhang and F. Yang, "The study of slit cut on the microstrip antenna and its applications", *Microwave Opt. Technol. Lett.*, vol.18, pp.297-300, 1998.
2. S. Dey and R. Mittra, "Compact microstrip patch antenna", *Microwave Opt. Technol. Lett.*, vol.13, pp.12-14, 1996.
3. K. L. Wong, C. L. Tang and H. T. Chen, "A compact meandered circular microstrip antenna with a shorting pin", *Microwave Opt. Technol. Lett.*, vol.15, pp.147-149, 1997.
4. F. Yang and X. X. Zhang, "Slitted small microstrip antenna", *1998 IEEE AP-S Dig.*, pp. 1236-1239, June 1998.
5. F. Yang, X. X. Zhang, X. Ye and Y. Rahmat-Samii, "Wide-band E-shaped patch antennas for wireless communications", *IEEE Trans. Antennas Propagat.*, vol. 49, pp. 1094-1100, 2001.
6. K. F. Lee, K. M. Luk, K. F. Tong, S. M. Shum, T. Huynh and R. Q. Lee, "Experimental and simulation studies of coaxially fed U-slot rectangular patch antenna", *IEE Proc. Microw. Antennas Propagat.*, vol. 144, pp. 354-358, 1997.
7. P. C. Sharma and K. C. Gupta, "Analysis and optimized design of single feed circularly polarized microstrip antennas", *IEEE Trans. Antennas Propagat.*, vol. 31, pp. 949-955, 1983.

8. C. Luxey, L. Dussopt, J. L. Sonn and J. M. Laheurte, "Dual frequency operation of a CPW-fed antenna controlled by PIN diodes", *Electronic Letters*, vol. 36, no. 1, pp. 2-3, Jan. 2000.
9. K. L. Virga and Y. Rahmat-Samii, "Low Profile Enhanced-bandwidth PIFA antennas for wireless communications packaging", *IEEE Trans. Microwave Theory Tech.*, vol. 45, pp. 1879-1888, 1997.
10. R. Simon, D. Chun and L. Katehi, "Reconfigurable array antenna using microelectromechanical systems (MEMSS) actuators", *2001 IEEE AP-S Dig.*, vol. 3, pp. 674-677, July 2001.
11. J. S. Dahele, K. F. Lee and D. P. Wong, "Dual frequency stacked annular-ring microstrip antenna", *IEEE Trans. Antennas Propagat.*, vol. 35, pp. 1281-1285, 1987.
12. F. Croq and D. M. Pozar, "Multifrequency operation on microstrip antennas using aperture coupled parallel resonators", *IEEE Trans. Antennas Propagat.*, vol. 40, pp. 1367-1374, 1992.
13. S. Maci, G. B. Gentili and G. Avitabile, "Single-layer dual frequency patch antenna", *Electronic Letters*, vol. 29, no. 16, pp. 1441-1443, Aug. 1993.
14. D. M. Pozar and S. M. Duffy, "A dual-band circularly polarized aperture-coupled stacked microstrip antenna for Global Positioning Satellite", *IEEE Trans. Antennas Propagat.*, vol. 40, pp. 1618-1625, 1992.
15. J. Y. Jan and K. L. Wong, "A dual-band circularly polarized stacked elliptic microstrip antenna", *Microw. Opt. Technol. Lett.*, vol. 24, pp. 354-357, 2000.
16. G. B. Hsieh, M. H. Chen and K. L. Wong, "Single-feed dual band circularly polarised microstrip antenna", *Electron. Lett.*, vol. 34, pp. 1170-1171, 1998.
17. M. G. Douglas, M. Okoniewski and M. A. Stuchly, "A planar diversity antenna for handheld PCS devices", *IEEE Trans. Veh. Technol.*, vol. 47, pp. 747-754, Aug. 1998.

18. S. T. Fang, "A novel polarization diversity antenna for WLAN applications", *2000 IEEE AP-S Dig.*, pp. 282-285, July 2000.
19. K. Hettak, G. Y. Delisle and M. G. Stubbs, "A novel variant of dual polarized CPW fed patch antenna for broadband wireless communications", *2000 IEEE AP-S Dig.*, pp. 286-289, July 2000.
20. M. Boti, L. Dussopt and J.-M. Laheurte, "Circularly polarized antenna with switchable polarization sense", *Electronic Letters*, vol. 36, no. 18, pp. 1518-1519, Aug. 2000.
21. X. X. Yang and S. S. Zhong, "Analysis of two dual-polarization square-patch antennas", *Microwave Opt. Technol. Lett.*, vol.26, No.3, pp.153-156, Aug. 2000.
22. J. Huang, "Miniaturized UHF microstrip antenna for a Mars mission", *2001 IEEE AP-S Dig.*, vol. 4, pp. 486-489, July 2001.

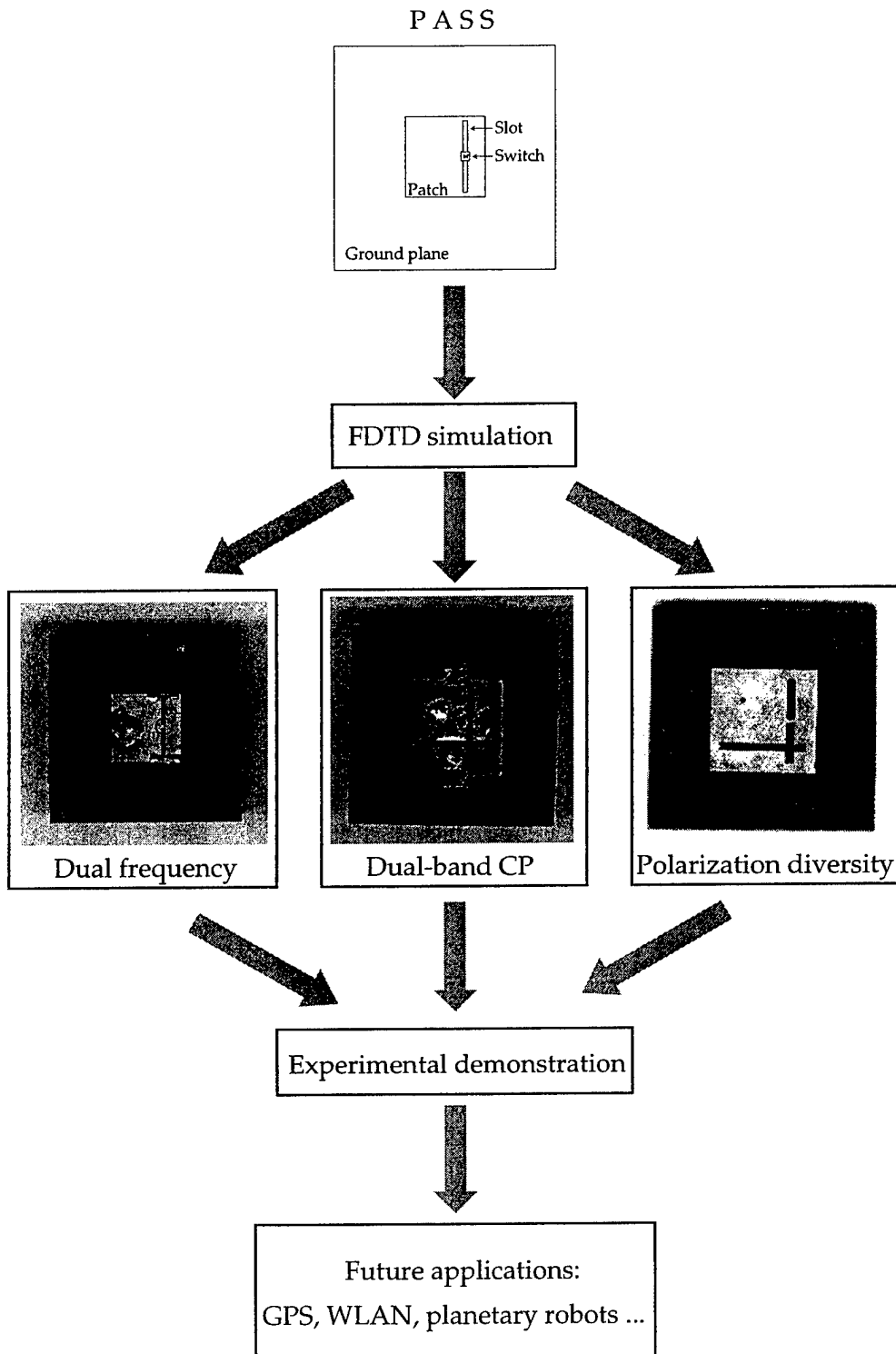


Figure 1: Patch Antennas with Switchable Slots (PASS): concept, theory and applications.

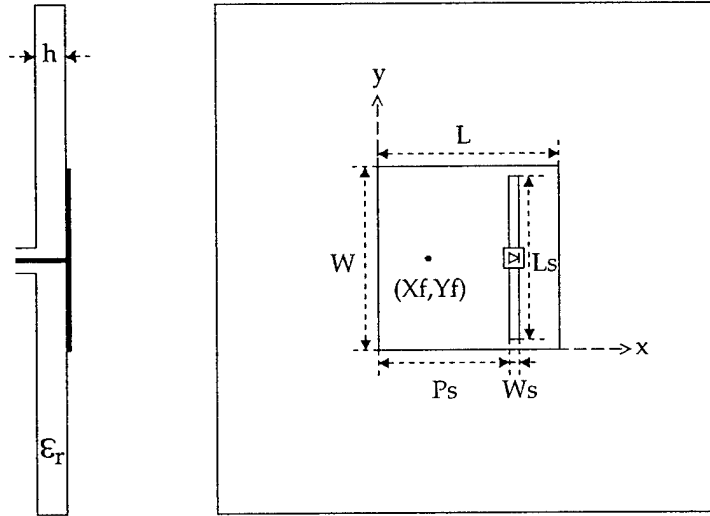


Figure 2: Geometry of a dual frequency Patch Antenna with a Switchable Slot (PASS).

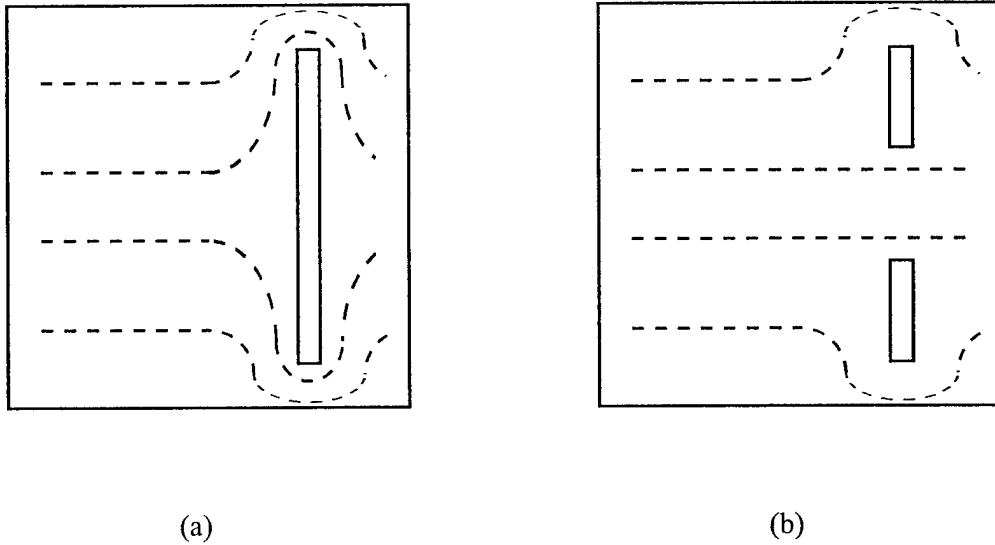


Figure 3: Electric currents on the patch antenna: (a) switch OFF mode, the current path has a long length so that the antenna resonates at a low frequency; (b) switch ON mode, the current path has a short length so that the antenna resonates at a high frequency.

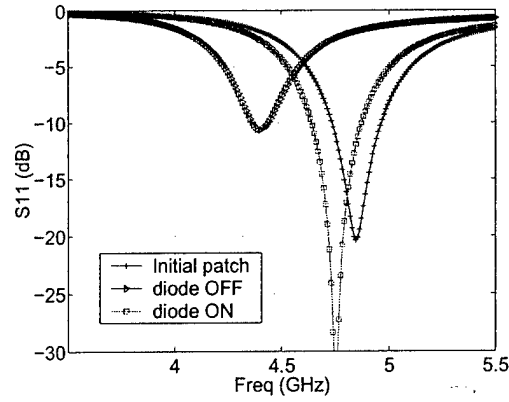
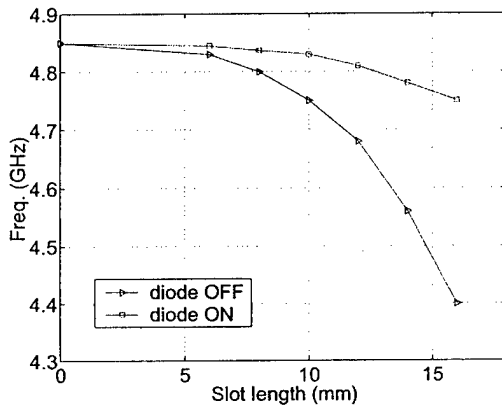
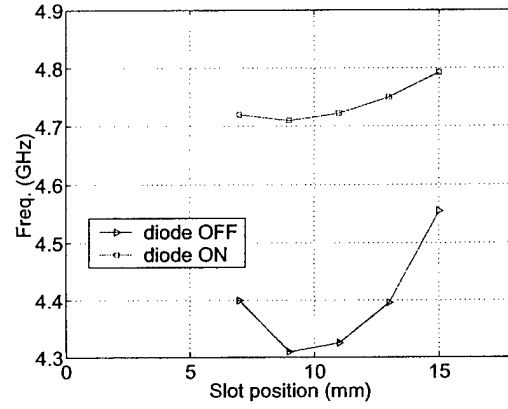


Figure 4: Simulated S_{11} results of a PASS under switch ON/OFF modes, compared to a patch antenna without slot. The frequency ratio of two modes is 1.10.

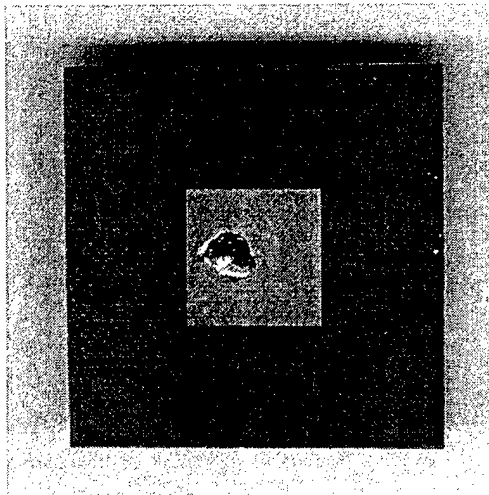


(a)

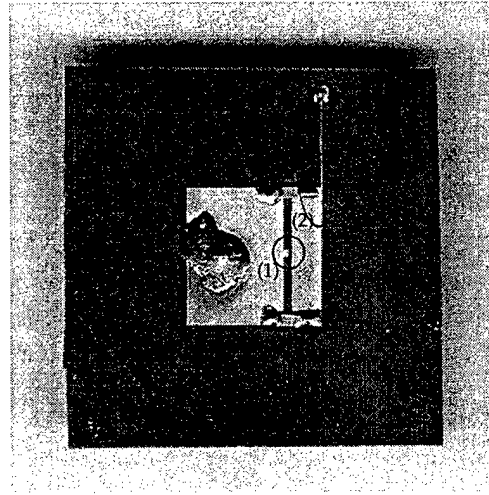


(b)

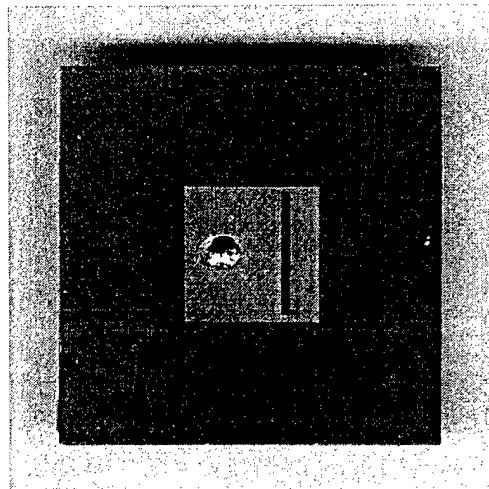
Figure 5: PASS resonant frequencies under switch ON/OFF modes (FDTD simulated) change with slot length (a) and with slot positions (b).



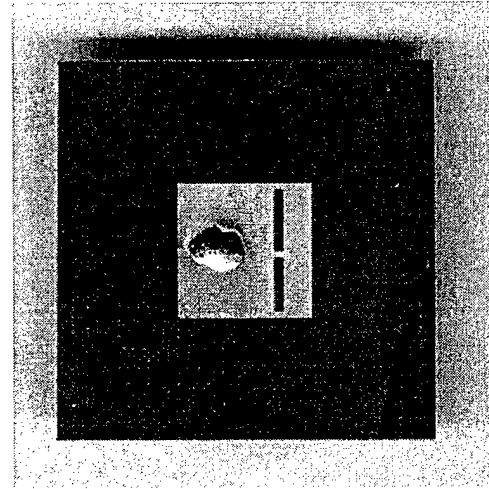
(a)



(b)



(c)



(d)

Figure 6: Photos of four patch antennas: (a) initial patch antenna, (b) PASS (1: a pin diode, 2: a shorted quarter-wavelength strip for DC bias), (c) reference patch antenna for switch OFF mode and (d) reference patch antenna for switch ON mode.

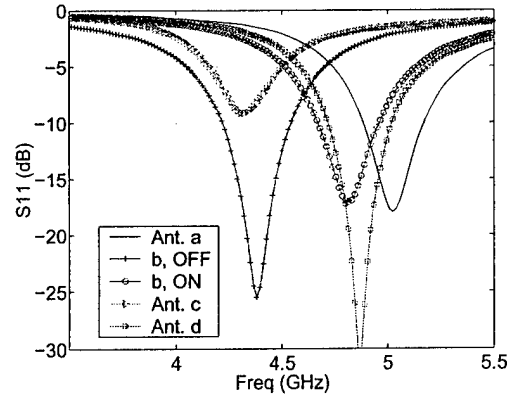


Figure 7: Measured S_{11} results of four patch antennas shown in Fig. 6. A 1.10 frequency ratio is achieved and the PASS shows similar resonant frequencies with reference patch antennas.

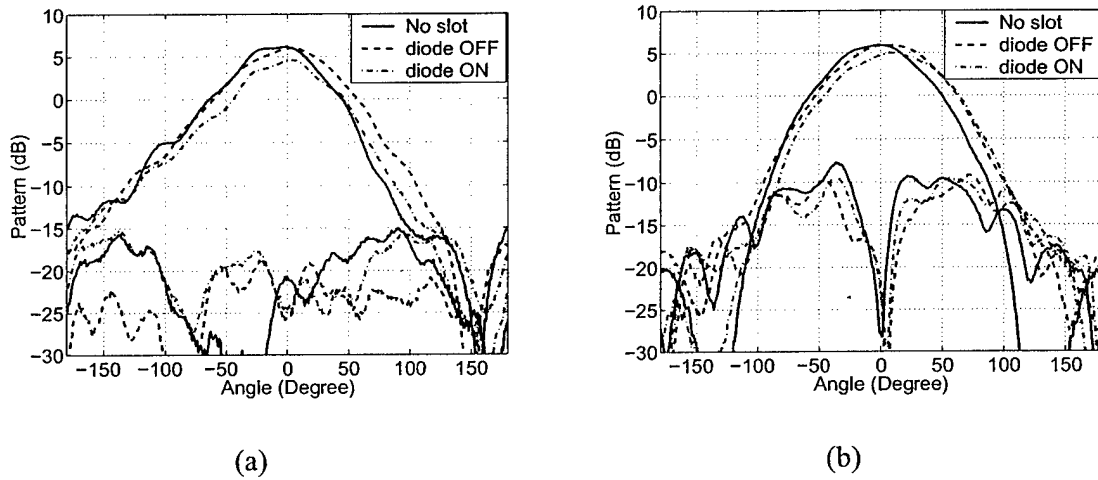
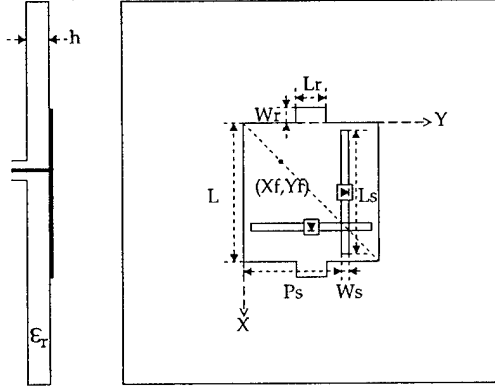
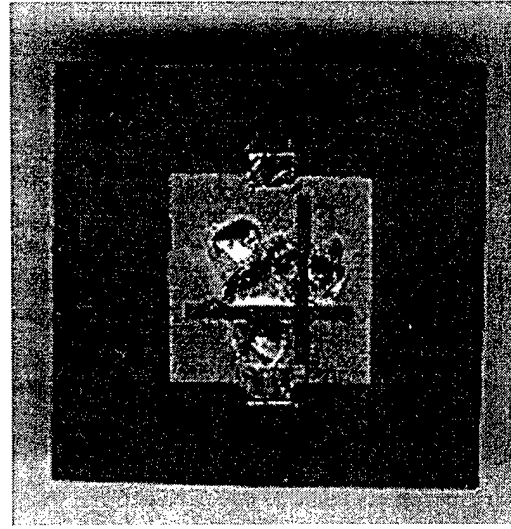


Figure 8: Comparison of measured radiation patterns: (a) E plane (xz plane) and (b) H plane (yz plane).

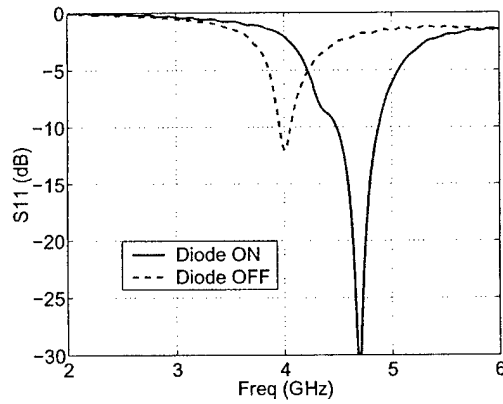


(a)

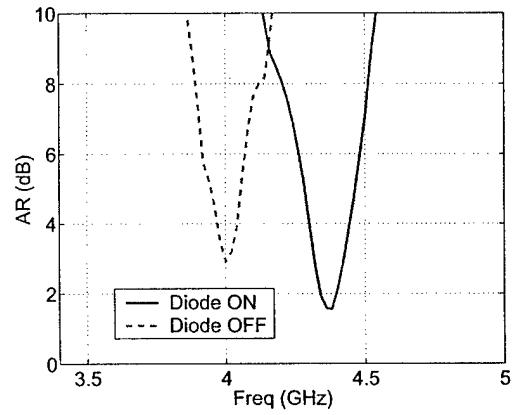


(b)

Figure 9: A PASS for dual-band CP operation: (a) geometry and (b) photo.



(a)



(b)

Figure 10: Measured results of the PASS for dual-band CP operation: (a) return loss and (b) axial ratio at the boresight under switches ON and OFF modes. A 1.09 frequency ratio is obtained with less than 3 dB axial ratio at each band.

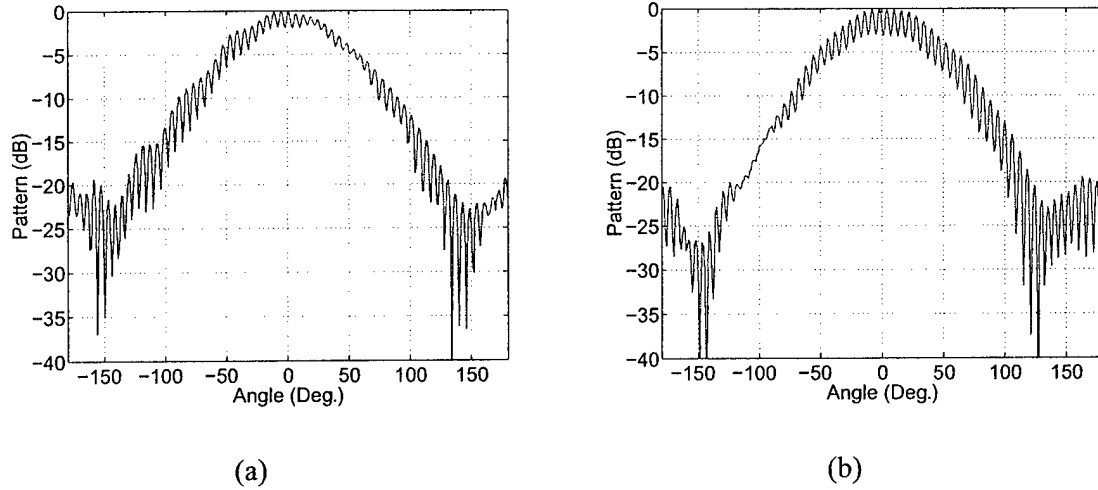


Figure 11: Measured spinning linear patterns of the antenna in xz plane: (a) Diodes ON mode, $f_1 = 4.0$ GHz and (b) Diodes ON mode, $f_1 = 4.0$ GHz.

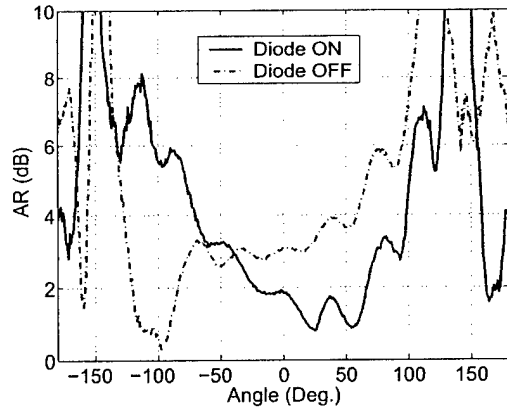


Figure 12: Measured axial ratio of the PASS in xz plane under switches ON and OFF modes.

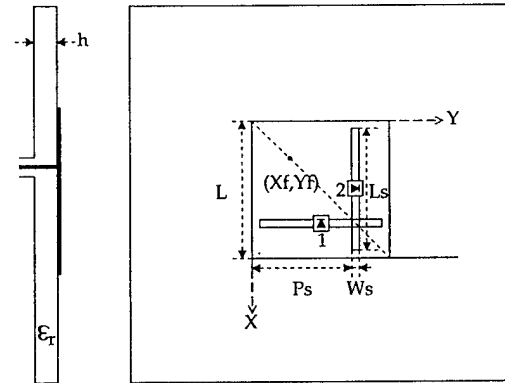
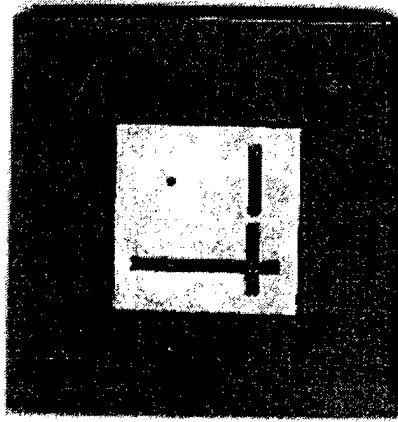
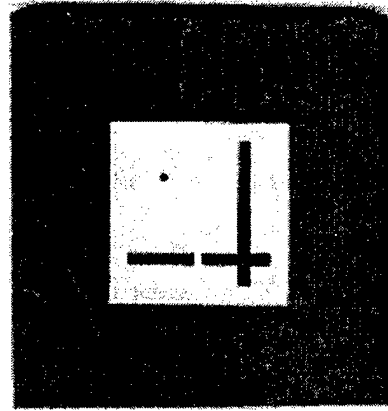


Figure 13: Geometry of a PASS for RHCP/LHCP diversity.



(a)



(b)

Figure 14: Photos of LHCP(a) and RHCP(b) patch antennas. The on status of the diodes in Fig. 13 are represented by conductive metal tabs in the center of the slots while the off status are represented by leaving the slots unchanged.

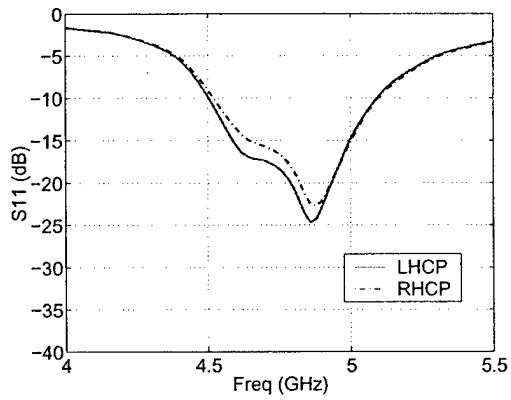


Figure 15: Measured return loss of the PASS for polarization diversity.

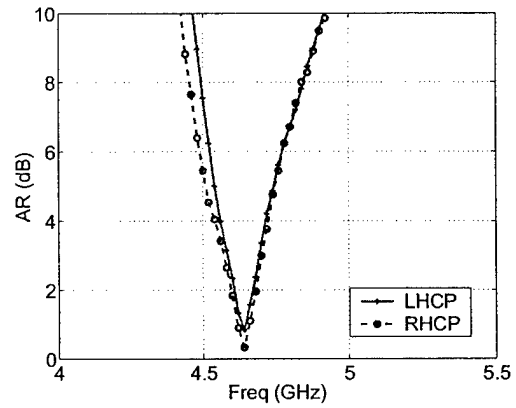
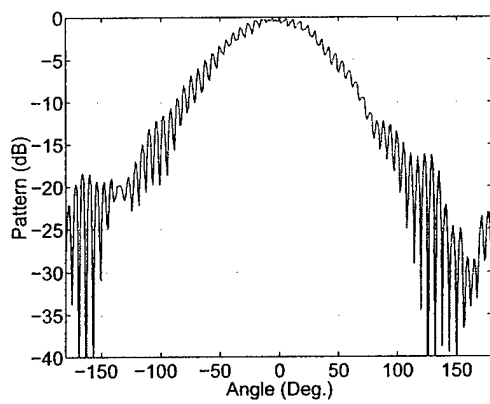
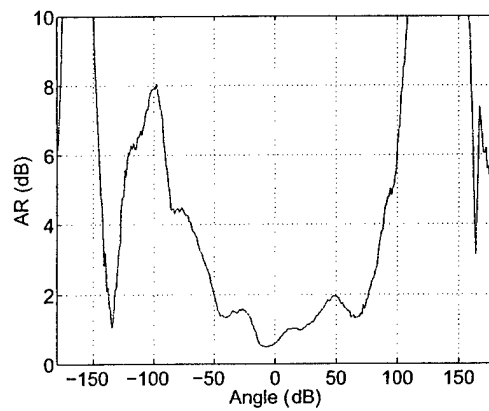


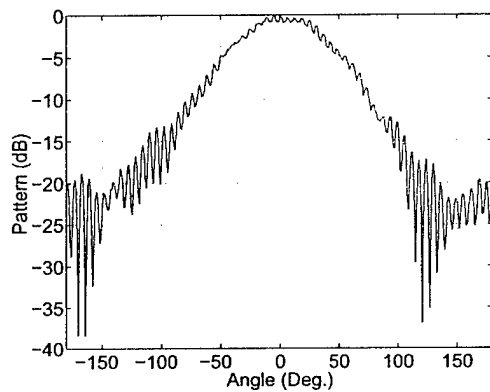
Figure 16: Measured axial ratio vs. frequency at the boresight of the PASS.



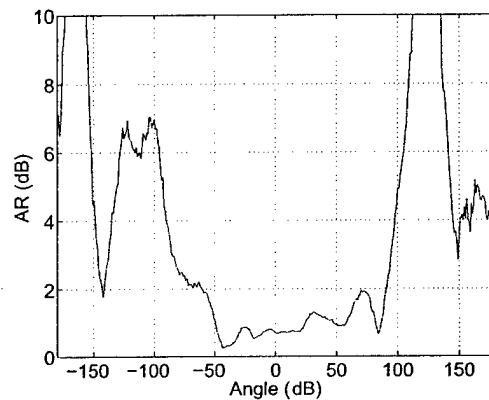
(a)



(b)

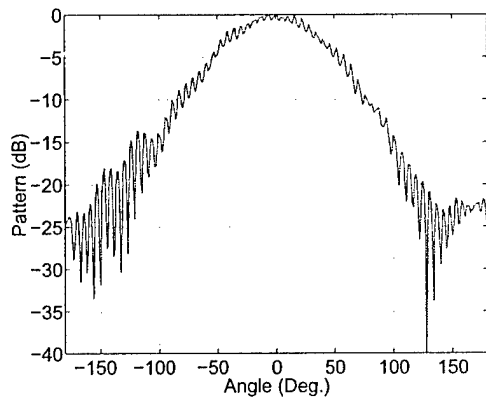


(c)

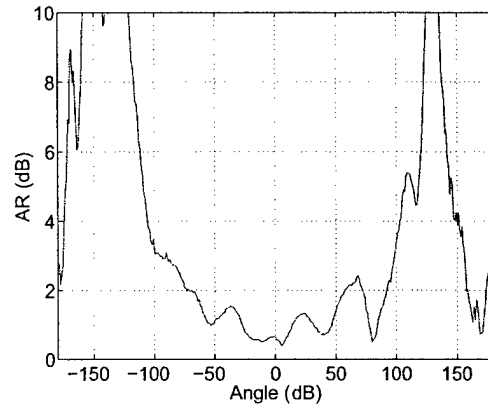


(d)

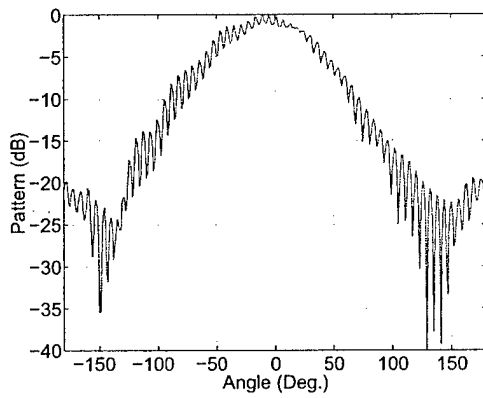
Figure 17: Measured radiation features at 4.64 GHz under RHCP polarization: (a) spinning pattern in xz plane, (b) axial ratio in xz plane, (c) spinning pattern in yz plane and (d) axial ratio in yz plane.



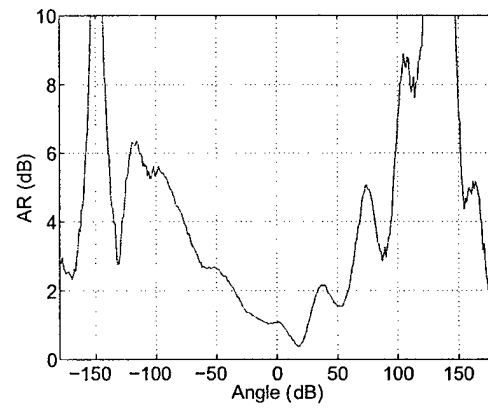
(a)



(b)



(c)



(d)

Figure 18: Measured radiation features at 4.64 GHz under LHCP polarization: (a) spinning pattern in xz plane, (b) axial ratio in xz plane, (c) spinning pattern in yz plane and (d) axial ratio in yz plane.

PIEZO-ELECTRIC MODULATION OF MICROSTRIP ELEMENTS

Mitali Banerjee
Dr. Probir K. Bondyopadhyay
MAHANAD COMMUNICATIONS INC.
14418 Oak Chase Drive
Houston, Texas 77062
E Mail : p.bondy@worldnet.att.net

ABSTRACT

Recently discovered powerful piezo-electric PZN-PT and PMN-PT single Crystals will permit direct modulation of microwave signals in a microstrip element. This paper analytically and computationally examines this possibility that leads to experimental verification and creation of a direct modulator in the microwave-millimeter wave range. This work has practical applications in remote sensing of smart structures [1].

1. INTRODUCTION

It has been experimentally determined that the piezo-electric response in PZN-PT and PMN-PT single crystals is over ten times stronger than that in ordinary piezo ceramics. This is exemplified by the fact that the well known piezo-electric parameter d_{33} is 2000 picocoulombs/Newton (pC/N) in the new crystals compared to 180 pC/N in ordinary piezo ceramics [2, 3]. The strong piezo strain then could be utilized to cause appreciable change in the microstrip resonator (mounted on an actuator) structural dimensions like the resonant length, the width, the thickness or even the dielectric constant of the substrate through compressive forces. Computational analysis has been carried out with estimation of the changes in the resonant frequency caused by substrate thickness change as well as the resonant length change.

2. NUMERICAL ANALYSIS OF CHANGES IN MICROSTRIP RESONANCE PARAMETERS

A rectangular microstrip resonator element is shown in Figure 1. An accurate numerical analysis of this sensor for resonant frequency already exists[4]. Such a microstrip antenna element could be bonded onto a multi-layer piezoelectric actuator such that the resonant dimension a is affected by the actuator. Also the piezo-electric

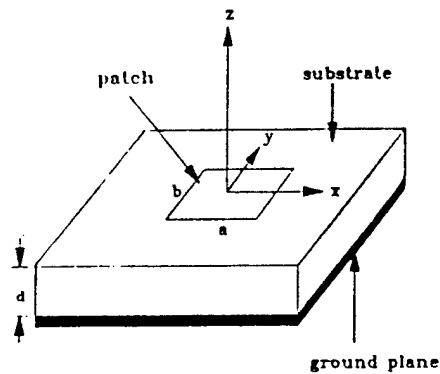


Figure 1. Low profile microstrip resonator structure. Structural dimensions will be changed by piezo-electric means to change the resonant frequency.

Crystal based actuator could be made to change the thickness of the substrate(could be an air gap) as shown in Figure 2.

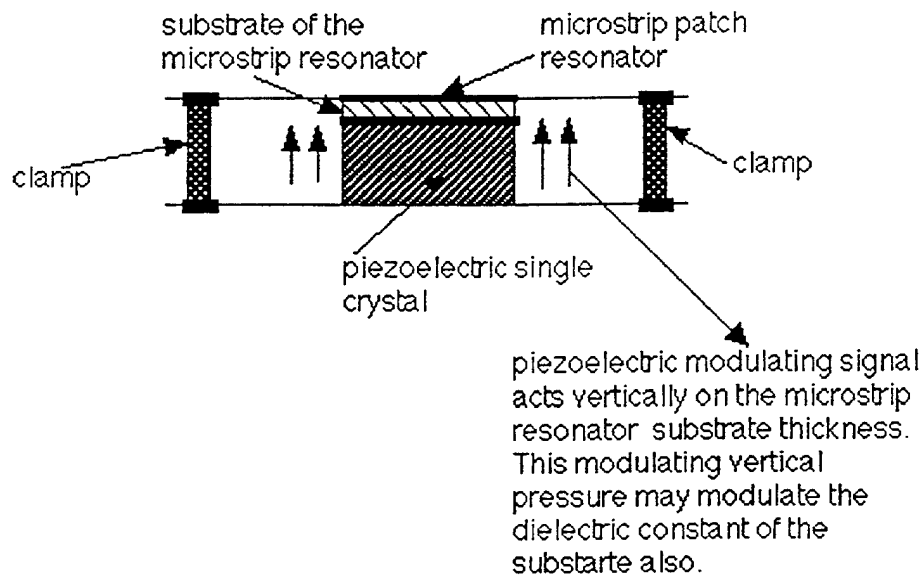


Figure 2 Experimental fixture for substrate thickness modulation.

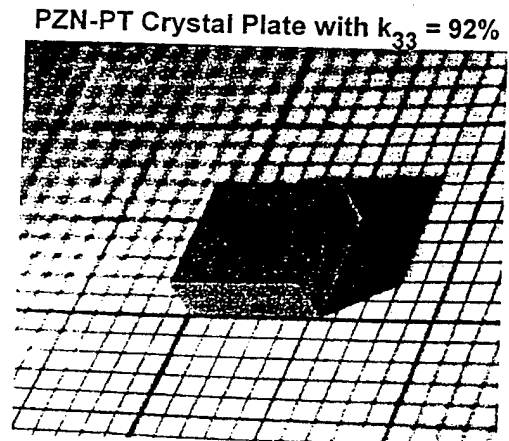
The new piezoelectric crystal can also be engaged to modulate the thickness of the microstrip resonator substrate. The dielectric constant of the substrate could be made to change due to pressure fluctuation. This action is going to change the resonant frequency of the microstrip resonator. The structure is outlined in Figure 2. The microstrip element is on a plate which is clamped with the multi-layer 33-mode actuator base plate. The actuator is supposed to compress the thickness of the microstrip resonator substrate. This will also modify the dielectric constant of the microstrip substrate which could be low dielectric constant PTFE material or higher dielectric constant ceramic impregnated composite substrate. The applications are at higher microwave frequency range like 20 GHz, 30 GHz or above where the substrate thickness could be like 5 mil, 10 mil or 20 mil.

3. PHYSICAL PROPERTIES OF THE CRYSTALS

Properties of the PMN-PT and PZN-PT crystals currently available is shown below.

PROPERTIES OF PIEZOELECTRIC SINGLE CRYSTALS

PROPERTY	PZN-PT (PT=0.08~0.09)	PMN-PT (PT=0.32~0.35)
K_3^T	4000~4200	4000~4500
$d_{33}(\text{pC/N})$ (150H, 0.3N)	1500~3000	1500~3500
e_{33} Strain (at 3KV/mm)	0.8~1.2%	0.6~1.0%
k_{33}	0.89~0.92	0.85~0.91
$T_c (^{\circ}\text{C})$	165~175	150~160
$E_c (\text{V/mm})$	300~600	250~500
$\text{tg}\delta$ (1kHz)	~0.01	~0.006
$P_s (\text{C/m}^2)$ (001)	0.35~0.45	0.30~0.40



4. APPLICATIONS

Although piezoelectric effect had been discovered in the 1880s by Pierre Curie and microstrip antennas came into existence in the 1950's, the two had no connections because piezoelectric materials are lossy at microwave frequencies and the effect is very very small in materials like quartz which could be a good substrate at microwave frequencies. Recent discovery of these powerful single crystals opened a new area of sensor research. Remote sensing of smart structures will be made possible by this discovery and investigation.

5. REFERENCES

1. Probir K. Bondyopadhyay, "Direct piezo-electric modulation of microstrip sensor elements", U.S. Patent Application, 22nd June 2001.
2. S-E. Park and T. R. Shrout, "Ultrahigh Strain and Piezoelectric Behavior in Relaxor Based Ferroelectric Single crystals", J. Appl. Phys, Vol. 82, No. 4, pp. 1804-1818, 1997.
3. S-E. Park and T. R. Shrout, "Characteristics of Relaxor Based Piezoelectric Single crystals for Transducers", IEEE Trans. Ultrasonics, ferroelectrics and frequency Control, vol. 44, no. 5, pp. 1140-1147, September 1997.
4. W.C. Chew and Q. Liu, " Resonance Frequency of a Rectangular Microstrip Patch," IEEE Trans. Antennas and Propagation, vol.AP-36, no.8, pp. 1045-1056, August 1988.

ANTENNA EFFICIENCY AND GAIN OF TWO NEW COMPACT MICROSTRIP ANTENNNAS

S. Zhang, G. Huff, and J. T. Bernhard
Electromagnetics Laboratory
Department of Electrical and Computer Engineering
University of Illinois at Urbana-Champaign
Urbana, IL 61801

Abstract: This paper presents the results of a study of antenna efficiency and gain of two new linearly polarized probe-fed microstrip antennas. Both antennas are characterized with measurements and simulations. The first antenna is a compact single-arm microstrip square spiral antenna with tuning arms. This antenna provides basic operating characteristics comparable to those of a traditional microstrip patch antenna while significantly reducing the antenna's physical extent and conductor area. The effect of the spiral nature of the current on overall antenna gain is discussed. The second antenna is a broadband rectangular microstrip antenna with a U-slot. This antenna possesses an impedance bandwidth of nearly 36% and a radiation bandwidth of 30% for linear polarization. The effect of the antenna's multiple resonances on efficiency and gain across the entire operating band is discussed. Comparisons of both antennas to simple rectangular microstrip antennas with identical ground plane sizes and feed probes are provided.

1. Introduction

Rectangular and circular microstrip antennas are widely used in communication receivers or antenna arrays. They have low profiles and light weight and are easy to fabricate and integrate. With the proliferation of personal wireless communication, designers search for small antennas for portable receivers. Many methods, such as addition of slots, parasitic elements and superstrates to the basic structure [1-3], have been proposed to reduce the size of microstrip patches.

In this paper, we study two different antennas. The first is a single-arm microstrip square spiral antenna with two tuning arms, and the second is a U-slot microstrip antenna. Both of them have two frequency bands with $VSWR < 2$ and a significantly smaller size than a traditional patch antenna. Additionally, the bandwidth of the U-slot antenna is much more broad than a traditional microstrip

antenna. The efficiency and gain of the spiral antenna and the U-slot antenna are measured and discussed.

2. Structure of Spiral Microstrip Antenna

The structure of the square spiral antenna is shown in Figure 1 [4]. It is fabricated on a substrate with height $H=3.175$ mm and relative permittivity $\epsilon_r = 2.2$. The spiral arm is 3 mm wide and the linear spacing between contiguous conductors is also 3 mm. Two tuning arms of 3×3 mm² are added symmetrically as shown. A coaxial feed probe is positioned at the origin. The dimensions of the antenna are 24×27 mm² with a conductor area of 403.5 mm².

A traditional square microstrip antenna operating at the same frequency on the same substrate has dimensions of 30.8×30.8 mm² with conductor area of approximately 948 mm². Therefore, the proposed spiral antenna provides a 32% reduction in dimension and a 57% reduction in conductor area compared to a square microstrip antenna.

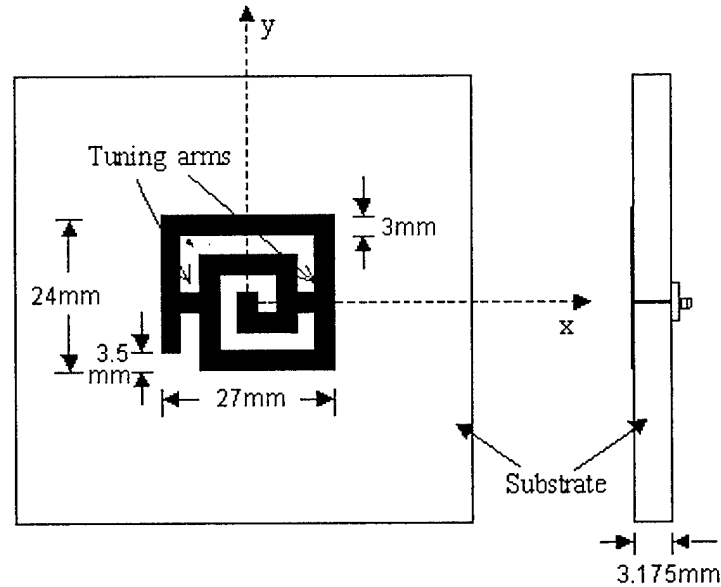


Figure 1: Geometry of the single-arm square microstrip spiral antenna with tuning arms.

3. Structure of U-slot Antenna

The geometry of the U-slot patch antenna, shown in Figure 2, is determined by the design procedure outlined in [5]. The structure is probe fed on Duroid© 5880

substrate with a height $H=3.175$ mm and relative permittivity $\epsilon_r = 2.2$. The overall dimension of the U-slot patch is 10.25×18.95 mm², approximately 194.24 mm², with a U-slot dimension $(6.625+6.0+6.625) \times 0.625$ mm², approximately 12.03 mm², for a total conductor area of 182.21 mm².

The standard rectangular patch antenna design with the same resonant frequency as that of the first U-slot resonance has a total conductor area of 214.13 mm², given by 12.83×16.69 mm². As with the U-slot, the antenna is probe fed on Duroid® 5880 substrate with a height $H=3.175$ mm and relative permittivity $\epsilon_r = 2.2$. This antenna was designed for maximum efficiency using [6]. With this design, there is a 9.3% reduction in total area and a 15.0% decrease in conductor area by using the U-slot over the square antenna.

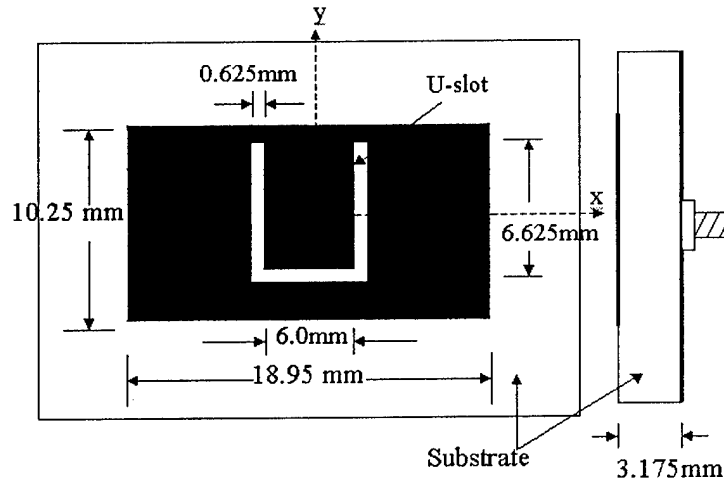


Figure 2: Geometry of the U-slot microstrip patch antenna.

4. Spiral Microstrip Antenna vs. Square Microstrip Antenna

The input impedance and S_{11} of the spiral antenna are shown in Figure 3. The frequency range extends from 2.5 GHz to 3.5 GHz. The antenna has two frequency bands with $VSWR < 2$. At the frequency of 3.0 GHz, the return loss is 11 dB and 2:1 VSWR bandwidth is 50 MHz (1.7%). It is larger than the 2:1 VSWR bandwidth of a traditional square antenna on the same substrate, which is about 1.4%. At 2.79 GHz, the S_{11} is -12.7 dB while the bandwidth is quite small. The two frequency bands indicate the antenna has the potential to work as a dual band antenna if the resonant frequencies and the bandwidth could be controlled

with judicious selection of antenna parameters. This is an attractive characteristic in some wireless communication systems where the transmitting and receiving channels are in different frequency bands.

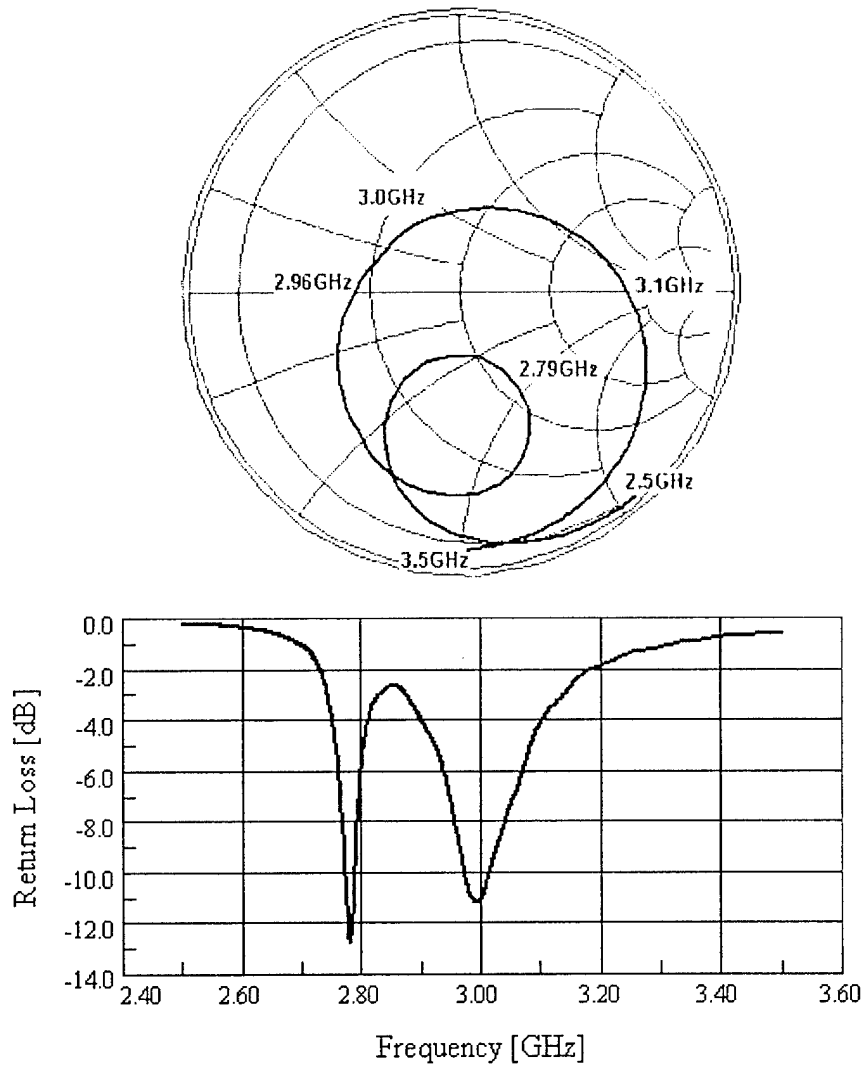


Figure 3: Input impedance and return loss of the single-arm square microstrip spiral antenna.

Table 1 compares characteristics of the spiral microstrip antenna with a traditional square antenna derived from experiments. Radiation efficiencies of 3.0 GHz measured using Wheeler cap method [7] are 7~10 percent higher than those simulated by IE3D [8]. A portion of the efficiency is contributed by the surface

wave that eventually radiates into free space [9]. In the measurement, most of the surface wave will contribute to the radiated fields because of diffraction effects. IE3D does not account for the surface wave when calculating the radiation efficiency using the method of moments, so the measured efficiency would normally be higher than simulated.

The radiation efficiency of the spiral antenna at 2.79 GHz could not be measured correctly by the Wheeler cap method because readings at this frequency fluctuated greatly. This may be due to a limitation of the Wheeler cap method. The Wheeler cap method models the radiation impedance and the loss impedance as a series or parallel combination. However in some antennas, such as our spiral antenna, this assumption fail since the structure is more complicated. Simulations using IE3D indicate an efficiency above 80% at 2.79 GHz for this structure.

Tab.1 Comparing of characteristics of the spiral antenna and square antenna

	Resonant Frequency (GHz)	2:1 VSWR Bandwidth (MHz)	Radiation Efficiency	Gain (dB)
Square Antenna	3.0	38	96%	7.7
Spiral Antenna	3.0	50	86.7%	7.6
	2.7875	<20	Not Measured	7.4

These measurements show that the spiral antenna has a slightly lower radiation efficiency than the square antenna. The current distribution could explain this phenomenon. Nearly all currents distributed on the square antenna go in the same direction so that no power is dissipated through cancellation. However, for the spiral antenna, currents curve along the spiral. Some of them go to the opposite direction of others, so that a small part of the radiation power is dissipated by cancellation. Moreover, the discontinuities of the currents around corners also could lead to lower efficiency.

Both the spiral antenna and the square antenna radiation patterns are broadside and linear polarized. The beamwidth of the spiral antenna is about 85°~90° at both frequencies [4]. Comparably, the beamwidth of the square antenna is about 80°. The cross-polarization of both antennas working at 3.0 GHz is more than 18

dB lower than the co-polarization. However, when working at 2.79 GHz, the spiral antenna's cross-polarization is only 10 dB lower than the co-polarization.

The measured gains are approximately 1 dB higher than simulated. An infinite ground was used in the simulations, while the actual antennas have grounds of $60 \times 60 \text{ mm}^2$. The finite ground makes the beamwidth narrower than that with a finite ground [10].

5. U-slot antenna vs. Rectangular Patch

The input impedance for the U-slot antenna is shown in Figure 4 over the frequency range 4-10 GHz. As with the spiral antenna, there are two frequency bands under investigation. The fundamental minimum S_{11} frequency is 7.3 GHz, at which point the antenna has a return loss of -16.1 dB and a 2:1 VSWR bandwidth of 1095 MHz (15%). This is significantly larger than the complimentary patch design at the onset of this band, which has a 2:1 VSWR bandwidth of 765 MHz (10.5%), nearly a 5% increase in percentage bandwidth. For the second band, centered at 9.775 GHz with a return loss of -14.7 dB , there is a 2:1 VSWR bandwidth greater than 1500 MHz (16%). Combined, these two bands could provide dual-band operation for very high bandwidth transmitting or receiving applications.

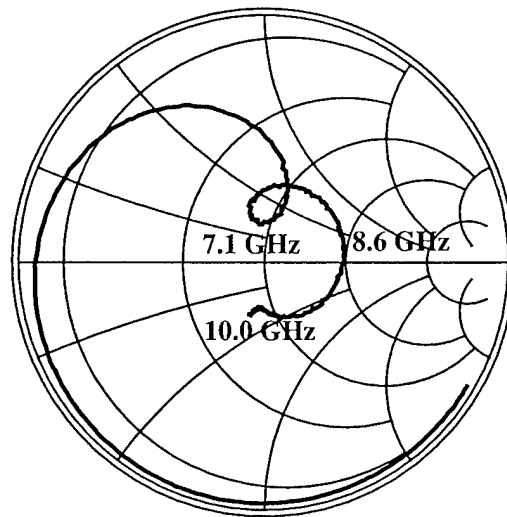


Figure 4: Input impedance frequency characteristics of the U-slot microstrip antenna.

Table 2 demonstrates the performance differences of the examined antenna figures of merit between the U-slot and rectangular patch. As with the spiral antenna, radiation efficiencies were measured using the Wheeler cap method [7]. Both antennas have broadside radiation patterns with at least 10dB of isolation from cross polarization. It should be noted that the beamwidth of the U-slot was slightly larger (by 11% and 18% for f_1 and f_2 respectively) as a performance trade-off for the decrease in measured gain when compared to the rectangular patch (which has a beamwidth of approximately 82°).

Tab.2 Comparing of characteristics of the U-slot antenna and rectangular patch antenna

	Resonant Frequency (GHz)	2:1 VSWR Bandwidth (MHz)	Radiation Efficiency	Gain (dBi)
Patch Antenna	7.1	765	96.1%	8.6
U-slot Antenna	7.1	1095	67.8%	6.9
	8.6	>1500	91.8%	2.7

In the U-slot antenna, ohmic losses are the leading factor for the decrease in efficiency at the first resonant frequency compared to the rectangular patch antenna. Figure 5 shows the simulated current distribution for the rectangular patch as well as for both resonant frequencies of the U-slot antenna. As the figure suggests, the current is high around the discontinuities provided by the U-slot. For the second U-slot operating band, the patch within the U-slot is effectively radiating and although there is high current density around the bends, the average electrical path length of the current is reduced and the efficiency of the structure is comparable to that of a patch.

6. Conclusion

Both a compact single-arm microstrip square spiral antenna and a U-slot antenna are studied. In comparison with traditional microstrip antennas, these antennas provide similar radiation characteristics. However, they significantly reduce the required physical dimensions and broaden the bandwidth, especially the U-slot antenna. These attributes come at the cost of decreased efficiency and gain, especially in the lower bands of both antennas. Both antennas can be useful for dual-band applications in small packages.

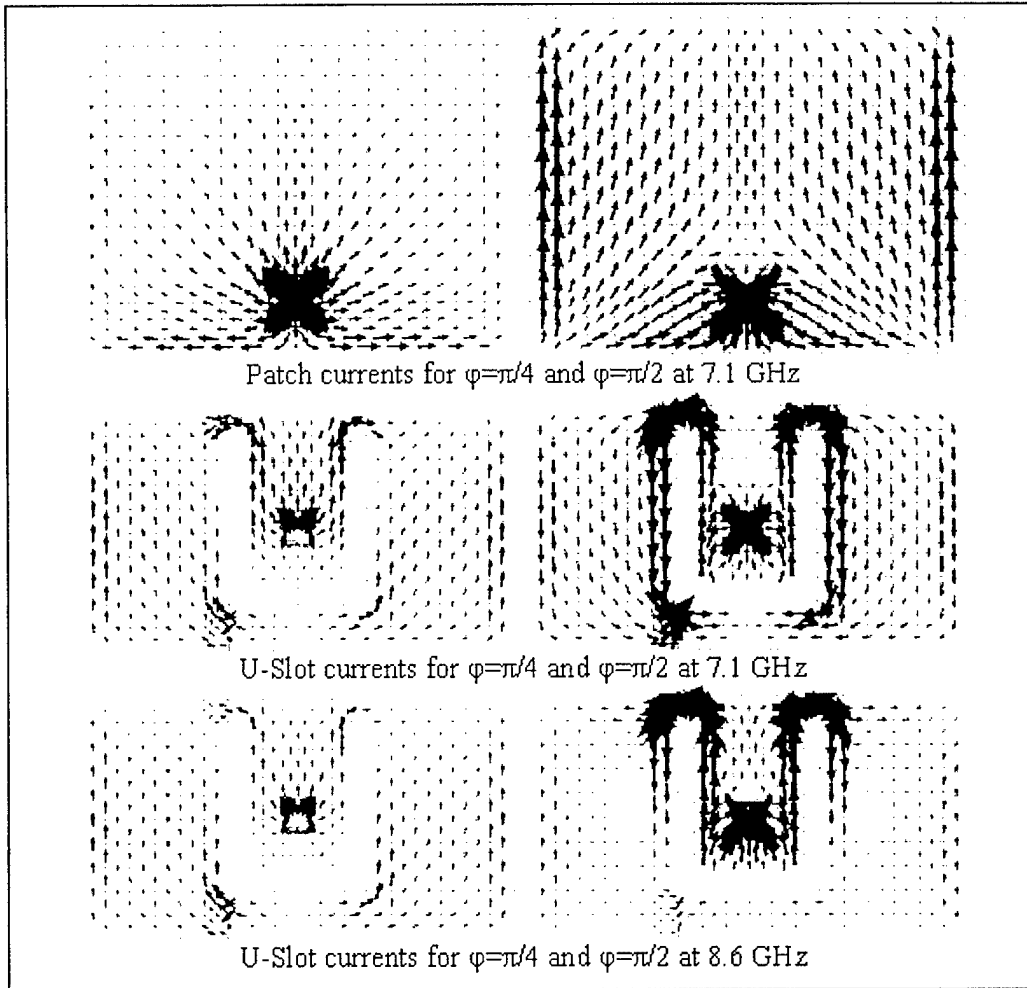


Figure 5: Average current densities for the rectangular patch and U-slot.

7. Acknowledgments

This work was funded in part by NSF grant #ECS-9983460. Dielectric substrates were provided by Rogers Corporation.

8. References

- [1] K. M. Luk, K.F. Tong, S.M. Shum, K.F. Lee, and R.Q. Lee, "FDTD analysis of U-slot rectangular patch antenna," IEEE AP-S Symposium Digest, 1997, pp. 2111-2114.

- [2] J.-H. Lu, C.-L. Tang, and K. L. Wong, "Slot-coupled compact broadband circular microstrip antenna with chip-resistor and chip-capacitor loading," *Microwave and Optical Technology Letters*, vol. 18, n. 5, 1998, pp. 345-349.
- [3] T. Holzheimer and T. O. Miles, "Thick multilayer elements widen antenna bandwidths," *Microwaves & RF*, vol. 24, n.2, 1985, pp. 93-95.
- [4] J. T. Bernhard, "Compact Single-Arm Square Spiral Microstrip Antenna with Tuning Arms," *Proc. IEEE/URSI Antennas and Propagation Soc. International Symp.*, vol. 2, 2001, p. 696-699.
- [5] S. Weigand, Student Member, G. Huff, K. Pan, and J. T. Bernhard, Member, "Analysis and Design of Broadband Single-Layer Rectangular U-slot Microstrip Patch Antennas," In review at *IEEE Trans. on Antennas and Propagation*.
- [6] K.G. Schroeder, "Miniature Slotted-Cylinder Antennas," *Microwaves*, pp. 28-37, Dec. 1964.
- [7] H. A. Wheeler, "The Radiansphere Around a Small Antenna," *Proc. IRE*, Aug. 1959, pp. 1325-1331.
- [8] IE3D, Version 8.1, Zeland Corporation.
- [9] David M. Pozar, and Barry Kaufman, "Comparison of Three Methods for the Measurement of Printed antenna efficiency," *IEEE Transactions on Antenna and Propagation*, vol. 36, no. 1, Jan. 1988, pp. 136-139.
- [10] S. Noghianian and L. Shafai, "Control of microstrip antenna radiation characteristics by ground plane size and shape," *IEE Proc.-Microwaves Antennas & Propagation*, vol. 145, no. 3, June 1998, pp. 207-212.

EXPERIMENTAL INVESTIGATION OF ANTENNA-HANDSET-FEED INTERACTION DURING WIRELESS PRODUCT TESTING

J. Haley,¹ T. Moore,² J. T. Bernhard¹

¹ Electromagnetics Laboratory
Department of Electrical & Computer Engineering
University of Illinois at Urbana-Champaign
Urbana, IL 61801

² Amphenol T & M Antennas*
825 Corporate Woods Pkwy
Vernon Hills, IL 60061

Abstract: Understanding interactions between the element and handset offers practical value for developers of antennas for portable applications. Chassis shape and element design dominate portable antenna circuit and radiation properties. Considerations of the entire operating environment enable ideal prediction of antenna radiation performance and regulatory compliance. This work investigates the interplay between the element, handset size, and feedline radiation suppression techniques. Radiation pattern and input reflection magnitudes are experimentally characterized at 1.6 and 1.9 GHz for several handset shape combinations.

1. Introduction

The typical handset measurement configuration inherently differs from that of a wireless device in operation. Handset chassis, antenna element, and environment [1] contribute to actual antenna performance, but during development the transmission line that supplies the signal to the antenna becomes another contributor [2], [3]. Quantifying the feedline contribution to

* T. Moore was with Amphenol T & M Antennas, Vernon Hills, IL. He is now with Northrop Grumman Corporation, Rolling Hills, IL.

antenna characteristics reduces uncertainty introduced by the measurement setup.

Radiating system design approaches include interpretation of the antenna development problem and antenna element specifications. Depending on the severity of element/chassis interactions, the antenna development problem is more appropriately cast in terms of contributions from the antenna and feed structure rather than separate consideration of the element and chassis. Especially in designs that require the ground metalization to achieve dipole resonance, the chassis ground comprises half of the antenna. Antenna element specifications inclusive of chassis effects provide more meaningful design guidelines. For example, the geometry-dependent element/chassis interaction can shift the measured near-resonance operating band away from values specified for the element.

Antenna performance aspects addressed in this work include return loss and pattern prediction for quarter-wave wire elements driven against variably-sized ground planes. The difference between chassis ground metalization and a traditional monopole/ground plane scenario accounts for observed asymmetric radiation patterns.

2. Antenna and Feed Structure Design

2.1 Handset Design

Appropriate selection of handset layout and antenna element enables measurements that yield the essence of chassis/antenna element interactions. To construct the handset, a double-side copper clad Rogers RO4350 ($\epsilon_r = 3.48$, $h = 60$ mil) substrate was milled and cut into rectangular boards (see Figure 2.1). In the layout, copper foil serves as the continuous ground reference/counterpoise on the board front, back, and edges. Although collinear, loaded whip antennas are commonplace, a simple quarter-wave (1.9 GHz) wire element is attached to a corner of exposed (front and back) substrate dielectric. Semi-rigid coaxial cable terminated in an SMA jack applies power to the wire element. Within the board periphery, soldering the cable shield to the board copper foil shunts stray currents along the line.

Handset dimensions vary as fractions of the free-space wavelength at 1.9 GHz. To explore the frequency sensitivity to substrate shape, board length and width dimensions shown in Table 2.1 assume both harmonic and non-harmonic wavelength fractions.

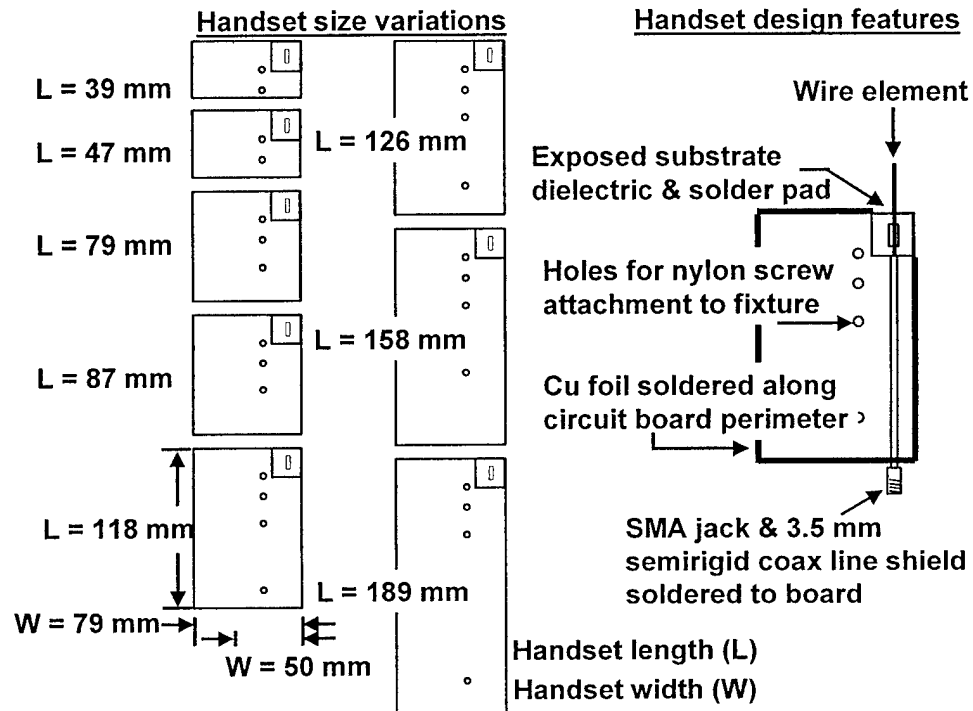


Fig. 2.1. Handset size variations and design detail.

Table 2.1 Antenna handset dimensions designed for 1.9 GHz.

L [mm]	39	47	79	87	W [mm]	50, 79
L/λ_0	0.25	0.30	0.50	0.55	W/λ_0	0.32, 0.50
L [mm]	118	126	158	189	W [mm]	50, 79
L/λ_0	0.75	0.80	1.00	1.20	W/λ_0	0.32, 0.50

2.2 Isolation Device Design

During the experiment, input impedance and radiation measurements for each handset antenna include either an isolation device (a sleeve balun) or equal-length, semi-rigid coaxial cable. Figure 2.2 depicts the handset measurement

and scattering-parameter reference plane. The coaxial sleeve balun designed for 1.9 GHz is constructed from 3.5 mm semi-rigid cable and brass tubing. Three short-circuited, quarter-wave coaxial sections reduce feedline currents that affect antenna characteristics.

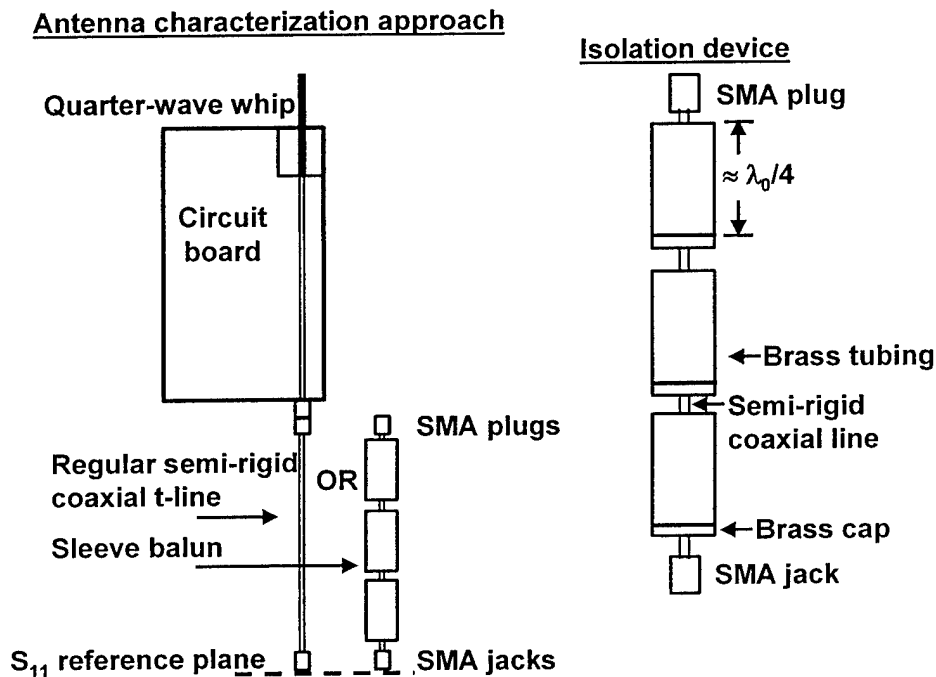


Fig. 2.2. Designs for experimental antenna characterization.

3. Handset Characterization Results

Antennas measured consist of quarter-wave wire elements fed against the handset double-sided circuit board ground metalization. The sleeve balun and equal-length, coaxial cable comprise the characterized feedline accessories. To correlate handset geometry and sleeve balun effects, antenna return loss and radiation pattern are measured for each design.

3.1 Isolation Device Reflection and Transmission Characteristics

For accurate assessment of antenna circuit behavior, devices employed to reduce parasitic feedline currents should introduce negligible in-line reflection and attenuation. Two-port characteristics are verified for the sleeve balun and equal-length semi-rigid coaxial cable. Measurement results for the two devices

exhibit reflection and attenuation magnitudes better than -35 dB and -0.15 dB, respectively (see Fig. 3.1).

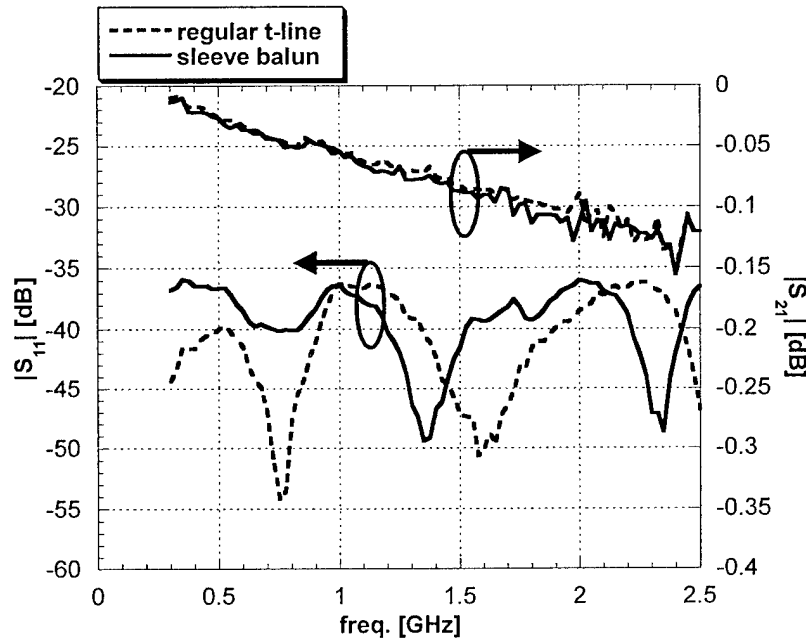


Fig. 3.1. Coaxial transmission line and sleeve balun measured S-matrix magnitudes.

3.2 Antenna Mismatch Characteristics

During measurement of the input impedance mismatch, either the sleeve balun or coaxial transmission line section is connected between the RF source and handset. One-port scattering parameter measurements of a fixed-length antenna element and handsets having three lengths and two widths investigate the extent to which induced feedline currents affect antenna circuit behavior.

For the 79 mm width handset, Figure 3.2 displays a drastic difference between the response with and without the sleeve. Since these dimensions support a dual resonance, omitting the sleeve erodes the dual-frequency match characteristic. Higher return loss observed for the 50 mm width handset and only slight variation between the transmission line and sleeve balun cases demonstrate the performance sensitivity to handset dimensions.

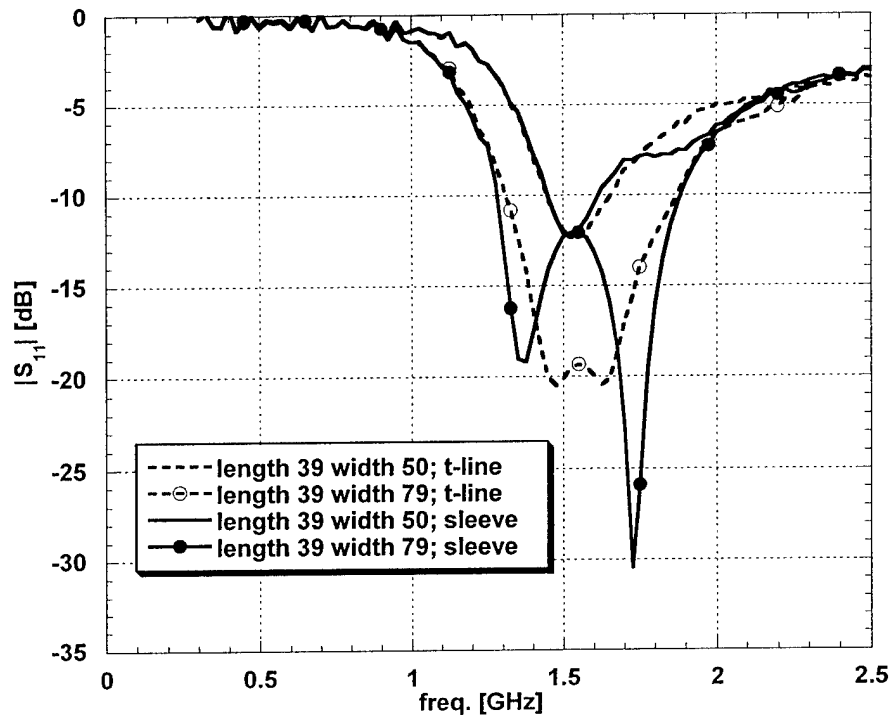


Fig. 3.2. Isolation device impact on handset antenna S_{11} magnitudes for the shortest handset (39 mm) of 50 and 79 mm width.

Increasing the board length in the 79 mm width design stabilizes the response and gives continuous operating bands at 1.6 GHz. Figures 3.3 and 3.4 illustrate reflection levels below -20 dB for lengths 87 and 189 mm. When the 50-ohm cable is replaced with the sleeve, magnitudes at resonance for the 87 mm handset differ slightly. However, shorter handsets exhibit pronounced differences.

For the 50 mm width board, the 1.6 GHz mismatch obtained over the length variation increases from -12 to -10 dB, but the sleeve's influence on antenna impedance diminishes.

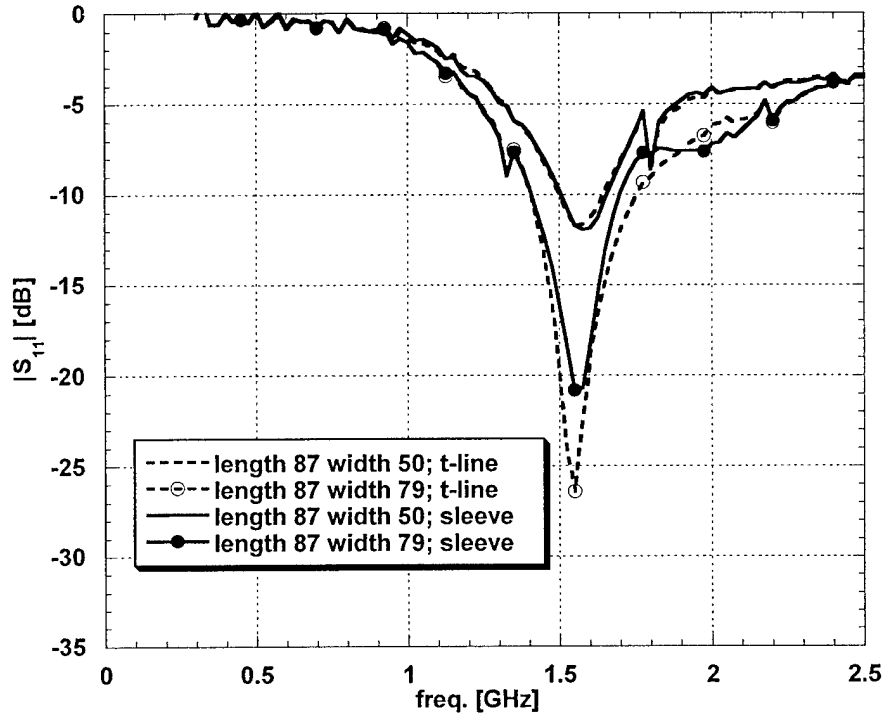


Fig. 3.3. Isolation device impact on handset antenna S_{11} magnitudes for the 87 mm handset length of 50 and 79 mm width.

Measurement results for all handsets display a match near 1.6 GHz, 300 MHz below the design frequency. Corresponding to a 1.9 GHz free-space quarter-wave, the 39 mm wire element drives against the handset copper cladding ground reference. Although not directly applicable to this asymmetric antenna design, the well-known length compensation technique [4] for producing resonant half-wave dipoles is consistent with the observed resonance shift. Considering the wire diameter ($2a = 2.1$ mm) and analogous dipole length ($L = 78$ mm), the ratio $L/2a$ of 37 approaches the ratio value 50 that produces resonance for $L = 0.455\lambda_0$ or 1.75 GHz [4]. The disparate antenna resonance and isolation device operating frequencies prompted the study of radiation patterns at both 1.6 and 1.9 GHz.

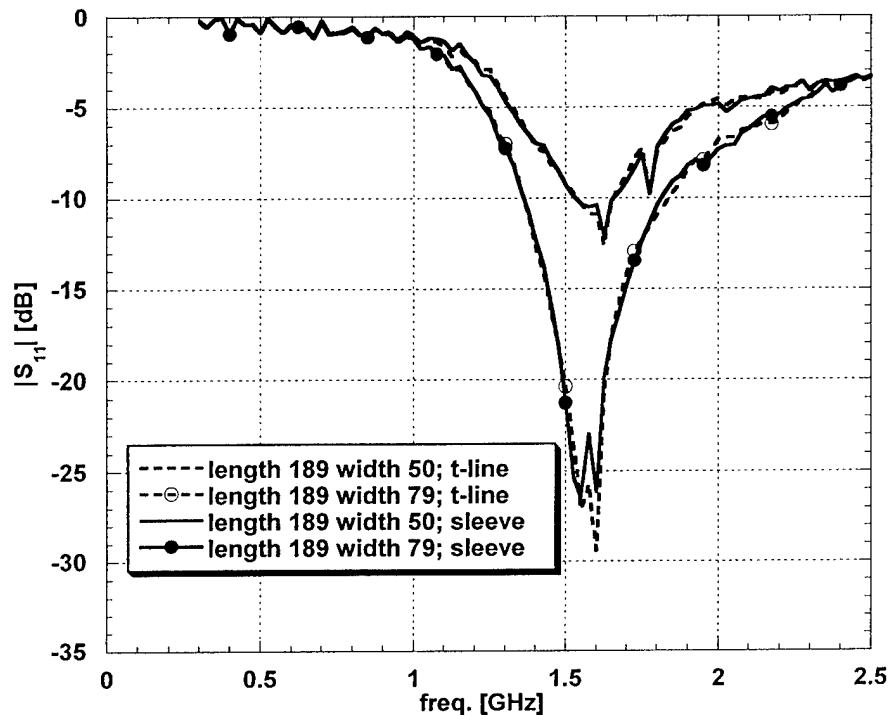


Fig. 3.4. Isolation device impact on handset antenna S_{11} magnitudes for longest handset (189 mm) of 50 and 79 mm width.

3.3 Radiation Pattern Analysis

Complementing the circuit viewpoint of antenna performance, elevational and azimuthal cuts of the far-field patterns are measured. The measurement configuration consisting of the energized, rotating handset and stationary pyramidal receive horn is illustrated in Figure 3.5. The handsets approximate asymmetric dipoles, and as such, are not particularly directive antennas. Instead of gain and side-lobe level considerations, we study the radiation pattern differences between the sleeve balun and regular transmission line. Angle annotations in the figure correspond to the viewing direction of the pattern plots, and plastic rotation fixtures place the handset center of rotation at the feedpoint end of the antenna wire element.

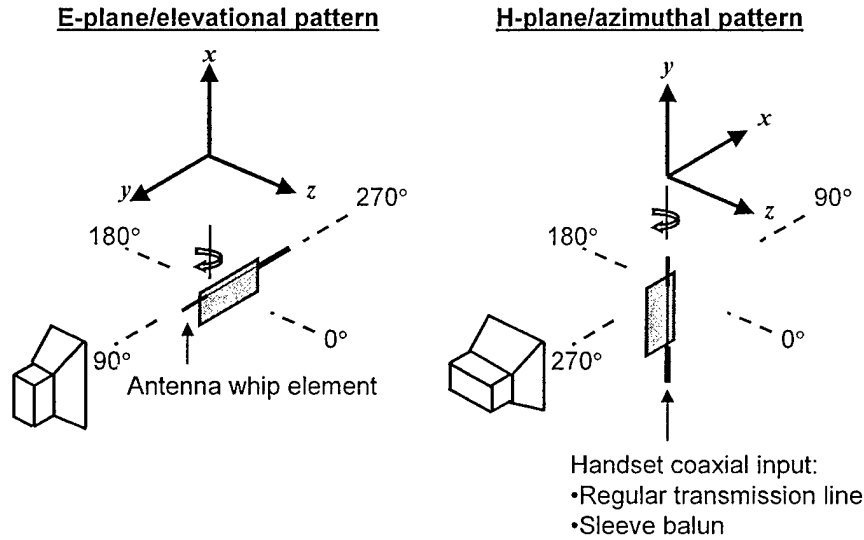


Fig. 3.5. Handset antenna radiation pattern measurement configuration.

The radiation pattern dataset consists of 128 copolarized measurements. To explore the isolation device's effect, elevational and azimuthal patterns are plotted for 1600 MHz in Figs. 3.6–8. An equivalent set of representative patterns measured at 1900 MHz include E-plane results for $\lambda_0/4$ and λ_0 board lengths and H-plane results for the $\lambda_0/4$ length (see Figs. 3.9–11). Measurements in each case (*t-line* and *sleeve*) are normalized to the peak magnitude observed within the two patterns. Including patterns for both 50 and 79 mm handset widths helps to convey the anticipated pattern sensitivity to harmonic ($79 \text{ mm} \approx \lambda_0/2$) circuit board dimensions.

An elevational cut perpendicular to the handset plane shows the antenna characteristics applicable to the scenario of a wireless device radiating while being held upright. Nulls observed near 90 and 270 degrees for both cases in Figures 3.6 and 3.9 are consistent with the dipole analogy, but the sleeve also eliminates pattern undulations introduced by the feedline. As expected for an electrically longer board, the additional lobes in Figures 3.7 and 3.10 highlight the pattern differences due to suppression of parasitic feedline currents.

Viewed on a scale down to -15 dB , azimuthal patterns in Figures 3.8 and 3.11 show the sleeve balun affecting the whole pattern. For the elevational plane, the comparison is based on how the two cases track the angular details of the

lobes, but the H-plane observations express how the sleeve spatially redistributes a major portion of the pattern along the length of the handset. Both elevational and azimuthal comparisons reveal that the sleeve balun reduces feedline radiation to yield accurate handset patterns.

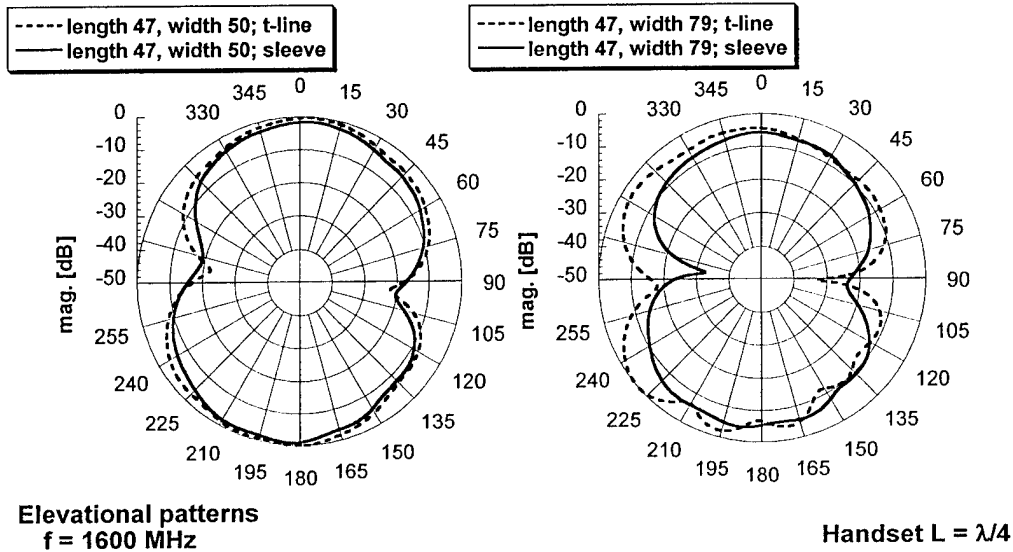


Fig. 3.6. Measured elevational pattern effects due to cable isolation device; measurement frequency 1600 MHz, handset length 47 mm, widths 50 and 79 mm.

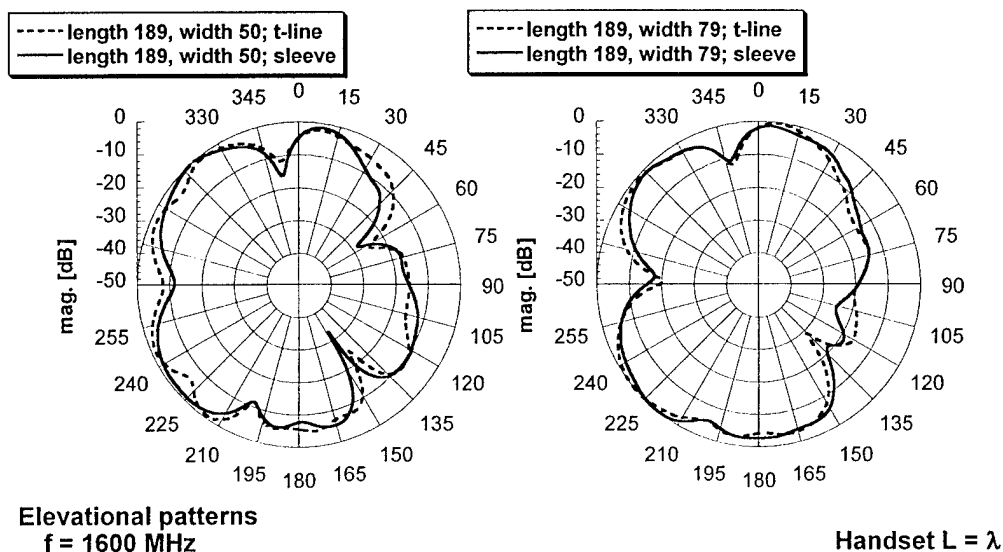


Fig. 3.7. Measured elevational pattern effects due to cable isolation device; measurement frequency 1600 MHz, handset length 189 mm, widths 50 and 79 mm.

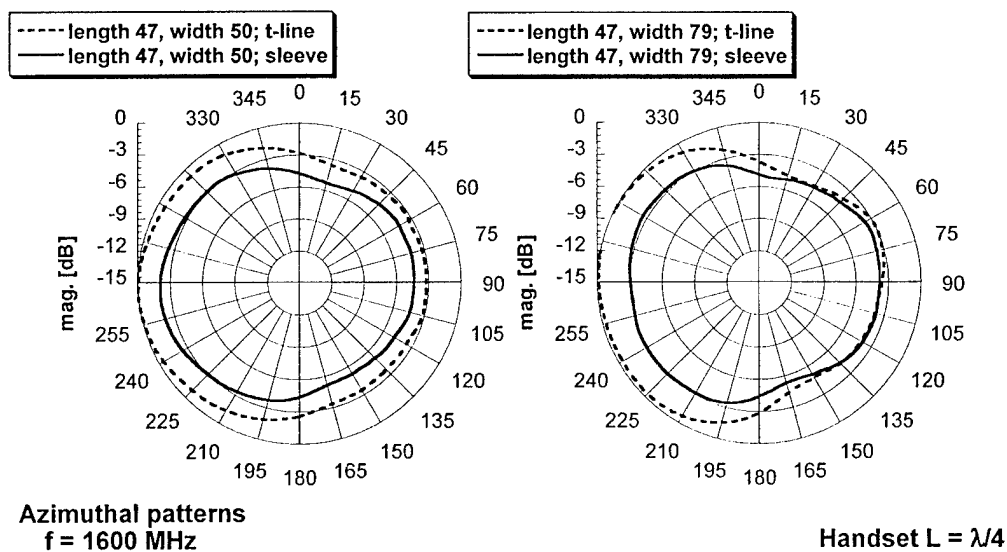


Fig. 3.8. Measured azimuthal pattern effects due to cable isolation device; measurement frequency 1600 MHz, handset length 47 mm, widths 50 and 79 mm.

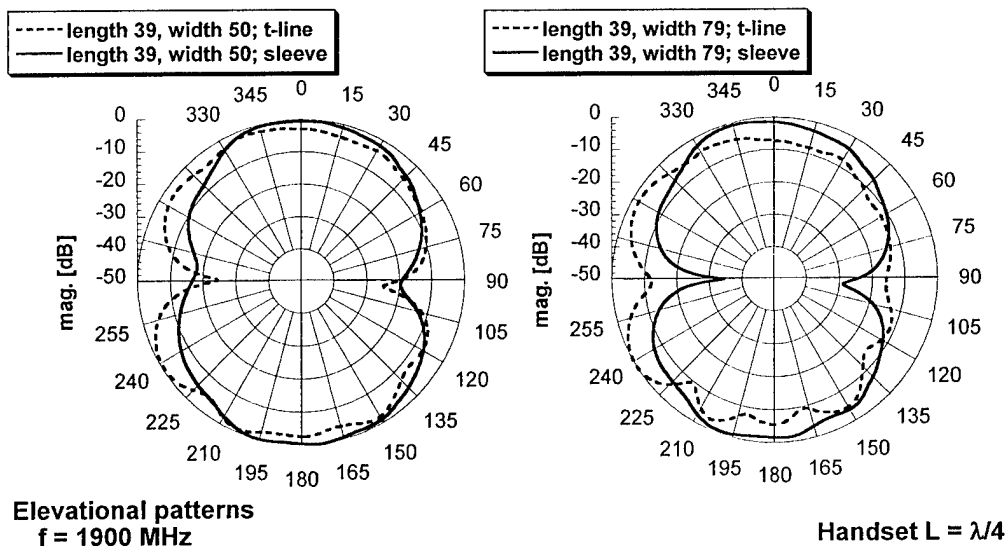


Fig. 3.9. Measured elevational pattern effects due to cable isolation device; measurement frequency 1900 MHz, handset length 39 mm, widths 50 and 79 mm.

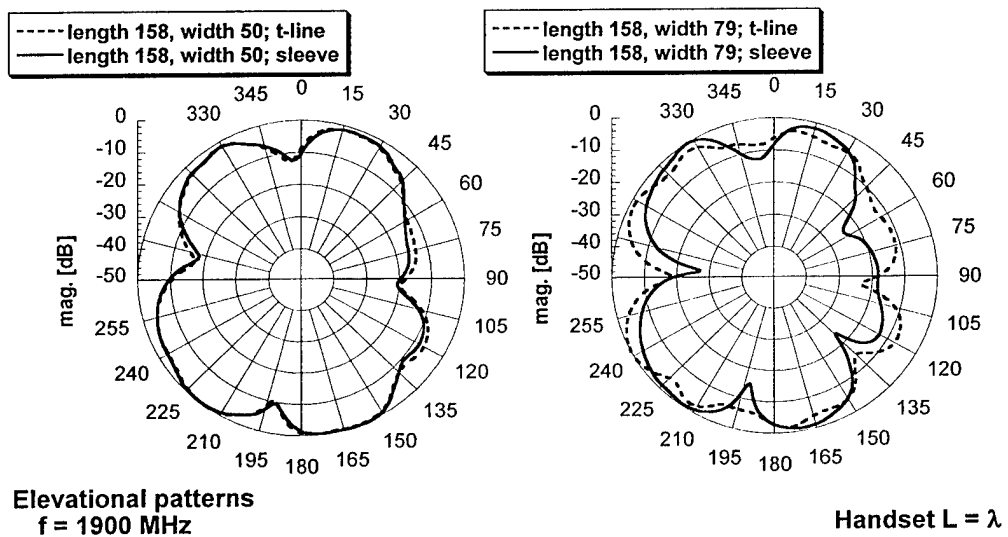


Fig. 3.10. Measured elevational pattern effects due to cable isolation device; measurement frequency 1900 MHz, handset length 158 mm, widths 50 and 79 mm.

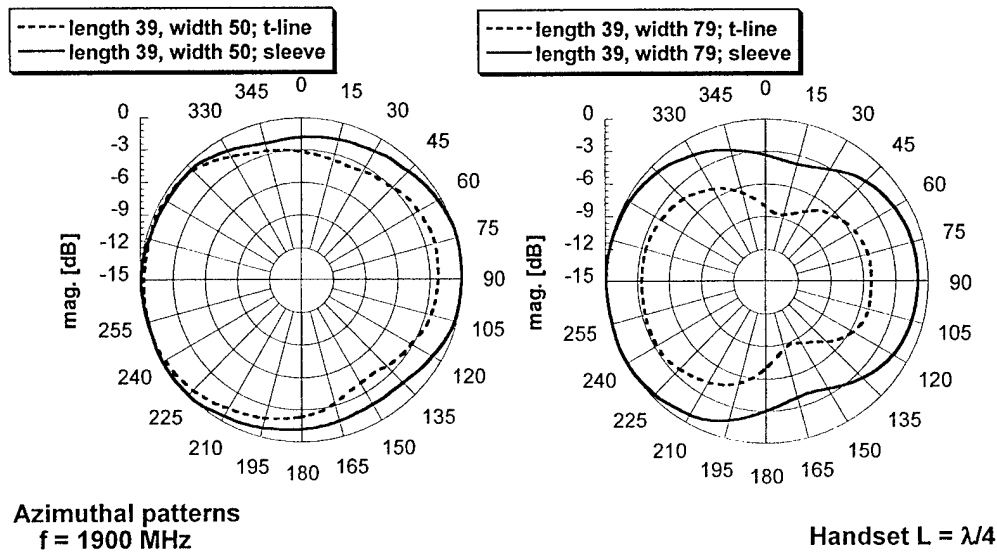


Fig. 3.11. Measured azimuthal pattern effects due to cable isolation device; measurement frequency 1900 MHz, handset length 39 mm, widths 50 and 79 mm.

Due to the extent of the measured dataset, the task of manual pattern plot comparison necessitates a more direct method. Calculation and analysis of pattern magnitude differences automate visual comparison. During the process, datasets are converted to linear magnitude and normalized. The pattern difference (*sleeve* magnitude – *t-line* magnitude) is a function between ± 1 and varies with angle. Calculating the pattern difference mean and standard deviation embeds angular complexity into two values that enable trend analysis with respect to handset geometry. Figures 3.12 and 3.13 consider the 1600 MHz elevational and azimuthal pattern statistics, respectively. Similarly, isolation device effects are observed in principal-plane patterns at 1900 MHz (see Figures 3.14 and 3.15).

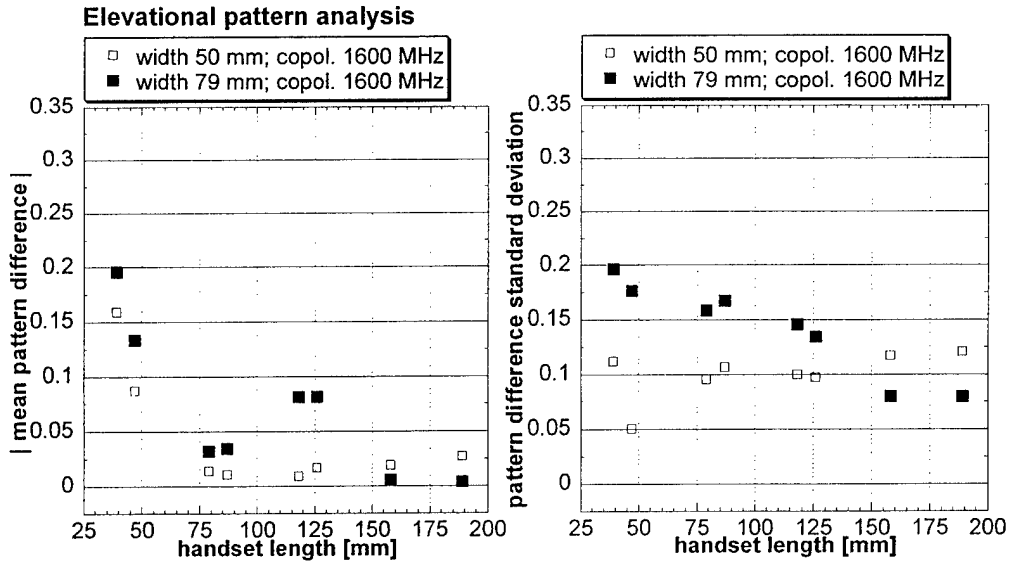


Fig. 3.12. Elevational pattern difference mean and standard deviation variation with handset shape; measurement frequency 1600 MHz.

The mean pattern difference (μ) expresses the sleeve balun's average effect on the whole pattern, while the standard deviation (σ) describes the directionality of the pattern change. To rank the severity of the observed effects, the following μ and σ magnitude ranges are established: *small* (0.000 to 0.075), *moderate* (0.075 to 0.150), and *large* (> 0.150). Four sample groups consist of two test frequencies (1600 and 1900 MHz) and two characteristic handset lengths (above and below $0.60\lambda_0 \approx 100$ mm). For each group both elevational and azimuthal antenna characteristics are considered together and compiled in Table 3.1. Results shown in the table are extracted from Figures 3.12 through 3.15 and enable correlation between pattern perturbations and handset geometry.

Two definitive trends embody the pattern sensitivity to handset shape and presence of a feedline radiation suppression device. As board length increases, overall pattern differences (μ trend) decrease for the near-resonance antenna (1600 MHz), regardless of handset width. Near the sleeve balun operating frequency (1900 MHz), the pattern change directionality (σ trend) diminishes with increased board length, regardless of handset width.

Table 3.1 Trend analysis for isolation device pattern effects.

Frequency		1600 MHz		1900 MHz	
Handset length	Pattern difference parameter	Handset width 50 mm	Handset width 79 mm	Handset width 50 mm	Handset width 79 mm
$L < 0.6 \lambda_0$	μ	moderate	moderate	small	large
	σ	small	moderate	moderate	large
$L > 0.6 \lambda_0$	μ	small	small	small	small
	σ	small	small	small	moderate

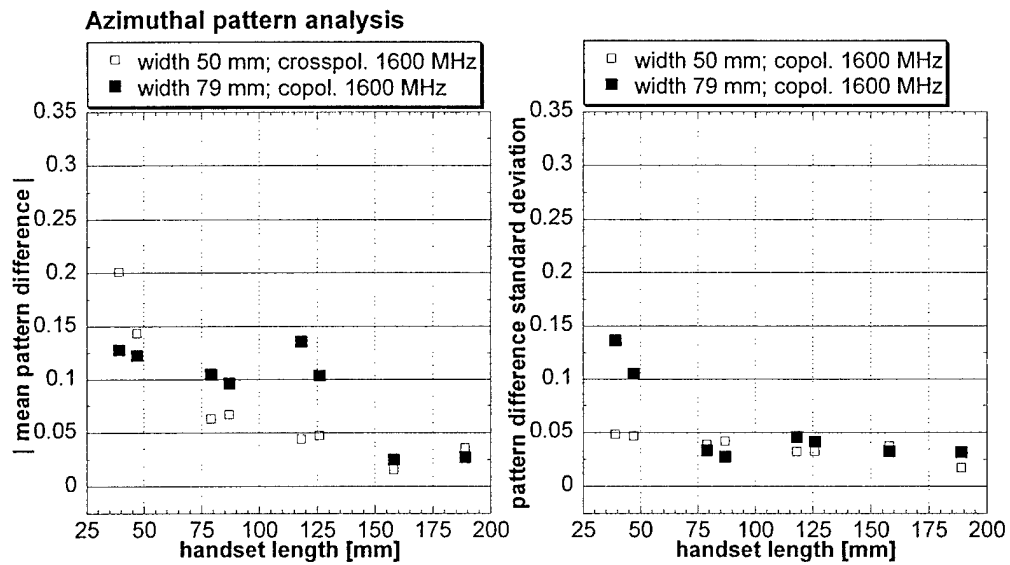


Fig. 3.13. Azimuthal pattern difference mean and standard deviation variation with handset shape; measurement frequency 1600 MHz.

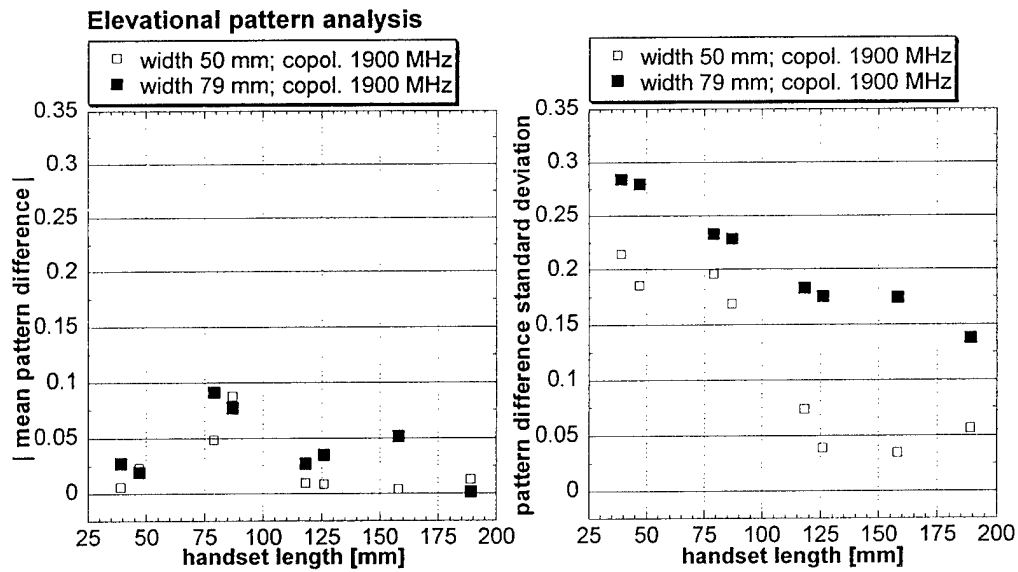


Fig. 3.14. Elevational pattern difference mean and standard deviation variation with handset shape; measurement frequency 1900 MHz.

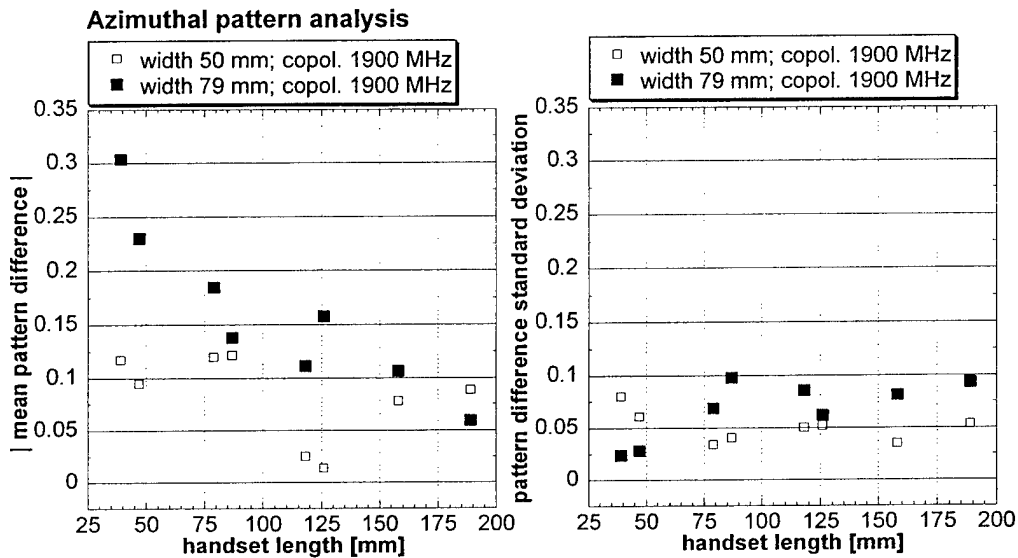


Fig. 3.15. Azimuthal pattern difference mean and standard deviation variation with handset shape; measurement frequency 1900 MHz.

4. Discussion

Antenna impedance sensitivity to board geometry was demonstrated through results presented for six handset designs. For electrically smaller handsets we observed significant response changes between measurements including either the sleeve or regular transmission line devices in the RF feed. Idealizing our antenna-handset radiator to be a half-wave dipole, calculations showed plausibility of a resonance shift from the intended 1.9 GHz operating frequency to 1.75 GHz. Since the antenna consists of dissimilar conductors, length compensation techniques were not employed during design. Uncertainties introduced by application of the dipole analogy to an asymmetric antenna prompted dimension choices referenced to free-space wavelength. The match observed at 1.6 GHz suggests that designers should account for board size while tailoring the antenna impedance.

Over the large design set characterized, trend extraction from plots of angular variation of pattern differences proved cumbersome. Instead, pattern difference mean and standard deviation were utilized to quantify pattern effects introduced by feedline radiation. The statistical parameters help to contrast measurements of an isolated handset with those that include detrimental feedline contributions.

The mean and standard deviation together capture the isolation device's overall magnitude and direction-dependent changes to the radiation pattern shape. A complete assessment of pattern effects requires both μ and σ values. For both handset width values, the 1.6 GHz mean pattern difference and 1.9 GHz standard deviation decrease with increasing board length. Pattern difference parameters μ and σ also show sensitivity to board widths equaling harmonic wavelength fractions. At 1.9 GHz the 79 mm ($\lambda_0/2$) width handset's measured μ and σ values dominate those corresponding to the 50 mm width design. Electrically-longer handsets show decreased sensitivity to cable radiation suppression techniques, while dimensions less than $\lambda_0/2$ require careful design consideration.

5. Acknowledgments

This work was sponsored by Amphenol T & M Antennas. Dielectric substrates were provided by Rogers Corporation.

6. References

- [1] H. -O. Ruoss and F. M. Landstorfer, "Measurement Techniques for Characterising Antennas of Hand-held Mobile Telephones Considering the User's Influence", *Proc. 1997 IEE Colloq. on Design of Mobile Handset Ant. for Optimal Performance in the Presence of Biological Tissue*, IEE Colloq. Dig. n. 022 1997, pp. 5/1–5/6, 1997.
- [2] C. Icheln and P. Vainikainen, "Dual-frequency Balun to Decrease Influence of RF Feed Cables in Small Antenna Measurements", *Electron. Lett.*, vol. 36, no. 21, pp. 1760–1761, October 2000.
- [3] Y. L. Chow, K. F. Tsang, and C. N. Wong, "An Accurate Method to Measure the Antenna Impedance of a Portable Radio", *Microw. Opt. Technol. Lett.*, vol. 23, no. 6, pp. 340–352, December 1999.
- [4] W. L. Stutzman and G. A. Thiele, *Antenna Theory and Design*, 2nd ed., pp. 165–173, New York: Wiley, 1997.

Accurate Analysis of Electrically Small Conical Antennas by Using the Low-Frequency Method

Jun-Sheng Zhao, Weng Cho Chew, and Paul E. Mayes

Center for Computational Electromagnetics
Electromagnetics Laboratory
Department of Electrical and Computer Engineering
University of Illinois at Urbana-Champaign
Urbana, IL 61801-2991

Abstract: In this paper, the loop-tree basis, which is designed for low-frequency problems, is applied to analyze the conical miniature antenna. Lumped load and lossy conductors are included in the full-wave analysis. Because the loop-tree basis performs the quasi-Helmholtz-decomposition at very low frequencies, compared with the high frequency approach, which does not give accurate results when the mesh size is small in terms of the wavelength, this approach works down to very low frequencies.

1. Introduction

The radiating resonator formed by two wide-angle coaxial conducting cones is useful as a low-profile, electrically small antenna. The cones are described in spherical coordinates by narrowly separated polar angles and radial limits, as depicted in Figure 1. In practice, a single resonator is excited by extending the center conductor of a coaxial cable through a small aperture at the tip of the lower cone and connecting it to the tip of the upper cone. The shield of the coax feed is attached to the lower cone as shown in Figure 2. The rotational symmetry of the resulting structure ensures that the radiation pattern will be omni-directional in azimuth and have nulls along the polar axis.

The conducting cones are respectively truncated at distances R_1 and R_2 from the origin. Although these distances are arbitrary, they are usually chosen to be equal or nearly so. The region between the cones may contain dielectric to provide support for the cones. Ordinarily, it will be desirable to limit the volume occupied by the dielectric in order to minimize the losses in the resonator.

Conical antennas were introduced by Barrow, *et al.* in 1939 [1]. Extensive measurements on conical monopoles with various flare angles were reported by Brown and Woodward in 1952 [2]. Much of the subsequent literature has focused on medium (sometimes called wide) flare angles since the input impedance for those angles converges toward the values of popular cables as frequency increases [3]. Hence, most of the conical antennas in use today are electrically large in order to use advantageously the wide impedance bandwidth of conical structures of sufficient size [4]. Recently, however, there has been an increasing demand for antennas for mobile and portable devices wherein reduced dimensions are of great practical importance.

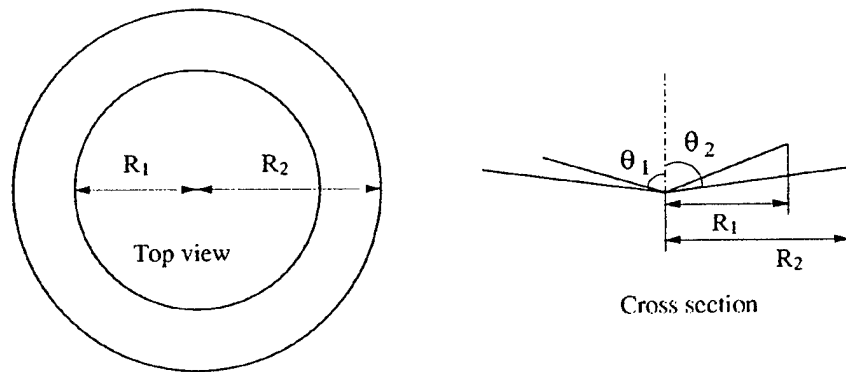


Figure 1: A conical radiating resonator (CRR) and its parameters

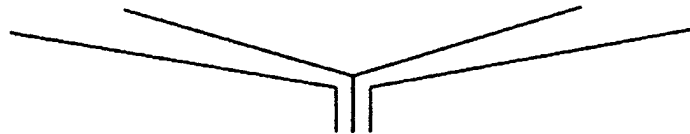


Figure 2: Rotationally symmetric excitation of a conical radiating resonator.

For impedance matching to the connected circuitry, a resistive input is usually desirable. When an antenna is electrically small ($ka < 1$, where a is the maximum radius), the impedance is naturally reactive, but can be made real by adding lumped reactive elements. Zero input reactance (resonance) is frequently obtained by adding a predominantly reactive lumped element at the feed-point. However, in the antennas considered here, resonance is achieved at small size by placing reactive elements across the aperture of the radiator.

When the polar angles of the cones of a conical resonator are near ninety degrees, the reactances can be conveniently connected between the outer rims of the two cones. Proper choice of inductive reactances can produce a high-impedance resonance for cones that are a small fraction of wavelength in radius. For such small antennas, excitation of the feed cable is likely unless means (e. g. chokes or ferrite rings) are provided to minimize currents on the outside of the shield. The radiation loss in this case is likely to be smaller than or comparable to the heat loss. Thus the efficiency is expected to be low [5] and the match bandwidth is dependent upon the device Q .

An early analysis of conical antennas was performed by Schelkunoff [6] who treated the antenna as a two-region boundary value problem. Several other authors later followed this method in finding solutions for special cases [7-9]. In recent years the preferred analytic tool has been a method-of-moments solution of the electric field integral equation. Algorithms for this analysis were first developed for thin wires. Smith, Butler and Umashankar [10] reported results of this type of analysis for conical antennas formed from wires. In the work reported here, integral equations formulated by applying the boundary conditions to the surfaces of the cones are used. At first, the code developed at the Lincoln Laboratory of Massachusetts Institute of Technology, called "Finite Element Radiation Model" (FERM) [11] was used. However, it was found that this code does not give accurate results when the patch size is small in terms of the wavelength. The purpose of this paper is to describe an alternative patch code that has no such limitation in accuracy.

2. Formulations

The integral representation of electric fields from the induced current is [12]

$$\mathbf{E}(\mathbf{r}) = i\omega\mu \int_S g(\mathbf{r}, \mathbf{r}') \mathbf{J}(\mathbf{r}') d\mathbf{r}' - \frac{1}{i\omega\epsilon} \nabla \int_S g(\mathbf{r}, \mathbf{r}') \nabla' \cdot \mathbf{J}(\mathbf{r}') d\mathbf{r}', \quad (1)$$

where $g(\mathbf{r}, \mathbf{r}')$ is the Green's function in free space,

$$g(\mathbf{r}, \mathbf{r}') = \frac{e^{ikR}}{R}, \quad R = |\mathbf{r} - \mathbf{r}'|.$$

The first and the second terms are contributions from the vector potential and the scalar potential, respectively. Let us denote

$$\mathbf{E}^V(\mathbf{r}) = i\omega\mu \int_S g(\mathbf{r}, \mathbf{r}') \mathbf{J}(\mathbf{r}') d\mathbf{r}', \quad (2)$$

$$\mathbf{E}^S(\mathbf{r}) = -\frac{1}{i\omega\epsilon} \nabla \int_S g(\mathbf{r}, \mathbf{r}') \nabla' \cdot \mathbf{J}(\mathbf{r}') d\mathbf{r}'. \quad (3)$$

Then (1) becomes

$$\mathbf{E}(\mathbf{r}) = \mathbf{E}^V(\mathbf{r}) + \mathbf{E}^S(\mathbf{r}) \quad (4)$$

For surface and wire basis functions, the dimension of $\frac{\mathbf{J}(\mathbf{r}')}{\nabla' \cdot \mathbf{J}(\mathbf{r}')}$ is a length unit.

Therefore, Equations (2) and (3) can be relatively frequency normalized as

$$\mathbf{E}^V(\mathbf{r}) = ik\eta \int_S \frac{e^{ikR}}{kR} k\mathbf{J}(\mathbf{r}') d\mathbf{r}', \quad (5)$$

$$\mathbf{E}^S(\mathbf{r}) = -\frac{ik\eta}{4\pi} \int_S \frac{ikR-1}{(kR)^2} e^{ikR} \hat{R} \nabla' \cdot \mathbf{J}(\mathbf{r}') d\mathbf{r}', \quad (6)$$

where

$$\hat{R} = \frac{\mathbf{r} - \mathbf{r}'}{R},$$

k and η are respectively the wavenumber and space impedance. From (5) and (6), we have

$$\frac{|\mathbf{E}^V(\mathbf{r})|}{|\mathbf{E}^S(\mathbf{r})|} \propto O(k^2 R^2), \quad kR \rightarrow 0. \quad (7)$$

Therefore, when $kR \rightarrow 0$, due to the finite machine precision, the contribution from the vector potential will be lost during the numerical process. However, it generates a non-vanishing magnetic field. The vector potential term is as important as the scalar potential term though it produces an electric field $O(k^2 R^2)$ smaller [14,21]. Furthermore, the scalar potential part in the above integral operator has a null space because of its divergence operator [21]. Hence, the loss of the contribution from the vector potential makes the matrix equation singular and the solution inaccurate. These problems are overcome by introducing the loop-star basis and loop-tree basis [14-22]. These bases separate the contributions from the vector potential and that from the scalar potential in the impedance matrix. In this manner, the contribution from the vector potential will not be swamped by that from the scalar potential, and the solutions are much more accurate.

The tangential component of the electric fields should vanish on the surface of the conducting surface. The electric field integral equation (EFIE) is

$$i\omega\mu\hat{\mathbf{t}}(\mathbf{r}) \cdot \int_S g(\mathbf{r}, \mathbf{r}') \mathbf{J}(\mathbf{r}') d\mathbf{r}' - \frac{1}{i\omega\epsilon} \hat{\mathbf{t}}(\mathbf{r}) \cdot \nabla \int_S g(\mathbf{r}, \mathbf{r}') \nabla' \cdot \mathbf{J}(\mathbf{r}') d\mathbf{r}' = -\hat{\mathbf{t}}(\mathbf{r}) \cdot \mathbf{E}^{inc}(\mathbf{r}), \quad \mathbf{r} \in S, \quad (8)$$

where $\mathbf{E}^{inc}(\mathbf{r})$ represents the incident electric fields. It can be the field of a impinging plane wave or the field created by a finite source residing within the structure. Here, $\hat{\mathbf{t}}(\mathbf{r})$ is an arbitrary tangential unit vector on the surface.

Using the loop-tree basis designed for low frequency problems

$$\mathbf{J}(\mathbf{r}') = \sum_{n=1}^{N_L} I_{Ln} \mathbf{J}_{Ln}(\mathbf{r}') + \sum_{n=1}^{N_T} I_{Tn} \mathbf{J}_{Tn}(\mathbf{r}') \quad (9)$$

where $\mathbf{J}_{Ln}(\mathbf{r}')$ and $\mathbf{J}_{Tn}(\mathbf{r}')$ are respectively divergence-free loop basis and non-divergence-free tree basis defined in [14, 21]. Equation (9) can be rewritten in the matrix form as

$$\mathbf{J}(\mathbf{r}') = \mathbf{J}'_L(\mathbf{r}') \cdot \mathbf{I}_L + \mathbf{J}'_T(\mathbf{r}') \cdot \mathbf{I}_T, \quad (10)$$

where $\mathbf{J}_L(\mathbf{r}')$, \mathbf{I}_L , $\mathbf{J}_T(\mathbf{r}')$, and \mathbf{I}_T are column vectors containing $\mathbf{J}_{Ln}(\mathbf{r}')$, I_{Ln} , $\mathbf{J}_{Tn}(\mathbf{r}')$, and I_{Tn} , respectively. The first term in (10) is divergence free, but (10) does not represent a complete Helmholtz decomposition because the second term is not curl-free. However, a complete Helmholtz decomposition is not mandatory to solve this problem as long as the second term always has a component in the curl free space. By substituting (10) into (8), testing with $\mathbf{J}_L(\mathbf{r})$ and $\mathbf{J}_T(\mathbf{r})$, and applying $\nabla \cdot \mathbf{J}(\mathbf{r}) = 0$, we have the matrix equation

$$\begin{bmatrix} \bar{\mathbf{Z}}_{LL} & \bar{\mathbf{Z}}_{LT} \\ \bar{\mathbf{Z}}_{TL} & \bar{\mathbf{Z}}_{TT} \end{bmatrix} \cdot \begin{bmatrix} \mathbf{I}_L \\ \mathbf{I}_T \end{bmatrix} = \begin{bmatrix} \mathbf{V}_L \\ \mathbf{V}_T \end{bmatrix}, \quad (11)$$

where

$$\mathbf{V}_L = -\langle \mathbf{J}_L(\mathbf{r}), \mathbf{E}^{inc}(\mathbf{r}) \rangle,$$

$$\mathbf{V}_T = -\langle \mathbf{J}_T(\mathbf{r}), \mathbf{E}^{inc}(\mathbf{r}) \rangle,$$

$$\bar{\mathbf{Z}}_{LL} = i\omega\mu \langle \mathbf{J}_L(\mathbf{r}), g(\mathbf{r}, \mathbf{r}'), \mathbf{J}'_L(\mathbf{r}') \rangle,$$

$$\bar{\mathbf{Z}}_{LT} = i\omega\mu \langle \mathbf{J}_L(\mathbf{r}), g(\mathbf{r}, \mathbf{r}'), \mathbf{J}'_T(\mathbf{r}') \rangle,$$

$$\bar{\mathbf{Z}}_{TL} = i\omega\mu \langle \mathbf{J}_T(\mathbf{r}), g(\mathbf{r}, \mathbf{r}'), \mathbf{J}'_L(\mathbf{r}') \rangle = \bar{\mathbf{Z}}'_{LT},$$

$$\bar{\mathbf{Z}}_{TT} = i\omega\mu \langle \mathbf{J}_T(\mathbf{r}), g(\mathbf{r}, \mathbf{r}'), \mathbf{J}'_T(\mathbf{r}') \rangle - \frac{i}{\omega\epsilon} \langle \nabla \cdot \mathbf{J}_T(\mathbf{r}), g(\mathbf{r}, \mathbf{r}'), \nabla' \cdot \mathbf{J}'_T(\mathbf{r}') \rangle.$$

In the above,

$$\langle \mathbf{A}(\mathbf{r}), g(\mathbf{r}, \mathbf{r}'), \mathbf{B}'(\mathbf{r}') \rangle = \int_S d\mathbf{r} \mathbf{A}(\mathbf{r}) \cdot \int_{S'} d\mathbf{r}' g(\mathbf{r}, \mathbf{r}') \mathbf{B}'(\mathbf{r}'),$$

$$\langle \mathbf{A}(\mathbf{r}), \mathbf{B}'(\mathbf{r}) \rangle = \int_S d\mathbf{r} \mathbf{A}(\mathbf{r}) \cdot \mathbf{B}'(\mathbf{r}).$$

From (11), we can see that the contribution from the vector potential is separated out. Hence, the low-frequency breakdown is avoided.

To make the conical antenna resonant, four inductors are connected at the outer boundary of the conical antenna. To try to keep the azimuthally symmetrical

property of the antenna, the four inductors are played with the same separation angle. The effect from lumped loads can be easily added to the EFIE by using different models [23-26]. When the antenna is not a perfect conductor, the loss effect can also be easily added to the equation [27, 28]. With surface impedance and lumped loads, Equation (11) becomes

$$\left\{ \begin{bmatrix} \bar{Z}_{LL} & \bar{Z}_{LT} \\ \bar{Z}_{TL} & \bar{Z}_{TT} \end{bmatrix} + \bar{Z}^S + \bar{Z}^L \right\} \cdot \begin{bmatrix} \mathbf{I}_L \\ \mathbf{I}_T \end{bmatrix} = \begin{bmatrix} \mathbf{V}_L \\ \mathbf{V}_T \end{bmatrix}, \quad (12)$$

where \bar{Z}^S and \bar{Z}^L are respectively the effects from the surface impedance and lumped loads.

3. Numerical Results

Because the height of the feed line is comparable to its diameter, a general wire model is inaccurate. We simulate the feed line as a circular cylinder whose radius is the same as the wire. As shown in Figures 3 and 4, the two cones are joined near their apices by a circular cylinder. The radius and the height of the circular cylinder are respectively 2 mm and 3.52893 mm. The structure is excited by a uniform distribution of δ -gap generators around the circumference of the circular cylinder, midway between the intersections of the cylinder and cones. The loop basis and tree basis are respectively shown in Figures 5 and 6.

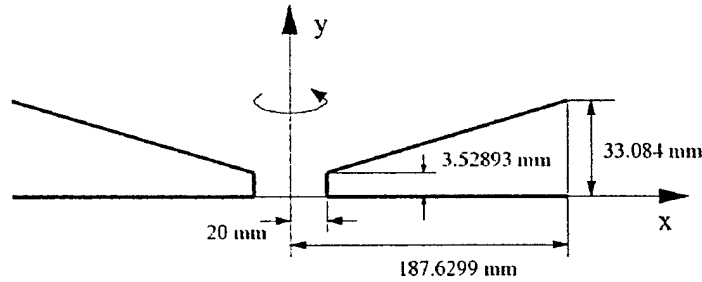


Figure 3: Dimensions of the conical antenna.

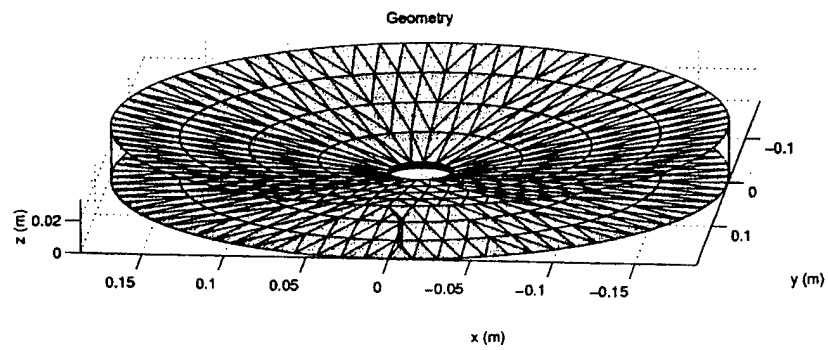


Figure 4: Geometry of the conical antenna with for strip terminations.

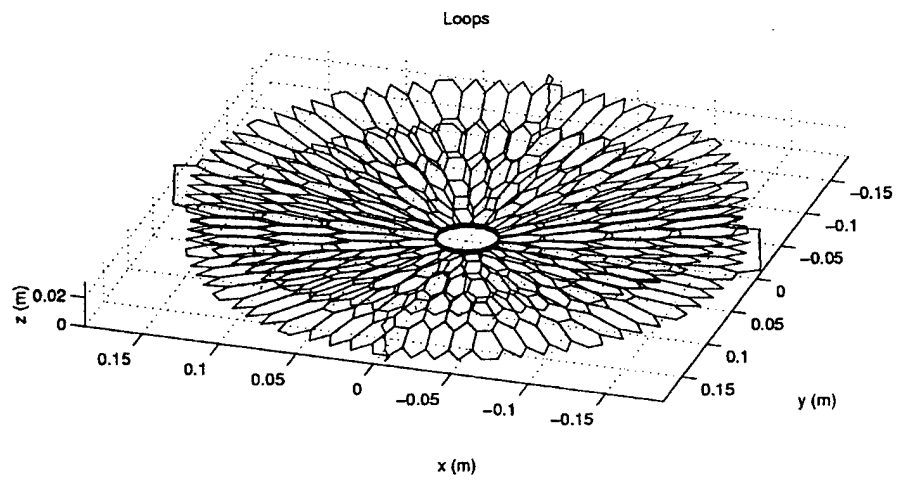


Figure 5: Loop basis of the conical antenna with four strip terminations.

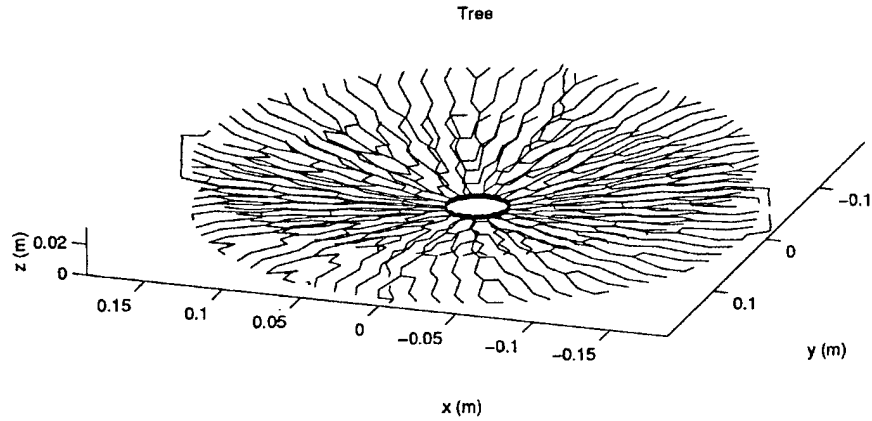


Figure 6: Tree basis of the conical antenna with strip terminations.

Figures 7 and 8 respectively show the comparison of the input conductance and susceptance of the unloaded conical antenna by using FERM and the low frequency method. It can be seen that FERM becomes unstable below 30 MHz. Figure 9 shows the input conductance and susceptance of a conical antenna by using the low frequency method. Because we apply the loop-tree basis, which captures the inductance and capacitance effects physically, the code works at very low frequencies. At very low frequencies, the structure is like a capacitor. When the frequency goes high, the distributed inductance becomes larger and makes the structure resonate.

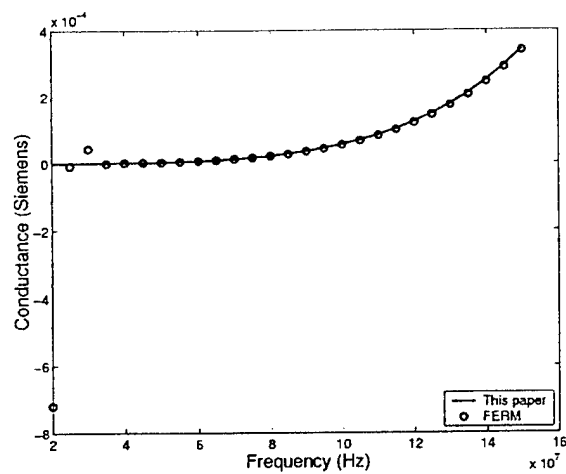


Figure 7: The comparison of input conductance of a open conical antenna by using different codes.

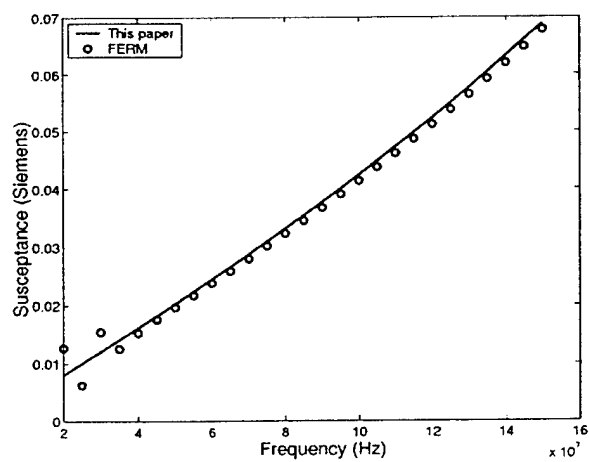


Figure 8: The comparison of input susceptance of a open conical antenna by using different codes.

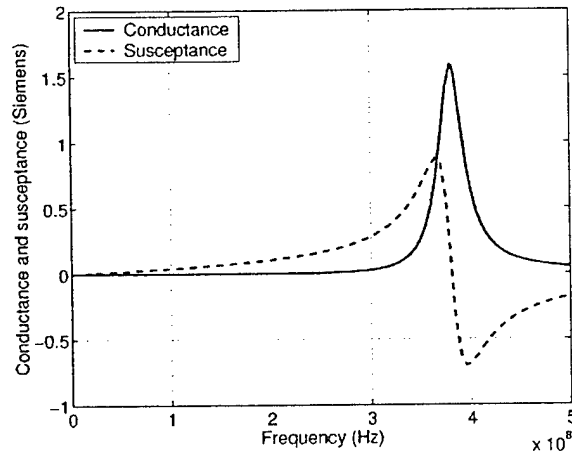


Figure 9: Input conductance and susceptance as a function of frequency for a open conical antenna.

We then uniformly connect four wires of a radius of 2 mm to the outer circumferences of these two cones. But no lumped load is connected. Figure 10 shows the input conductance and susceptance of this conical antenna with four wire terminations. At very low frequencies, because these four wires form loops, the structure is like an inductor. The applied loop basis can physically capture the conductance information at low frequencies. When the frequency goes high, the distributed inductance becomes bigger and make the structure resonate. This property is clearly shown in Figure 10.

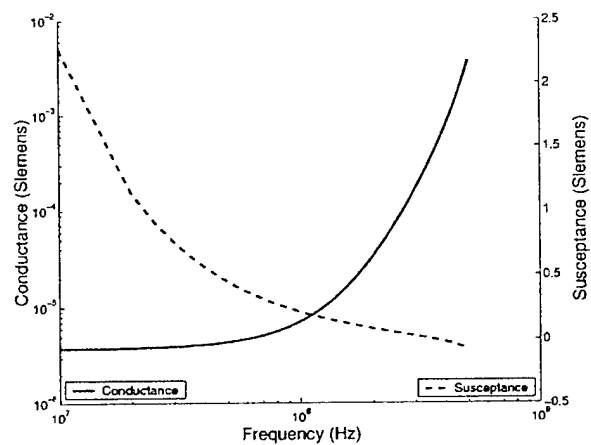


Figure 10: Input conductance and susceptance as a function of frequency for a conical antenna with four wires.

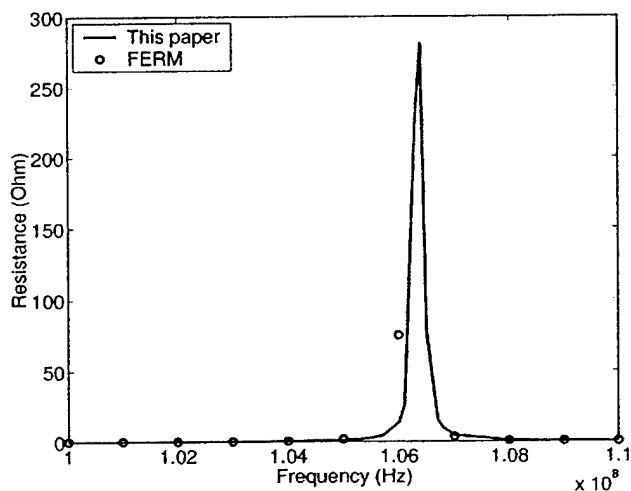


Figure 11: The comparison of input resistance near the resonant frequency of an open conical antenna by using different codes.

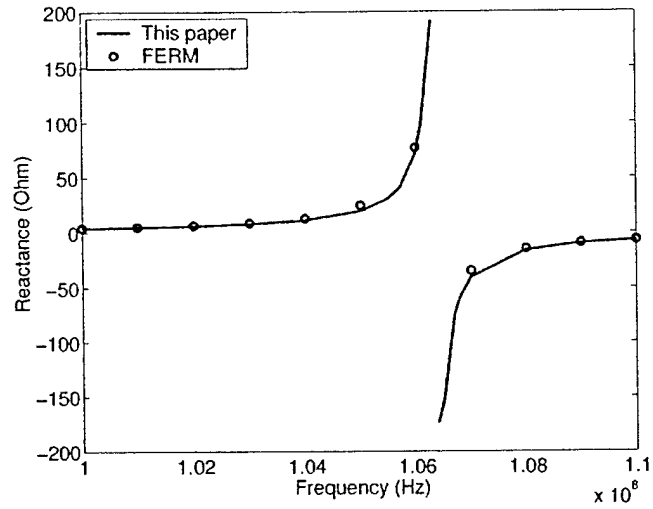


Figure 12: The comparison of input reactance near the resonant frequency of a open conical antenna by using different codes.

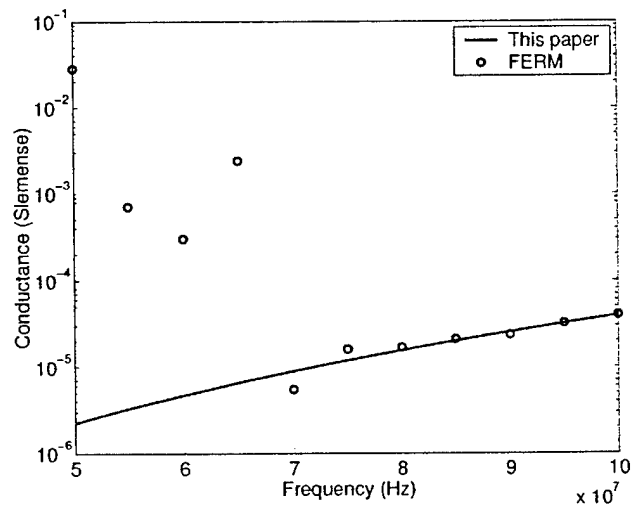


Figure 13: The comparison of input conductance at relative low frequencies of a open conical antenna by using different codes.

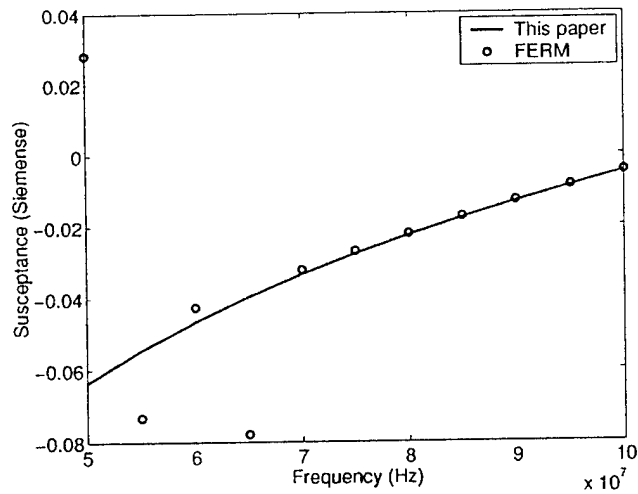


Figure 14: The comparison of input susceptance at relative low frequencies of a open conical antenna by using different codes.

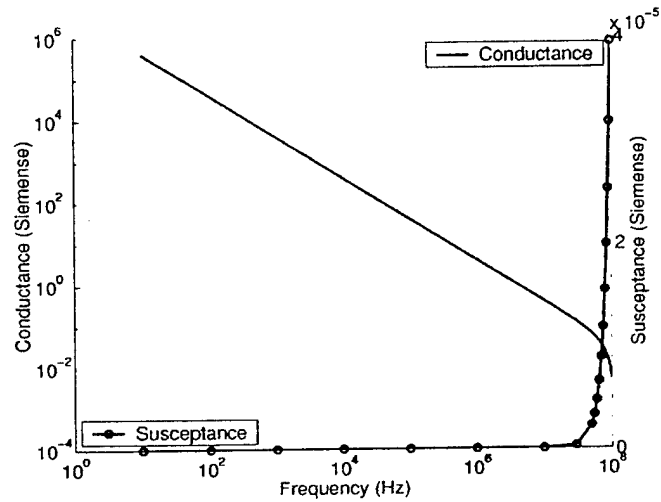


Figure 15: Input conductance and susceptance as a function of frequency for a loaded conical antenna at low frequencies.

Figures 11-14 show the comparison of input resistance and reactance around and below the resonant frequency of a conical antenna with four 96.8 nH inductors

terminated by thin strips by using our approach and FERM. It can be seen that FERM becomes unstable below 70 MHz.

Figure 15 shows the input conductance and susceptance as a function of frequency for a loaded antenna with four 96.8 nH inductors terminated by thin strips by using the low frequency approach.

4. Conclusions

In this paper, the loop-tree basis, which is designed for low-frequency problems, is applied to analyze the conical miniature antenna. Lumped loads and lossy conductors are included in the full-wave analysis. Because the loop-tree basis performs the quasi-Helmholtz-decomposition property at very low frequencies, this approach works down to very low frequencies. At high frequency, we switch the basis from loop-tree to general RWG-type basis. Therefore, the code works all the way from very low frequencies to high frequencies.

5. References

- [1] W. L. Barrow, L. J. Chu and J. J. Jansen, "Biconical electromagnetic horns," *Proceedings of IRE*, vol. 27, pp. 769-779, Dec. 1939.
- [2] G. H. Brown and O. M. Woodward. Sr., "Experimentally determined radiation characteristics of conical and triangular antennas," *RCA Review*, vol. 13, No. 4, pp. 425-452, Dec. 1952.
- [3] C. H. Papas and R. King, "Input Impedance of a Wide-Angle Conical Antenna Fed by a Coaxial Line," *Proc. IRE*, vol. 37, pp. 1269-1271, 1949.
- [4] Y. T. Lo and S. W. Lee (eds), *Antenna Handbook*, pp. 3-29, New York: Van Nostrand Reinhold, 1988.
- [5] W. L. Stutzman and G. A. Thiele, *Antenna Theory and Design*, pp. 49-50, New York: Wiley, 1981.
- [6] S. A. Schelkunoff, *Electromagnetic Waves*, New York: Van Nostrand, 1943.

- [7] S. A. Schelkunoff, "General theory of symmetrical biconical antenna," *Jour. Appl. Phys.*, vol. 22, pp. 1330-1332, Nov. 1951.
- [8] C. H. Papas and R. W. P. King, "Radiation from wide-angle conical antennas fed by a coaxial line," *Proc. IRE*, vol. 39, pp. 40-50, Jan. 1951.
- [9] C. S. Smith, "The conical dipole of wide angle," *Jour. Appl. Phys.*, vol. 19, 1948.
- [10] C. E. Smith, C. M. Butler, and K. R. Umashankar, "Characteristics of a wire biconical antenna," *Microwave Jour.*, pp. 37-40, Sept. 1979.
- [11] S. Lee, D. A. Shnidman and F. A. Lichauco, "Numerical modeling of RCS and antenna problems," Technical Report No.785, Lincoln Laboratory, Massachusetts Institute of Technology, Dec. 1987.
- [12] W. C. Chew, *Waves and Fields in Inhomogeneous Media*, New York: Van Nostrand Reinhold, 1990, reprinted by IEEE Press, 1995.
- [13] R. G. Harrington, *Time-Harmonic Electromagnetic Fields*, McGraw-Hill, New York, 1961.
- [14] D. R. Wilton and A. W. Glisson, "On improving the electric field integral equation at low frequencies," *URSI Radio Science Meeting Digest*, p. 24, Los Angeles, CA, June 1981.
- [15] J. R. Mautz and R. F. Harrington, "An E-field solution for a conducting surface small or comparable to the wavelength," *IEEE Trans. Antennas Propagat.*, vol. 32, pp. 330-339, April 1984.
- [16] E. Arvas, R. F. Harrington, and J. R. Mautz, "Radiation and scattering from electrically small conducting bodies of arbitrary shape," *IEEE Trans. Antennas Propagat.*, vol. 34, pp. 66-77, Jan. 1986.
- [17] J. S. Lim, S. M. Rao, and D. R. Wilton, "A novel technique to calculate the electromagnetic scattering by surfaces of arbitrary shape," *URSI Radio Science meeting Digest*, p. 322, Ann Arbor, Michigan, June 1993.
- [18] M. Burton and S. Kashyap, "A study of a recent, moment-method algorithm that is accurate to very low frequencies," *Applied Computational Electromagnetic Society Journal*, vol. 10, no. 3, pp. 58-68, Nov. 1995.

- [19] W. Wu, A. W. Glisson, and D. Kajfez, "A study of two numerical solution procedures for the electric field integral equation at low frequency," *Applied Computational Electromagnetic Society Journal*, vol. 10, no. 3, pp. 69-80, Nov. 1995.
- [20] G. Vecchi, "Loop-star decomposition of basis functions in the discretization of the EFIE," *IEEE Trans. Antennas Propagat.*, vol. AP-47, no. 2, pp. 339-346, Feb. 1999.
- [21] J. S. Zhao and W. C. Chew, "Integral Equation Solution of Maxwell's Equations from Zero Frequency to Microwave Frequencies," *IEEE Trans. Antennas Propagat.*, James R. Wait Memorial Special Issue. vol. AP-48, no. 10, pp. 1635-1645, Oct. 2000.
- [22] J. S. Zhao and W. C. Chew, "Applying LF-MLFMA to Solve Complex PEC Structures," *Microwave Opt. Technol. Lett.*, vol. 28, no. 3, pp. 155-160, Feb. 5, 2001.
- [23] B. D. Popovic, M. B. Dragovic, and A. R. Djordjevic, *Analysis and Synthesis for Wire Antennas*, Research Studies Press, 1982
- [24] J. H. Richmond, "Radiation and scattering by thin-wire structures in the complex frequency domain," *Computational Electromagnetics*, edited by E. K. Miller, L. Medgyesi-Mitschang and E. H. Newman, pp. 156-169, IEEE Press, 1992.
- [25] W. A. Johnson, D. R. Wilton, and R. M. Sharpe, "Modeling scattering from and radiation by arbitrary shaped objects with the electric field integral equation triangular surface patch code," *Electromagnetics*, Vol. 10, pp. 41-62, 1990.
- [26] J. S. Zhao and W. C. Chew, "Modeling Lumped Impedance Loads in Full Wave Electromagnetic Analysis," submitted to *IEEE Trans. Microwave Theory Tech.*, June 2001.
- [27] T. B. Senior, "Scattering by resistive strips," *Radio Science*, vol. 14, pp. 911-924, 1979.
- [28] J. S. Zhao and W. C. Chew, "Full wave electromagnetic simulation of crosstalks between lossy conducting structures," submitted to *IEEE Trans. Circuits and Syst. I: Fundamental Theory and Appl.*, Sept. 2001

INDUCTIVELY LOADED, STACKED SECTOR ANTENNAS

Paul E. Mayes

Electrical and Computer Engineering Department
University of Illinois at Urbana-Champaign
1406 West Green Street
Urbana, IL 61801

Abstract: The concept of series-connected, size-reduced, radiating resonators is here applied to sector shapes. When used singly, small, low-profile sector radiators produce wide radiation beams directed generally normal to the planes of the sectors. Symmetry of the beam is improved when two sectors are used to produce a symmetry plane between them. Four sectors disposed with rotational symmetry and fed with 90-degree phase progression produce circular polarization on axis, with sense determined by the direction of the phase progression. Small single sectors can be matched at resonance to a wide range of real impedances. Only an external transformer is required, but such devices are high-Q with very narrow match bandwidth. The bandwidth can be increased by adding resonators stacked in the vertical direction, thus preserving the small footprint of the antenna. The principles of operation of the antenna are demonstrated by means of computer simulations done with the FERM software developed at Lincoln Laboratories of MIT.

1. Introduction

It was previously shown how conical radiating resonators could be reduced in size by means of inductors across a peripheral radiating aperture [1]. It was further shown that the electrically small conical resonators could be stacked and effectively connected in series in order to increase the match bandwidth of the system [1]. In this paper, the idea of inductive aperture loading of a series-connected set of radiating resonators is applied to elements with sector shape. In contrast to the system of conical resonators, the sector resonators produce appreciable radiation in the vertical (broadside) direction [3]. By using two opposing sectors, having geometry similar to the bow-tie antenna, a symmetric vertical beam of linearly polarized radiation can be produced. Adding an orthogonal set of sectors fed with a ninety-degree phase difference will yield a beam of predominantly circular polarization.

2. Geometries of Sector Antennas

The top-view geometries of a single sector and several possible combinations thereof are shown in Figure 1. Each case shows one or more triangular

conducting sheets that are placed over and very close to a ground plane (not shown). Each sector is fed by the center conductor of a coaxial cable whose outer conductor is connected around the periphery of a circular aperture in the ground plane. Each sector may be parallel or canted with respect to the ground, the latter being preferred in many cases.

The single sector when constructed on a dielectric substrate rendering it parallel to the ground plane is just a triangular microstrip patch antenna fed at the apex of the sector. Ordinarily, such an antenna is operated near resonance to produce a real value of input impedance with a rather large value of Q . It is possible, however, to obtain very large impedance bandwidth by extending the frequency range upward until the antenna operates in semi-resonant or non-resonant mode. There are two significant problems with making use of this property of a sector antenna: (a) the patterns are not necessarily useful across the band of near-constant impedance, and (b) the antenna becomes quite large in terms of the wavelength. It is the objective of this paper to attack the second of these problems whereby the first is also ameliorated. Assuming that the above problems have been solved, or are not important to a given application, the versatility of sector antennas in producing controllable polarization is shown in Figure 1.

The asymmetry in the E-plane of a single sector naturally leads to asymmetry in the radiation pattern in that plane. This asymmetry becomes more pronounced as frequency increases. Using two diametrically opposed sectors with balanced feed, while removing the asymmetry in the E-plane, does not eliminate the problem of pattern variation with increasing frequency. So, although the polarization of orthogonal balanced sectors can be widely controlled by amplitude and phase differences between the orthogonal pairs of feed terminals, the operating bandwidth is still likely to be associated with variation in the radiation pattern.

Traces in the vertical plane of several possible arrangements of sectors are shown in Figure 2. When flat (planar and parallel to ground), the sectors discussed here are distinguished from conventional "bow-tie" antennas by the small values of h , the perpendicular distance between the sector and ground. For these small distances, the sectors differ from microstrip patches by the substantial replacement of dielectric by free space. In the canted versions of the sector elements, the angle between the sector and ground plane, α , is allowed to be a small, but non-zero, value. When, as is frequently the case for canted sectors, the tip of the sector lies on the ground surface, the height parameter, h , is determined by the angle, α , and also by the distance from the apex to the end of the sector. When the tip does not lie in the plane of the ground, there will be an additional parameter, the vertical distance from ground to the sector tip.

Although other methods are feasible, reduction in size at resonance is achieved in this work by placing inductive elements at the corners of the sector. When the tip of the sector is very close to the ground plane, the connection to a feed cable requires little extension of the center conductor above the ground. Then, the

inductive elements are located only at those corners away from the feed, as shown in the lower right of Figure 2 (where one edge of the sector lies in the plane of the page). As mentioned previously, the impedance bandwidth of a resonant element of dimensions that are small compared to the wavelength is also small. Enhancement of the impedance bandwidth is achieved in this work by using multiple resonators, effectively connected in series, so that the input impedance is dominated by the values at the various resonant frequencies. The vertical geometry of such a system is shown at the lower left of Figure 2. Note that the center conductor of the feed coax is connected only at the tip of the uppermost sector. The tips of the remaining sectors, although spaced very close to the center conductor of the coax, are not connected to it. In this simple manner, the series connection of the radiating resonators is accomplished.

3. Evaluation of Sector Antennas by Numerical Analysis

One advantage of canted conical sectors, from a theoretical point of view, is that there exists a TEM solution for the fields between the sector and ground (or between two sectors with a common tip). In a system in which the TEM fields are dominant, the simple approximate circuit shown in Figure 3 can be used to analyze each resonator of the system. Each resonator formed by two adjacent sectors can be represented approximately by a section of uniform transmission line with length equal to the distance from the tip of the sector to the gap between their distant ends. The phase constant for the lines is the intrinsic phase constant for the homogeneous medium between the sectors. The length of the line is equal to the distance from the (virtual) apices of the sectors to the aperture between them. Existing theory can be used to calculate the characteristic impedances of these lines [2]. Thus, all parameters of the model are known except the termination at the aperture end of the line. The terminating impedance is the parallel combination of a resistance that absorbs power equal to that radiated by the sector resonator and a reactive element that represents the (near-field) energy stored near the aperture. Evaluation of the terminal impedance requires a solution of the electromagnetic boundary-value problem represented by the radiating resonators of Figures 1 and 2.

Numerical solutions for the sector radiating resonator (SRR) have been obtained using the method of moments as implemented in the software package FERM (Finite Element Radiation Model) originally developed at the Lincoln Laboratory of Massachusetts Institute of Technology [4]. Figure 4 shows the geometry of a typical set of patch subsections used in the analysis of a low-profile planar SRR. Single resonators with sectors having polar angles near ninety degrees satisfy the requirement of some applications for reduced height. Resonators with small polar angles between the sectors can be packaged in multi-resonator systems, as will be shown later.

4. Input Impedance Computed for a Single Sector Resonator

The input impedance computed for a single sector resonator of the type shown in Figure 5 is shown plotted on a Smith chart in Figure 6. In this case the width of the aperture was divided into six sections ($n_{\text{pap}}=6$) and the terminating strap width was one-half the width of one of these sections ($d_{\text{sodw}}=0.5$). For the parameters shown on the figure, the impedance locus crosses the real axis, from inductive to capacitive side of the chart, at approximately 2.65 GHz (wavelength = 11.32 cm). So the impedance behavior is similar to that of a parallel RLC circuit which is resonant near 2.65 GHz. Since the length from tip to aperture is only about one-sixth of the wavelength at resonance, the radiation in the neighborhood of resonance is small and the impedance locus is close to the outer rim of the chart. As a result, the match to 50 ohms is poor, even at resonance, and much of the power incident on a 50-ohm line would be reflected.

If the data in Figure 6 were computed for finer frequency divisions, the result that would be obtained in practice by inserting a transformer at the input of the antenna could also be plotted as it traverses the region near the center of the chart. However, the band within the region $\text{SWR} < 2$ would be very narrow. The objective of the present work is to increase the match bandwidth without increasing the horizontal dimension or decreasing the efficiency of the antenna.

5. Results for a Two-Resonator Antenna

Fano has shown that the maximum bandwidth for a given degree of match is obtained when the impedance locus follows the specified SWR circle around the Smith chart [5]. Using two resonators to construct a sector antenna introduces two resonant frequencies at which the impedance locus crosses the real axis. Between the resonant frequencies the impedance locus will form a loop and the size of the loop will depend upon the frequency span between the resonances. Figure 7 shows the view looking into the aperture of a two-resonator sector antenna. Although the sizes of the resonators are basically the same, each resonator is tuned to a different frequency by changing the width of the terminating straps seen connected across the apertures. Adding the second resonator does not increase the horizontal dimension and, since the resonators are thin, adds little to the vertical dimension.

Figures 8, 9 and 10 show the input impedances versus frequency for a two-resonator system as the widths of the terminal straps on the upper resonator are changed. A system requirement for one potential application is to cover the band from 2.7 to 3.5 GHz. At these frequencies, the inductance of a conducting strap alone is sufficient; no lumped inductors are needed. In Figure 8, the strap widths were adjusted so that the lower resonance was just above 2.7 GHz and the upper resonance was just below 3.5 GHz. The impedance loop for the frequency band between these two resonances is seen to be somewhat larger than might be desired. There are several ways to reduce the size of the loop: (a) the resonances could be moved closer together, in which case the frequency band within the loop

would be reduced, (b) loss could be added, in which case the efficiency of the antenna would be reduced, or (c) the size of the antenna could be increased.

The effect on the impedance of exercising the first option is illustrated in Figures 9 and 10. The widths of the terminal straps are normalized with respect to the widths of the aperture patches. In the cases shown here, the aperture was divided into six sections. The relative widths of the patches on the strap of the lower resonator were fixed at 0.01. The inductances of these relatively thin straps produced resonances at about 2.8 GHz in all three of Figures 8, 9 and 10. The relative widths of the straps on the upper resonator were changed from 0.2 to 0.15 to 0.1 in Figures 8, 9 and 10, respectively. As a result of this stepped variation in the inductances across the aperture, the upper resonances were decreased from about 3.41 to about 3.34 to about 3.23 GHz. As the upper resonances decrease, the size of the loop also decreases.

Although the smaller loops represent a smaller variation in impedance versus frequency, the variation is with respect to a rather high value of mean impedance. Match to a lower impedance can be improved greatly by adding an external matching circuit. Some care has been taken to make the impedance loop symmetrical about the real axis of the Smith chart. So, approximate centering of the loop on the chart can be achieved by adding a transformer at the input. Figure 11 shows the data of Figure 8 after transformations by factors of 2, 3, 4 and 5, thus simulating the effect of adding transformers of those ratios. When the ratio is equal to 2, the loop passes very near the center of the chart, producing excellent match, but over a rather limited frequency range. The ratio of 5 produces a loop that is most nearly centered on the chart; coming closest to satisfying Fano's criterion for widest bandwidth. The effect of these transformations on the SWR is shown in Figure 12. The ratio of 2 yields the lowest minimum SWR and narrowest band for $\text{SWR} < 5.0$; while the ratio of 5 produces the wider band, but also higher SWR. Proceeding in this way, it is possible to achieve almost constant SWR of various values by adding a transformer with the proper impedance ratio at the input terminals of a two-resonator sector antenna of proper parameters.

Figure 13 shows the input impedances after transformers with ratios of 2, 4, 6 and 8 have been introduced to the antenna of Figure 10. In Figure 14, the input SWR for these four cases are compared. The trade-off between bandwidth and SWR is clearly seen.

6. Flat versus Canted Sectors

The evaluation of systems of flat (planar, parallel to ground) sector radiating resonators is underway. The view of Figure 15 shows the elongation of the feed conductor that is required when the tips of the sectors are raised to make the elements parallel to the ground plane. The width of the feed conductor is comparable to the widths of the terminal straps used to tune each resonator. It is not surprising, therefore, to find that a flat sector of the same dimensions and

loading as a canted sector does not resonate at the same frequency. The computed data of Figure 16 shows that the resonance of the lower resonator cannot be adjusted by changing the widths of the terminal straps so that it can be approximately 2.7 GHz, as before. However, by adding small surface reactances to the patches on the terminal straps the desired resonance can be achieved. The upper resonance remains above 4.0 GHz, the upper limit of the computed band. The next step will be to add surface reactances to the straps on the upper resonator until the desired band (2.7 to 3.5 GHz) is covered.

7. Plans for the Future

Although some radiation patterns have been calculated that demonstrate the expected dipole shape, additional patterns may be needed to verify that there is little variation in the directivity over the band of best impedance match. These computations of far fields would also be useful in evaluation of the antenna gain. A fundamental question about the performance of electrically small antennas pertains to the efficiency and gain. New software that is capable of making these computations over extended frequency bands that include very low frequencies has recently been written [6]. Its application to the evaluation of both flat and canted sector antennas is planned for the near future.

8. References

1. P. E. Mayes and W. Gee, "Using Multiple Resonant Radiators for Increasing the Impedance Bandwidth of Electrically Small Antennas", *Proc. 24th Annual Antenna Applications Symposium*, Allerton Park, Illinois, September 2000.
2. R. L. Carrel, "The Characteristic Impedance of the Fin Antenna of Infinite Length", Tech. Rep. No. 16, Contract No. AF33(616)-3220, Antenna Laboratory, University of Illinois, 1957.
3. J. T. Bernhard, N. W. Chen, R. Clark, P. Mayes and E. Michielssen, "A Canted Sector Antenna with Broad Impedance Bandwidths for High Performance Arrays," *Proc. 24th Annual Antenna Applications Symposium*, Allerton Park, Illinois, September 2000.
4. S. Lee, D. A. Shnidman, and F. A. Lichauco, "Numerical Modeling of RCS and Antenna Problems," Tech. Rep. 785, Lincoln Laboratories, Massachusetts Institute of Technology, Lexington, MA, December 1987.
5. R. M. Fano, "Theoretical Limitations on the Broadband Matching of Arbitrary Impedances," Ph. D. Thesis, Massachusetts Institute of Technology, 1947.
6. Jun-Sheng Zhao, Weng Cho Chew, and Paul E. Mayes, "Accurate Analysis of Electrically Small Conical Antennas by Using the Low-Frequency Method," *Proc. 25th Annual Antenna Applications Symposium*, Allerton Park, Illinois, September 2001.

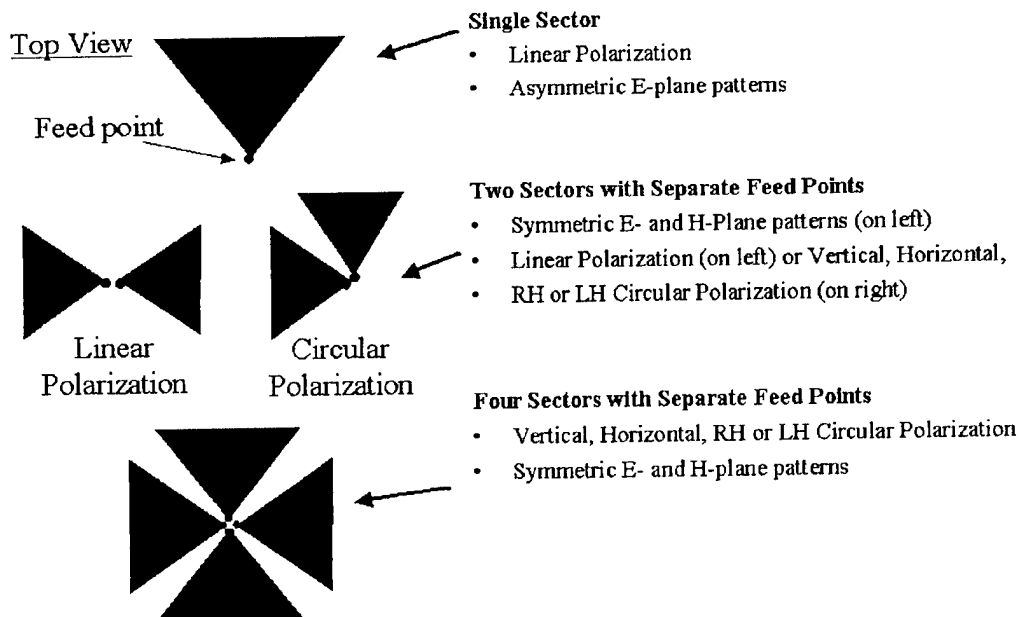


Figure 1. Top views of sector antennas with combinations that permit control of the polarization of the radiated field.

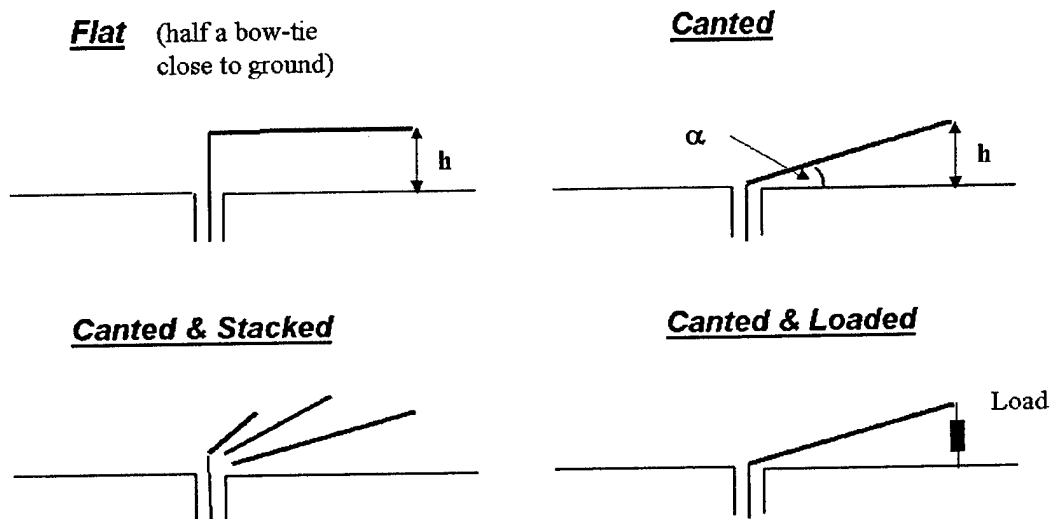


Figure 2. Traces in the vertical plane of sector antenna elements showing arrangements and parameters of interest.

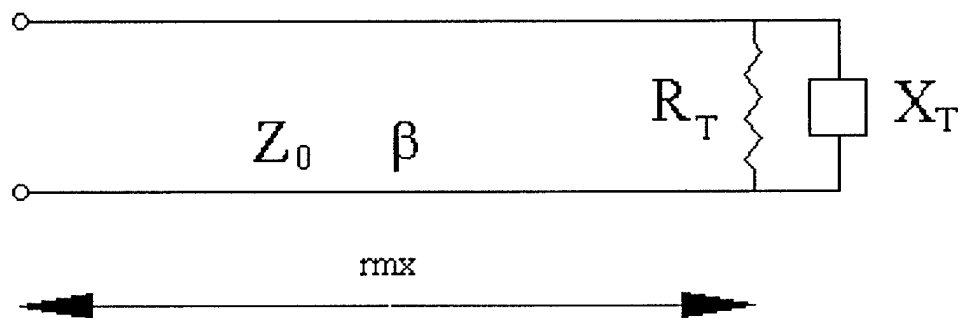


Figure 3. Approximate equivalent circuit for a single radiating conical sector resonator. The length rmx is the distance from the feedpoint to the aperture. Z_0 is the characteristic impedance for the TEM fields between the two sectors that form the upper and lower boundaries of the resonator. β is the intrinsic phase constant for the medium surrounding the conducting sectors. R_T is the terminating resistance that simulates the power lost in radiation from the aperture and X_T is the terminating reactance that provides energy storage equivalent to that in the non-radiating fields near the aperture.

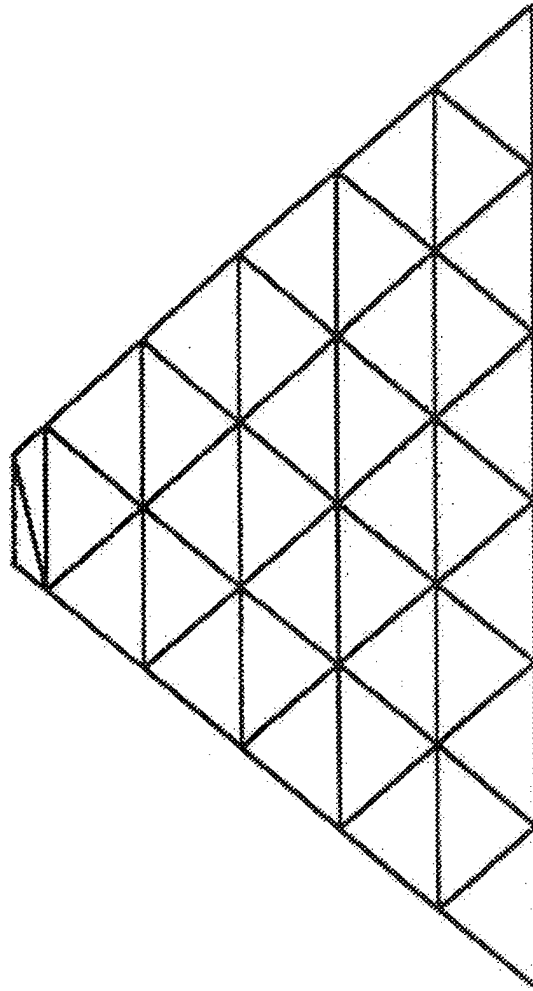


Figure 4. Example of subsectional divisions used in the analysis of a planar radiating sector with the FERM software.



Figure 5. View looking into the aperture of a radiating planar sector element showing the inductive straps connected across the aperture to reduce the size of the element at resonance. The interior lines are the boundaries of subsectional patches used in the moment method analysis of the antenna using the FERM software.

Input Impedance Computed for 80-Deg Loaded Sector
 Theta1=90 deg, Theta2=80 deg, xtrcm=0.25 cm, Radius=1.8 cm
 Two Inductive Straps, npap=6, dsodw=0.5, h=0.75

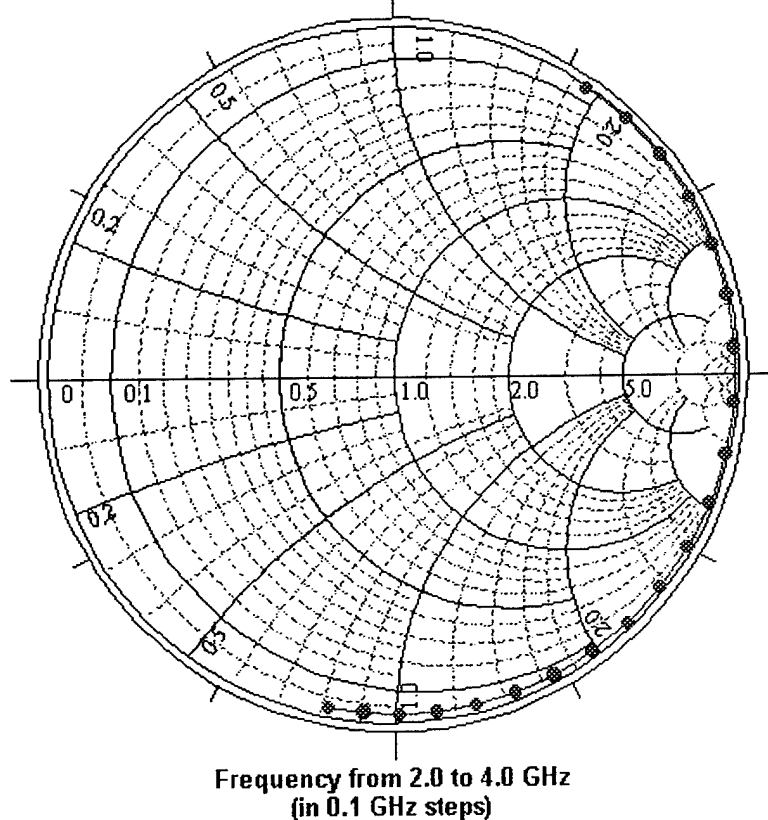


Figure 6. Input impedance computed for an 80-degree wide canted sector making an angle of 10 degrees above ground plane. The distance from tip to aperture, measured along the ground plane, is 1.8 cm. The tip is truncated 0.25 cm from the virtual apex (xtrcm=0.25 cm). The resonant frequency is approximately 2.65 GHz (wavelength = 11.32 cm) so the length at resonance is slightly less than one-sixth of the wavelength. Resonance at this size is obtained by connecting two conducting straps across the aperture (side away from the feed). Each strap has a vertical dimension equal to three-quarters of the vertical dimension of the aperture (h=0.75).

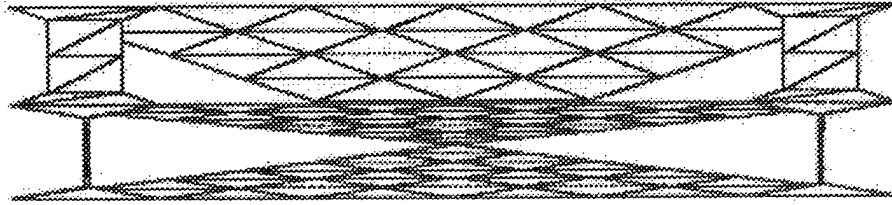
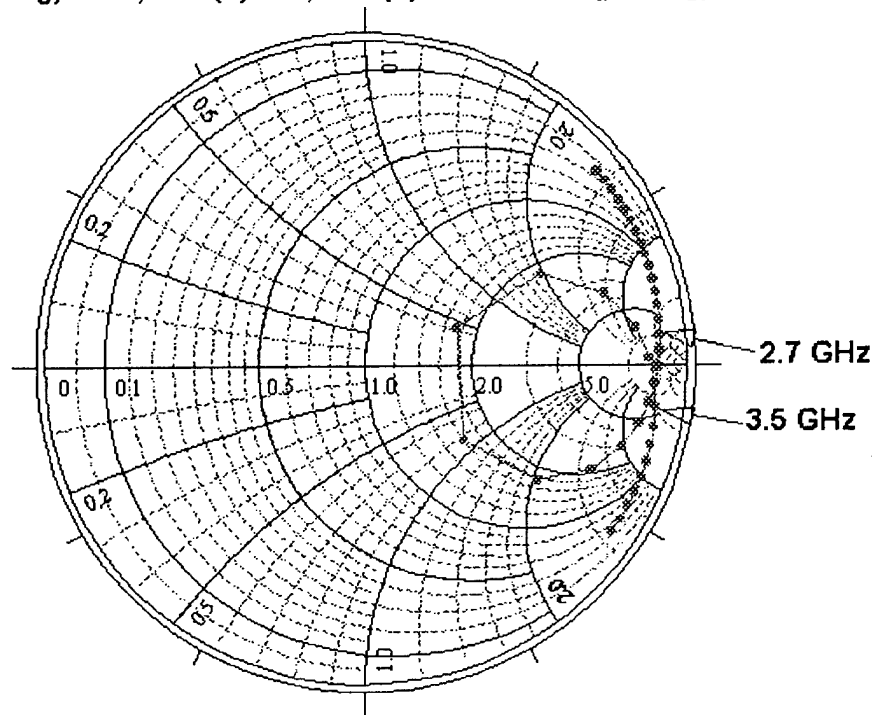


Figure 7. View looking into the apertures of a two-resonator canted sector system showing the inductive straps connected across the apertures to reduce the size of the element at resonance. The interior lines are the boundaries of subsectional patches used in the moment method analysis of the antenna using the FERM software. Note the difference in the widths of the terminal straps across the upper and lower resonators. Although the resonators have almost the same size, the resonant frequencies differ because of the difference in inductances of the straps.

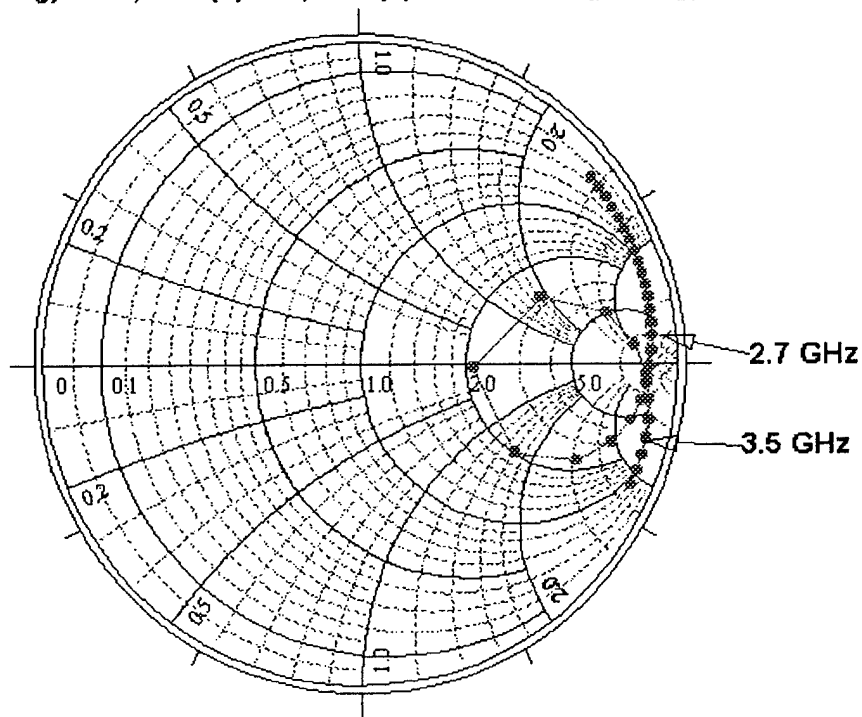
Input Impedance Computed for Two Stacked 80-Deg Loaded Sectors
 Theta1=90 deg, Theta2=80 deg, Theta3=70 deg, Radius=1.2 cm
 xtr(1)=xtr(3)=0.01 cm, xtr(2)=0.05 cm, dsodw(1)=0.01, dsodw(2)=0.2
 h(j)=0.75, rsurf(1)=0.1, rsurf(2)=1.0 ohms/sq, xsurf(j)=0.0



Frequency from 2.0 to 4.0 GHz, (in 0.05 GHz steps)

Figure 8. A Smith chart plot of impedance computed for a system of two stacked eighty-degree triangular sector resonators loaded with straps of relative width (dsodw(2))=0.2 at the corners of the upper resonator and straps of relative width (dsodw(1))=0.01 at the corners of the lower resonator. The upper and lower sectors are truncated at xtr(1)=xtr(2)=0.01 cm and the center sector is truncated at xtr(2)=0.05 cm. The vertical dimension of the straps is h(j)=0.75 of the height of the corresponding resonator aperture. The lower strap has a surface resistance rsurf(1)=0.1 ohms/square. The upper strap has a surface resistance rsurf(2)=1.0 ohms/square. No surface reactance (xsurf(j)) is added to any strap.

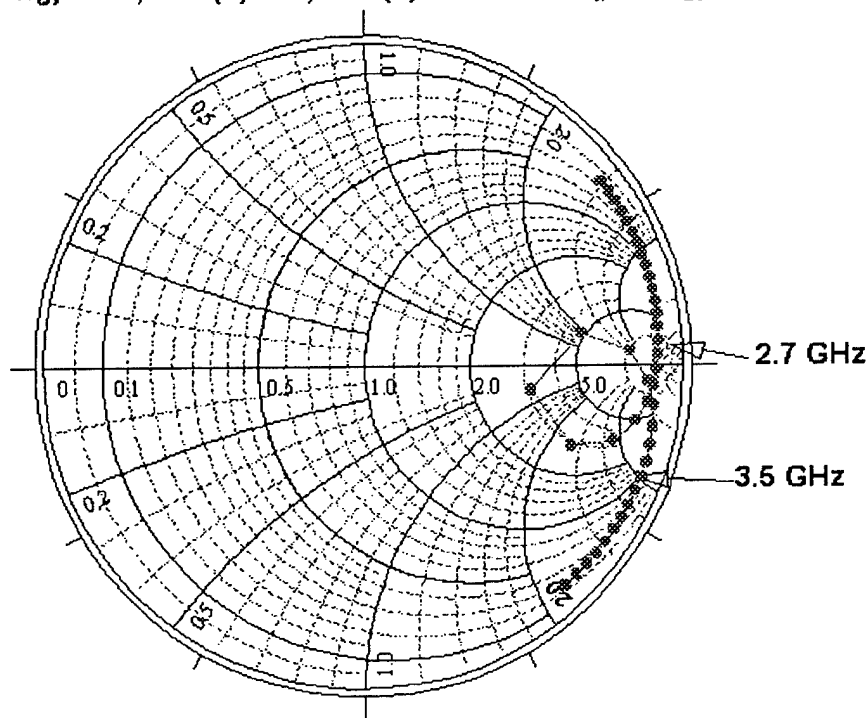
Input Impedance Computed for Two Stacked 80-Deg Loaded Sectors
 Theta1=90 deg, Theta2=80 deg, Theta3=70 deg, Radius=1.2 cm
 $x_{tr}(1)=x_{tr}(3)=0.01$ cm, $x_{tr}(2)=0.05$ cm, $dsodw(1)=0.01$, $dsodw(2)=0.15$
 $h(j)=0.75$, $rsurf(1)=0.1$, $rsurf(2)=0.7$ ohms/sq, $xsurf(j)=0.0$



Frequency from 2.0 to 3.65 GHz, (in 0.05 GHz steps)

Fig. 9. Smith chart plot of impedance computed for a system of two stacked eighty-degree triangular sector resonators loaded with straps of relative width=0.15 at the corners of the upper resonator and straps of relative width=0.01 at the corners of the lower resonator. See Figure 8 for a definition of the parameters listed above.

Input Impedance Computed for Two Stacked 80-Deg Loaded Sectors
 Theta1=90 deg, Theta2=80 deg, Theta3=70 deg, Radius=1.2 cm
 xtr(1)=xtr(3)=0.01 cm, xtr(2)=0.05 cm, dsodw(1)=0.01, dsodw(2)=0.1
 h(j)=0.75, rsurf(1)=0.1, rsurf(2)=0.5 ohms/sq, xsurf(j)=0.0



Frequency from 2.0 to 3.95 GHz, (in 0.05 GHz steps)

Fig. 10 Smith chart plot of impedance computed for a system of two stacked eighty-degree triangular sector resonators loaded with straps of relative width=0.1 the corners of the upper resonator and straps of relative width=0.01 at the corners of the lower resonator. See Figure 8 for a definition of the parameters listed above.

Transformed Impedance Computed for Two Stacked 80-Deg Loaded Sectors
 Theta1=90 deg, Theta2=80 deg, Theta3=70 deg, Radius=1.2 cm
 xtr(1)=xtr(3)=0.01 cm, xtr(2)=0.05 cm, dsodw(1)=0.01, dsodw(2)=0.2
 h(j)=0.75, rsurf(1)=0.1, rsurf(2)=1.0, xsurf(j)=0.0 ohms/sq

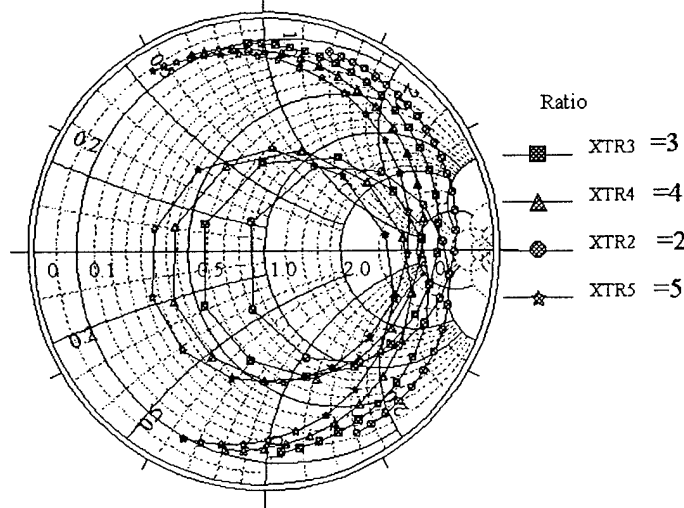


Figure 11. Impedance loops for the sector antenna data of Figure 7 after applying various ratios to simulate the effect of adding a transformer at the input. See Figure 8 for a definition of the parameters listed above.

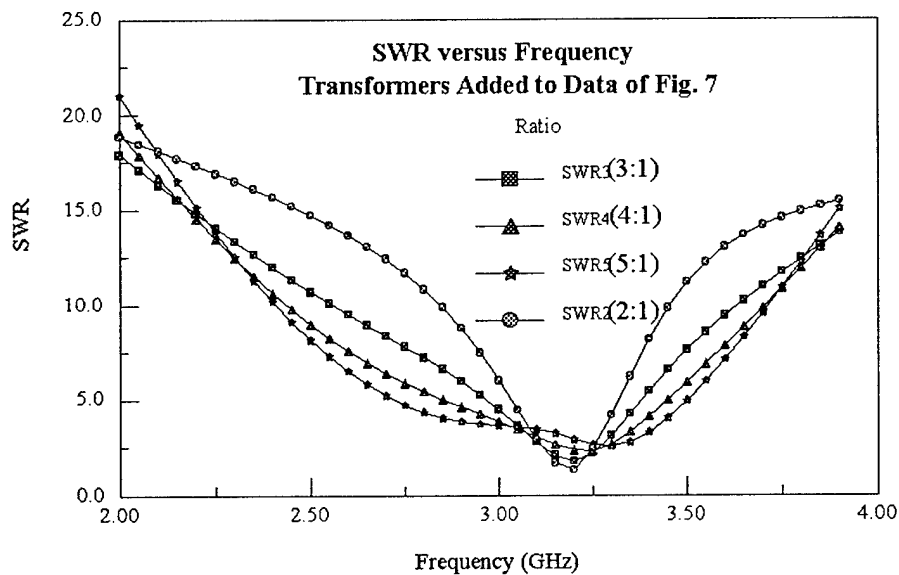
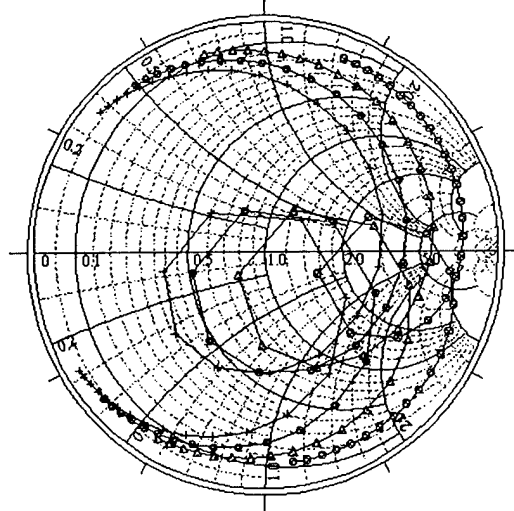


Figure 12. SWR versus frequency computed from the data of Figure 11.

Input Impedance Computed for Two Stacked 80-Deg Loaded Sectors
 Theta1=90 deg, Theta2=80 deg, Theta3=70 deg, Radius=1.2 cm
 xtr(1)=xtr(3)=0.01 cm, xtr(2)=0.05 cm, dsodw(1)=0.01, dsodw(2)=0.1
 h(j)=0.75, rsurf(1)=0.1, rsurf(2)=0.5 ohms/sq, xsurf(j)=0.0



Frequency from 2.0 to 3.95 GHz, (in 0.05 GHz steps)

Figure 13. Impedance loops for the sector antenna data of Figure 10 after applying ratios of 2, 4, 6 and 8 to simulate the effect of adding transformers at the input. See Figure 8 for a definition of the parameters listed above.

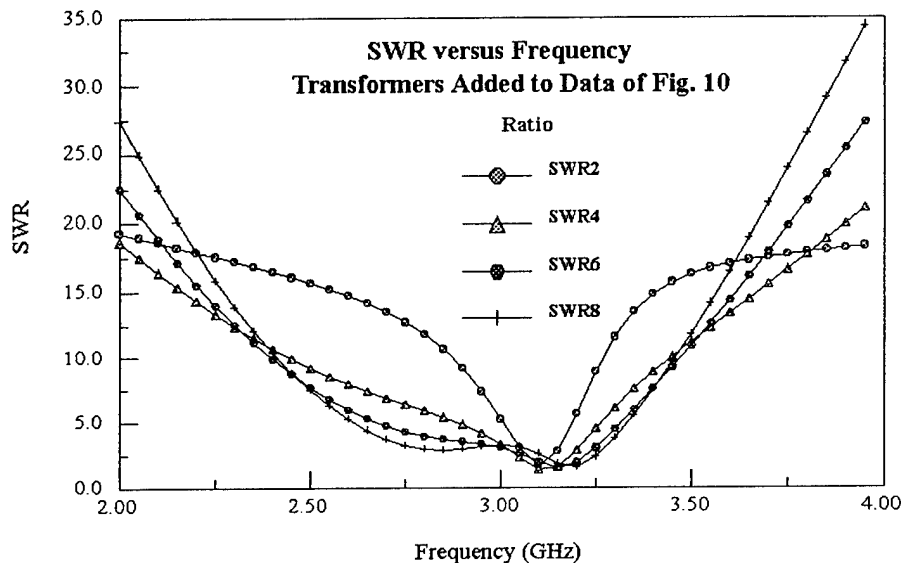


Figure 14. SWR versus frequency computed from the data of Figure 13.

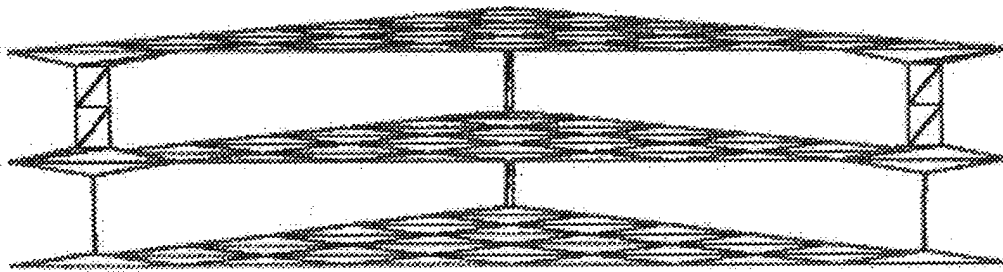


Figure 15. View looking into the apertures of a radiating flat (planar and parallel to ground) sector antenna system showing the inductive straps connected across the apertures to reduce the size of the element at resonance.

The interior lines are the boundaries of subsectional patches used in the moment method analysis of the antenna using the FERM software. Note the difference in the widths of the terminal straps across the upper and lower resonators. Although the resonators have almost the same size, the resonant frequencies differ because of the difference in inductances of the upper and lower straps. In addition, surface reactances may be needed on the aperture straps to compensate for the effect of the inductance of the longer feed strap (seen at the tip of the sector).

Input Impedance Computed for Two Stacked 80-Deg Loaded Parallel Sectors
 $T1=T2=T3=90$ deg, $z1=0.0$, $z2=0.2116$, $z3=0.4368$ cm, Radius=1.2 cm
 $xtr(1)=xtr(3)=0.01$ cm, $xtr(2)=0.05$ cm, $dsodw(1)=0.01$, $dsodw(2)=0.1$
 $h(j)=0.75$, $rsurf(1)=0.1$, $rsurf(2)=1.0$ ohms/sq, $xsurf(1)=0.8$, $xsurf(2)=0.0$

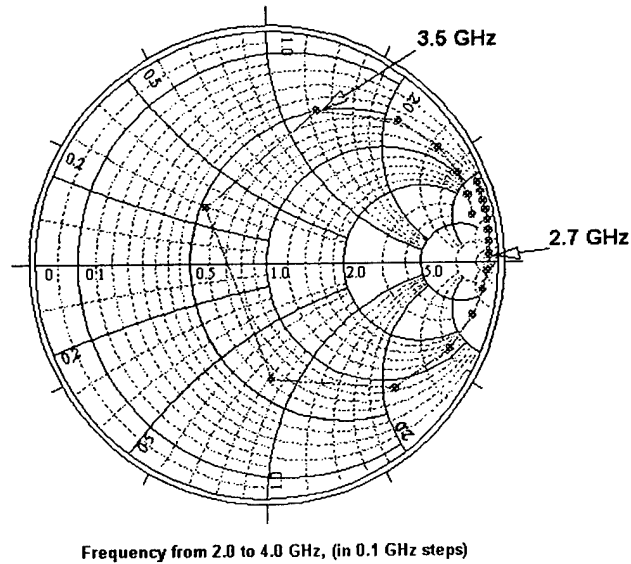


Figure 16. Input impedance computed for a set of two flat sector radiating resonators with terminal strap widths the same as for the antennas of Figures 11, 12 and 13, but with lumped inductance added to the straps on the lower resonator to place the lower resonance near 2.7 GHz. Note that additional inductance will also be required on the upper resonator to make the loop smaller by reducing the value of the second resonant frequency. See Figure 8 for a definition of the parameters listed above.

Performance Enhancements with Applications of the Coaxial Cavity Antenna

Dr. Tim Holzheimer, P.E.
Raytheon, C3I
Garland, Texas 75042

Dr. Stephen Schneider
WPAFB/AFRL-SN
Dayton, Ohio 45433

Abstract:

The Initial presentation of the Coaxial Cavity Antenna occurred at the Antenna Applications Symposium 2000. Additional work has been undertaken using the coaxial cavity antenna in taking advantage of the four-fold feed symmetry and out of band roll-off. This antenna is unique in its configuration providing the capability for multiple polarizations as described previously. The new performance data illustrates the relevant use of this element for interferometry and direction finding systems. The flat phase and amplitude over an octave in frequency and a +/- 60 degree field of view demonstrate the use of these elements in numerous wideband systems.

The latest performance data, to be presented, shows a slow out of band roll-off on the lower side and a sharp roll-off on the upper side of the designed operating band edges. The four-fold symmetry has been demonstrated with a simple four element butler matrix resulting in a classic mode 0 and mode 1 (alternatively mode 1 and mode 2) radiation pattern shape.

Based on the latest performance enhancements, a new version 360 degree circular DF antenna can be built in a smaller volume. A design that is being fabricated and tested has a volume of only 9.0 inches in diameter with approximately a 4.5 inch height. This DF antenna works over the 2 to 18 GHz frequency range.

1.0 Introduction:

There are numerous antennas that attain multi-octave bandwidth. They are documented by others and examples include spirals, sinuous, TEM type structures and other variations such as Zig-Zags and Interlogs.[1-3] Extensive work with regard to wide band or wide bandwidth antennas, that operate over multiple octaves, has been performed by numerous researchers such as Mayes, and others. The designs have accomplished multi-octave frequency coverage typically 2 to 18 GHz or 6 to 18 GHz frequency bands. Unlike the Coaxial Cavity antenna these structures are generally traveling wave type structures.[4] However, they are complimentary just like the Coaxial Cavity antenna.

The sub-system perspective desires an antenna that covers multiple octaves, has multiple polarization capability, flat amplitude and phase response over field of view and among similar elements, low cross-polarization and high efficiency. The coupling among arrayed elements should be small, and when installed should have high isolation.

The Coaxial Cavity Antenna was initially presented at the Antenna Applications Symposium 2000.[5] This was the first time a published paper had been presented describing the Raytheon patented Coaxial Cavity Antenna and is shown in figure 1. This antenna is fully scalable over any octave or multi-octave frequency range, and has been demonstrated over the 400 MHz to 40 GHz frequency range. This antenna design is a balanced complimentary structure that has four discrete feed points, is light weight, and generally is unloaded, i.e. no dielectrics are introduced into the cavity structure.

The differences are illustrated when these various elements are introduced into systems such as interferometers, direction finding arrays, tracking systems and various types of phased array antennas.[6-7]

The obvious next step is to determine how far out of band these antennas can be taken before they are unusable in a system based on currently available technology. Electrically small antennas, using active devices at the antenna feed are known examples of antennas operating at extremely large out of band frequencies and are small in size compared to the operating wavelength.

The, patent pending, concentric cavity or coaxial cavity antenna has been investigated in regard to operation out of its normal in band frequency of design and operation. The concentric or coaxial cavity antenna presents itself as a moderate gain element with excellent phase and amplitude tracking over the

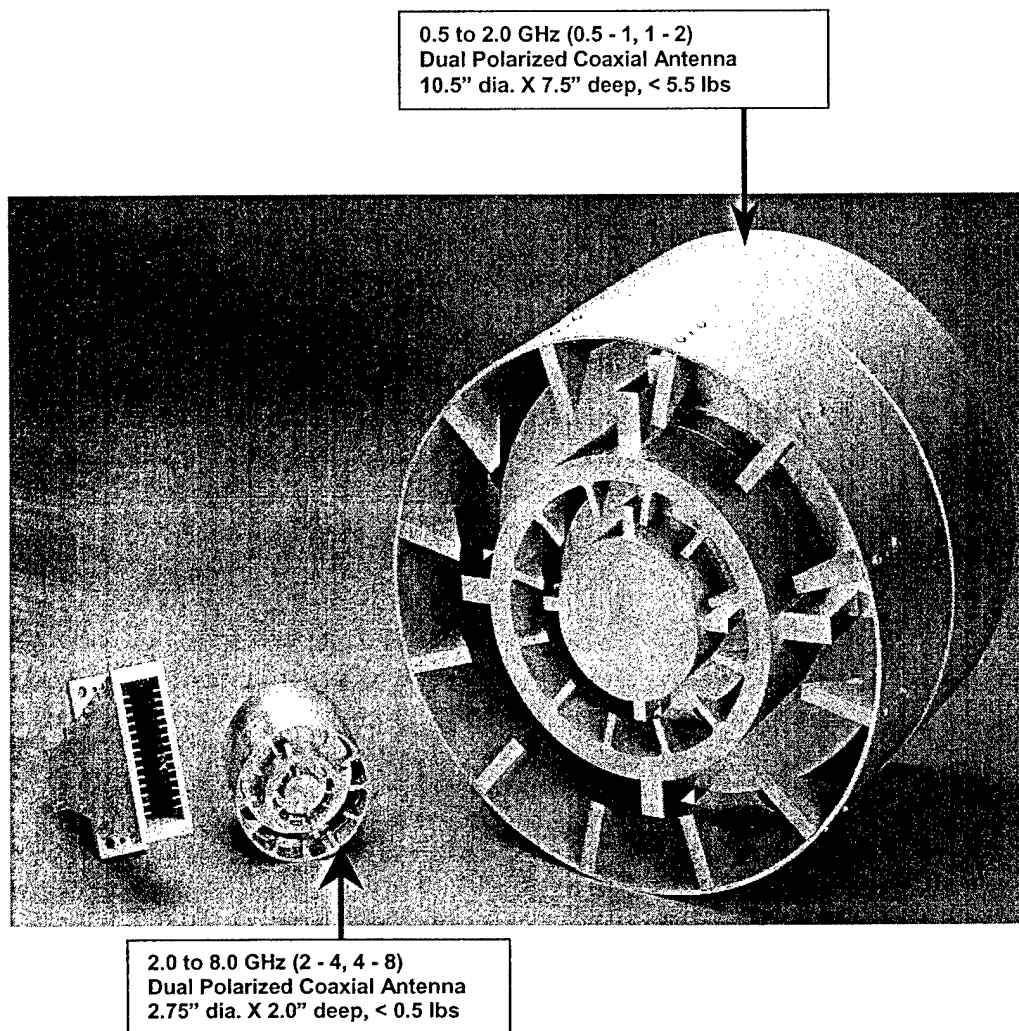


Figure 1. Coaxial cavity antennas illustrating scaling.

desired field of view and exhibits potential for wide applicability to numerous types of systems.

2.0 Applications:

Typical applications for these types of antennas, regardless of whether they are spirals, horns or coaxial cavity antennas, are in use as interferometer elements, direction finders, radar warning receiver (RWR) antennas, phased array elements, polarimeters and others. The interferometer and the polarimeter place the most stringent requirements on the antennas of the applications listed above. They require flat amplitude and phase over both field of view and frequency of operation. Stated another way, if the antenna can radiate an exact duplicate of an impulse then it will have the desired properties for use as an interferometer and polarimeter antenna element.

The elements that are used in these systems must be balanced against desired polarizations (usually all-polarization capable), operational frequency range, useful field of view and detection range, which translates into the amount of gain required of the antenna element. Mechanical considerations also exist, such as weight, complexity, and reliability of the design to survive operational vibration, shock, altitude, and/or other environmental factors.

The following discussions will show the performance of the coaxial cavity antenna for use in various applications such as electrically small structures, tracking systems and phased arrays. The coaxial cavity data will illustrate the single and the arrayed performance that can be obtained. This will demonstrate the potential for use in phased arrays and electrically small antennas.

3.0 Results:

Principal plane radiation patterns are shown for the vertical probe pairs in figures 3 through 5 for the in-band performance of a typical 2 to 4 GHz coaxial cavity antenna. These patterns illustrate the frequency range of an octave from 2 to 4 GHz. These patterns are representative of the typical field of view equated at the 3 dB beamwidth points. There are no dips in the main field of view of any of these patterns and both principal planes are well balanced to each other. Out of band principal plane radiation patterns are shown in figures 6 through 9 over the frequency range of 0.5 to 2 GHz. These patterns show excellent tracking to the respective principal planes out of band by at least two octaves. The high side of the band, above 4 GHz falls off within approximately 100 MHz and is not illustrated here. This implies that the 2 to 4 GHz antenna can actually operate fairly well at 2 octaves out of band if the system requires only a sum radiation pattern. However, additional information as illustrated in the following paragraphs is required in order to use this antenna out of band over two octaves.

Antenna gain was measured as the secondary measurement to verify the usage of these elements out of band by two octaves. The in-band antenna gain is shown in figures 10 and 11. The gain has a slight roll-off at the lower end, but for the most part is averaging +6 dBli. This antenna works in band based on this data. The gain plotted in figures 12 and 13 shows the performance of the 2 to 4 GHz coaxial cavity antenna out of band by two octaves. There is roll-off, but it exhibits roll-off on the order of 10 to 12 dB per octave. This is slower roll-off than other types of antennas and shows the ability to use this antenna at least two octaves out of band, albeit on the low side. What is not shown is that the VSWR, does go high out of band and as a result, makes this a reasonable receive antenna and unsuitable as a transmit antenna.

The antenna has been noted as a complimentary four feed device and because of this a standard four-port modeformer was attached to the back of the antenna to investigate the capability of acquiring mode 0 and mode 1 radiation patterns. The mode 0 or sum patterns are actually those of figures 3 through 9. The difference patterns or mode 1 patterns are shown in figures 14 through 16. Well behaved difference radiation patterns were measured which illustrates the use of this antenna for a tracking system as a low gain element or as a tracking feed for a reflector dish antenna.

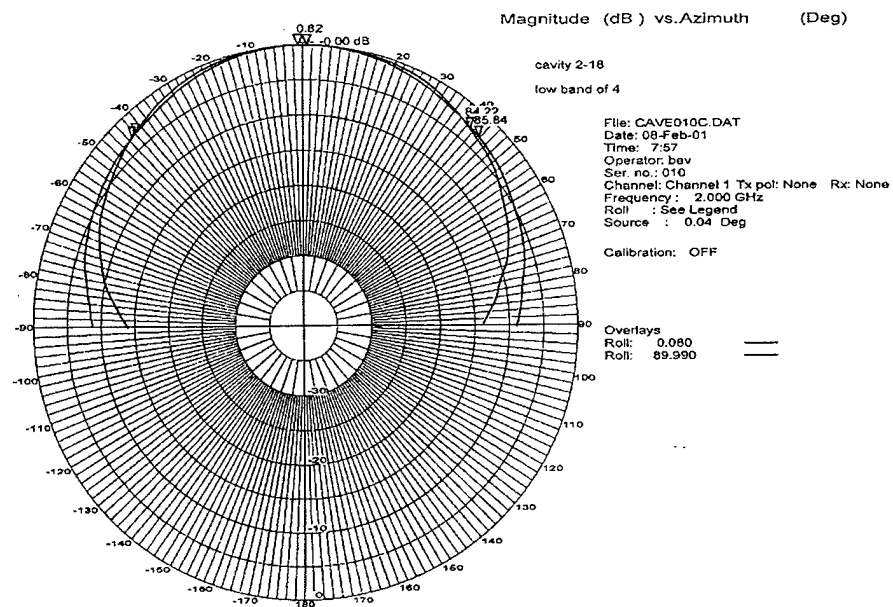


Figure 3. Principal plane patterns for single coaxial cavity antenna at 2GHz.

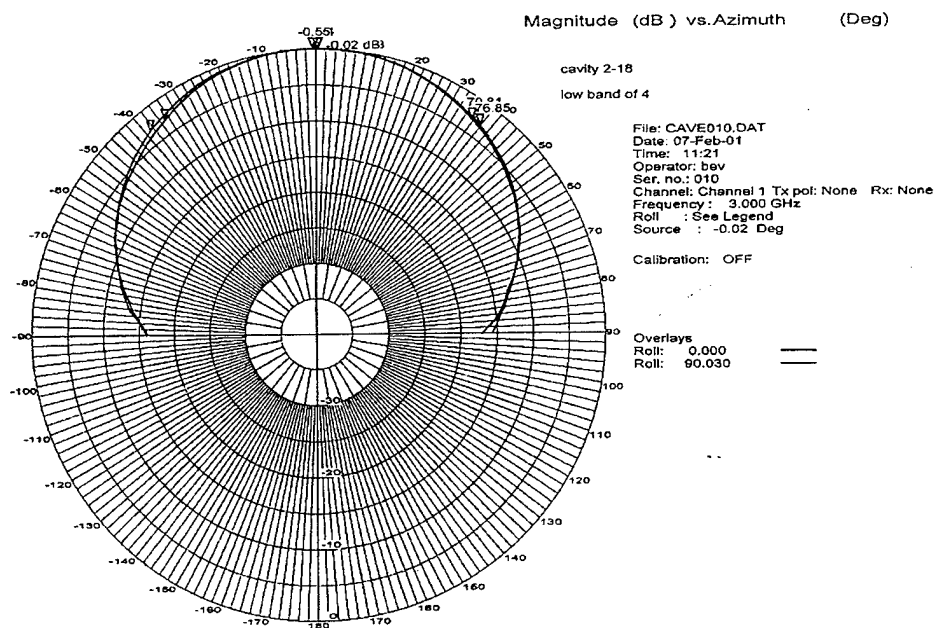


Figure 4. Principal plane patterns for single coaxial cavity antenna at 3 GHz.

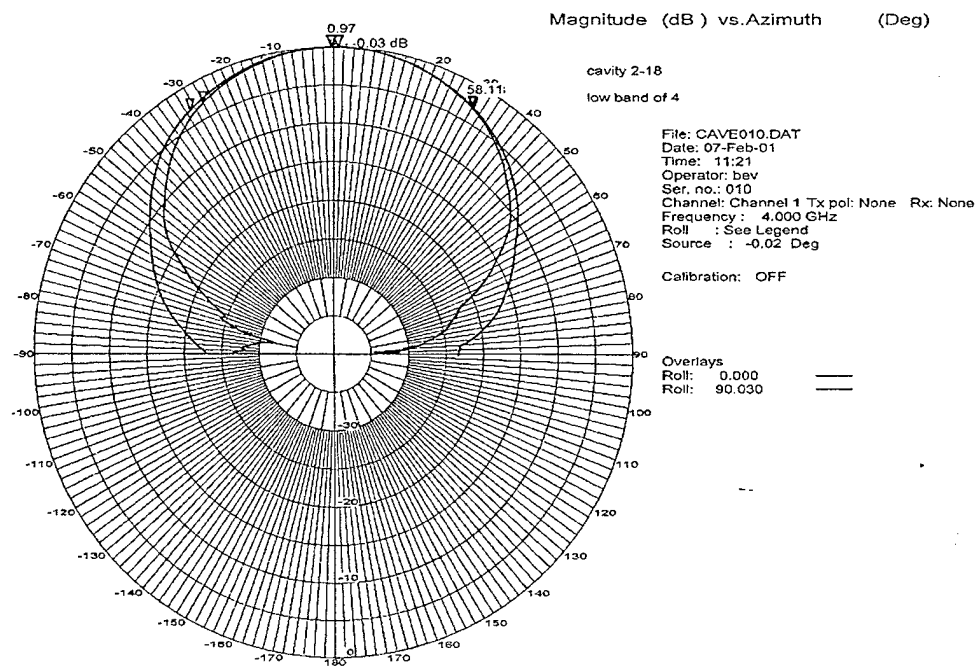


Figure 5. Principal plane patterns for single coaxial cavity antenna at 4 GHz.

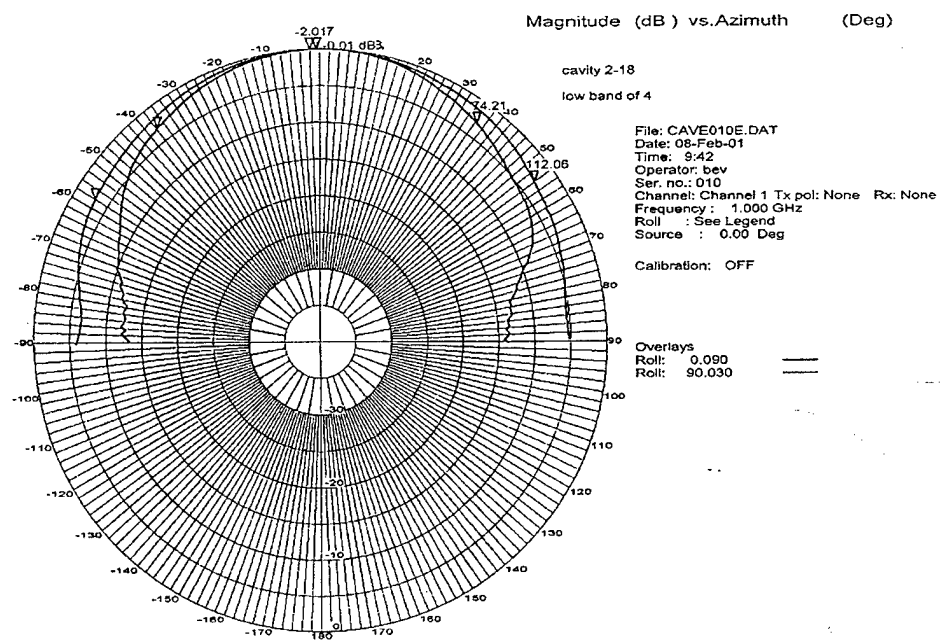


Figure 6. Principal plane patterns for single coaxial cavity antenna at 1 GHz.

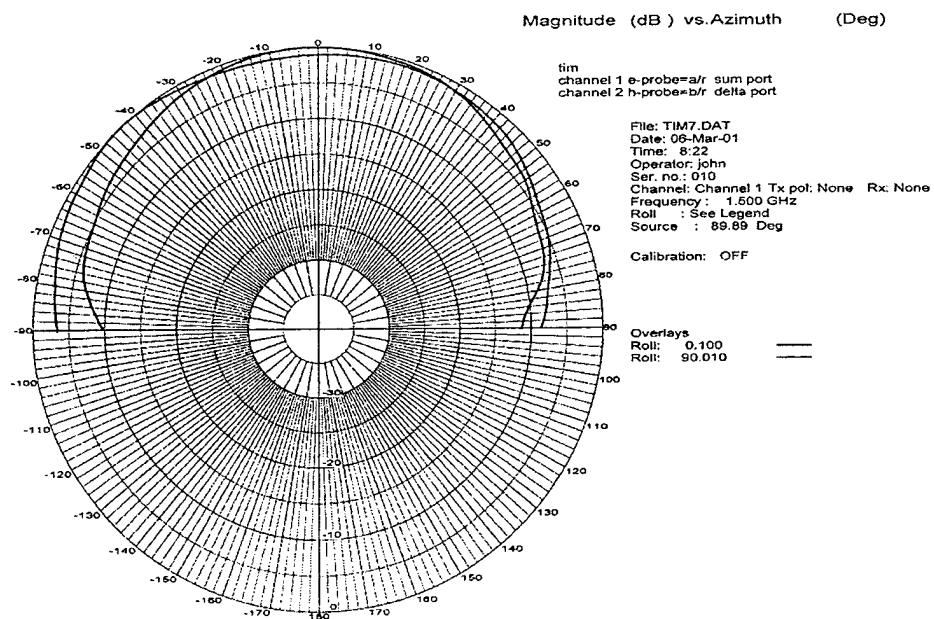


Figure 7. Principal plane patterns for single coaxial cavity antenna at 1.5 GHz.

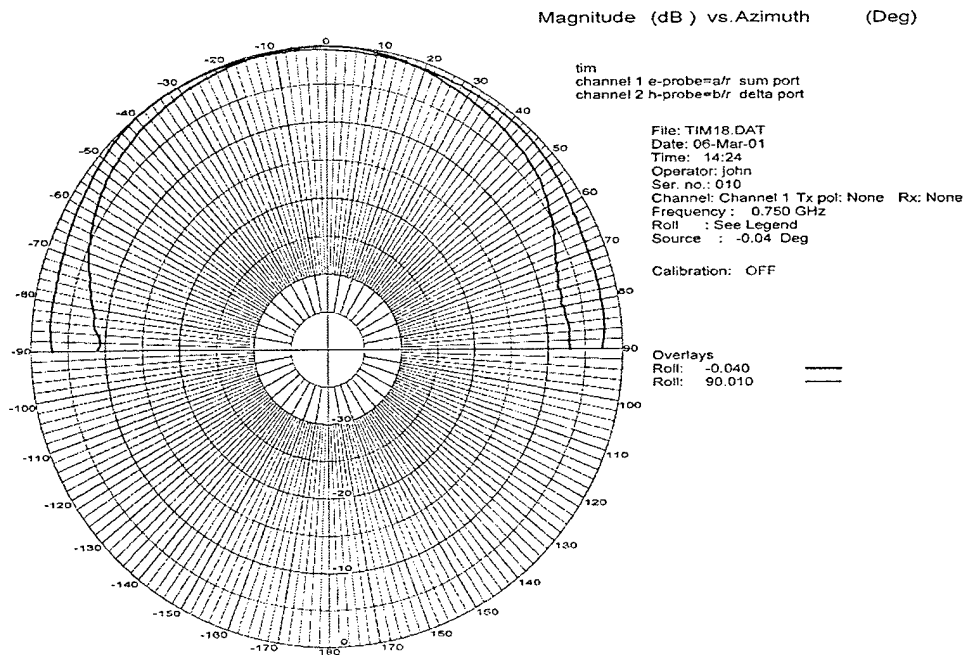


Figure 8. Principal plane patterns for single coaxial cavity antenna at 0.75 GHz.

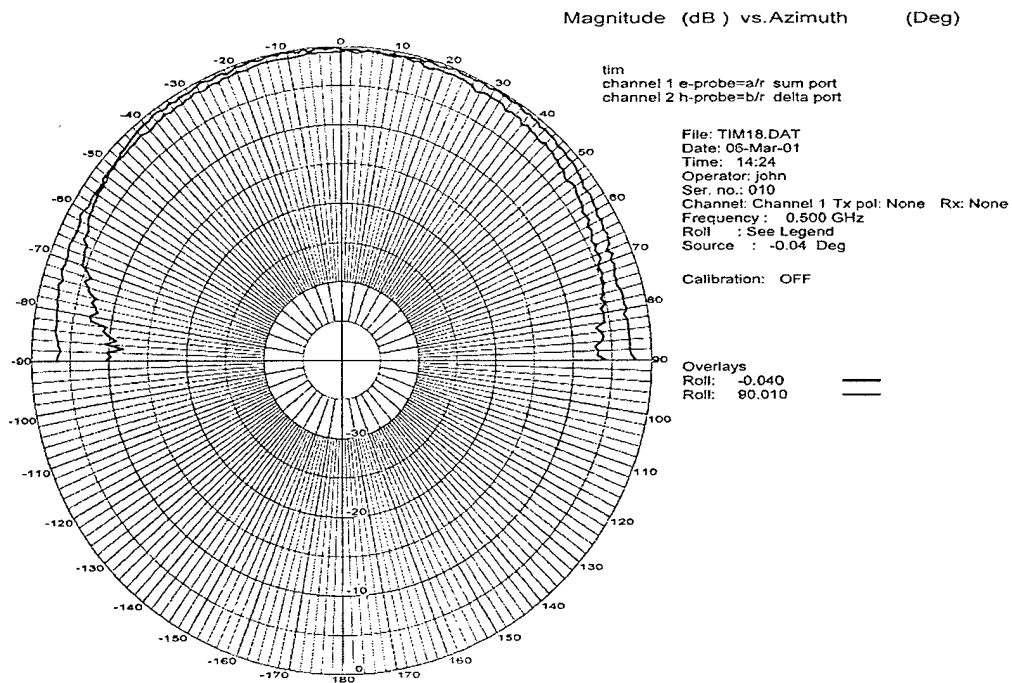


Figure 9. Principal plane patterns for single coaxial cavity antenna at 0.5 GHz.

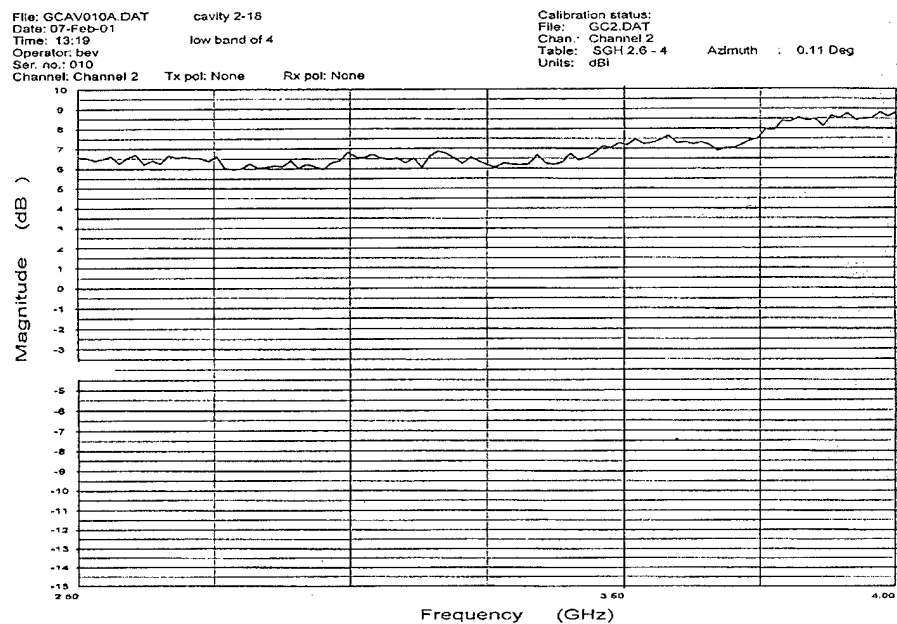


Figure 10. Coaxial cavity antenna gain in band 2.5 to 4 GHz.

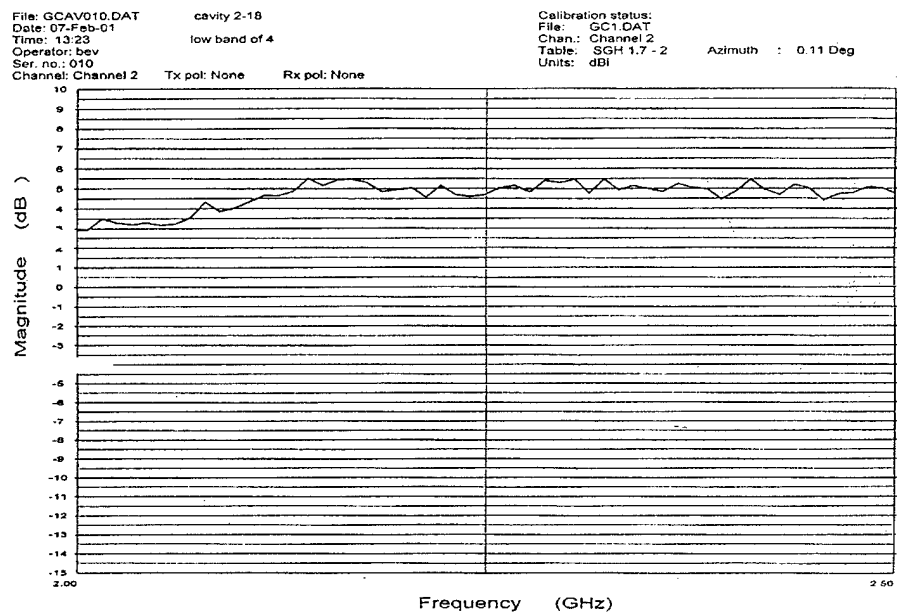


Figure 11. Coaxial cavity antenna gain in band 2 to 2.5 GHz.

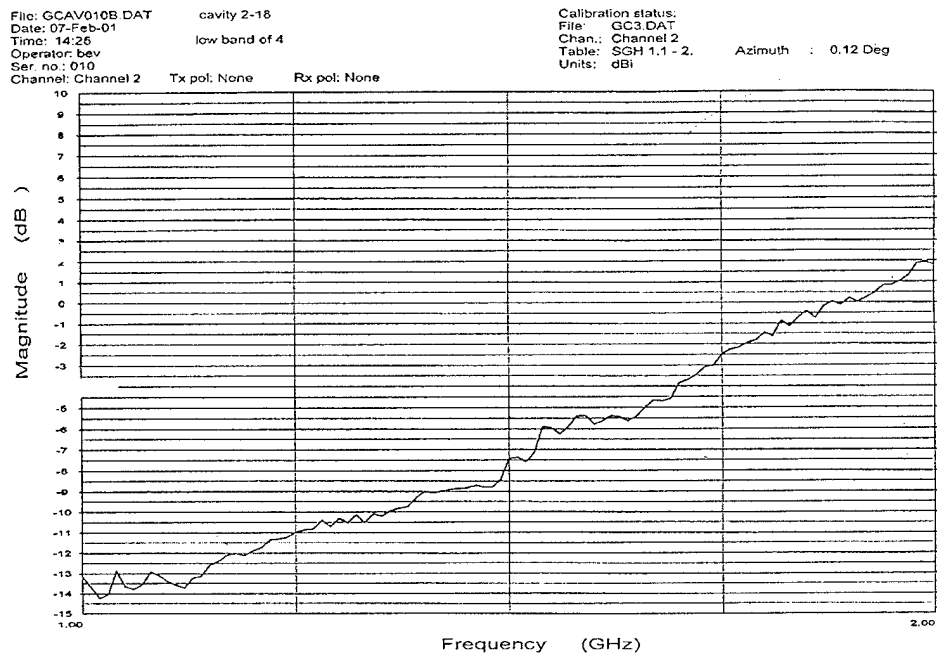


Figure 12. Coaxial cavity antenna gain out of band 1 to 2 GHz.

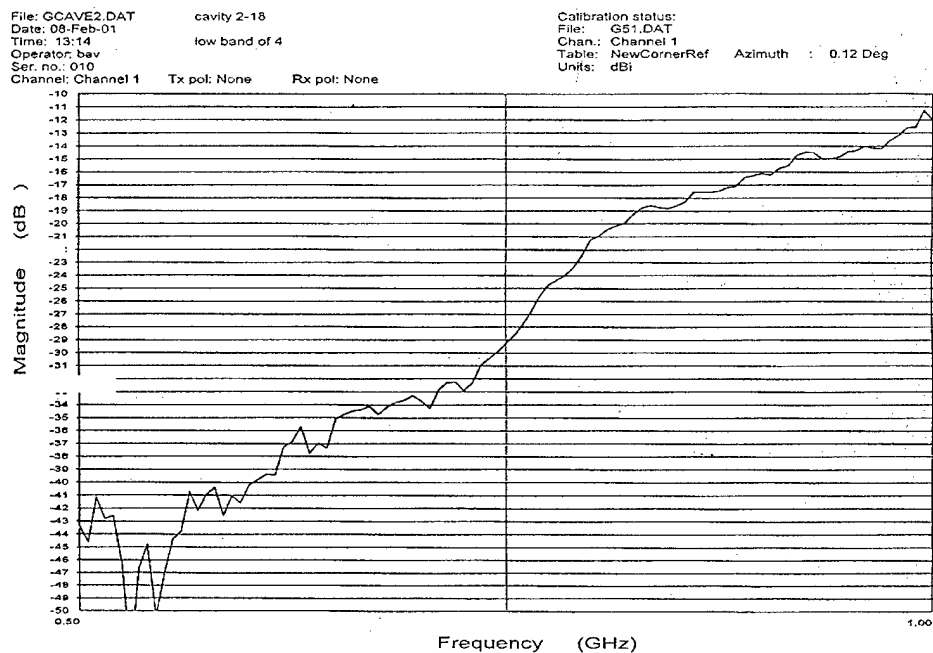


Figure 13. Coaxial cavity antenna gain out of band 0.5 to 1 GHz.

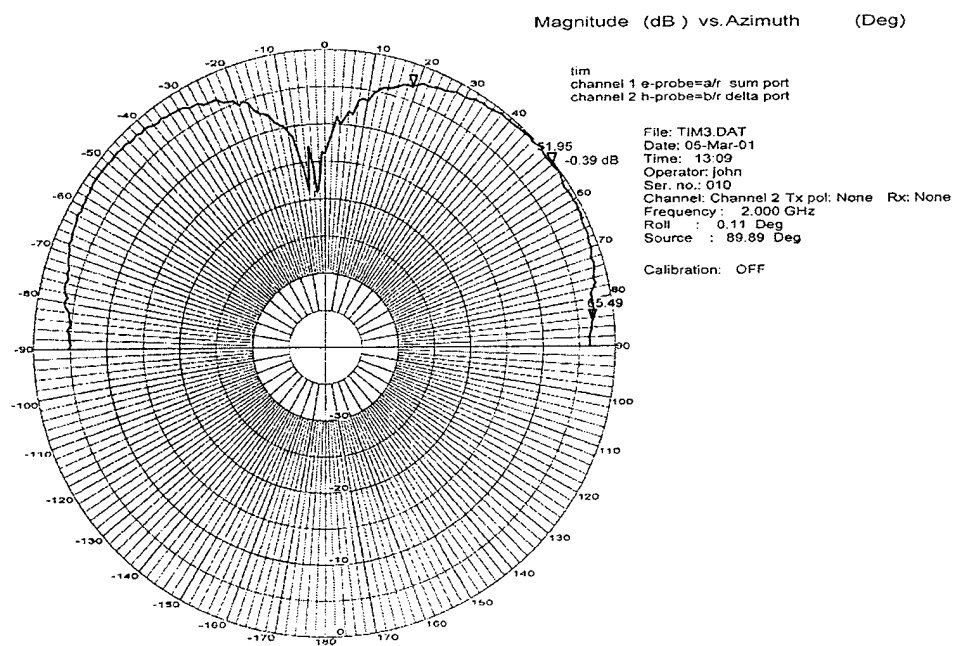


Figure 14. Delta pattern using the coaxial cavity antenna at 2 GHz.

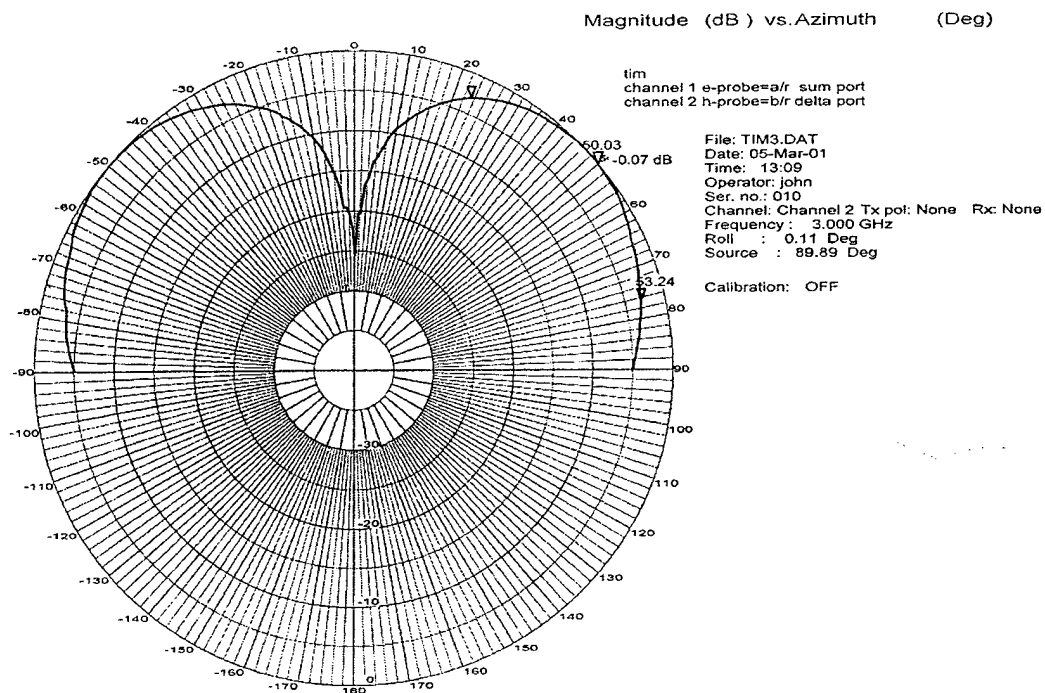


Figure 15. Delta pattern using the coaxial cavity antenna at 3 GHz.

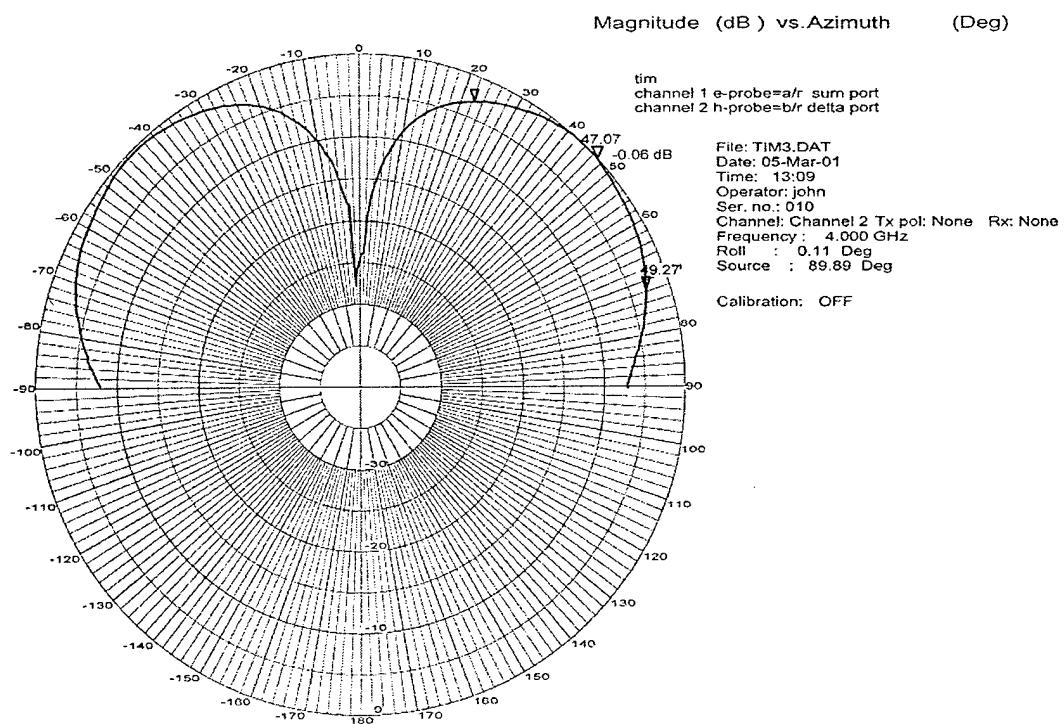


Figure 16. Delta pattern using the coaxial cavity antenna at 4 GHz.

4.0 Arrayed Coaxial Cavity Antennas:

The coaxial cavity antennas have been arrayed in two-element and four-element line array form factor with the elements butting right up to each other, i.e. the outer cavities were physically touching. The premise prior to performing this set of measurements was that the coaxial cavity antennas exhibit almost zero coupling as predicted from the measured high efficiency (approximately 65%) of the antenna.[5]

The gain of the array is shown in figure 17. Included on this plot is the gain of a single reference element whose patterns are shown later in this report for comparison. What stands out is the gain of the array of two coaxial cavity antennas is almost at the theoretical 3 dB over the gain of a single element. This points to almost zero coupling between the elements and the higher efficiency over other types of antennas. The other point is that the coaxial cavity elements are well balanced, illustrating and alluding to the amplitude and phase tracking of the elements. The gain for the vertical and horizontal port outputs is almost identical. The gain of four elements stacked is not quite 3 dB due to the fact that a less than optimum four-way power combiner was used in the measurements. This has not been accounted for in the plot, but when it is the delta from 3 dB is less than 0.25 dB which again illustrates the lack of element coupling when the elements are butted up to each other.

A cylindrical reflector antenna was designed, built and implemented with a line array feed of eight, 8 to 12 GHz coaxial cavity elements and is shown in figure 18 and 19. There was no sidelobe tapering as illustrated by the approximately 13 dB sidelobes which theoretically should be 13.6 dB shown in figure 20. The gain for this array is shown in figure 21, and when all feed network losses are accounted for, the measured value is within approximately 1 dB of a theoretical envelope calculation. However, the important point is that the coaxial cavity elements can be arrayed, and used for complex feeds in reflector type antennas.

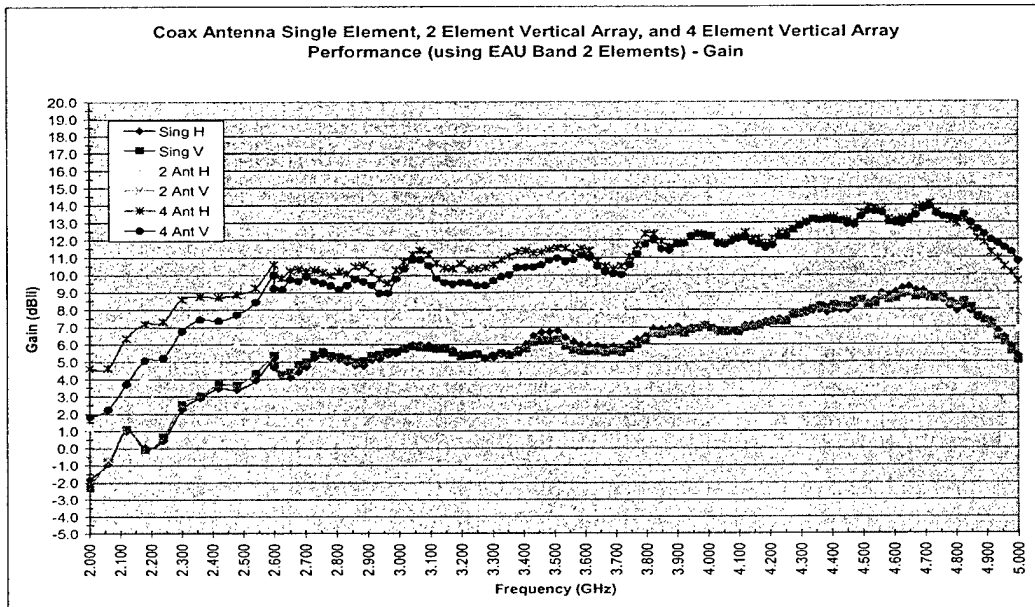


Figure 17. Arrayed Coaxial cavity antenna gain.

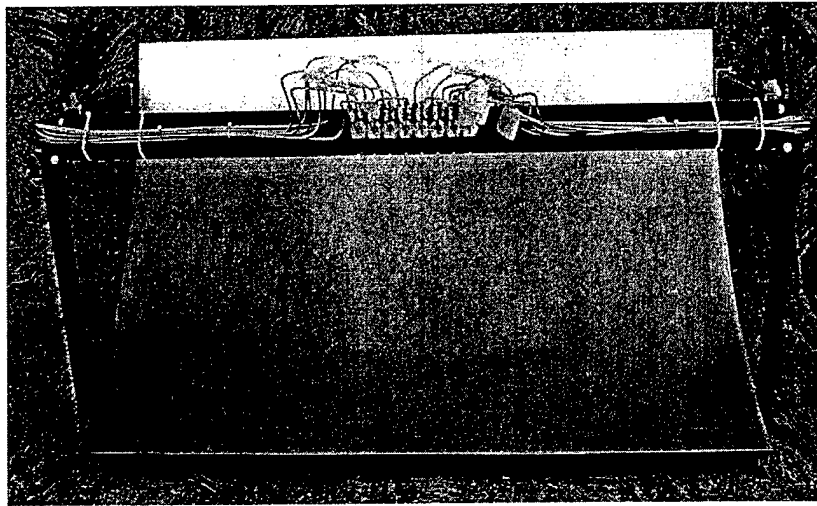


Figure 18. Coaxial cavity antenna line array reflector antenna operating over the 8 to 12 GHz frequency band.

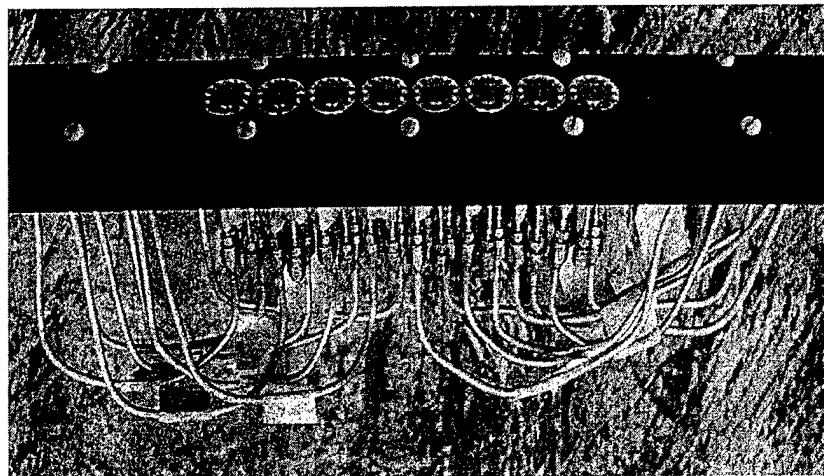


Figure 19. Close up of the 8 to 12 GHz Coaxial cavity antenna line array feed for the cylindrical reflector.

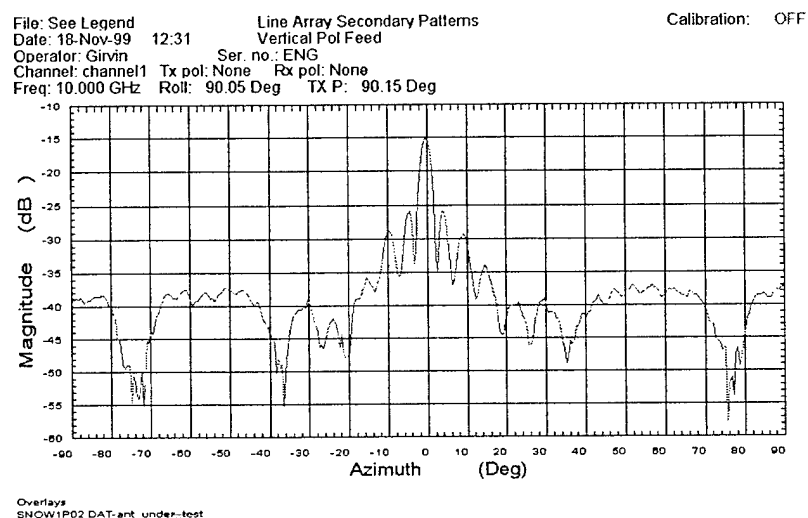


Figure 20. Typical Coaxial cavity array fed cylindrical reflector radiation pattern at 10 GHz.

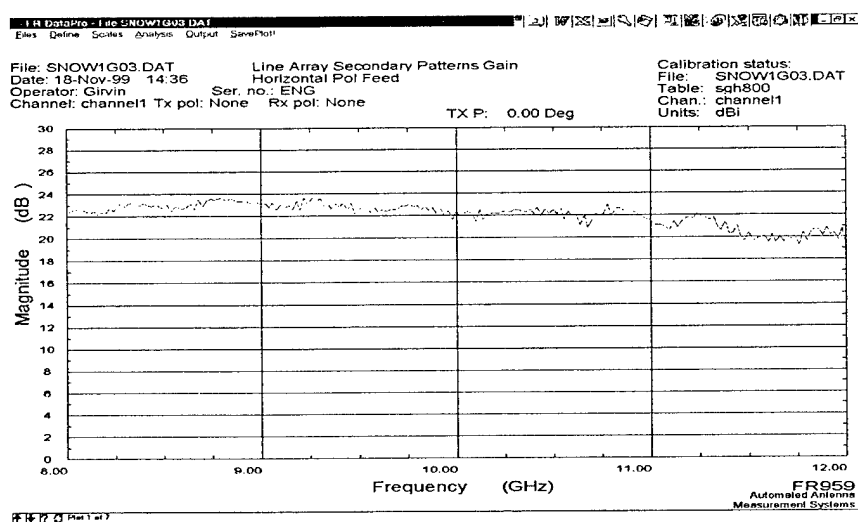


Figure 21. Gain of the Coaxial cavity line array fed cylindrical reflector antenna over the 8 to 12 GHz frequency band.

5.0 Application Examples:

Several application concepts using the coaxial cavity antenna have been designed, built and tested both in the laboratory and in real world field exercises. Various direction finding antennas have been reported at this symposium in the past where the 2 to 18 GHz version of this simultaneous circular DF antenna was built and tested in a 11.0 inch diameter with approximately a 3.5 inch height. This is illustrated in figure 22. A newer version is presently being configured for field exercise that is 9.0 inches in diameter and 4.5 inches in height, and is illustrated in figure 23. The goal with these systems is to achieve 0.5 RMS angle of arrival over a 360 degree azimuthal field of view and over the 2 to 18 GHz frequency range.

Figures 24 through 26 show actual hardware of several varieties prior to being taken on an unclassified field exercise. The antennas used in the field exercise consisted of two reflector types fed by coaxial cavity antennas and single low band coaxial cavity antennas. The cylindrical reflector fed with a band configured set of eight coaxial cavity line arrays operating from 2 to 18 GHz is shown in figure 24. Two single, multi-octave coaxial cavity antennas that worked as low as 400 MHz up 2 GHz are shown in figure 25. Two, 1 meter dish antennas with single element coaxial feeds that worked from 2 to 18 GHz are shown in figure 26. These antennas are shown in an operational configuration in figure 27.

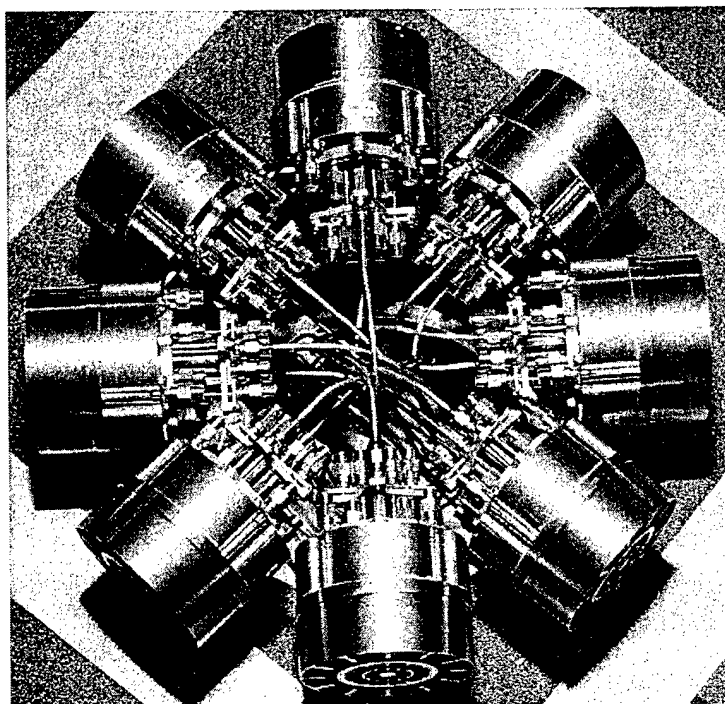


Figure 22. 11 inch diameter direction finding antenna using 2 to 18 GHz Coaxial cavity antennas.

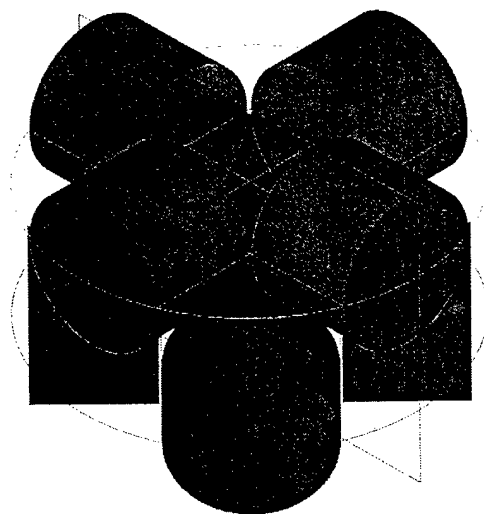


Figure 23. A compressed direction finding antenna approximately 9 inches in diameter operating over 2 to 18 GHz.

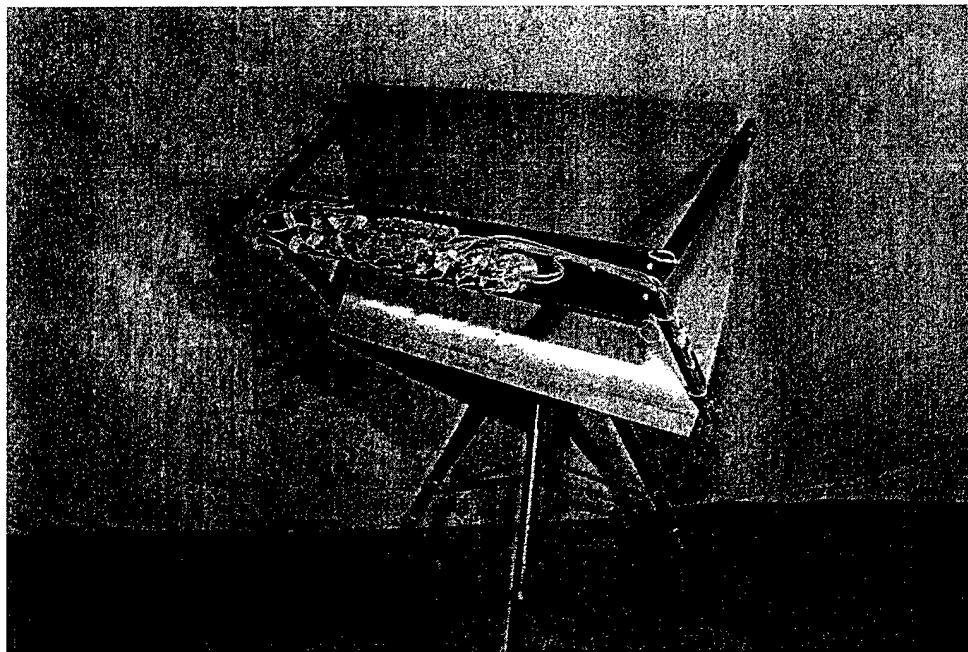


Figure 24. Eight, coaxial cavity element fed, cylindrical reflector array antenna.

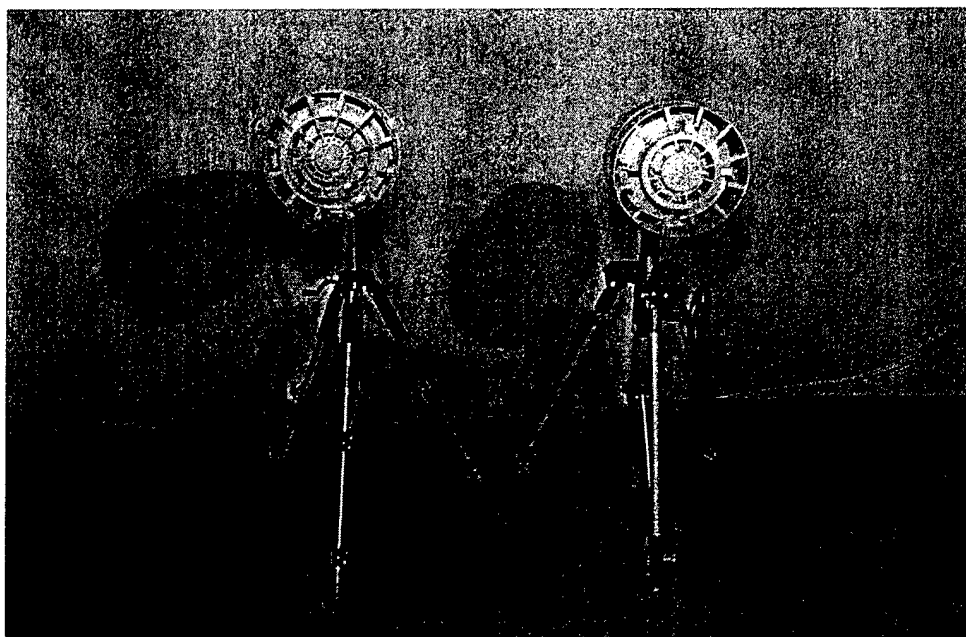


Figure 25. Two, low band coaxial cavity antennas.

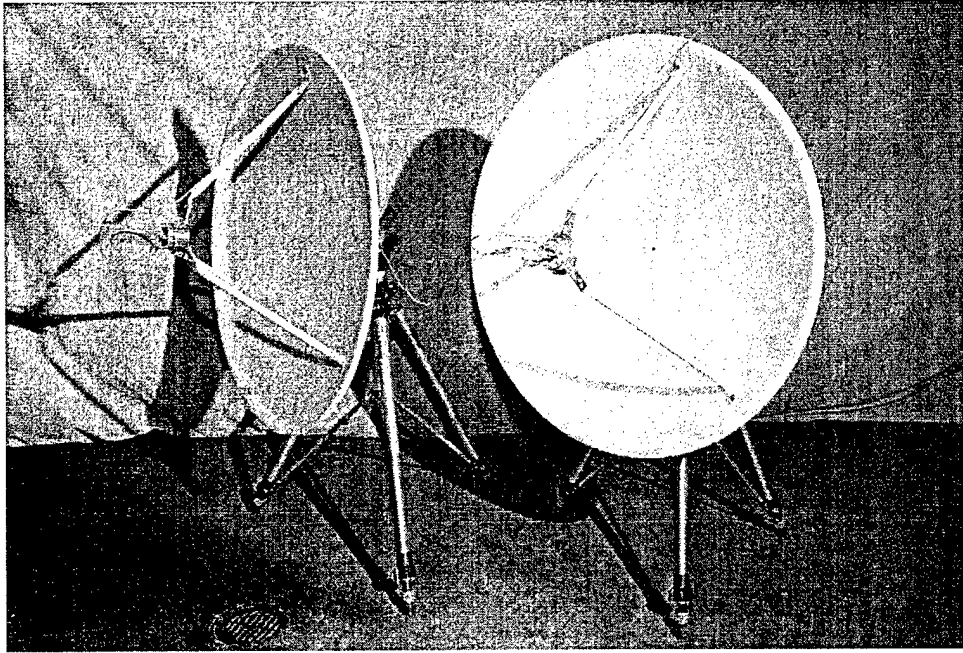


Figure 26. Two, 1 meter reflectors fed with single coaxial cavity antenna.

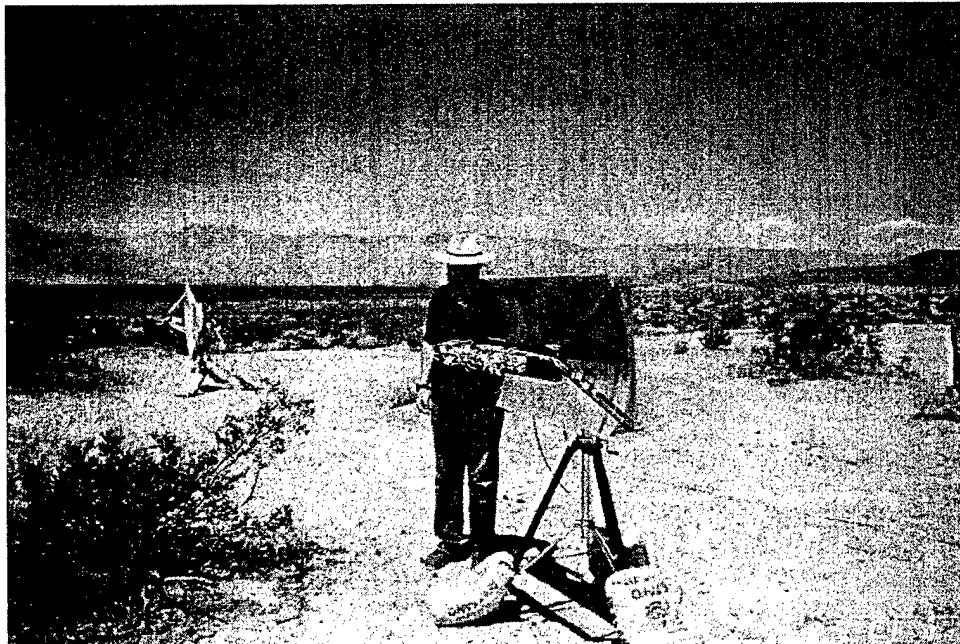


Figure 27. Actual field test of these different coaxial cavity antenna concepts.

6.0 Conclusions:

The coaxial cavity antenna has been described and data illustrating its low dispersion performance has been presented previously.[5] The coaxial cavity antenna is scaleable over octave, multi-octave and any other desired frequency band. Numerous aperture sizes can be determined based on desired operating frequency bands and desired gain. The self-complimentary structure of the coaxial cavity antenna has been verified by using a four-element modeformer resulting in very acceptable sum (mode 0) and difference (mode 1) radiation patterns. The most surprising result is that the coaxial cavity antenna appears to work at least 2 octaves out of band on the lower operating frequency side. The high end falls very quickly due to the natural cut-off nature of the annular slot.

These results illustrate the potential use of the coaxial cavity antenna in electrically small configurations where the available aperture area is non-existent. The cost in performance is the slow roll-off of approximately 10 to 12 dB per octave in antenna gain. The radiation patterns appear to be unaffected within the 3 to 5 dB beamwidth that is typical of useful fields of view. This allows size compression versus total operational frequency for the 360 degree DF antenna. It also allows the use of the coaxial cavity antenna as a tracking feed in a reflector antenna system.

The arrayed 2-element and 4-element coaxial cavity data illustrates the lack of coupling from cavity to cavity element. This provides the potential of using these elements in a multitude of array environments. This has been investigated and fielded in several types of arrays in a recent unclassified field exercise as shown in figure 27.

These antennas can also be used as radar warning antennas (RWR), and because of the excellent phase and amplitude tracking over both field of view and the operational frequency range, are an excellent choice for use in interferometers, polarimeters and circular direction finding antennas

Ongoing work is being performed in the 360 degree circular DF antenna where the size is already down to 11.0 inches in diameter and a novel approach has been discovered for decreasing the size to a 9.0 inch diameter. This 360 degree DF antenna version works over the frequency range of 1 to 18 GHz taking advantage of the roll off, as in a spiral antenna.

Design curves and scaling data for impedance matching and frequency band determination have been developed. This data and antenna design are presented in a pending patent.[5]

7.0 Acknowledgments:

The author wishes to thank the personnel, attached to the Raytheon - Antenna Engineering Laboratory, Garland, Texas, where all of this work has been accomplished and is presently continuing.

8.0 References:

1. R. G. Corzine and J. A. Mosko, Four-Arm Spirals, Artech House, Norwood, MA, 1990.
2. C. H. Walter, Traveling Wave Antennas, Dover Publications, Inc., New York, 1965.
3. Y. Mushiake, Self-Complimentary Antennas: Principle of Self-Complementary for Constant Impedance, Springer-Verlag, New York, 1996.
4. R. Jaeger, T. Holzheimer, R. Rudd and R. Ackerman, "Coaxial Cavity Antenna," Patent Pending, 20 October, 1998.
5. T. R. Holzheimer A Coaxial Cavity Antenna Exhibiting Low Dispersion Over a Wide Field of View," 2000 Antenna Applications Symposium, Allerton Park, Monticello, Illinois, 20-22 September, 1995, pp. 281-310.
6. T. R. Holzheimer, "An Implementation of a 0.5 to 2.0 GHz Circular 360 Degree Direction Finding Antenna," 1999 Antenna Applications Symposium, Allerton Park, Monticello, Illinois, 17-19 September, 1999, pp. 374-404.
7. T. R. Holzheimer, "High Accuracy DF Antenna Using COTS Hardware," 1995 Antenna Applications Symposium, Allerton Park, Monticello, Illinois, 20-22 September, 1995, pp. 12-1-12-30.

THE KOCH FRACTAL MONOPOLE ANTENNA: THE SIGNIFICANCE OF FRACTAL GEOMETRY IN DETERMINING ANTENNA PERFORMANCE

**Steven R. Best
Cushcraft Corporation
48 Perimeter Road
Manchester, NH 03103**

Abstract: The use of fractal geometries in antenna design has generated a significant level of interest within the engineering and wireless communications communities. In the previous literature, it has been demonstrated that fractal antennas exhibit compressed resonance and multi-band behavior when their impedance properties are compared to those of Euclidean antennas having the same overall size. These performance properties have generally been attributed to the self-similar fractal geometry of the antenna. Fractal antennas have also been shown to exhibit lower resonant frequencies than Euclidean antennas of the same overall size. This property can be advantageous in applications requiring reduced size antennas. However, noticeably absent in the previous literature is a comparison of fractal antennas to antennas with non-fractal wire geometries having the same overall size and total wire length. Here, the impedance properties of several Koch fractal monopole antennas are presented and then compared to the impedance properties of antennas with non-fractal wire geometries. Through this comparison, it is demonstrated that the non-fractal antennas perform in a manner similar to the fractal antennas and that the fractal geometry is not the significant factor causing the antenna to exhibit lower resonant frequency behavior. It is demonstrated through numerical analysis and measurement that the increase in total wire length, and the compression of this wire length into the same overall size as the Euclidean antenna, are the significant factors causing the antenna to exhibit lower resonant frequencies. Finally, it is demonstrated that when the self-similar fractal and non-fractal antennas are made to be resonant at the same frequency, they exhibit virtually identical impedance characteristics through several resonant frequencies.

1. Introduction

Fractal antennas represent a class of radiators where the overall structure is comprised of a series of repetitions of a single geometry basis, where each geometric repetition is typically on a different scale [1] - [6]. In most cases, a portion of the fractal geometry has the same shape as the overall geometry. In this case, the fractal antenna is defined to be

self-similar. It has been shown that when a fractal antenna is of the same overall size as a Euclidean antenna, the fractal antenna has a lower resonant frequency and it exhibits resonance compression or multi-band behavior as a function of frequency [1] – [6].

Since fractal antennas exhibit a lower resonant frequency than the same size Euclidean antenna, they are well suited for use in applications requiring reduced size antennas. While this has been discussed in the literature, the performance properties of fractal antennas have not been compared to the performance properties of other antenna types that similarly exhibit lower resonant frequency behavior. In previous discussions of the Koch fractal monopole antenna [6], the performance properties of the Koch fractal monopole are typically compared to the properties of a non-fractal Euclidean antenna of the same overall size or height. This discussion does not compare the impedance properties of the Koch fractal monopole to antennas with non-fractal wire geometries that also have the same total wire length or the same resonant frequency. Without these additional comparisons, the relationship between the antenna's impedance characteristics and the antenna's height, total wire length and fractal geometry is not evident.

Here, the impedance properties of the Koch fractal monopole antenna are examined as a function of frequency. In all cases, the Koch fractal monopole's height is held the same as that of the straight Euclidean monopole antenna. As a result, the Koch fractal monopole's total wire length must increase with increasing fractal iteration. The Koch fractal monopole is shown to exhibit a lower resonant frequency and compressed resonance behavior relative to that of the Euclidean monopole. Two non-fractal bent wire antenna geometries are then considered: the simple meander line and the normal mode helix antenna. These antennas are first made to have the same overall height and same total wire length as the Koch fractal monopoles and it is demonstrated that these antennas exhibit similar behavior. With increasing total wire length, these antennas exhibit lower resonant frequency and compressed resonance behavior. Finally, when these antennas are made to be resonant at the same frequency as the Koch fractal monopole, they exhibit virtually the same impedance and resonance characteristics as the Koch fractal. It is also demonstrated that these antennas are more effective at lowering resonant frequency than the self-similar Koch fractal monopole.

From this analysis and performance comparison, it is demonstrated that the antenna volume and total wire length are the significant factors related to the antenna exhibiting lower resonant frequency behavior.

2. The Koch Fractal Monopole Antenna

The geometry configurations of the self-similar Koch fractal monopole antennas are depicted in Figure 1 for fractal iterations 0 through 4, designated K0 through K4, respectively. The reference antenna for comparison purposes is the straight Euclidean monopole antenna, designated as fractal iteration K0. The progressive self-similar fractal

nature of these monopoles and the associated increase in total wire length is evident for each increase in fractal iteration. These antennas were modeled with NEC 4 using EZNEC Pro [7]. In each case, the wire diameter was set at 0.2 mm and the antennas were modeled over an infinite, perfectly conducting ground plane. Additionally, the copper wire loss option was selected. The K0 Euclidean monopole was modeled using 31 wire segments, while the K1, K2, K3 and K4 monopoles were modeled with 44, 80, 192, and 256 wire segments, respectively.

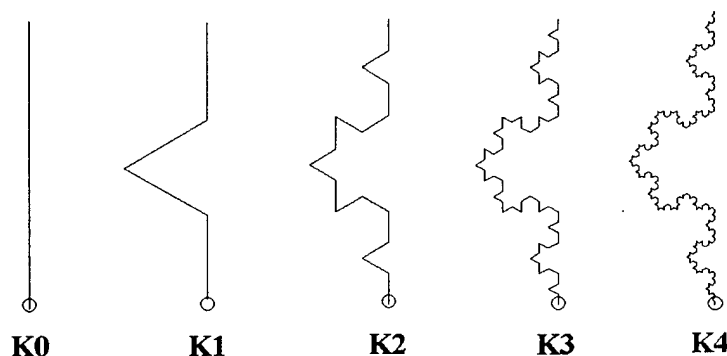


Figure 1. Geometry of Euclidean (K0) and Koch Fractal Monopole Antennas.

The Koch fractal monopole antennas considered are those having the same total height as the K0 Euclidean monopole antenna. Since the total monopole height is the same in each case, the total wire length in the antenna must increase in order to maintain the fractal geometry. In this case, the K0 Euclidean monopole has a height of 6 cm. The height of the K1 through K4 fractal monopoles is also 6 cm, however, the wire length increases as follows: K1: 8 cm, K2: 10.67 cm, K3: 14.22 cm and K4: 18.96 cm.

The feed point impedance properties of these antennas from 200 MHz to 3000 MHz are presented in Figure 2. With each increase in fractal iteration, the resonant frequency of the Koch fractal monopole decreases relative to that of the K0 Euclidean monopole. Additionally, the fractal antennas exhibit resonance compression behavior as their resonant frequencies are more closely spaced and they exhibit more resonant frequencies over a given frequency bandwidth. A graph of the Koch monopole's resonant frequency as a function of increasing fractal iteration is presented in Figure 3. The Koch monopole's resonant frequency is compared to the resonant frequency of a straight Euclidean K0 monopole having the same total wire length as the Koch fractal. It is evident, that for the same total wire length, the Koch fractal is less effective in the lowering of resonant frequency than the Euclidean monopole. Resonant frequency information for the Koch fractal monopole is also detailed in Table 1. It is significant to also note that with decreasing wire diameter, the resonant frequency of the Koch fractal monopole will decrease, improving its effectiveness in lowering of resonant frequency.

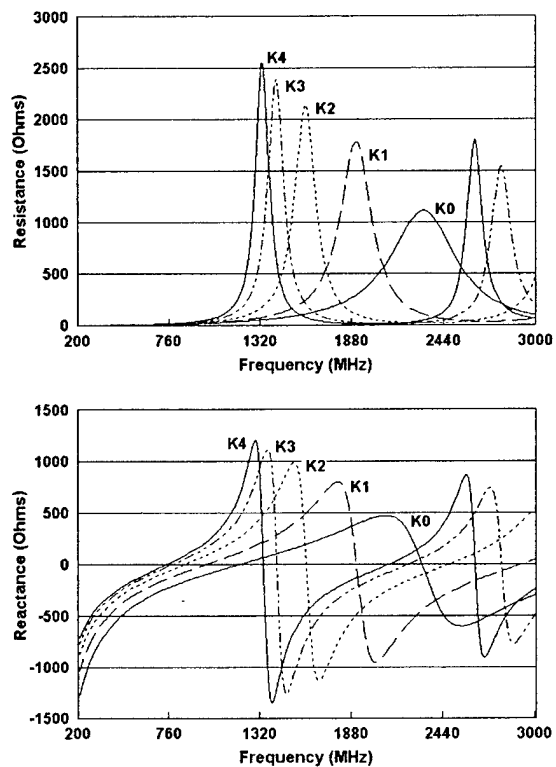


Figure 2. Impedance Properties of the Koch Fractal Monopole Antennas.

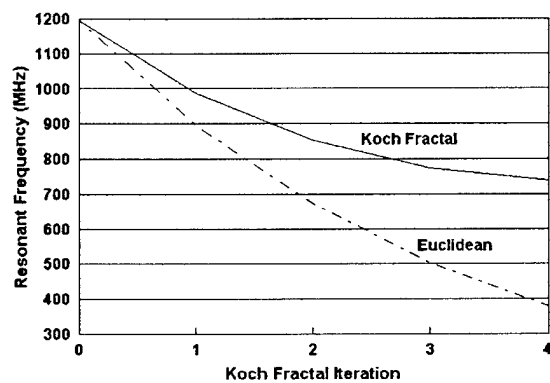


Figure 3. Resonant Frequency Comparison for the Koch Fractal Monopole and the Euclidean Antenna with the Same Total Wire Length.

Antenna	Antenna Height (cm)	Total Wire Length (cm)	Resonant Frequency (MHz)	Resonant Frequency K0 Monopole of same Total Wire Length (MHz)
Euclidean (K0)	6	6	1195.2	1195.2
K1	6	8	987.2	898.5
K2	6	10.67	853.2	675.2
K3	6	14.22	777.8	507.4
K4	6	18.96	740	381.2

Table 1. Resonant Frequency Comparison of the Koch Fractal Monopole and the Euclidean Monopole.

3. The Meander Line Antenna

The performance properties of fractal antennas have primarily been attributed to the antenna's fractal geometry. The physical parameter seemingly neglected in the analysis of these antennas is the fact that the antenna's total wire length increases dramatically with increasing fractal iteration. It is well known that increasing the total wire length in a fixed size antenna reduces the antenna's resonant frequencies. This lowering of resonant frequencies results in resonance compression over any fixed frequency spectrum. As a result, it is reasonable to conclude that an antenna of any geometry, having a fixed size and increased total wire length will exhibit resonance compression behavior. This behavior is primarily a function of the increase in total wire length and the antenna's geometry, fractal or otherwise, is a secondary factor. However, since the antenna geometry is a factor in determining antenna performance, antennas of the same overall size and total wire length will have differing resonant frequencies. This will especially be true as the operating frequency increases and the antenna becomes larger with respect to the operating wavelength. With increasing frequency, the fractal antenna will behave significantly different than antennas of other geometries.

To evaluate these points further, several simple meander line geometry antennas are considered as depicted in Figure 4. These meander line antennas, designated M1, M2, M3 and M4 have the same height and total wire length as the Koch fractal monopole antennas, K1 through K4, respectively. The feedpoint impedance properties of these meander line antennas are illustrated in Figure 5 and it is evident that these antennas exhibit lower resonant frequencies and resonance compression behavior similar to that exhibited by the Koch fractal monopole antennas.

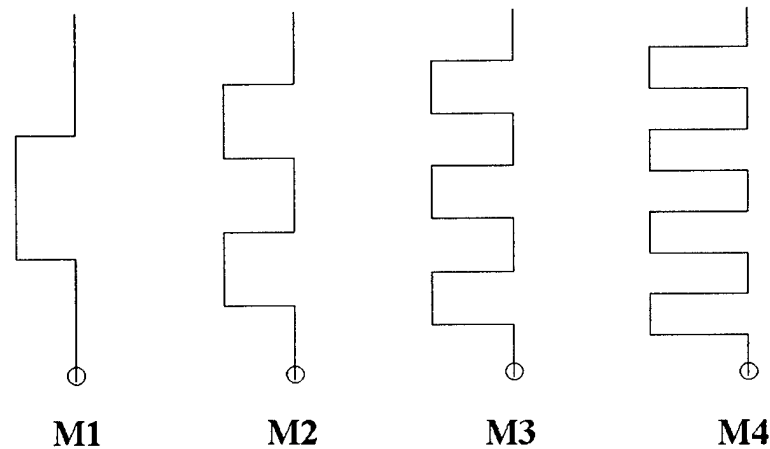


Figure 4. Meander Line Monopole Antenna Geometry.

An interesting point to note is that with increasing fractal and meander line iteration, the simple meander line antennas exhibit a lower resonant frequency than the Koch fractal monopole. The resonant frequency of these antennas as a function of increasing meander line iteration is illustrated in Figure 6. Comparison is made between these resonant frequencies and those of the Koch fractals and the Euclidean monopole (K0) having the same total wire length. With increasing fractal iteration, the self-similar fractal antenna is less effective at lowering resonant frequency than the simple meander line structure. This is primarily a result of the fact that in the self-similar fractal antenna, the increase in total wire length occurs in much smaller increments over the entire antenna structure. This has the effect of compressing the increased total wire length into a smaller effective (electrical) perimeter relative to the operating wavelength. While a disadvantage in the lowering of resonant frequency, it is a necessary factor in the Koch fractals exhibiting multi-band behavior with increasing frequency. Although the meander line antennas exhibit lower resonant frequencies and resonance compression behavior, they will not exhibit multi-band behavior in the same manner as fractal antennas.

Since the simple meander line antennas exhibit a lower resonant frequency than the Koch fractal monopole of the same size and total wire length, it follows that the meander line antennas will operate at the same resonant frequency as the Koch fractals, with less wire. This is validated with meander line configurations having the following shortened wire lengths: M2: 10.216 cm, M3: 12.042 cm and M4: 13.424 cm. The total height of each of the meander line antennas was not shortened and remained at 6 cm. A comparison of the impedance properties of the modified meander line antennas and the Koch fractal antennas is presented in Figure 7. It is evident that when modified to have the same resonant frequency as the Koch fractal antennas, the meander line and Koch fractal

antennas exhibit virtually identical impedance characteristics, even though their geometries are remarkably different.

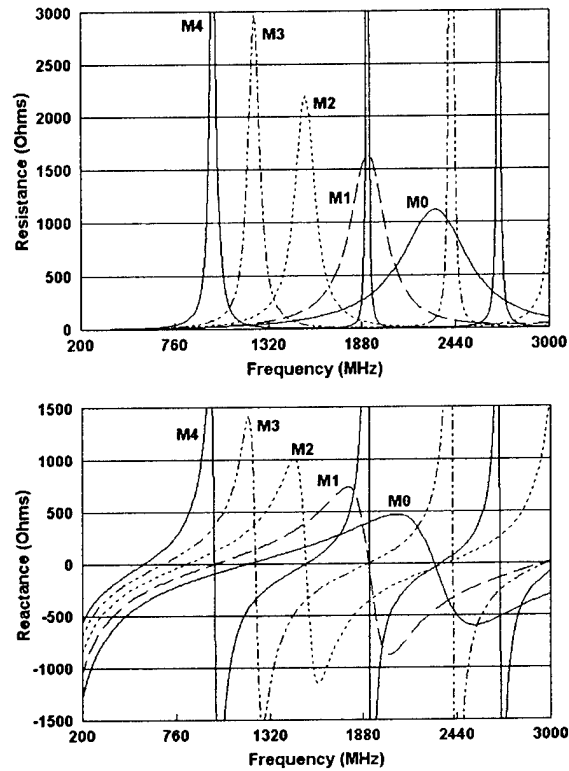


Figure 5. Impedance Properties of the Meander Line Monopole Antennas.

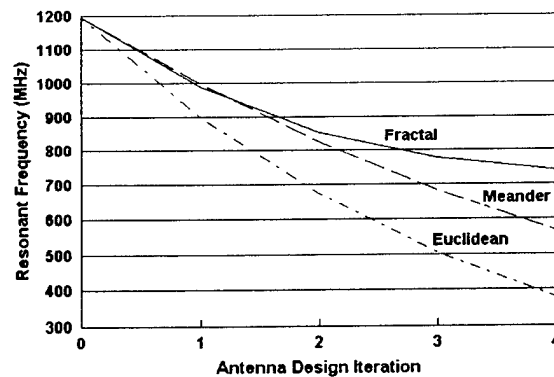


Figure 6. Resonant Frequency Comparison between the Koch Fractal and Meander Line Monopoles as a Function of Increased Total Wire Length.

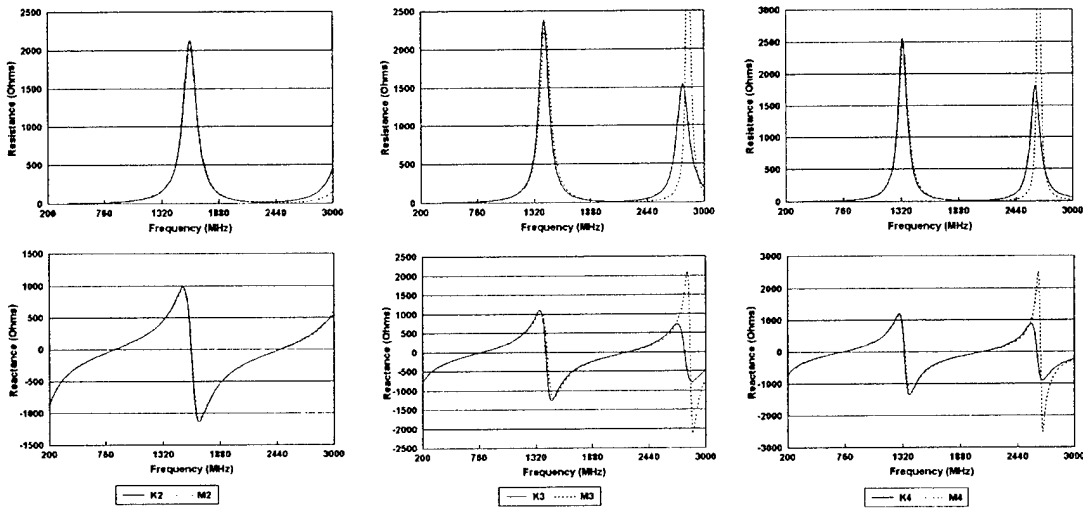


Figure 7. Impedance Properties of the Modified Meander Line Antennas and the Koch Fractal Antennas.

4. The Normal Mode Helix Antenna

In the previous section, it was demonstrated that simple meander line antennas exhibit the same behavior as the Koch fractal monopoles as the meander line and fractal iteration increases. In this section, a similar comparison is made between the Koch fractal monopole and the normal mode helix antenna commonly used where space constraints limit the use of full size, resonant Euclidean antennas.

The normal mode helix antennas considered here have the same height (6 cm) and resonant frequency as the Koch fractal monopole. The normal mode helix antennas have an overall diameter of approximately 1 cm. The resonant frequency of the helix was adjusted to match that of the Koch fractal monopole by adjusting the number of helical turns. Depictions of the normal mode helix antennas are presented in Figure 8. The resonant frequencies of the H2, H3 and H4 helices match those of the K2, K3 and K4 Koch fractal monopoles, respectively. The H2, H3 and H4 helical antennas have $2\frac{1}{4}$, $2\frac{3}{4}$, and $3\frac{1}{8}$ turns, respectively. As with the meander line antennas, the normal mode helices have less wire length than the Koch fractal monopoles. The total wire length in each antenna is: H2: 9.7 cm, H3: 11.03 cm and H4: 11.86 cm.

The impedance properties of the normal mode helix antennas and the Koch fractal monopole antennas, both resonant at the same frequency are presented in Figure 9. Similar to the meander line antennas, the normal mode helix and the Koch fractal

monopoles exhibit virtually identical impedance characteristics, though their geometries are significantly different.

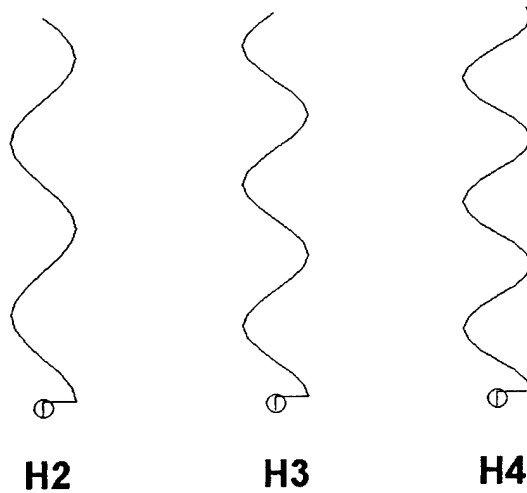


Figure 8. Geometry Configuration of the Normal Mode Helix Antennas.

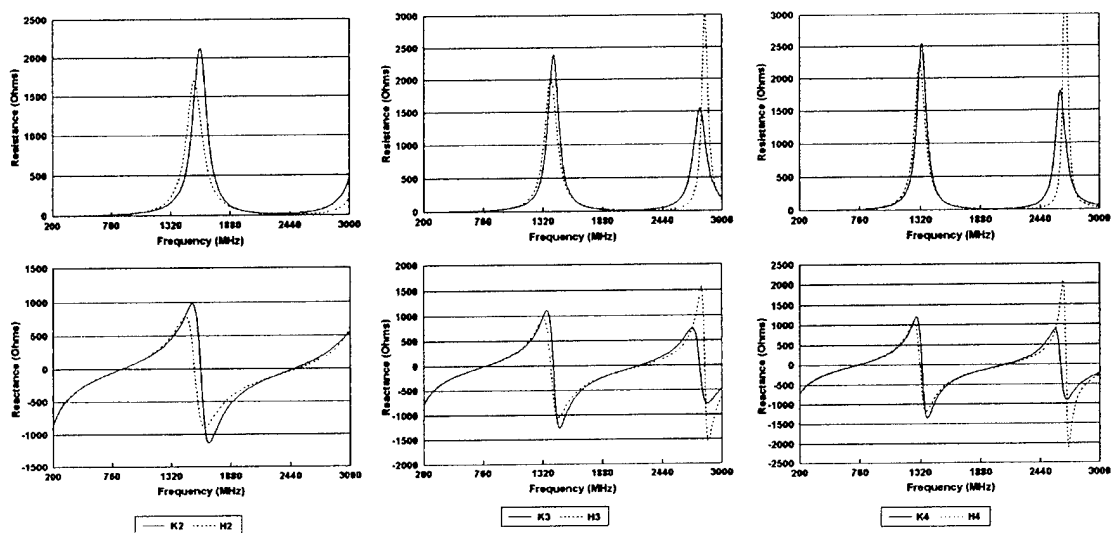


Figure 9. Impedance Properties of the Normal Mode Helix Antennas and the Koch Fractal Monopole Antennas.

5. Measured Results

In order to validate the results of the NEC numerical modeling, the impedance properties of the K0, K3, M3 and H3 antenna configurations were measured. In the first instance, each of the antennas had the same total height and the K3, M3 and H3 antennas had the same total wire length. In order to facilitate ease of fabrication of these antennas, an antenna height of 15.24 cm (6 in) was selected, requiring that the modeled frequency range of 200 to 3000 MHz be scaled to approximately 78.74 to 1181.1 MHz. The measured data for these antenna configurations is presented in Figure 10. From the data presented in Figure 10, it is evident that the modeling results are validated. As previously discussed, the meander line and normal mode helix antennas exhibit a lower resonant frequency than the Koch fractal of the same height and total wire length.

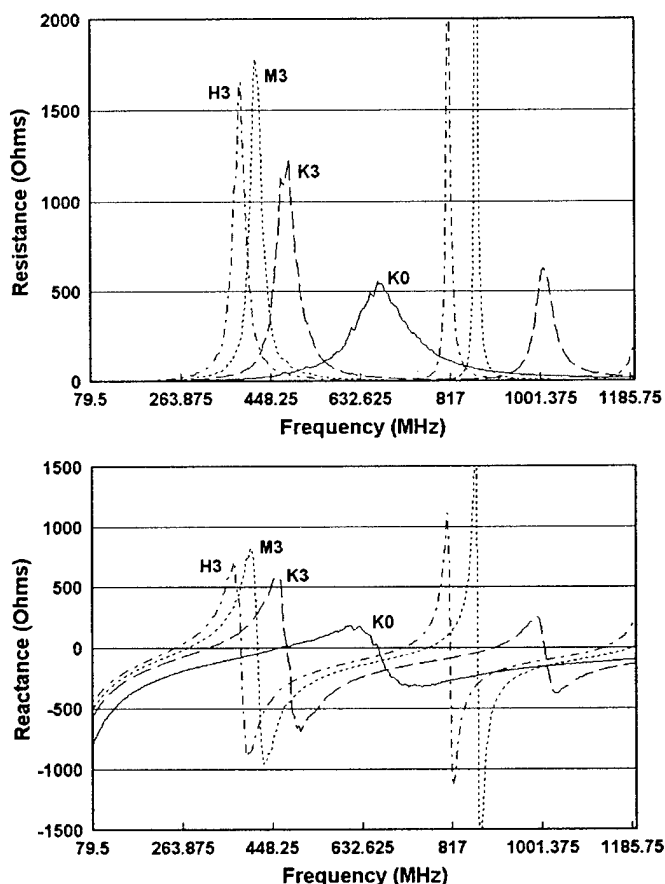


Figure 10. Measured Impedance Data of the K0 Euclidean Monopole and the K3, M3 and H3 antennas having the same height and the same total wire length.

The second set of antennas fabricated were the M3 and H3 configurations designed to be resonant at the same frequency as the K3 Koch fractal monopole. The impedance properties of these antennas compared to the K3 Koch fractal and the K0 Euclidean antenna are presented in Figure 11. From the data presented in Figure 11, it is evident that the modeled results are validated. In this case, when the M3 and the H3 are made to be resonant at the same frequency as the Koch fractal, they exhibit virtually the same impedance characteristics. As stated previously, the impedance characteristics will diverge with increasing frequency as the operating wavelength decreases and the antennas become electrically larger. As this occurs, differences in antenna geometry start to significantly differentiate antenna performance. At very high frequencies, all of the antennas will exhibit multi-resonance behavior but the Koch fractal will exhibit multi-band performance which is characterized by regions of low SWR with respect to a pre-defined impedance, typically 50 ohms.

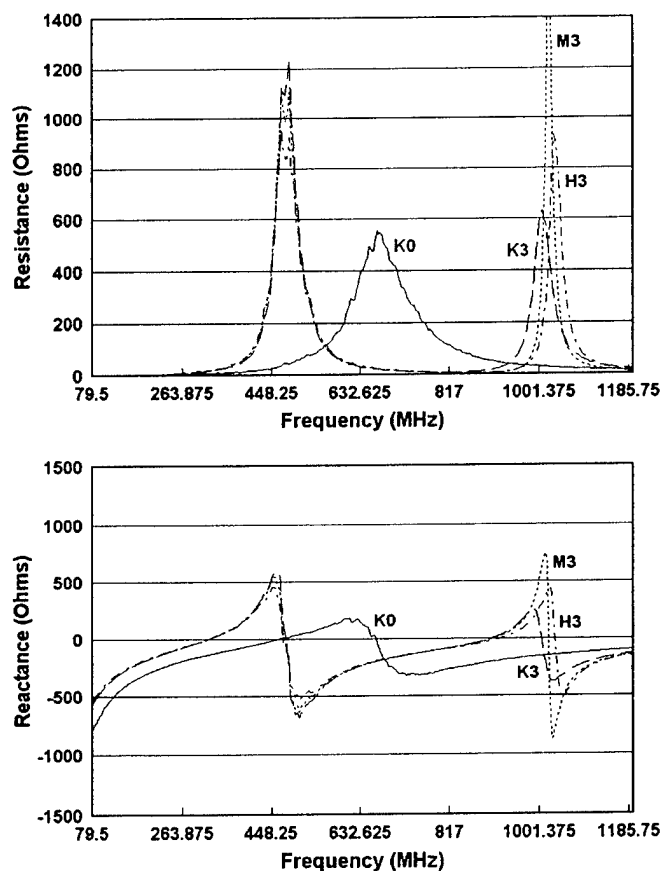


Figure 11. Measured Impedance Data of the K0 Euclidean Monopole and the K3, M3 and H3 antennas designed to be resonant at the same frequency.

6. Summary

The properties and performance characteristics of the Koch fractal antenna were presented and discussed. Although fractal antennas are known to exhibit a lower resonant frequency than a Euclidean antenna of the same size, it was demonstrated that simple meander line and normal mode helix antennas exhibit the same behavior. In fact, any linear wire antenna of fixed overall size and of any geometry will exhibit similar behavior with an increase in total wire length. When the length of the meander line antenna and normal mode helix antennas are adjusted to be resonant at the same frequency as the Koch fractal, all of the antennas exhibit virtually identical impedance characteristics even though their geometries are quite different.

REFERENCES

- [1] Nathan Cohen, "Fractal Antennas Part 1," *Communications Quarterly*, pp. 7 – 22, Summer 1995.
- [2] Nathan Cohen, "Fractal Antennas Part 2," *Communications Quarterly*, pp. 53 - 65, Summer 1996.
- [3] Nathan Cohen, "Fractal Loops and the Small Loop Approximation," *Communications Quarterly*, pp. 77 – 81, Winter 1996.
- [4] Carles Puente-Baliarda, J. Romeu, R. Pous and A. Cardama, "On the Behavior of the Sierpinski Multiband Fractal Antenna," *IEEE Transactions on Antennas and Propagation*, Vol. 46, pp. 517 – 524, April 1998.
- [5] Carles Puente-Baliarda, C. Borau, M. Rodero and J. Robert, "An Iterative Model for Fractal Antennas: Application to the Sierpinski Gasket Antenna," *IEEE Transactions on Antennas and Propagation*, Vol. 48, pp. 713 – 719, May 2000.
- [6] Carles Puente-Baliarda, J. Romeu and A. Cardama, "The Koch Monopole: A Small Fractal Antenna," *IEEE Transactions on Antennas and Propagation*, Vol. 48, pp. 1773 – 1781, November 2000.
- [7] EZNEC/4 Antenna Modeling Software, Roy Lewallen, P.E., <http://www.eznec.com>.

ON THE PERFORMANCE TRADE-OFFS ASSOCIATED WITH FRACTAL ANTENNA DESIGNS

Steven R. Best
Cushcraft Corporation
48 Perimeter Road
Manchester, NH 03103

Abstract: Fractal antennas have been shown to exhibit lower resonant frequencies than Euclidean antennas of the same overall size. Therefore, fractal antennas with a reduced overall physical size can be made resonant at the same frequency as the Euclidean antenna. This size reduction capability is advantageous in the design of antennas for wireless devices where space constraints can limit the design and use of Euclidean antennas. The performance properties of fractal antennas having the same size as a Euclidean antenna have been described in the literature. However, little comparison of relative performance has been made where the fractal and Euclidean antennas are designed to be resonant at the same frequency. As a result, the performance trade-offs associated with using fractal geometries in reduced size antenna designs have generally been understated. Here, the performance properties of several Koch fractal monopole antennas are examined and compared to the properties of a non-fractal Euclidean monopole antenna. These performance properties are examined for the case where all of the antennas are made to be resonant at the same frequency. It is demonstrated that with increasing fractal iteration and size reduction, the fractal antennas exhibit a lower resonant feed point resistance, less bandwidth and lower efficiency. Finally, the resonant performance properties of the Koch fractal monopole are compared to the resonant properties of simple meander line antennas of the same size, and it is demonstrated that the fractal antenna offers little or no inherent performance advantage.

1. Introduction

It has been previously demonstrated that when a fractal antenna is of the same overall size as a Euclidean antenna, the fractal antenna has a lower resonant frequency [1] – [6]. Therefore, when the fractal antenna and the Euclidean antenna are designed to be resonant at the same frequency, the fractal antenna will be physically smaller. However, with increasing fractal iteration and overall size reduction, the fractal antenna will have a corresponding increase in total wire length.

In the design of many wireless devices, space constraints limit the design and use of Euclidean antennas and alternate, reduced size antenna designs must be considered. The use of fractal geometries provides a convenient method of size reduction in antenna design. However, an important aspect of using fractal geometries not sufficiently covered in the previous literature, is understanding the performance trade-offs associated with reduced size fractal antenna designs. In order to understand these performance trade-offs, the performance of the reduced size fractal antenna should be compared to the full size resonant Euclidean antenna it replaces.

Here, the performance properties of the Koch fractal monopole antenna [6] are examined at resonance and as a function of frequency. In all cases, the Koch fractal monopoles are made to be resonant at the same frequency. The performance properties of the Koch fractal monopoles are then compared to those of the resonant Euclidean antenna as a function of increasing fractal iteration. The performance trade-offs associated with the Koch fractal antennas are considered in terms of the antenna's resonant resistance, bandwidth and radiation efficiency.

Additionally, the simple meander line antenna is considered as a reduced size antenna. In each case, the meander line antenna has the same overall height and is made to be resonant at the same frequency as the Koch fractal monopole. The relative performance of these different antenna designs is also compared in terms of the antenna's resonant resistance, bandwidth and radiation efficiency.

2. The Koch Fractal Monopole Antenna

The geometry configurations of the self-similar Koch fractal monopole antennas are depicted in Figure 1 for fractal iterations 0 through 4, designated as K0 through K4, respectively. The reference antenna for comparison purposes is the straight Euclidean monopole antenna, designated as fractal iteration K0. These antennas were modeled with NEC 4 using EZNEC Pro [7]. In each case, the wire diameter was set at 0.2 mm and the antennas were modeled over an infinite, perfectly conducting ground plane. The copper wire loss option was selected in EZNEC so that the radiation efficiency of the antennas could be determined as a function of increasing fractal iteration. The K0 Euclidean monopole was modeled using 31 wire segments, while the K1, K2, K3 and K4 monopoles were modeled with 44, 80, 192, and 256 wire segments, respectively.

The Koch fractal monopole antennas considered have the same primary resonant frequency as the K0 Euclidean monopole antenna. In this case, the K0 Euclidean monopole height is set at 25.17 cm and its modeled resonant frequency is 287.6 MHz. Since the resonant frequency of the Koch fractal monopoles is the same as that of the Euclidean monopole, the Koch fractals will have decreasing overall size and increasing total wire length with increasing fractal iteration.

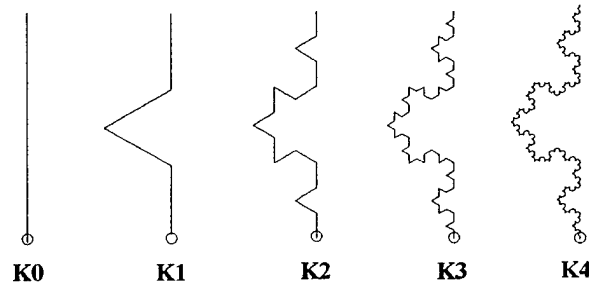


Figure 1. Geometry of Euclidean (K0) and Koch Fractal Monopole Antennas.

The feed point impedance properties of these antennas from 50 MHz to 1000 MHz are presented in Figure 2. Although the overall size, total wire length and geometry are remarkably different with each fractal iteration, all of the antennas exhibit similar behavior over this frequency band. The performance of these antennas is virtually identical at frequencies below the primary resonance where the antennas are relatively small with respect to the operating wavelength. As the operating frequency increases, and the antennas become larger relative to the wavelength, the performance properties of the antennas diverge.

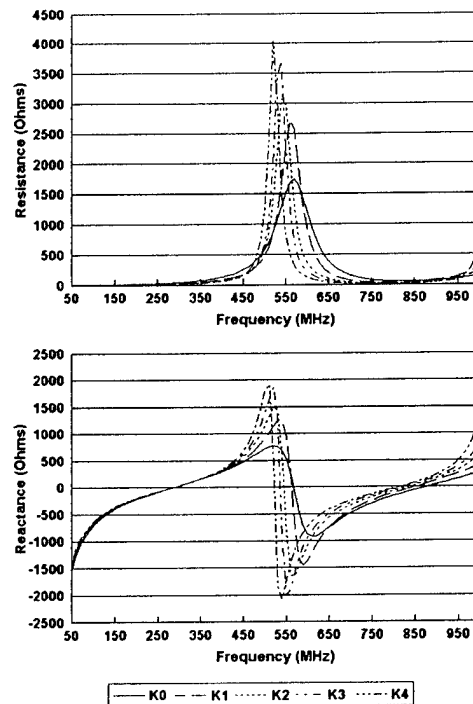


Figure 2. Impedance Properties of the Koch Fractal Monopole Antennas.

A performance comparison of these antennas is presented in Table 1. Performance information presented in Table 1 includes the antenna's overall height, total wire length, resonant resistance, inherent bandwidth and radiation efficiency. The inherent bandwidth is defined by the 2:1 SWR with respect to the antenna's resonant resistance. With increasing fractal iteration, the antennas have a smaller overall size and increasing total wire length. With increasing fractal iteration, the antennas exhibit a lower resonant resistance, less bandwidth and lower radiation efficiency. These are typical performance trade-offs associated with reduced size antenna designs.

Antenna	Antenna Height (cm)	Total Wire Length (cm)	Resonant Resistance (Ohms)	Bandwidth (%)	Radiation Efficiency (%)
Euclidean (K0)	25.17	25.17	36.9	7.8	97.1
K1	20.4	27.2	24	5.2	95.7
K2	17.26	30.67	17.9	3.9	93.4
K3	15.24	36.12	14.4	3.1	90.6
K4	14.22	44.93	13	2.8	87

Table 1. Performance Comparison of the Koch Fractal Monopoles Resonant at the Same Frequency.

3. The Meander Line Antenna

In addition to the use of fractal geometries, other reduced size antenna designs have been used for many years in applications where space constraints limit the use of full size Euclidean antennas. These designs typically involve some form of bent wire geometry where an increase in total wire length is compressed into a reduced physical size. Compressing a fixed wire length into a smaller physical size increases the antenna's resonant frequency. Increasing the total wire length in a fixed size decreases the antenna's resonant frequency. Therefore, with an appropriate decrease in size and increase in total wire length, an antenna of bent wire geometry can be designed to maintain a fixed resonant frequency. In addition to fractal antennas, simple meander line geometries can be used in reduced size applications. Here, several simple meander line geometries are considered and designed to have the same resonant frequency as the K0 Euclidean antenna discussed in the previous section. The performance of these meander line antennas is compared to the performance of the Koch fractals.

The simple meander line antennas considered here are depicted in Figure 3. These meander line antennas, designated M1, M2, M3 and M4 have the same height and resonant frequency as the Koch fractal monopole antennas, K1 through K4, respectively.

The feedpoint impedance properties of K0 Euclidean monopole (M0) and the meander line antennas are illustrated in Figure 4. It is evident that these antennas exhibit behavior similar to that exhibited by the Koch fractal monopole antennas.

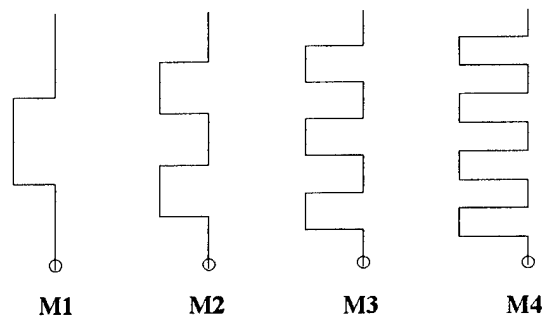


Figure 3. Meander Line Monopole Antenna Geometry.

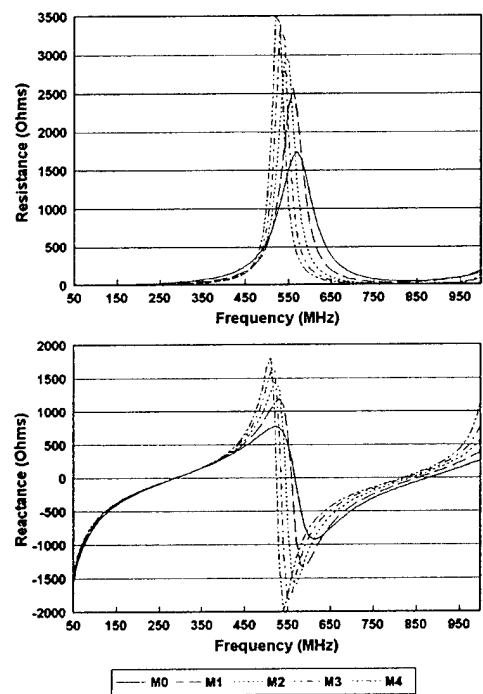


Figure 4. Impedance Properties of the Meander Line Monopole Antennas.

A performance comparison of these antennas is presented in Table 2. As in the case of the Koch fractal monopoles, with increasing meander line iteration, these antennas have a smaller overall size and increasing total wire length. However, it is interesting to note that the simple meander line geometries do not require as much wire as the Koch fractals to maintain the same resonant frequency in the same height. This is a result of the Koch fractal's self-similar geometry restricting the total wire length increase into smaller segments with increasing fractal iteration. Increasing the total wire length in smaller increments or segments is less effective than increasing the wire length in larger segments. As with the Koch fractals, with increasing meander iteration, the antennas exhibit a lower resonant resistance, less bandwidth and lower radiation efficiency. It is also significant to note that the performance of these antennas is virtually identical to the performance of the Koch fractals.

Antenna	Antenna Height (cm)	Total Wire Length (cm)	Resonant Resistance (Ohms)	Bandwidth (%)	Radiation Efficiency (%)
Euclidean (K0)	25.17	25.17	36.9	7.8	97.1
M1	20.4	27.5	24.2	5.2	95.9
M2	17.26	29.66	18.1	3.9	93.6
M3	15.24	31.77	14.7	3.5	91.4
M4	14.22	38.8	13.2	4.6	90

Table 2. Performance Comparison of the Meander Line Monopoles Resonant at the Same Frequency.

4. Measured Results

In order to validate the results of the NEC numerical modeling, the impedance properties of the K0, K3, and M3 antenna configurations were measured where each antenna was fabricated to be resonant at the same frequency. The K3 and M3 monopole antennas had an overall total height of 15.24 cm and were both resonant at 316.48 MHz, which is different than the modeled resonant frequency of 287.6 MHz. This difference in resonant frequency is attributed to the difference in wire diameter used in the modeled (0.2 mm) and fabricated (0.9 mm x 0.51 mm strip) antennas. The K0 monopole resonant at 316.48 MHz had a height of approximately 22.48 cm. The physical wire length in the K3 monopole was 36.12 cm while the physical wire length in the M3 monopole was approximately 30 cm.

The measured impedance properties of these antennas from 50 MHz to 1000 MHz are presented in Figure 5. The measured behavior exhibited by these antennas is consistent

with that predicted by NEC. The measured resonant resistance of these antennas was as follows: K0: 37 ohms; K3: 17.4 ohms; and M3: 18.5 ohms.

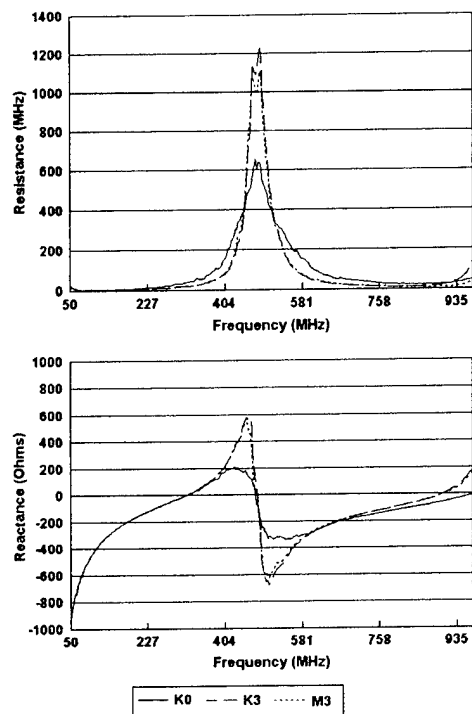


Figure 5. Measured Impedance Properties of the K0, K3 and M3 Antenna Configurations.

5. Summary

The properties and performance characteristics of the Koch fractal monopole antenna were presented and discussed as they relate to the antennas being used in reduced size applications. The performance trade-offs associated with the use of the Koch fractal monopole were considered in terms of the antenna's resonant resistance, bandwidth and radiation efficiency. It was demonstrated that with increasing fractal iteration and size reduction, the Koch fractal monopole exhibits lower resonant resistance, less bandwidth and lower efficiency. Additionally, the performance properties of several meander line antennas, designed to be resonant at the same frequency as the Koch monopoles, were presented and it was demonstrated that they exhibited virtually identical performance. In fact, the meander line antennas exhibited the same performance with less overall total wire length. In reduced size applications, the Koch fractal offers no inherent performance advantage over other commonly used geometries.

REFERENCES

- [1] Nathan Cohen, "Fractal Antennas Part 1," *Communications Quarterly*, pp. 7 – 22, Summer 1995.
- [2] Nathan Cohen, "Fractal Antennas Part 2," *Communications Quarterly*, pp. 53 - 65, Summer 1996.
- [3] Nathan Cohen, "Fractal Loops and the Small Loop Approximation," *Communications Quarterly*, pp. 77 – 81, Winter 1996.
- [4] Carles Puente-Baliarda, J. Romeu, R. Pous and A. Cardama, "On the Behavior of the Sierpinski Multiband Fractal Antenna," *IEEE Transactions on Antennas and Propagation*, Vol. 46, pp. 517 – 524, April 1998.
- [5] Carles Puente-Baliarda, C. Borau, M. Rodero and J. Robert, "An Iterative Model for Fractal Antennas: Application to the Sierpinski Gasket Antenna," *IEEE Transactions on Antennas and Propagation*, Vol. 48, pp. 713 – 719, May 2000.
- [6] Carles Puente-Baliarda, J. Romeu and A. Cardama, "The Koch Monopole: A Small Fractal Antenna," *IEEE Transactions on Antennas and Propagation*, Vol. 48, pp. 1773 – 1781, November 2000.
- [7] EZNEC/4 Antenna Modeling Software, Roy Lewallen, P.E., <http://www.eznec.com>.

Printed Circuit Board Implementation of Log-periodic Parasitic Monopole Arrays

P.G. Ingerson¹, S.C. Kuo², P.E. Mayes³, C.C. Liu¹

Abstract

This paper briefly reviews the analysis technique previously published by the authors [Ref 1] which has proven successful for analysis of log-periodic dipole and monopole arrays which include parasitic elements between the driven elements [Ref 2]. The analysis model is an extension of the analysis technique developed by Carrel for the log-periodic dipole array (LPDA) [Ref 3].

The authors have shown that in addition to the coupling between all the radiating elements as developed by Carrel for the analysis of LPDA (where all the elements are connected to the feedline), that the analysis model for LP scaled antenna arrays with parasitic elements requires the inclusion of the coupling between the feed transmission line and the parasitic elements to achieve proper operation. This coupling ideally scales from cell-to-cell by increasing the parasitic element to transmission line separation as the cells increase in size away from the feed point.

This paper reviews the importance of this transmission line coupling to the proper operation of the antenna array and how to compensate the antenna's parameters to allow implementation on constant thickness printed circuit board.

The paper also briefly covers the group delay properties of the LP antennas showing the group delay is a simple function of only the antenna scale factor τ .

1 Antenna Systems Center, TRW, Redondo Beach, CA.

2 California Electromagnetics, Mountain View, CA

3 Center for Computational Electromagnetics, University of Illinois, Urbana, IL

Printed Circuit Board Implementation of Log-periodic Parasitic Monopole Arrays

P.G. Ingerson , S.C. Kuo , P.E. Mayes , C.C. Liu

1.0 Introduction

The purpose of this paper is to describe the method of implementing log-periodic parasitic monopole arrays (LPPMA) on printed circuit boards (PCB). The LPPMA is a compact means of implementing LP scaled monopole arrays which can then be used as building blocks for several types of wideband feeds. In a previous paper presented at this Antenna Applications Symposium [Ref 1], the authors showed implementations of the LPPMA on a ground plane as a single array as well as implementations of 3, 4 and 6 arrays fed against a central boom. In these configurations, it is usual to refer to the arrays as arms or wings. For 3 and 4 arms, the central boom diameter is small in terms of wavelengths, whereas a larger central cone (or pyramid) is used for 6 or more arms. The larger diameter central cone (0.3 to 0.5 wavelengths) allows the antenna to support dual polarized sum and difference modes for wideband tracking and angle-of-arrival applications.

The conventional log-periodic dipole array (LPDA) (as will be discussed) lacks feedline symmetry and can not be implemented as a monopole array fed against a ground plane. The introduction of parasitic elements into the LP dipole array by Barbano [Ref 2] allows a monopole implementation.

In the analysis model developed by Carrel for the analysis of the LPDA [Ref 3], all the elements are connected to the feedline. The model includes all the mutual coupling between the radiating elements, but does not include coupling between the elements and the feedline. This analysis model was highly successful and has shown excellent correlation with measured LPDA performance.

The authors have shown that in addition to the coupling between radiating elements, LP scaled arrays with parasitic elements require the inclusion of the coupling between the feed transmission line and the parasitic elements to achieve proper operation. This coupling ideally scales from cell-to-cell by increasing the parasitic element to transmission line separation as the cells increase in size away from the feed point.

In earlier applications, the LPPMA wings have been built using freestanding elements where the separation between the parasitic elements and a biconical transmission line used as the feedline for the driven elements was increased by the scale factor cell-to-cell. This increasing separation properly scaled the coupling of the parasitic elements to the transmission line required for wideband operation.

These arrays have been build with well over 18:1 bandwidths with upper frequencies of 18 GHz.

In this paper, we will review the importance of this transmission line coupling to the proper operation of the antenna array and how to compensate the antenna's parameters to allow implementation on constant thickness printed circuit board and achieve the same performance as the freestanding implementation.

2.0 Background

2.1 Log-periodic dipole arrays

The log-periodic dipole array (LPDA) has been one of the most successful of the numerous log-periodic structures that have been investigated.

Log-periodic antennas are generally composed of cascaded cells, each of which is related in dimensions to its nearest neighbor by a scale factor (usually called τ) that remains constant for pairs of cells between the largest and the smallest. Such a structure is said to satisfy a self-scaling principle in that successive scalings by τ lead to the same geometry except at the ends.

Log-periodic antennas are usually provided with a feedpoint at the end of the smallest cell at which point connection is made to a cable leading to a transmitter or receiver.

Consider the transmitting case. At some mid-band frequency, energy that is introduced at the feedpoint propagates along the structure until it encounters the "active region" wherein it radiates into the surrounding space. The radiated fields usually propagate in the direction back towards the feedpoint and thus suffer minimal scattering from the encountered elements since they are relatively small compared to the wavelength.

Besides requiring an array of linear dipoles with lengths and separations that satisfied the scaling principle, the LPDA needs properly phased excitation of the dipoles in the active region. This is accomplished by connecting the inner ends of the dipoles to a two-wire transmission line and either (a) transposing the conductors of the line in the space between each pair of adjacent dipoles, or (b) connecting the corresponding inner ends of adjacent dipoles to different conductors of a parallel pair as shown in Figure 2.1. In the latter case, the feed conductors can remain straight and parallel and are often used to provide mechanical support for the dipoles.

Soon after the development of the LPDA, it was recognized that a similar array of monopoles would have numerous applications. However, because the required active region phasing of monopole elements could not be achieved in the manner of the LPDA, the development of a successful log-periodic monopole array was some time in coming.

2.2 LP Monopole Arrays Using Delay Lines

The effect of the feedline transposition or alternating connection of dipole halves to different feedline conductors in an LPDA is to change the phase between adjacent dipoles by 180 degrees. Another way to add 180 degrees to the phase shift along a feedline is to increase the length of the line by one-half wavelength. Hence, some early attempts to feed log-periodic arrays of thin monopole elements involved the insertion of extra length of feedline between each pair of adjacent monopoles. However, this procedure was not immediately successful and the first LPMA's with excess length of feedline displayed poor input impedance. The cause was found to be a "stop region", an area of high reflection situated between the feedpoint and the active region. This problem was later shown by Ingerson and Mayes [4] to be associated with the structural stopband in periodic structures when the phasing between loading elements is near $1/2\lambda$ or multiples of $1/2\lambda$ and which could easily be overcome by changing or modulating the feedline impedance.

2.3 LP Parasitic Dipole Array

In 1965, N. Barbano's log-periodic dipole array with parasitic elements [2,5], shown in Figure 2.2 was introduced. On this antenna, the active (or driven) dipoles are connected to the feeder and alternated with parasitic (not physically connected to the feeder) dipoles. This antenna is excited using a conventional two-parallel wire balanced transmission line. The phase reversal of the excitation currents of the adjacent dipoles is accomplished by the presence of the parasitic dipoles. The resulting log-periodic parasitic dipole array (LPPDA) has a plane of symmetry centered between the parallel feedline conductors. Hence, it is possible to take one-half of this structure, the half on one side of the plane of symmetry, and feed it against ground to produce an LP parasitic monopole array (LPPMA). In the early literature the success of the LPPDA was attributed to only mutual coupling between the driven and parasitic dipoles. However, it has been shown by the authors [Ref 1] that the most important contribution to successful operation is made by proximity coupling between the feedline and the parasitic dipoles.

The LPPMA has a strong advantage over the delay line implementations of monopole arrays. The disadvantage of the delay line LPMA is that it requires a larger ground plane (or volume) to accommodate the delay lines. Although the delay line can be meandered to reduce the size of the ground plane, this will limit the useful high frequency because fabrication is difficult. In addition, unless care is taken the delay line will radiate and increase the cross-polarization level.

Using the parasitic element technique for achieving the correct phasing in the active region, however, makes the LPPDA or LPPMA significantly more sensitive to a change in geometric parameters than the LPDA. Thus, the method of construction for LPPDA or LPPMAs must be chosen carefully to ensure repeatability. Antenna and feedline dimensions must be accurately realized and the separation between feedline and parasitic monopoles must be carefully adjusted. The higher the operating frequency band, the more critical are the requirements for accurate construction.

2.4 Freestanding Element LPPMA

It was found that a successful LPPMA antenna could be constructed from planar elements in free space. For use in multi-arm configurations the arms must closely track each other in phase and amplitude. The accuracy needed for the antenna arms to track each other and operate at centimeter wavelength can be achieved by an electrostatic machining process applied to thin sheets of conducting material. Both the parasitic and driven arrays are fabricated in a similar fashion. The parasitic arrays are mounted directly to the ground plane (or central boom), while the planar feedline and driven monopoles are mounted above the ground plane (or central boom) and held in place with dielectric spacers. The feedline is bounded by lines arranged so that constant angles were maintained between the edges of the feedline and the ground plane, and also between the vertical surface of the feedline and the plane of the parasitic elements.

2.5 PCB LPPMA Implementation

Given the need for monopole arrays for centimeter and shorter wavelengths, the photo-lithographic methods used to make printed circuits seem most appropriate for the construction of LPPMA antennas for the higher frequencies. In the PCB implementation, the driven monopoles are printed on one side of the substrate and the parasitic monopoles on the other side. Thus the spacing between the transmission line and the parasitic dipoles is constant due to the constant thickness of the PC board.

Numerous attempts at constructing wide bandwidth printed LPPMA antennas met with little success. The PCB LPPMA has a smaller useful bandwidth due to the constant thickness of the conventional PC board and is limited to about 5 or 6:1. To achieve wider bandwidths, the PCB sections were scaled to a second substrate thickness and cascaded.

To increase this bandwidth, compensations had to be made for the constant thickness of the substrate material. Since this separation is fixed throughout the array by the thickness of the substrate, the separation between feedline and

parasitic monopoles provides an excess of capacitance for the longer monopoles. This capacitance can be reduced by changing the area in the region where feedline and parasitic monopoles cross over one another as shown in Figure 2.3. Experimentation with antenna models using the above guidelines finally led to printed LPPMA antennas that operate well at centimeter wavelengths. Figure 2.4 shows the measured VSWR of a PCB LPPMA wing with a driven $\alpha = 15$ degrees. Figure 2.5 shows an example of a freestanding and corresponding PCB LPPMA on a ground plane. Figure 2.6 shows the VSWR comparison between the freestanding and corresponding PCB implementation.

3.0 Analysis Model

The importance of coupling between the feedline and the parasitic elements was demonstrated by analysis using an approximate model. In formulating the model, the parasitic elements are excited not only by fields due to radiation from other elements, but also by electromagnetic coupling to the feedline, even though no conducting connections between parasitic elements and the feeder exist. So the excitation of the parasitic elements of a LPPMA differs from that of conventional parasitics, but because of the lack of conducting connections, the term "parasitic" is used to distinguish them from the driven elements.

The analysis technique is an extension of the method used by Carrel to analyze log-periodic dipole (LPD) arrays. The first step is to use image theory to convert the LPPMA to an LPD with parasitic elements (LPPDA), an array of dipoles excited by a balanced twin-fin feeder. Following Carrel, approximate field techniques are used to compute the elements of the impedance matrix, Z_A for the dipoles. All of the dipoles are driven at one extremity in the LPD, but for the LPPDA, the coupling of a parasitic element to the feeder takes place mostly in the region where the planar dipole overlays the planar feedline, forming thereby a parallel-plate capacitor. The midpoint of this region is chosen as a terminal for the parasitic element. The driven elements and the portions of the parasitic elements beyond the feedline are analyzed by a procedure very much like Carrel used to solve the "exterior problem" to find the impedance matrix for the dipoles of the LPD.

Figure 3.1 shows the division of an LPPDA into exterior and interior problems. A uniform line is used to represent the triangular fin conductors of the balanced feeder. The capacitances, C_P , are connected between the transmission line and the terminals of the parasitic elements. These network elements are introduced as approximate models for the proximity coupling between the feeder and the parasitics. The sections of the parasitic elements between the feeder conductors,

not having been included in the exterior problem, are taken into account by connecting inductances, LP, between the "terminals" on the parasitics.

The main component of the feeder for the planar LPPDA arrays is a coplanar, triangular-fin transmission line with small included angle of the fin and small angle of separation between the fins.

The capacitances in the feeder network of Figure 3.1 have been estimated using the parallel plate formula with the given dimensions of the overlap region between each monopole and the feeder as shown in Figure 3.2. Note that the scaling of dimensions from element to element in a log-periodic fashion means that the area of the capacitor at the second longest parasitic element (element four) will be τ^2 times the area of the capacitor at the longest parasitic (element two).

The inductance values for the network have been estimated using the formula for the inductance per meter of a circular cylinder conductor of length b, radius a and the conventional equivalence between strip width, w, and cylinder radius, a, $w = 4a$.

$$L_p = \frac{\mu b_p}{2\pi} \ln \left\{ \frac{2\lambda}{\pi w_p} \right\} \quad (1)$$

Examples

Figure 3.3 shows the corresponding LPPDA ($\tau = .9$, $\sigma = .1$ between driven elements) with values approximately corresponding to the current design. Figure 3.4 shows the same antenna with the parasitic element to transmission line coupling set to zero. With the coupling set to zero and the length of the parasitic elements varied, it has been found that the lowest VSWR is about 6:1. With the current feed parameters the calculated VSWR is not as good as the conventional LPDA, but shows that acceptable values well below 1.5:1 are possible.

4.0 Applications

In addition to allowing, a monopole implementation for ground plane applications, LPPMAs can be used to implement multi-arm feeds obtained by placing elements circumferentially around a rod, a pyramidal, or conical base cone.

Figures 4.1 and 4.2 show three and four arm configurations. The three-arm configuration has been used for its ability to be packed in a hexagonal array. The

four-arm version could be implemented in two cross LPDAs, but the four-arm LPPMAs have superior cross polarization properties at higher frequencies.

Figure 4.3 shows a multi-arm LPPMA where the monopoles are built around a cone. These multi-arm feeds can then provide tracking and angle of arrival information by exciting the arms with proper phase progression

5.0 Group Delay

Log-periodic antennas can be made to cover extremely wide frequency bands, but they are inherently dispersive. Thus a narrow pulse presented to the feed point (or incident upon the antenna) is not transmitted (or received) undistorted. The LPDA as shown by Carrel and the LPPMA both introduce a 180 degree phase shift every log cycle. Group delay is defined by the mathematical formula

$$\text{Group Delay} = \frac{-d\phi}{360df} \quad (2)$$

Where group delay is in seconds, ϕ is the phase in degrees and f is the frequency in Hertz.

For log-periodically scaled antennas, the group delay reduces to a simple formula:

$$\text{Group Delay} = \frac{\sqrt{\tau}}{2(1-\tau)f} \quad (3)$$

The interesting feature of the group delay is that it is only a function of the scale factor τ and does not depend on the other parameters of the antenna.

Figure 5.1 shows measured group delay (referenced to the feed point) of two LP antennas with different scale factors which covered approximately a 1 to 10 GHz frequency bandwidth. The Group delay was measured using an HP 8510 using the S12 measurement capability after calibration to remove the effects of the transmit antenna and connecting cables. Figure 5.2 shows the corresponding calculations using the group delay equation (3). Figure 5.3 shows the group delay in nanoseconds for a 1 GHz signal as a function of the scale factor τ .

6.0 Conclusions

The control of the coupling between the parasitic elements and the feedline is critical for proper LPPMA operation

In LPPMA using freestanding elements, the separation between the biconical transmission lines used as the feedline for the driven elements and the parasitic elements is increased by the scale factor cell-to-cell. This increasing separation properly scales the coupling of the parasitic elements to the transmission line required for wideband operation.

In the PCB implementation, the driven monopoles are printed on one side of the substrate and the parasitic monopoles on the other side. Thus the spacing between the transmission line and the parasitic dipoles is constant due to the constant thickness of the PC board. This constant spacing limits the PCB bandwidth to about 5 or 6:1.

To increase this bandwidth, compensations must be made for the constant thickness of the substrate material. Since this separation is fixed throughout the array by the thickness of the substrate, the separation between feedline and parasitic monopoles provides an excess of capacitance for the longer monopoles. The capacitance can be reduced by changing the area in the region where feedline and parasitic monopoles cross over one another

When the coupling is compensated, implementation on constant thickness printed circuit board can achieve essentially the same performance as the freestanding implementation.

7.0 References

- [1] P.G. Ingerson, S.C. Kuo, P.E. Mayes, "Analysis and Applications of Log-periodic Monopole Arrays", Proc. Antenna Applications Symposium, Sept. 1994.
- [2] N. Barbano, "Log-periodic Dipole Array with Parasitic Elements," microwave Jour., vol. 8, pp. 41-69, October 1965.
- [3] R.L. Carrel, "Analysis and Design of Log-periodic Dipole Antennas," Tech. Rep. No. 52, Contract AF33(616)-6079, Antenna Laboratory, University of Illinois, Urbana, October 1961.
- [4] Ingerson and Mayes, "Log- periodic Antennas with Modulated Impedance Feedline," IEEE Trans. Antennas Propag., vol. AP-16, pp. 633-642, November 1968.
- [5] N. Barbano, "Log-periodic Yagi-Uda Array," IEEE Trans. Antennas Propag., vol. AP-14, no. 2, pp 235-238, March, 1966.

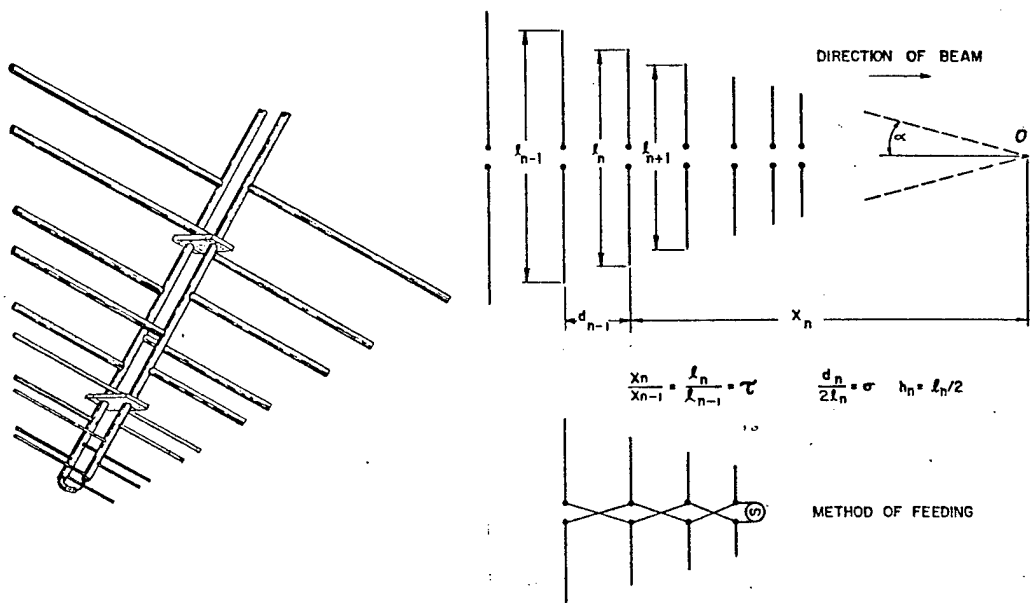


Figure 2.1 Log-periodic dipole array parameters and method of feeding

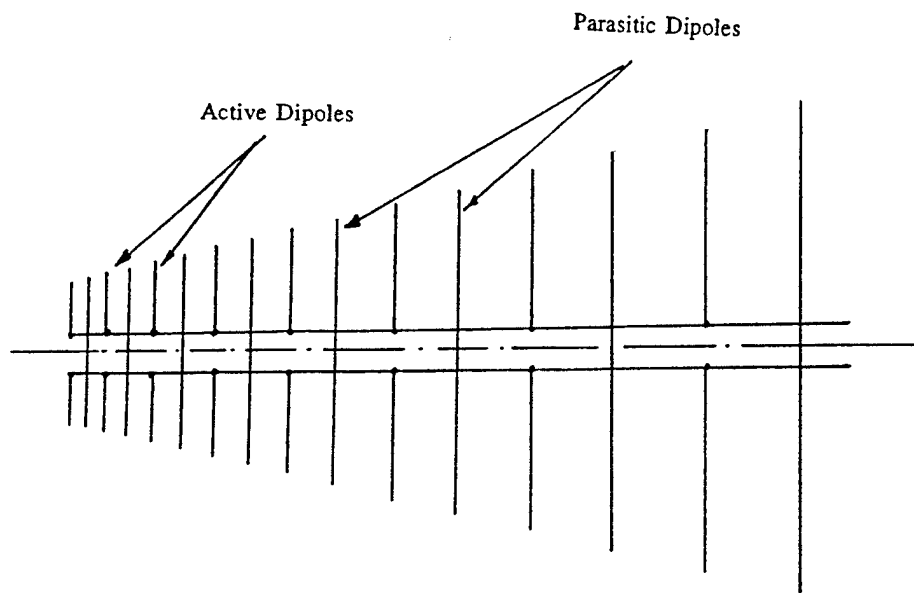


Figure 2.2 Log-periodic dipole array with parasitic elements

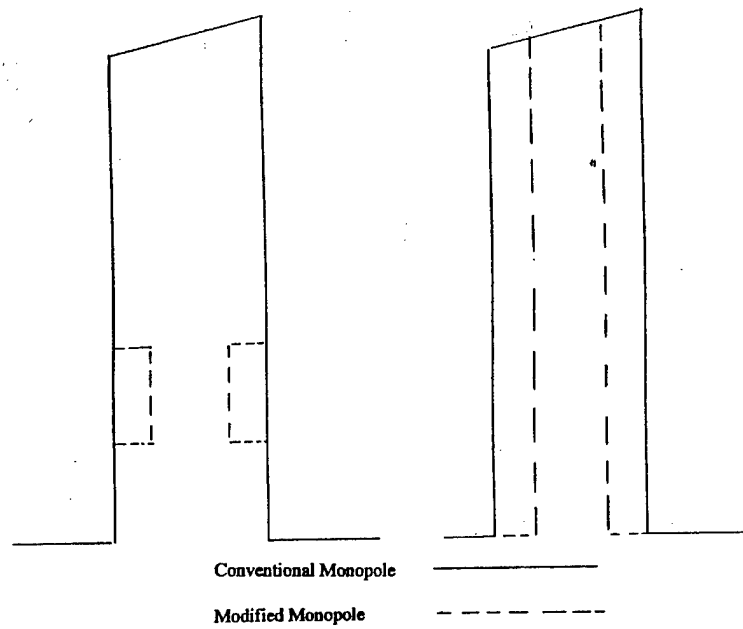


Figure 2.3 Parasitic element to feedline coupling reduction method by reducing coupling area

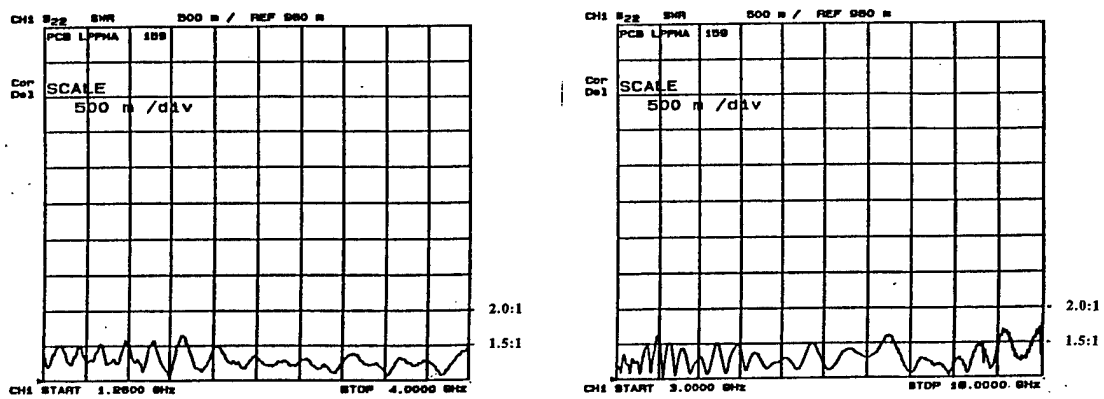


Figure 2.4 Measured VSWR of a PCB LPPMA with a 15 degree α

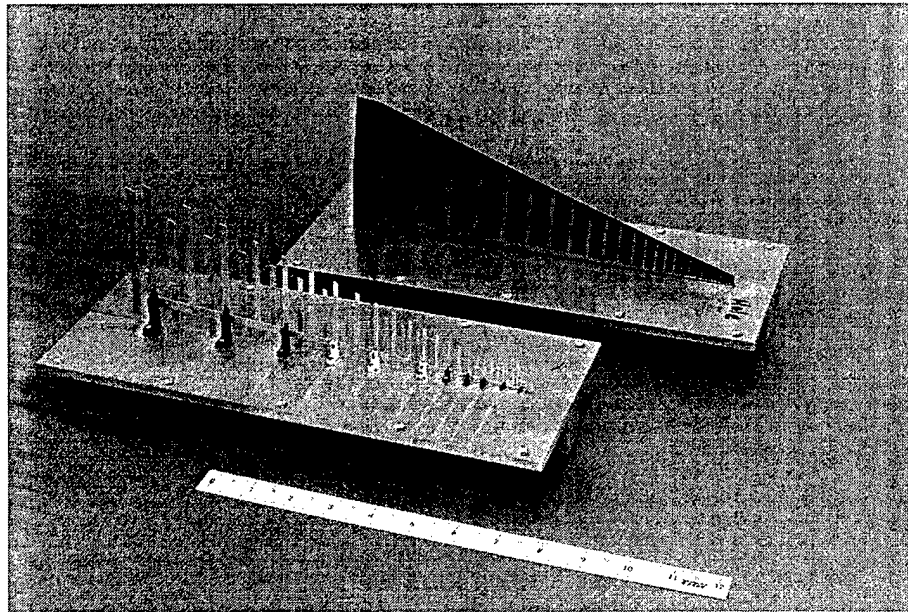


Figure 2.5 Freestanding and PCB LPPMA on a ground plane

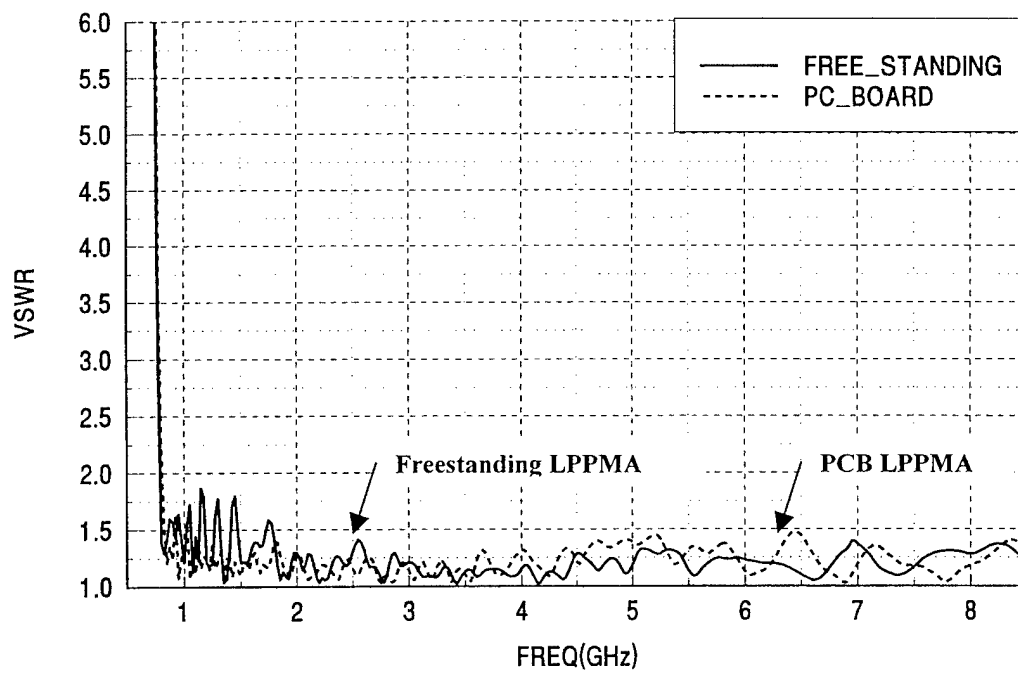


Figure 2.6 Comparison of VSWR for a freestanding and PCB LPPMA

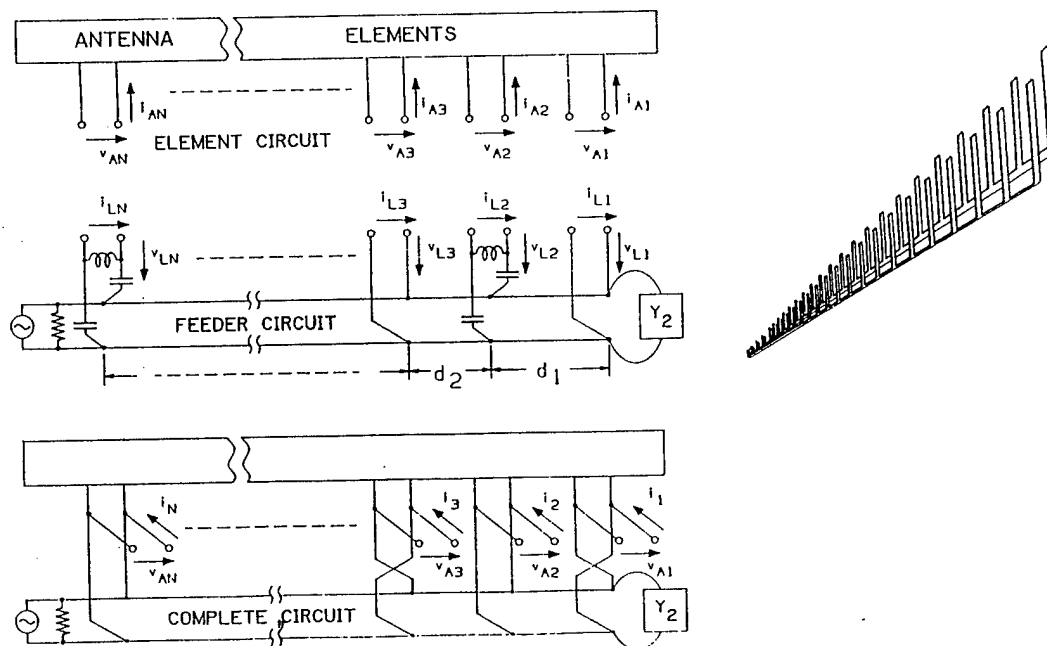


Figure 3.1 Analysis model for the LPPDA and LPPMA with feedline coupling

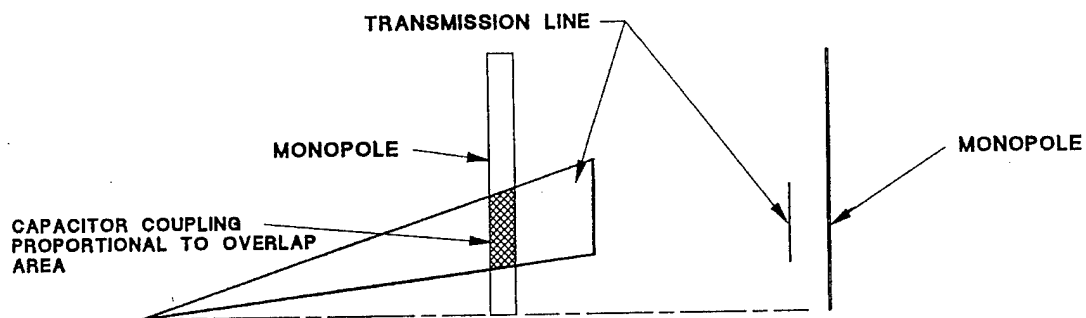


Figure 3.2 Parasitic element to feedline coupling model

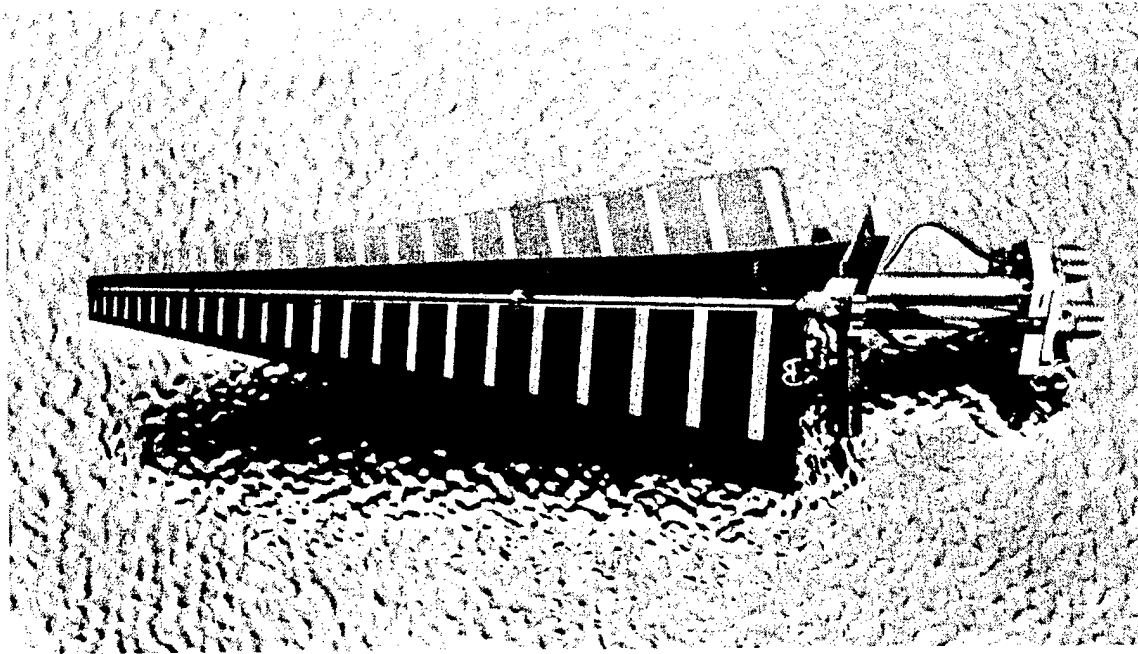


Figure 4.1 Three-arm LPPMA

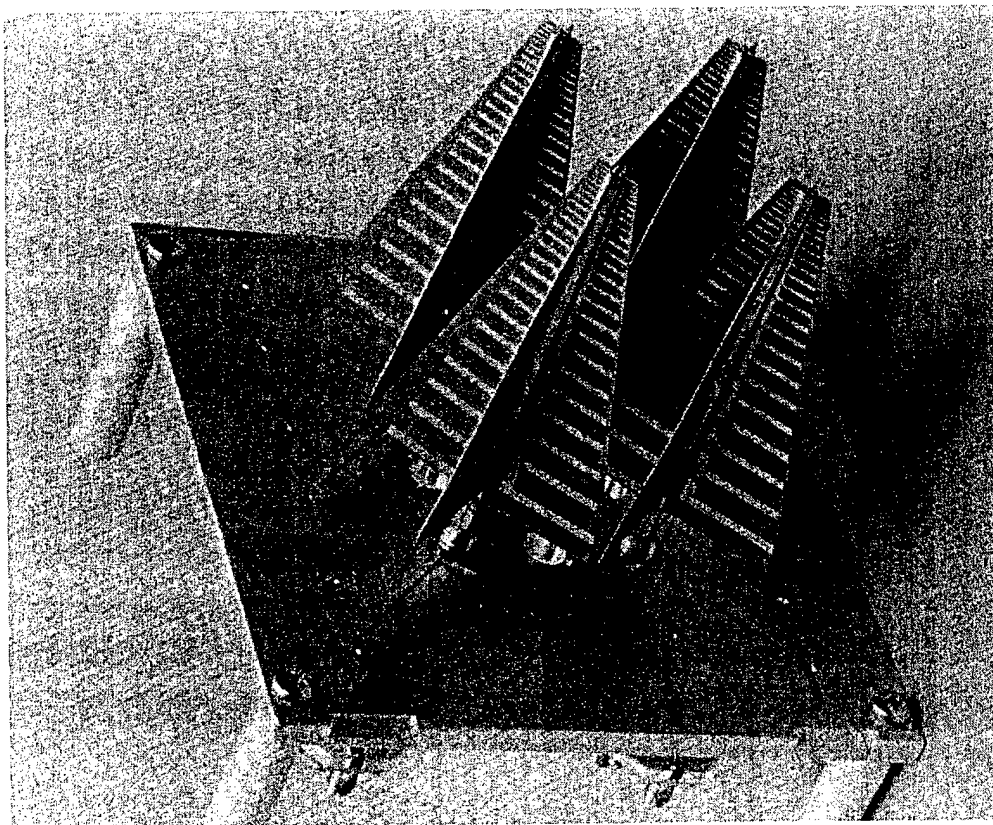


Figure 4.2 Four element array of four-arm LPPMAs

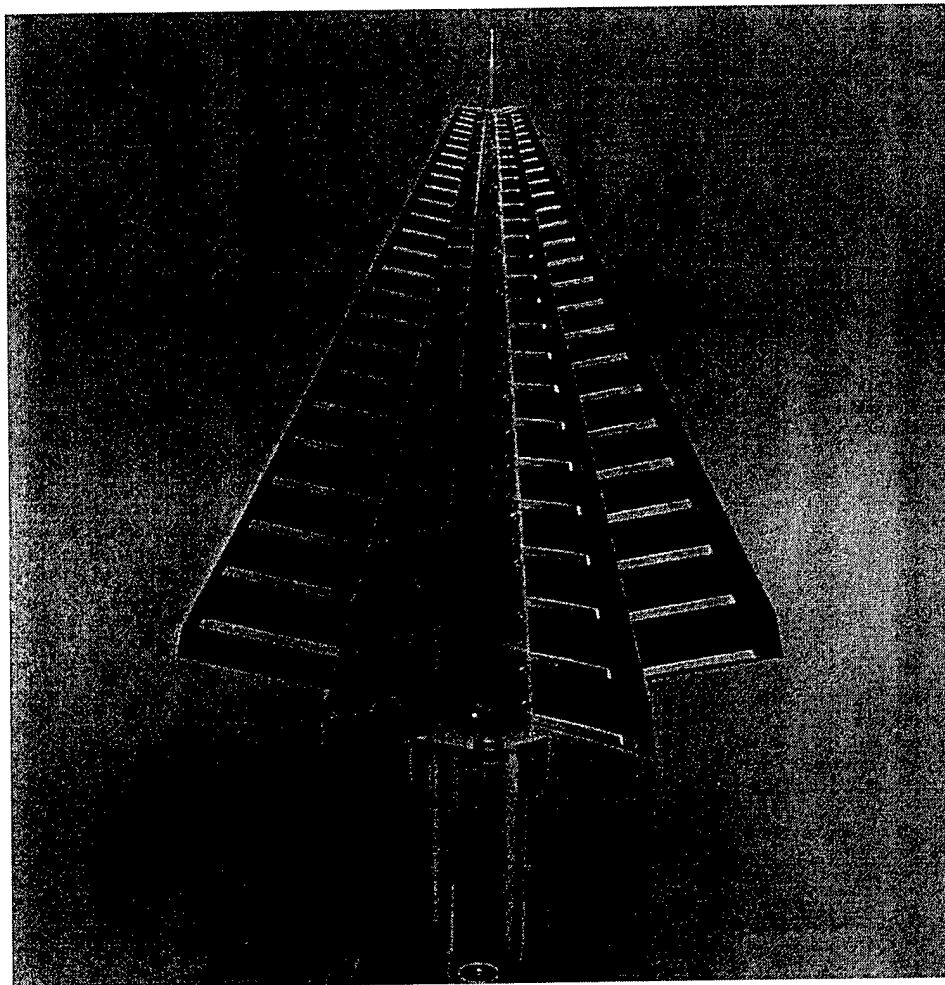


Figure 4.3 Six-arm PCB LPPMA

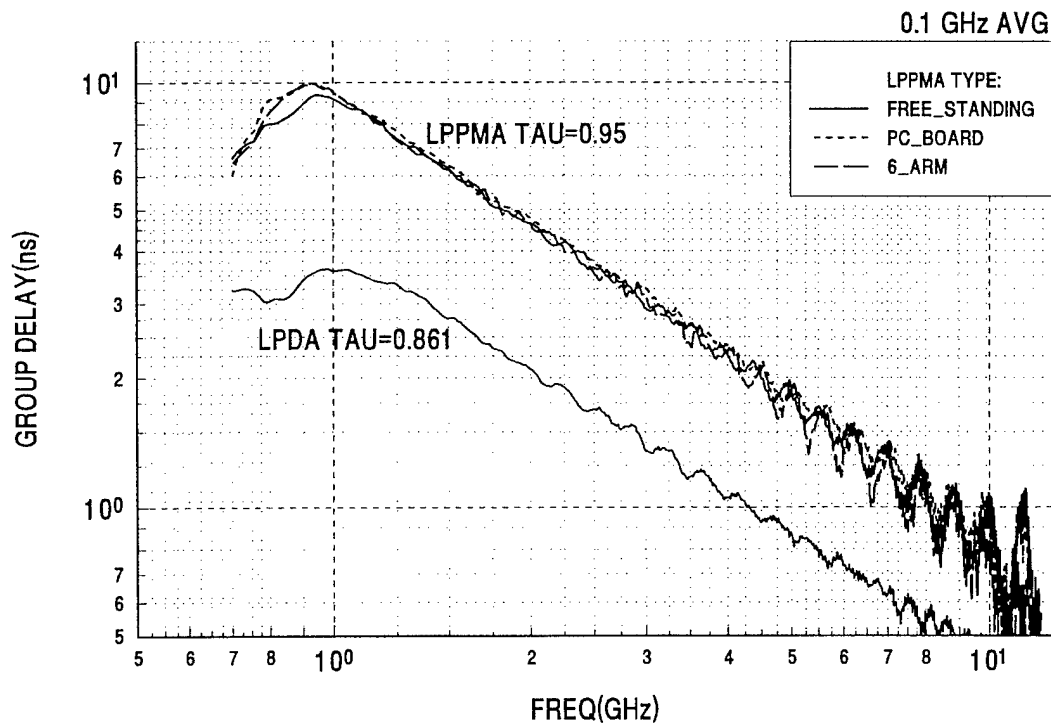


Figure 5.1 Measured group delay for a LPDA and LPPMA with different scale factors

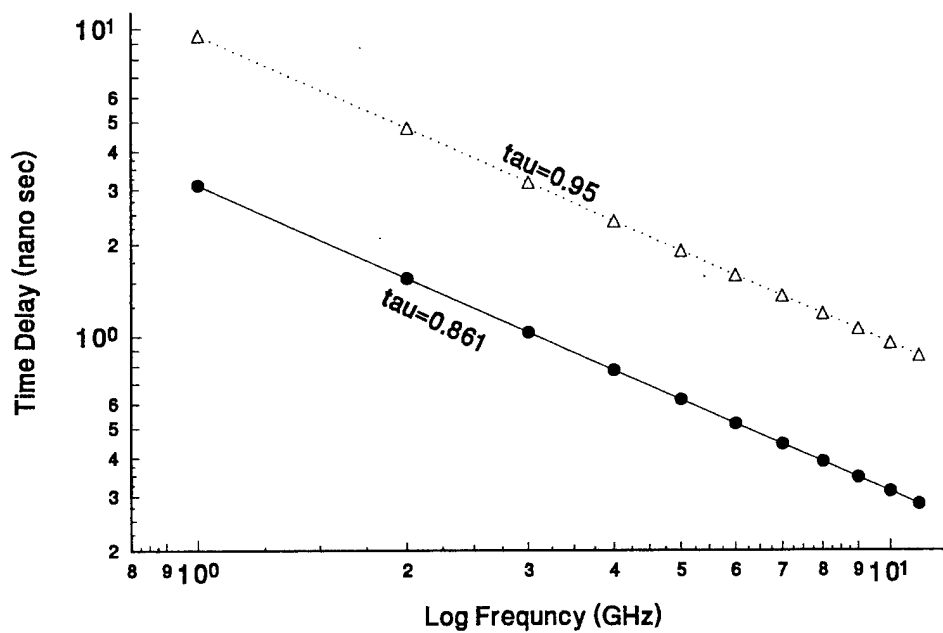


Figure 5.2 Calculated group delay using equation 3

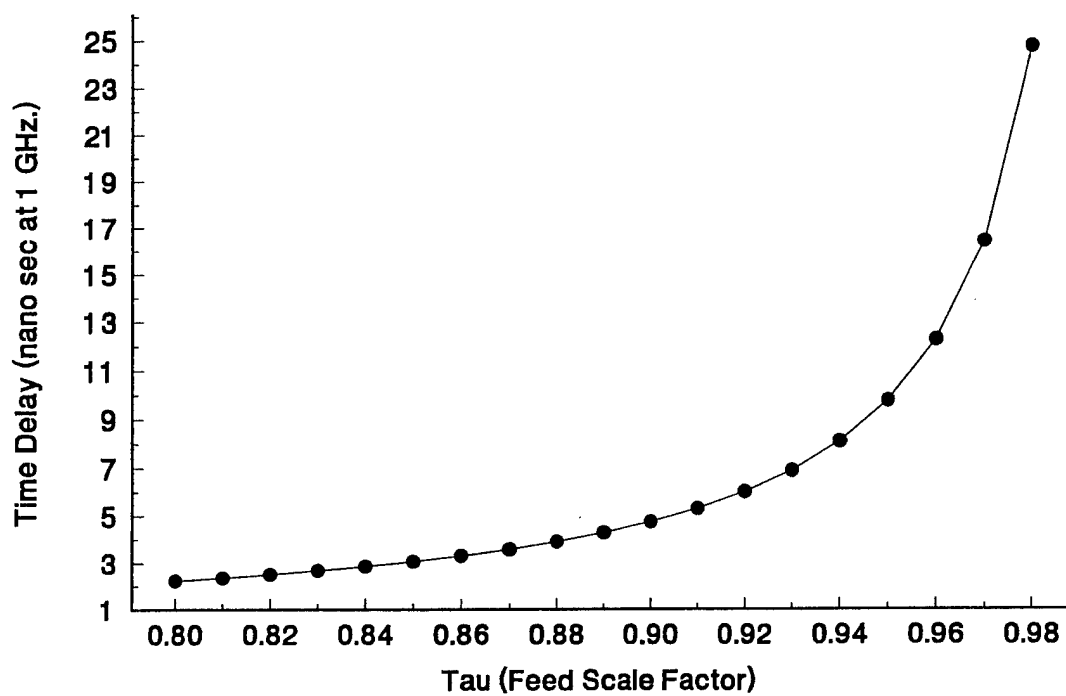


Figure 5.3 Group delay as at function of tau at 1 GHz.